

**Shear capacity of reinforced concrete slab bridges under a wheel load  
close to the support**  
*Literature review*  
**CONCEPT v. 16-08-2012**

Author:  
Ir. E. Lantsoght

**Shear capacity of reinforced concrete slab bridges under a wheel load  
close to the support**  
*Literature review*  
**CONCEPT v. 16-08-2012**

Author:

Ir. E. Lantsoght

© 2012

Delft University of Technology  
Faculty of Civil Engineering and Geosciences  
Department of Design & Construction – Concrete Structures  
Stevinlaboratorium  
Postbus 5048  
2600 GA Delft  
Telephone 015 2783990/4578  
Telefax 015 2785895/7438

AUTEURSRECHTEN

Alle rechten voorbehouden. Niets uit deze uitgave mag worden verveelvoudigd, opgeslagen in een geautomatiseerd gegevensbestand, of openbaar gemaakt, in enige vorm of op enige wijze, hetzij elektronisch, mechanisch, door fotokopieën, opnamen of enig andere manier zonder voorafgaande schriftelijke toestemming van de universiteit.

All rights reserved. No part of this publication may be reproduced, stored in a retrieval system of any nature, or transmitted, in any form or by any means, electronic, mechanical, photocopying, recording or otherwise, without the prior written permission of the university.

AANSPRAKELIJKHEID

De TU Delft en degenen die aan deze publicatie hebben meegewerkt, hebben een zo groot mogelijke zorgvuldigheid betracht bij het samenstellen van deze uitgave. Nochtans moet de mogelijkheid niet worden uitgesloten dat er toch fouten en onvolledigheden in deze uitgave voorkomen. Ieder gebruik van deze uitgave en gegevens daaruit is geheel voor eigen risico van de gebruiker en de TU Delft sluit, mede ten behoeve van al degenen die aan deze uitgave hebben meegewerkt, iedere aansprakelijkheid uit voor schade die mocht voortvloeien uit het gebruik van deze uitgave en de daarin opgenomen gegevens, hetzij de schade die mocht voortvloeien uit opzet of grove schuld zijdens de TU Delft en/of degenen die aan deze uitgave hebben meegewerkt.

## Table of contents

1.	Introduction.....	6
2.	Scope.....	7
2.1.	Existing slab bridges.....	7
2.1.1.	Slab bridges.....	7
2.1.2.	Reinforced concrete slabs.....	10
2.1.2.1	Forces in slabs.....	10
2.1.2.2	The difference between slabs and beams.....	12
2.1.3.	Existing concrete bridges.....	12
2.2.	Wheel loading.....	15
2.3.	Influence of the support.....	18
3.	Shear in slabs.....	21
3.1.	Shear transfer.....	21
3.1.1.	What is shear in reinforced concrete?.....	21
3.1.1.1	A historical overview.....	21
3.1.1.2	Horizontal shear and diagonal tension.....	24
3.1.1.3	Which forces define the shear resistance?.....	25
3.1.2.	Types of shear failure.....	27
3.1.2.1	The influence of flexure.....	27
3.1.2.2	Classification of types of shear failure.....	28
3.1.2.3	The influence of arching action on the failure mode.....	32
3.1.3.	The mechanisms of shear transfer.....	33
3.1.3.1	Concrete compression zone.....	37
3.1.3.1.1	Models based on the capacity of the concrete compressive zone	37
3.1.3.1.2	Determination of the capacity of the concrete compressive zone	38
3.1.3.1.3	Contribution of concrete compressive zone to shear carrying capacity	39
3.1.3.2	Residual tension over crack.....	39
3.1.3.3	Aggregate interlock.....	41
3.1.3.3.1	What is aggregate interlock.....	41
3.1.3.3.2	Models.....	44
3.1.3.3.3	Contribution of aggregate interlock to shear carrying capacity	53
3.1.3.4	Dowel action.....	53
3.1.3.4.1	What is dowel action?.....	53
3.1.3.4.2	Models.....	54
3.1.3.4.3	Contribution of dowel action to shear carrying capacity.....	58
3.1.3.5	Arch action.....	59
3.1.3.5.1	What is arch action?.....	59
3.1.3.5.2	Experiments.....	61
3.1.3.5.3	Models.....	62
3.1.3.5.4	Contribution of arch action to shear carrying capacity.....	64
3.1.4.	The size effect.....	64
3.1.4.1	Observations related to size effect.....	65
3.1.4.2	Size effect explained by aggregate interlock.....	70
3.1.4.3	Size effect explained by fracture mechanics.....	71
3.1.4.4	Size effect related to type of shear failure.....	76
3.2.	One-way and two-way shear.....	77
3.2.1.	Distinction.....	77

3.2.2.	Similarities and transition zone.....	81
3.2.3.	Effective width in wide beams.....	87
3.2.3.1	Observations and measurements with regard to effective width ....	88
3.2.3.2	Design methods for effective width.....	94
3.3.	Models for shear .....	98
3.3.1.	Compression field theory models .....	98
3.3.1.1	Development of the compression field theory .....	98
3.3.1.2	Design method: modified compression field theory .....	105
3.3.1.3	Methods based on a compression field .....	109
3.3.1.4	Discussion of compression field theory models .....	113
3.3.2.	Critical shear crack theory .....	116
3.3.2.1	Development of CSCT.....	116
3.3.2.2	Design procedure based on CSCT .....	116
3.3.2.3	Non-axis-symmetrical punching based on CSCT.....	119
3.3.2.4	Discussion of CSCT.....	122
3.3.3.	Strut and tie models and truss models.....	123
3.3.3.1	Development of strut and tie models .....	123
3.3.3.2	Truss with concrete tensile contribution .....	125
3.3.3.3	3D strut and tie model.....	126
3.3.3.4	Discussion of strut and tie models .....	129
3.3.4.	Mechanical models .....	131
3.3.4.1	Tooth model .....	131
3.3.4.2	Bond model.....	138
3.3.5.	Plasticity-based models.....	141
3.3.5.1	Failure criteria.....	141
3.3.5.1.1	Coulomb's hypothesis and the modified Coulomb criterion ...	141
3.3.5.1.2	Parabolic Mohr failure criterion.....	144
3.3.5.2	Plasticity models .....	145
3.3.5.2.1	Introduction .....	145
3.3.5.2.2	Shear capacity explained by plasticity models.....	146
3.3.5.2.3	Punching shear capacity explained by plasticity models .....	150
3.3.5.2.4	Discussion of plasticity models.....	151
3.3.6.	Fracture mechanics models.....	152
3.3.6.1	Introduction to fracture mechanics models.....	152
3.3.6.2	Modeling material behavior .....	153
3.3.6.3	Fracture mechanics models for shear.....	157
3.3.6.4	Discussion of fracture mechanics models.....	163
3.3.7.	Empirical models .....	164
3.3.7.1	Regan's formula for concentrated loads close to supports .....	164
4.	Experimental data .....	166
4.1.	Test data by Regan.....	166
4.2.	Test data by Furuuchi et al.....	168
4.3.	Test data from University of Toronto .....	169
4.4.	Test data from EPFL.....	173
4.5.	Test data from ETH .....	178
4.6.	Experiments on wide beams and slabs.....	182
4.7.	Experiments on bridge decks .....	207
5.	Code provisions .....	216
5.1.	NEN 6720 .....	216
5.2.	EN 1992-1-1:2005 .....	220



5.3.	ACI 318-08 .....	225
5.4.	Model Code 2010.....	229
6.	Discussion.....	235
7.	Conclusions.....	238
8.	References.....	239
9.	Annex: Database of test results.....	263

# 1. Introduction

This report is a summary and review of the literature which will serve as a background to study the shear capacity of existing reinforced concrete slab bridges without shear reinforcement under wheel loads close to the support.

Chapter 2 gives background information with regard to the scope of the research. Information about concrete slabs, slab bridges and existing concrete bridges as well as wheel loading is given and the influence of the position of the load near to the support is discussed.

Chapter 3 is the core of this literature review and contains an overview of the literature about the shear capacity of slabs without shear reinforcement. Slabs under point loads containing sufficient flexural reinforcement can fail as a wide beam (one-way shear) or in punching shear (two-way shear). As very few shear tests have been carried out on one-way slabs, the one-way shear theory is mainly based on the shear capacity of reinforced concrete beams. The concepts of shear failure, the mechanisms of shear transfer and the majority of the discussed models are entirely based on beam shear. The models for punching (two-way) shear on the other hand are based on the shear capacity of slab-column connections. The punching capacity for a slab under a wheel load is calculated based on this configuration.

Chapter 4 contains test data from the literature concerning shear tests of one-way slabs and wide beams without shear reinforcement. To compare with the tests carried out at Delft University of Technology, data from test series with comparable widths (0,5m and larger) and shape ( $b/h \geq 1$ ) have been gathered. The full database is given in the Annex.

Chapter 5 gives an overview of some current code provisions for beam shear and punching shear. The code formulations are cited, and the assumptions and research leading to the current code formulas are emphasized.

Chapter 6 discusses the information that is gathered in this document and conclusions are given in chapter 7.

## 2. Scope

### 2.1. Existing slab bridges

#### 2.1.1. Slab bridges

The results of this research will be used to study the shear capacity of existing reinforced concrete solid slab bridges. Concrete slab bridges are economical for spans in the range of 3 to 8 m. However, spans up to 16m can also be feasible. These bridges are normally reinforced with reinforcing bars, but prestressing strands and I-beams can be used in practice. An example of an existing Dutch slab bridge is shown in Fig. 2.1, Fig. 2.2 and Fig. 2.3. The reinforcement ratio for bridge deck slabs with  $d > 25\text{cm}$  and a reasonable maximum amount of reinforcement of  $25\text{cm}^2/\text{m}$  will always be below  $\rho_l = 1\%$  (Rombach et al. 2009).

According to Aktan et al. (1992): “Certain bridge types, such as reinforced concrete slab bridges with sound piers and abutments, are inherently more resistant to collapse than others.” Testing a deteriorated bridge shows that it still can carry 22 rating trucks, a load exceeding four times the bridge rating. Beal (1982) tested scale models of reinforced concrete bridge decks and discovered that the failure load was 6 times higher than calculated. The failure mode was punching shear and not flexure as assumed in design. The high capacities in solid slabs are the result of the compressive membrane action. The membrane action in slabs enhances the flexural and punching shear capacity, as shown in Azad et al. (1994); Chamululu (2009); Eyre (1997); Guice, Slawson and Rhomberg (1987); Hewitt and de Batchelor (1975), Hon, Taplin and Al-Mahaidi (2005); Taylor and Hayes (1965); Taylor et al. (2003) and Vecchio and Collins (1990). As the flexural capacity of concrete slabs is larger due to the compressive membrane action, shear failure modes become more important (Ebeido and Kennedy, 1996). Likewise, Azizinamini et al. (1994) point out that experimental results indicate that reinforced concrete slab bridges possess a much higher strength than that indicated by current rating procedures. The authors refer to tests by Fenwick and Dickson (1989), in which it was found that for all three specimens the stresses in the reinforcement were considerably lower than the analytical predictions using thin plate theory (60%, 50% and 35% for the simply supported, flexurally restrained and fully restrained slabs, respectively). This is attributed to wider distribution of flexural

forces across the slab width, residual tensile capacity of the concrete at a crack and, for the restrained slab, compressive membrane action.

Azizinamini et al. (1994) tested a five span continuous reinforced slab bridge. This bridge failed in flexure after forming two yield lines. While the bridge was rated to carry a maximum truck load equivalent to 67% of the HS20 truck, it carried 3 times the HS20 truck load while behaving in a perfectly linear elastic manner. More than seven HS20 trucks loads on each span were required to reach the ultimate capacity. The results corresponded well to the ultimate load calculated with yield line analysis. However, Jackson (2010) in a discussion to Zheng et al. (2010) argues that accounting for compressive membrane action leads to good results for single wheel loads, but not necessarily whole vehicles or combinations of vehicles.

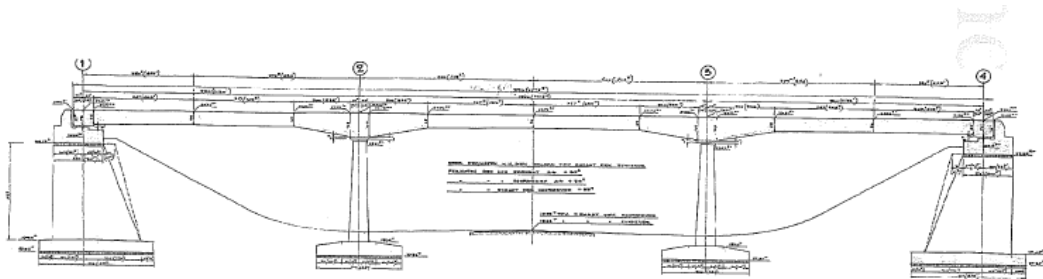


Fig. 2.1: Side view of slab bridge, TNO report 2010.

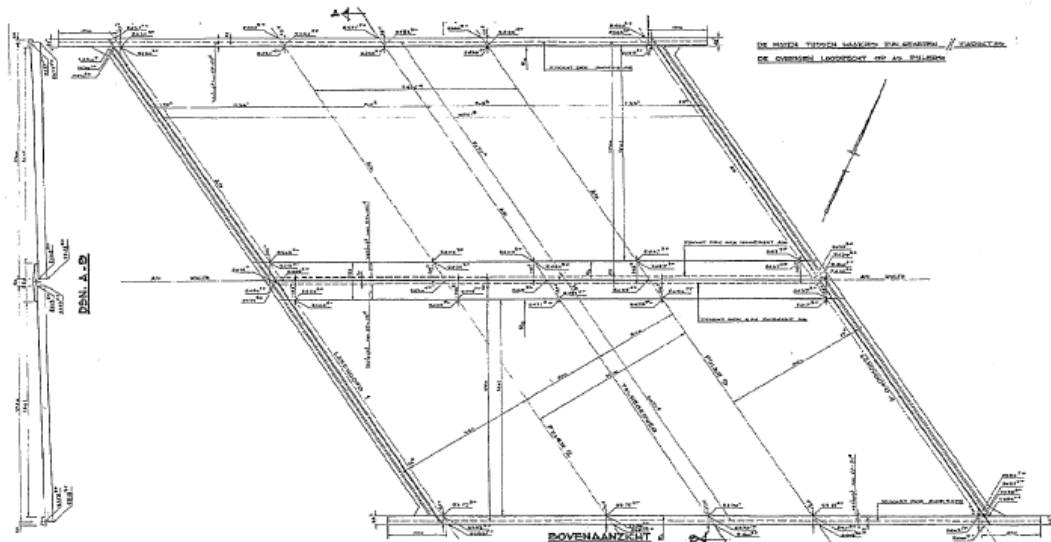


Fig. 2.2: Top view of slab bridge, TNO report 2010.

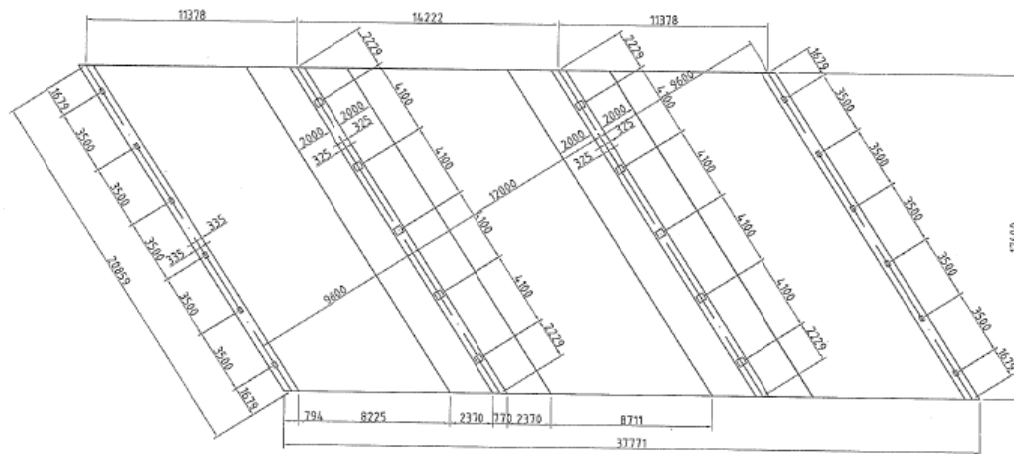


Fig. 2.3: Geometry of slab bridge, TNO report, 2010.

A recent example of a collapse of a bridge due to shear is the collapse of the de la Concorde overpass in Laval, Quebec (Wood, 2008).



Fig. 2.4: Collapse of the de la Concorde overpass (Wood, 2008).



Fig. 2.5: Shear failure of the Laval bridge (Massicotte, 2007).

Cope (1985) pointed out that when the deck has a skew angle, the concentration of shear forces increases considerably, owing to the additional twisting action. Increasing skew angles reduce the shear capacity. According to Ebeido and Kennedy (1996) skew effects become important when the skew is larger than  $20^\circ$ . In the current study, skew effects are not considered.

Rombach and Velasco (2005) observed that due to the new code provisions, shear is often the governing failure mode in slabs without shear reinforcement. This results from the increase in the sectional forces due to the more concentrated wheel loading. Moreover, the maximum shear stress which a member without transverse reinforcement can resist, is reduced. Rombach et al. (2009) contribute the underestimation of the load bearing capacity to neglecting the shear-bending interaction in the code formula and the redistributions of shear forces after the formation of shear and bending cracks.

## 2.1.2. Reinforced concrete slabs

### 2.1.2.1 Forces in slabs

According to EN1992-1-1:2005: “A slab is a member for which the minimum panel dimension is not less than 5 times the overall slab thickness.” A slab has an extra dimension to carry load as compared to a beam and is therefore statically multiply indeterminate. The additional dimensions in a slab lead to additional force components. Marti (1999) states that for plates and shells: “similar to shear forces in

beams and frames, it can be seen that principal and diaphragm shear forces in slabs provide the key to understanding the internal force flow.” According to Marti (1990), conventional design methods consider potential shear failures of a slab as a wide beam as well as punching failures in the vicinity of concentrated loads or reactions. Nominal shear stresses at well-defined critical sections are limited to guard against such failure modes. While such methods are simple and conservative, they have at least three shortcomings:

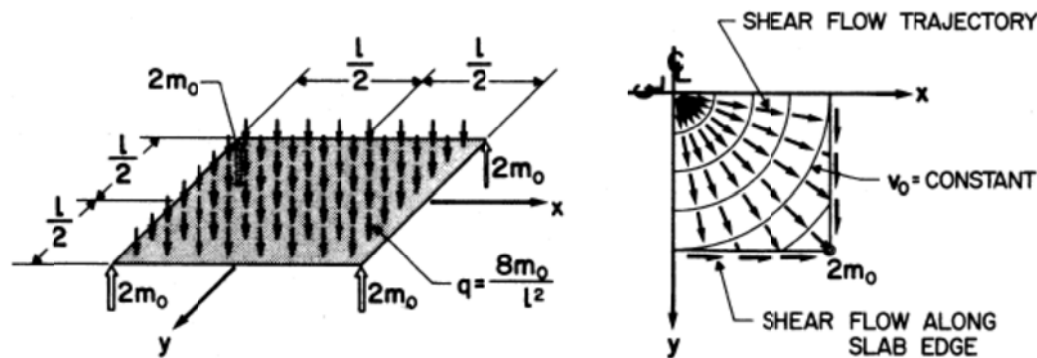
1. They do not provide a basic understanding of how transverse shear forces are transferred in the interior of reinforced concrete slabs.
2. They do not recognize shear transfer by twisting moments along slab edges.
3. They do not provide a consistent model for the dimensioning of transversely reinforced slabs.

Marti (1999) analyses shear in slabs based on the 8 stress resultants, out of which he takes the components  $v_x$  and  $v_y$  to form the principal shear  $v_0 = \sqrt{v_x^2 + v_y^2}$  at an angle

$\varphi_0 = \tan^{-1}\left(\frac{v_y}{v_x}\right)$  to the  $x$ -axis. The direction of the principal shear does not coincide

with the direction of the flexural reinforcement in slabs. Other authors use the sum  $v_x + v_y$  (Rombach and Latte, 2009). Some examples of force flow in slabs are shown in Fig. 2.6. More details about force flow in slabs can be found in Marti (1990, 1999, 2003).

Vaz Rodrigues et al. (2008) state that intermediate cases between one- and two-way shear where shear forces in a slab develop neither parallel nor radially can be found in practice. The strength of these intermediate cases between one- and two-way shear is not always covered by current codes of practice.



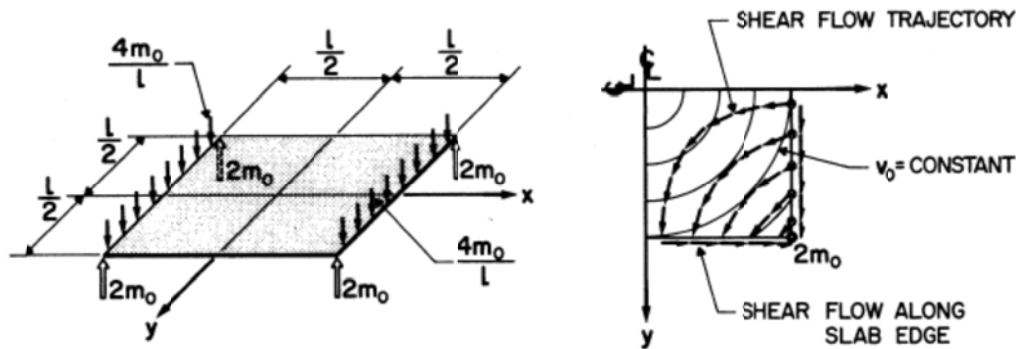


Fig. 2.6: Notation and shear flow and lines of equal principal shear for slab quadrant (Marti, 1990)

### 2.1.2.2 The difference between slabs and beams

Coin and Thonier (2007) point out that the French practice allows for 3.43 times larger shear stresses in slabs than when using EN 1992-1-1:2005. They argue that due to the three-dimensional behavior of a slab the shear capacity of slabs is higher because of a lateral redistribution. Iyengar et al. (1988) found a decreasing shear strength for an increasing  $d/b$  ratio, meaning that slabs have a significant higher shear strength than beams, which may be due to “plate action”. Rensaa (1967) in a discussion to Kani (1967) suggests allowing 10% or higher shear in ordinary one-way slabs, since slabs are typically shallow and have a minimum amount of transverse reinforcement which “undoubtedly puts slabs in a better class than ordinary rectangular beams without web reinforcement.” He added: “If practical experience counts, it might be mentioned that many European building codes, without any adverse effect known to the writer, for more than 30 years have allowed considerably higher shear stresses for slabs than for beams.” Kani (1967) replied in the closure that: “The impression that slabs fail at higher shear stresses than beams probably originated from the comparison of test results of slabs, which usually have small depths, with the results of beams of greater depths.”

### 2.1.3. Existing concrete bridges

Mabsout et al. (2004) wrote: “According to the U.S. Federal Highway Administration’s 2001 National Bridge Inventory data, about 27% of the nation’s 590984 bridges are structurally deficient or functionally obsolete as reported in *Better Roads* magazine (November 2001). Single-span concrete bridges represent about 163000 of these, of which 23% are structurally deficient or functionally obsolete. The majority are short spans, averaging less than 15m in length.” Out of 2000 bridges in



the state of Georgia that require posting, 800 are governed by deficient shear rating of their reinforced concrete pier caps (Wang et al. 2010). Wang et al. (2010) showed that the shear capacity of reinforced concrete pier caps ( $a/d < 1,5$ ) when calculated using a strut and tie model or finite element analysis is higher than when using the traditional ACI 318-08 equations for the shear capacity.

In Europe, it has been estimated that repairs could account for 40% of the total construction contract costs (Pearson-Kirk, 2010). In 1989 inspections in the UK led to the conclusion that only 12% of the concrete bridges were in good condition.

However, when the results of corrosion testing and laboratory testing of samples were reviewed, 30% of the bridges were considered in good condition (Pearson-Kirk, 2010).

In the Netherlands, about 600 slab bridges are under discussion. Investigations on the existing bridges in The Netherlands are carried out, with the aim to determine the actual shear bearing capacity. As the Dutch government decided to extend a large number of existing highways with an additional lane, a large round of assessments was deemed necessary (Walraven, 2007).

Existing bridges typically contain poor flexural anchorage and cutoff details and smaller sized and more widely spaced stirrups than permitted currently. These bridges can be vulnerable to low-cycle fatigue, which is fatigue caused by repeated plastic deformations (Forrest et al., 2010).

When there are existing flaws in a slab, the punching shear capacity is reduced. The most critical angle for cracks is  $20^\circ$  to  $30^\circ$ , for which the punching shear capacity is reduced by as much as 50% (Azad et al., 1994). In deteriorated structures, corroded reinforcement leads to different bond conditions and hence a different behavior in shear (Coronelli and Radaelli, 2010). Cullington, Daly and Hill (1996) report that a number of bridges have been found insufficient in shear capacity as a result of poor anchorage of the longitudinal reinforcement. On site testing to failure of a slab strip, however, led to flexural failure. The influence of ASR on existing slab bridges was studied by den Uijl (2005). If the swelling due to ASR is not restrained, tensile stresses which lead to cracks result. In slab bridges, this can lead to compressive stresses in the horizontal direction because of the reinforcement. In the vertical direction (no reinforcement), horizontal cracks can occur. The tensile strength will then depend on the direction. Even for a significant decrease of the tensile strength, the failure mechanism is still flexure for slab bridges with a reinforcement ratio

smaller than 1,3%. It is also shown that in slab bridges not affected by ASR, the uni-axial tensile strength is very low, while the splitting tensile strength is unaffected. Methods of assessing the remaining service-life of existing bridges are given in Enright and Frangopol, 2000; Estes and Frangopol, 2001; Li et al., 2004; Stewart and Val, 2003 and Wang, Ellingwood and Zureick, 2010. The cost of constructing and maintaining a bridge over its lifetime is denoted as whole life costing (WLC) (Taylor et al., 2007). The present value is taken as:

$$PV = \frac{c}{(1+r)^t} P \quad (3.1)$$

with

$c$  the cost  
 $r$  the discount rate  
 $t$  time in years.

The cost of delaying traffic can be up to 10 times higher than the cost of the associated bridge works. The interruption to traffic tends to be the highest cost influence in the whole life cost of bridges. A comparison of different bridge types is shown in Fig. 2.7.

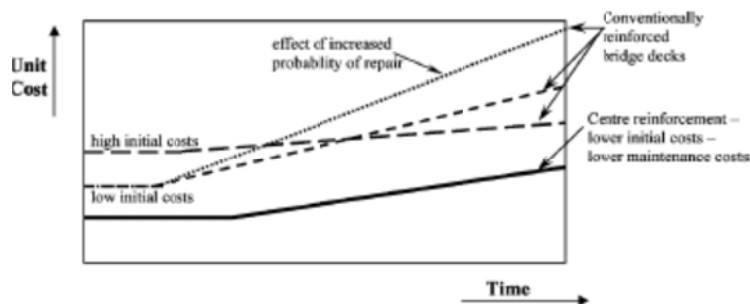


Fig. 2.7: Comparison of total unit cost for bridges with different initial and maintenance costs (Taylor et al., 2007)

These existing bridges have been designed for the traffic loads and volumes of their era. It is however predicted that between 2010 and 2025 an additional increase in transport of goods of 80% will occur (Naumann, 2010), Fig. 2.8. The author points out that the previous prediction for 1998 – 2015 was already reached in 2008. The existing bridges typically contain less prestressing and less reinforcement (flexural as well as shear reinforcement). Regardless of the increase in admissible traffic loads, overloading of trucks is also a long-standing practice, Fig. 2.9. It is therefore

necessary to investigate whether the existing bridges can support the ever-increasing traffic loads and volumes, or if retrofitting or replacements are necessary.

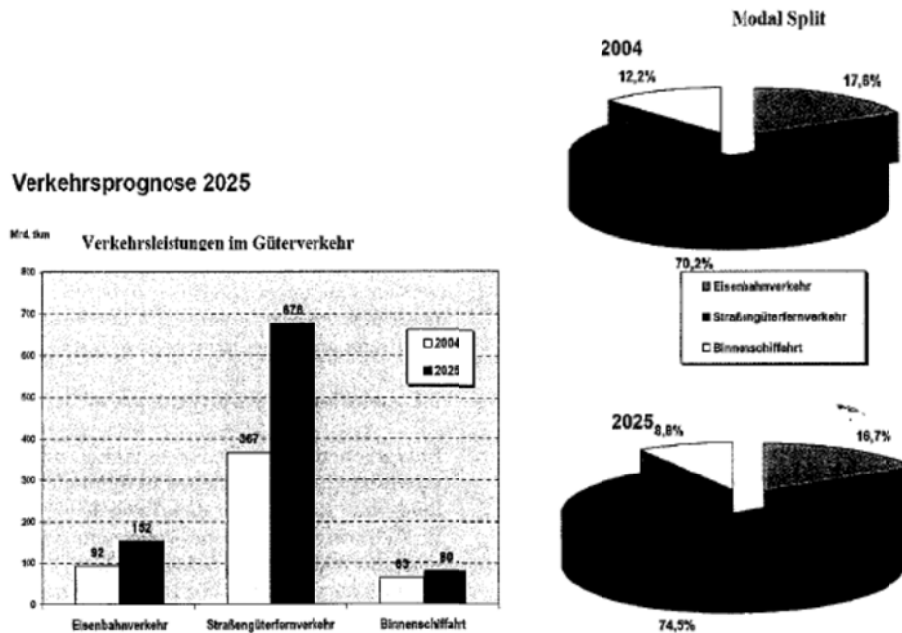


Fig. 2.8: Current traffic forecast (Naumann, 2010).

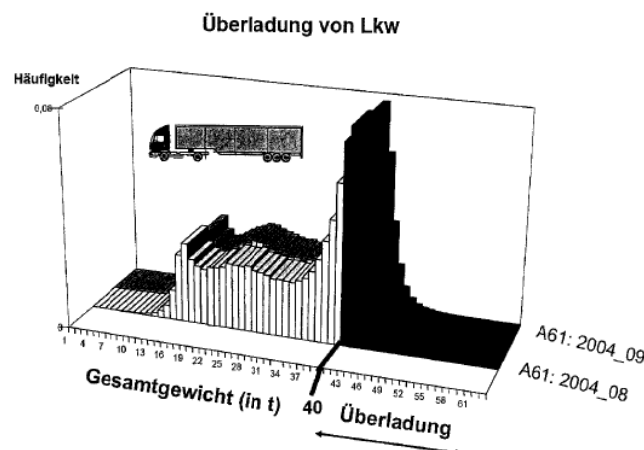


Fig. 2.9: Traffic measurement Brohltal Bridge (Naumann, 2010).

## 2.2. Wheel loading

Recent research (Fernandez Ruiz et al., 2009) showed that: “For road bridges, in general, concentrated loads are decisive for the dimensioning of the slab for flexure as well as for shear.” Bridge deck slabs under wheel loads behave in a complex way. Several load-carrying mechanisms can develop and coexist, depending on the loading and the geometry of the structure. Two-way shear can become prevalent over one-way shear but with a flow of inner forces quite different from that of symmetric punching shear (Vaz Rodrigues, 2007). According to Cope (1985) the critical loading case occurs with a design truck (HB bogie) near a free edge.

The tire contact area as prescribed in EN 1991-2 is 400mm × 400mm with an axle load of 300kN in load model 1 (Fig. 2.10a) and 600mm × 350mm in load model 2 (twin tires, normally relevant to orthotropic decks, Fig. 2.10b). In AASHTO LRFD 2007 the tire contact area is 510mm × 250mm (20in × 10in) for design truck and tandem with axle loads of 45kN and 2 times 145kN. For other design vehicles, the tire contact area should be determined by the engineer. The Dutch VBB uses a tire contact area of 320mm × 250mm.

Nowak (1995) showed that the actual moments and shears caused by the heaviest vehicles observed in truck surveys, range from 1,5 to 1,8 times the design moments and shears calculated using the HS-20 load.

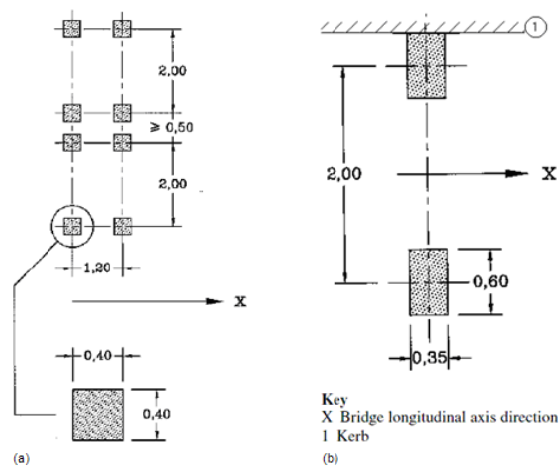


Fig. 2.10: (a) Application of tandem systems for local verifications, Figure 4.2b from EN1991-2:2003; (b) Load model 2, Figure 4.3 from EN1991-2:2003.

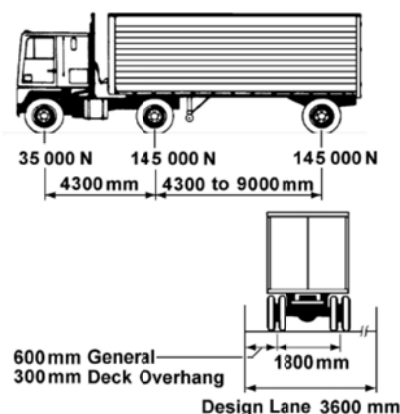


Fig. 2.11: Characteristics of design truck, AASHTO (2007).

The resulting shear forces from the load model from EN1991-2:2003 are shown in Fig. 2.12 for a practical case. The force distribution as a result from one wheel load is shown in Fig. 2.13 and for two wheel loads in Fig. 2.14.

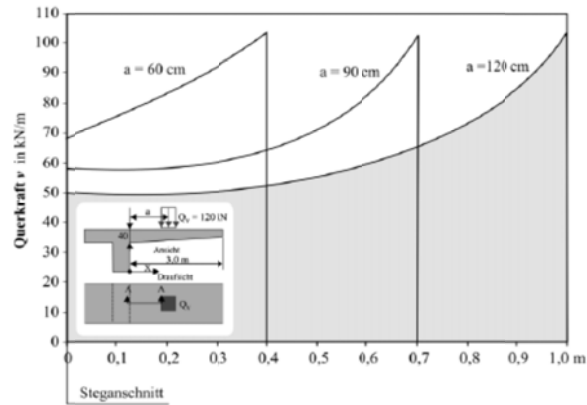


Fig. 2.12: Shear force distribution in section A-A (Rombach and Velasco, 2005).

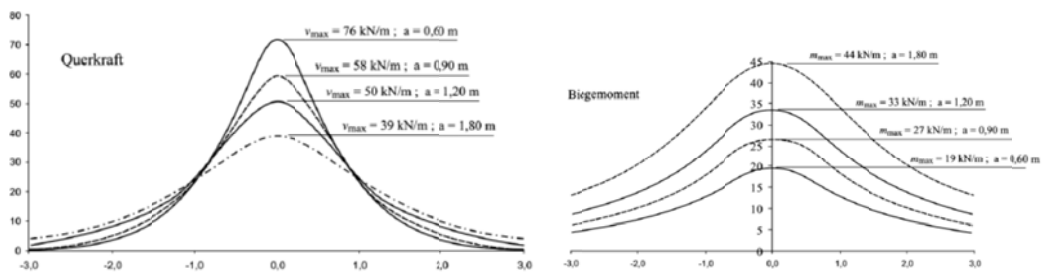


Fig. 2.13: Moment- and shear force distribution in longitudinal direction at the relevant section for a wheel load of  $Q_v = 120\text{kN}$  (cantilever length  $L_k = 3\text{m}$ , depth of the slab  $h = 0.4\text{m}$ ).

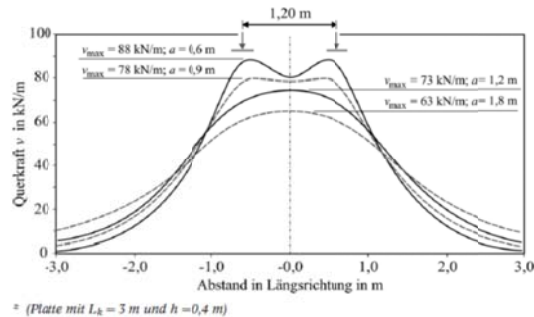


Fig. 2.14: Shear force distribution for two wheel loads in longitudinal direction in the relevant section (Rombach and Velasco, 2005).

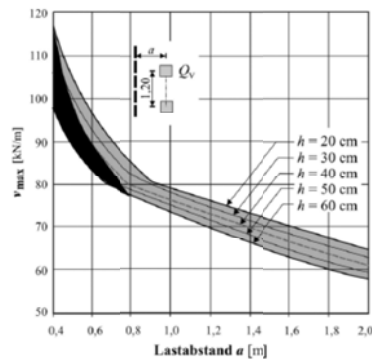


Fig. 2.15: Greatest shear force  $v_{max}$  for 2 wheel loads of  $Q_v = 120\text{kN}$  according to load model 1 (Rombach and Velasco, 2005).

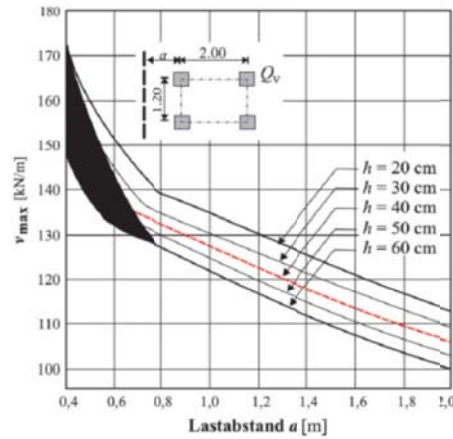


Fig. 2.16: Greatest shear force  $v_{max}$  for 4 wheel loads of  $Q_v = 120\text{kN}$  according to load model 1 (Rombach and Velasco, 2005).

Kirkpatrick, Rankin and Long (1984) report that wheel loads, delivered by rubber pneumatic tires result in a better load distribution and thus improve the load capacity of the slab as compared to steel loading plates which are used in laboratories. Vaz Rodrigues (2007) concluded likewise that the punching shear capacity under a wheel with pneumatic pressures is less critical because curvatures tend to be distributed over the surface of the applied load rather than concentrated near the edges, Fig. 2.17.

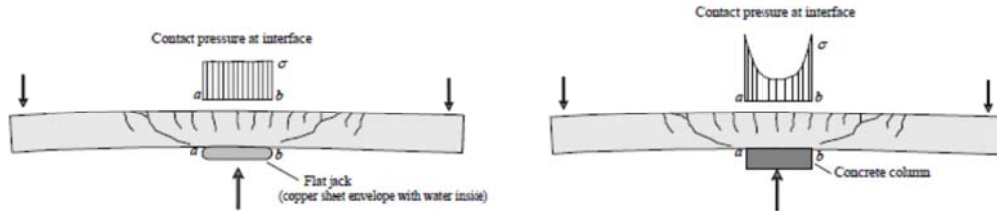


Fig. 2.17: Stress distribution on slab under wheel load and slab-column specimen (Vaz Rodrigues, 2007).

### 2.3. Influence of the support

The influence of the distance to the support on beam shear was first explained by Kani (1962) on the basis of the tooth model. The resulting “Kani valley” is also related to the amount of flexural reinforcement, Fig. 2.18. Zsutty (1968, 1971) used a statistical analysis of published data of beam shear tests to validate the widely accepted assumption that slender members having an  $a/d$  of 2,5 or greater should be considered separately from shorter members.

Test results combined with North-American code methods are shown in Fig. 2.19.

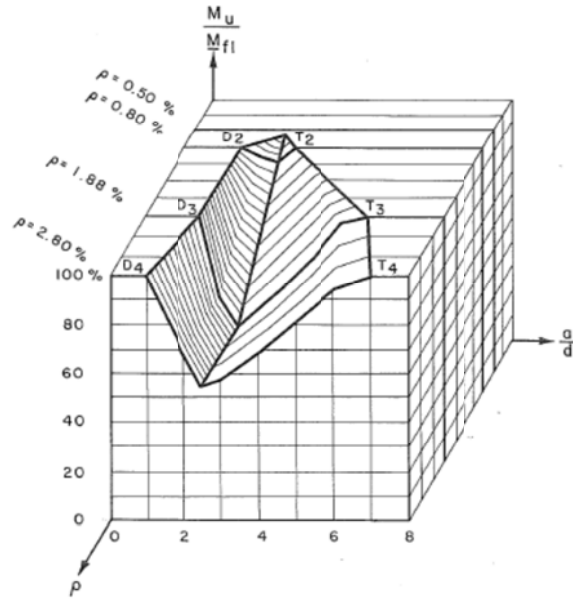


Fig. 2.18: Relative beam strength  $M_u/M_{f1}$  versus  $a/d$  and  $\rho$ , Kani (1979).

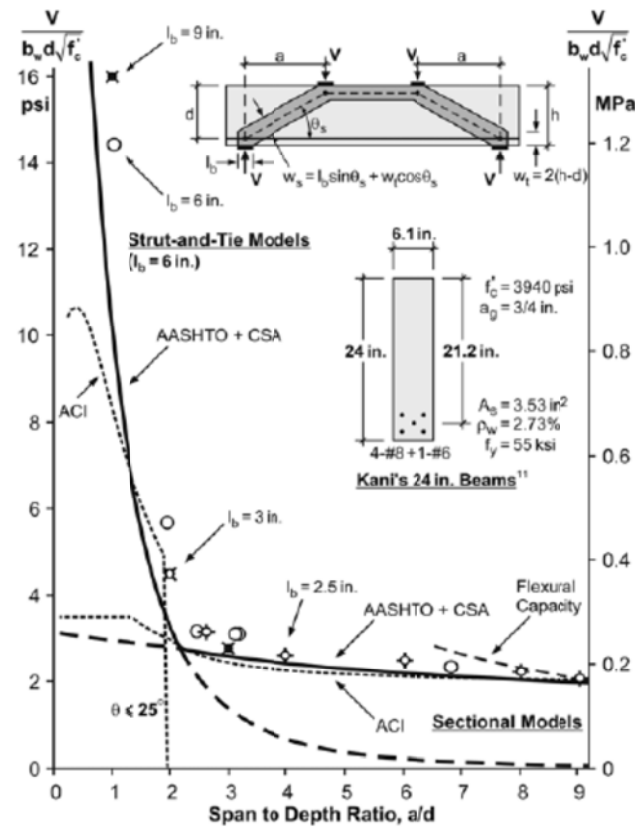


Fig. 2.19: Influence of shear span-depth ratio on failure shear stress. (Collins, Bentz and Sherwood, 2008).

Rombach and Latte (2008, 2009) point out that the ratio of bending moment to shear force  $m/v$  is not directly proportional to the geometrical ratio  $a/d$  for bridge deck slabs under concentrated loads, because  $m/v$  depends on the elastic distribution of shear and

bending moments in the support region, Fig. 2.20. Also,  $m$  and  $v$  are spread over different effective widths.

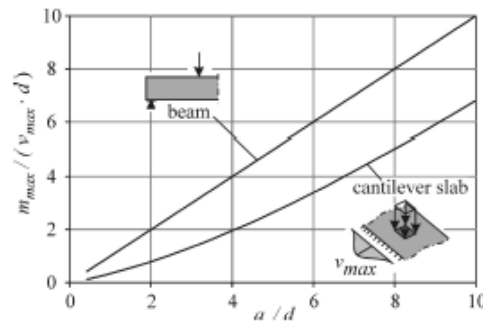


Fig. 2.20: Comparison between the ratio  $a/d$  and the bending moment to shear ratio  $m/v$  for a beam and a slab with concentrated load, Rombach and Latte (2008).

In the vicinity of the loads and support, the concrete is in biaxial compression and therefore has an increased strength and deformation capacity (Manuel, 1973). The ultimate strain in the concrete can then be taken as 0,008.



### 3. Shear in slabs

#### 3.1. Shear transfer

##### 3.1.1. What is shear in reinforced concrete?

###### 3.1.1.1 A historical overview

Researchers worldwide have been trying to solve the riddle of shear failure for the past 110 years. A lot of work was done up to about 1914 and then since the mid 1950's (Regan, 1993). In 1948, Richart wrote: "diagonal tension seems to be the point of weakness in current design practice". An overview of the amount of experimental work that has been done over the past century is shown in Fig. 3.1 and Fig. 3.2. As early as 1909, Talbot indicated the percentage of longitudinal reinforcement, the shear span to effective depth ratio and the concrete compressive strength as the main factors influencing the shear capacity. He also pointed out that the actual diagonal tension is considerably greater than the vertical shearing stress. He distinguished the horizontal or longitudinal component stresses for the calculation of resisting moments from the diagonal, vertical and horizontal stresses like shear and diagonal tension and diagonal compression and termed these web stresses.

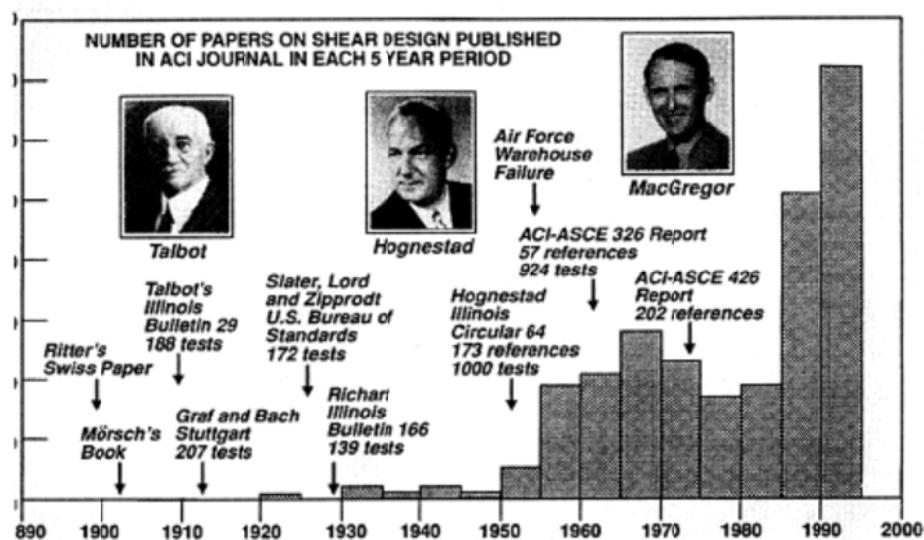


Fig. 3.1: Research into shear design methods (Collins et al., 1996).

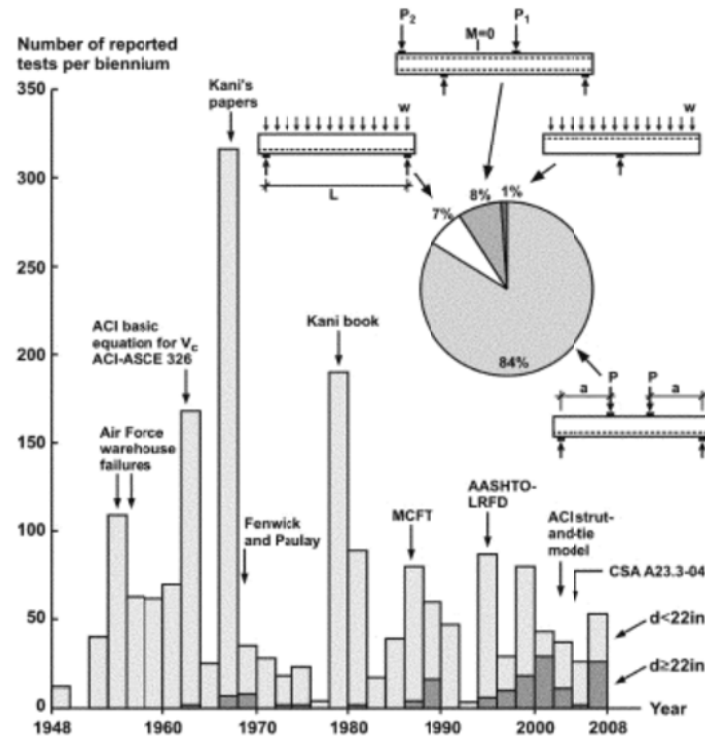


Fig. 3.2: Sixty years of shear research (Collins, Bentz and Sherwood, 2008).

The complex internal force system was pointed out very early on as the cause for the ongoing debate on shear. The joint committee on concrete and reinforced concrete (1916) wrote: “For the composite structure of reinforced concrete beams, an analysis of the web stresses, and particularly of the diagonal tensile stresses, is very complex; and when variations due to a change from no horizontal tensile stress in the concrete at the remotest fiber to the presence of horizontal tensile stress at some point below the neutral axis are considered, the problem becomes more complex and indefinite. Under these circumstances, in designing, recourse is made to the use of the calculated vertical shearing stress, as a means of comparing or measuring the diagonal tensile stresses developed, it being understood that the vertical shearing stress is not the numerical equivalent of the diagonal tensile stress and that there is not even a constant ratio between them.” Zararis and Papadakis (2001) too state that one of the major difficulties in developing a theoretical expression for shear is due to the indeterminacy of the internal force system of a cracked member.

Particularly the biaxial stress situation which results due to shear loading is seen as a challenge. Clark (1951) described the problem as: “Vertical stresses caused by the end shear combines with longitudinal stress from bending in the beam and produces tensile and compressive stress components.” Combined tension and compression

loadings, which are the shear stresses, reduce both the tensile and compressive stresses at failure, ASCE-ACI committee 426 (1973), Fig. 3.3. Leonhardt (1978) points out that shear must be considered as the combined action of inclined principal tension and compression. Shear stresses are the projections of the principal stresses while shear cracks are the result of inclined principal tension. According to Leonhardt (1978) it is wrong to “relate the upper limit of the shear stresses to the tensile strength of the concrete or to a so-called shear strength of concrete which does not exist.”

Bresler and Pister (1958) examined the combination of shear stress and uniaxial compression, Fig. 3.4.

Moreover, the diagonal direction of shear failure requires designers to think out of the scope of the traditional cross-sectional analysis. Unlike flexural failures, which are confined to a cross-section normal to the longitudinal axis, members failing in shear have failure surfaces that encompass inclined cracks in addition to the normal section through uncracked portions of the compression zone at the crack tip (Lubell, 2006).

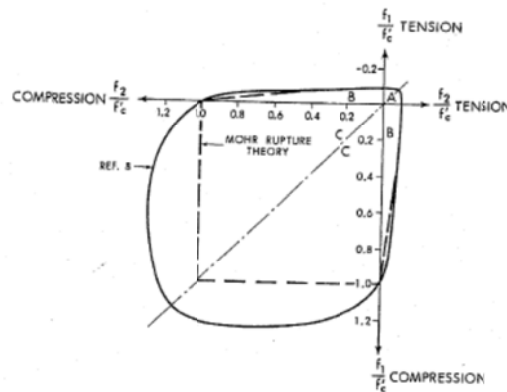


Fig. 3.3: Biaxial strength of concrete, ASCE-ACI committee 426 (1973).

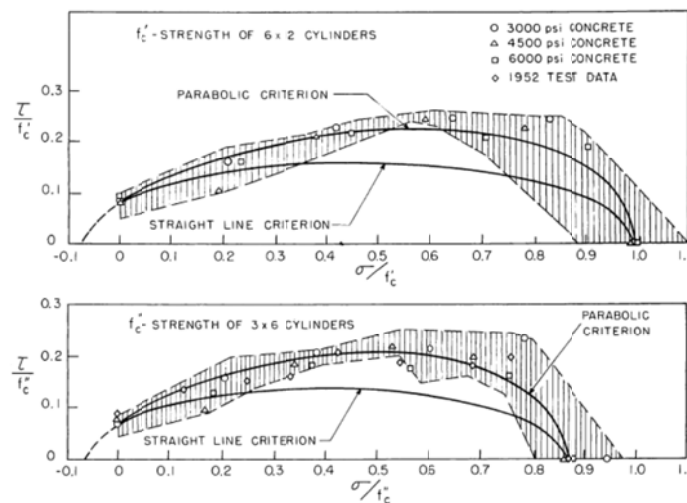


Fig. 3.4: Shear-compression strength (Bresler and Pister, 1958).

### 3.1.1.2 Horizontal shear and diagonal tension

In the early 1900's two ideas for shear transfer were competing: horizontal shear (as in other materials) and diagonal tension. The idea for diagonal tension was first formulated by Ritter (1899) who stated that stirrups resist tension and not horizontal shear. Mörsch (1922) further developed this for beams in shear without and with web reinforcement. Experimental proof and nominal shearing stresses close to the tensile strength of concrete led to the classic diagonal tension equation, based on the assumed stress distribution shown in Fig. 3.5 (ACI-ASCE committee 326, 1962):

$$v = \frac{8V}{7bd} \quad (3.1)$$

with

- |     |   |
|-----|---|
| $v$ | the unit horizontal shear stress at a distance $y$ from the neutral axis; |
| $V$ | the total vertical shear at the section;                                  |
| $b$ | the width of the cross section at a distance $y$ from the neutral axis;   |
| $d$ | the effective depth to the longitudinal reinforcement.                    |

Equation (3.1) is based on the following assumptions:

1. Concrete and steel are homogeneous and isotropic.
2. Stresses do not exceed the proportional limits.
3. Beams have constant cross sections.
4. Distribution of the shearing stresses is uniform across the width of the beam.
5. Concrete carries no flexural tension below the neutral axis.
6. The concentration of reinforcement at the tension face does not influence the distribution of shear stresses (van den Berg, 1962).

Van den Berg (1962) showed that the measured stress concentration gave comparably

good results for both  $v = \frac{8V}{7bd}$  and  $v = \frac{V}{bjd}$ . It is then a safe estimate ( $j \approx 0,9$ ) to use

the formula that is nowadays used in design:

$$v = \frac{V}{bd} \quad (3.2)$$

However, this assumption is only true for uncracked concrete. The internal stresses in the cracked state depend upon the shape and extent of the cracks and the layout of the reinforcement (Leonhardt and Walther, 1962). Laupa et al. (1953) also pointed out

that the formation of a diagonal crack changes the state of stress in a reinforced concrete beam, as no stress can be transferred across a crack. Hence, the popular conception of the distribution of shearing stresses in a reinforced concrete beam cannot be true and it is believed that any agreement between an empirical expression based on the nominal shearing unit stress  $v$  and test results is coincidental.

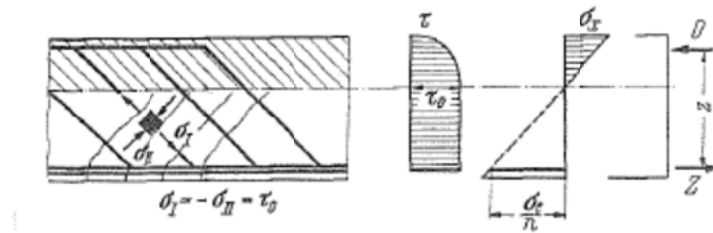


Fig. 3.5: Idealized stress distribution in the cracked state (Leonhardt and Walther, 1962).

Measurements have shown that the average principal tensile stress for diagonal cracking is smaller than the concrete tensile strength. According to ASCE-ACI committee 445 (1998) this observation is due to the stress concentration at the tip of the initial cracks and the reduction of the cracking stress due to the coexisting transverse compression, or because of the non-uniform shear stress distribution at a flexural crack from the concentration of bond stresses and the reduction of the internal lever arm due to arch action in a flexurally cracked zone.

### 3.1.1.3 Which forces define the shear resistance?

Bažant and Kim (1984) and Alexander and Simmonds (1991) write the shear force as

$$V = \frac{d(Tjd)}{dx} = \frac{d(T)}{dx} jd + \frac{d(jd)}{dx} T \quad (3.3)$$

which emphasizes the combination of beam and arch action.

Kani (1979) claimed that shear stress is not directly related to shear failure, and renamed it “diagonal failure”. According to Kani (1969) as well as Bresler and Pister (1958) the problem of shear strength is not the transfer of the smaller component  $V$  (the shear force) to the support while neglecting the component  $C$ , but rather how to transfer both of them, Fig. 3.6. Kani (1964) stated that bond, not shear, is the important parameter in the determination of the shear strength. He also showed that diagonal failures can exist without the presence of a shear force, Fig. 3.7. The force transfer from a reinforcing bar anchored by bond in concrete is described by the

equilibrium of shear stresses on the interface. The shear stresses cause principal tensile and compressive stresses in the adjacent concrete. If compression is the weakest component, then the bar is just pulled out. If the failure mode is tension, then cracks in the transverse direction to the stresses around the bars develop (Reineck et al., 1997). According to Marti (1999): “shear, bond and development problems are inseparable and should be treated in a unified manner”. Reineck (1990) links shear and bond together by showing that the nominal shear stress  $v_n$  has the physical relevance of an average tooth-bond stress over the beam width  $b_w$  due to  $\Delta T$ .

$$v_n = \frac{\Delta T}{b_w s_{cr}} = \frac{V}{b_w z} \quad (3.4)$$

This tooth-bond is by equilibrium related to the bond stress  $\tau_b$  at the bar surface:

$$v_n = 4\tau_b \rho \frac{d}{d_b} \quad (3.5)$$

Therefore, the bond may principally limit the possible transfer of  $\Delta T$  to the tooth, and consequently, according to (3.4) also the ultimate shear force. In slender B-regions this is not the case. It should be noted that structural concrete codes of about 40 years ago had clauses related to ‘local bond’, which could be a problem at points of low-moment/high-shear such as simple supports and points of contraflexure. Local bond often required a larger number of smaller bars. In order to demonstrate that anchorage and local bond are a major part of the shear strength riddle, one must first make some assumptions about anchorage strength (Gurley, 2011).

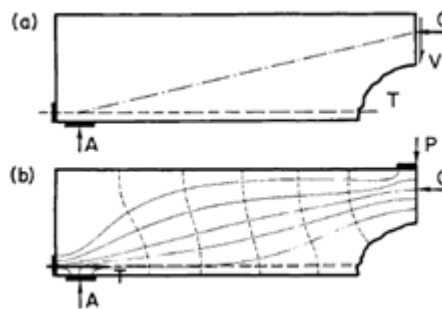


Fig. 3.6: Forces in the shear span (Kani, 1969).

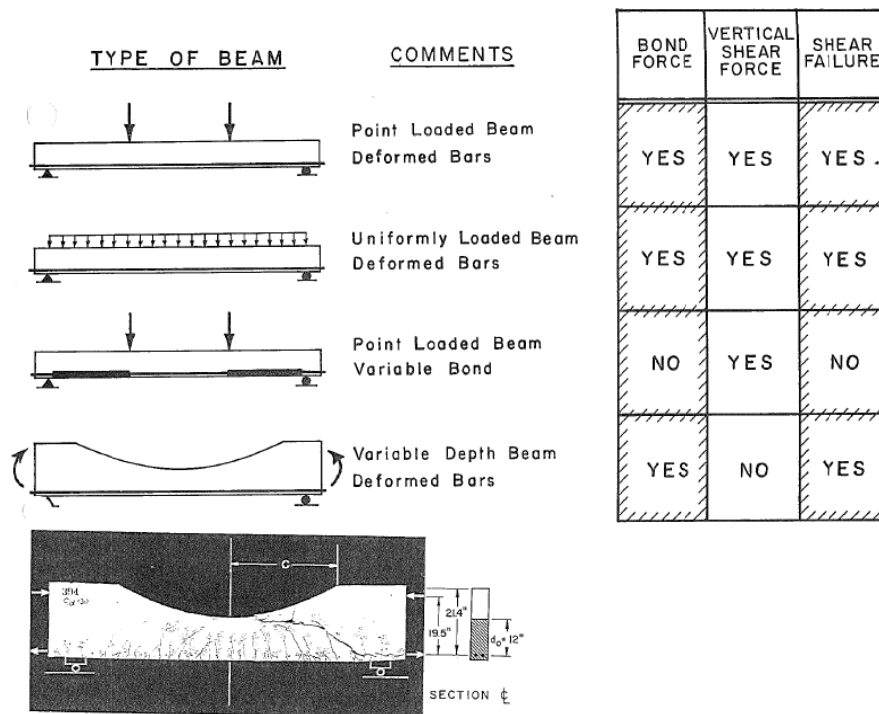


Fig. 3.7: Correspondence of shear failure with the presence of bond forces and shear forces, Kani, 1979.

### 3.1.2. Types of shear failure

#### 3.1.2.1 The influence of flexure

When loading a beam with two point loads (Fig. 3.8) a series of observations can be made.

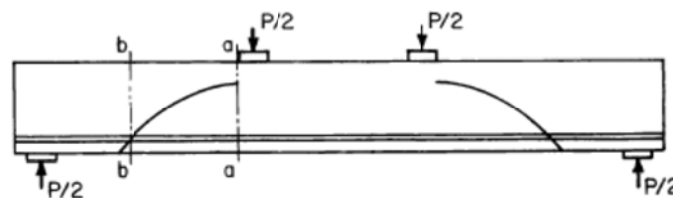


Fig. 3.8: Typical test setup for a beam shear test, ACI-ASCE committee 326 (1962).

First, vertical tension cracks will appear at the location of maximum moment. Then, inclined cracks will form towards the load. This cracking sequence is called **flexure-shear** (Fig. 3.9b) cracking, while **web shear cracking** (Fig. 3.9a) is inclined cracking before the occurrence of flexural cracking. The formation of flexure-shear cracks is complicated by the disturbed force flow in the concrete previously cracked in flexure (Lubell, 2006).

### 3.1.2.2 Classification of types of shear failure

For beams with a long span and a small percentage of reinforcement, a **flexural failure** (Fig. 3.9c) will occur and the capacity of the beam is not affected by shear. For beams with an intermediate span and a high percentage of longitudinal reinforcement, a critical **diagonal tension crack** (Fig. 3.9d) will appear and the failure mode will be **flexure-shear failure**. The shear cracks then rise so high that eventually the compressive zone fails (Leonhardt and Walther, 1962). Diagonal tension failure is related to the failure of the concrete teeth, Fig. 3.10. The transformation of a flexural crack into a flexure-shear crack depends on the rate of growth and the height of the shear crack in the shear region and the magnitude of shear stresses near the tops of the flexural cracks (MacGregor and Hanson, 1969). The combination of shear and flexure is discussed in Vaz Rodrigues et al. (2010). Mathey and Watstein (1963) also identify a failure mode which they call “**shear proper**”, in which the diagonal tension crack develops gradually until full development, but crushing of the concrete does not occur as in shear-compression failures.

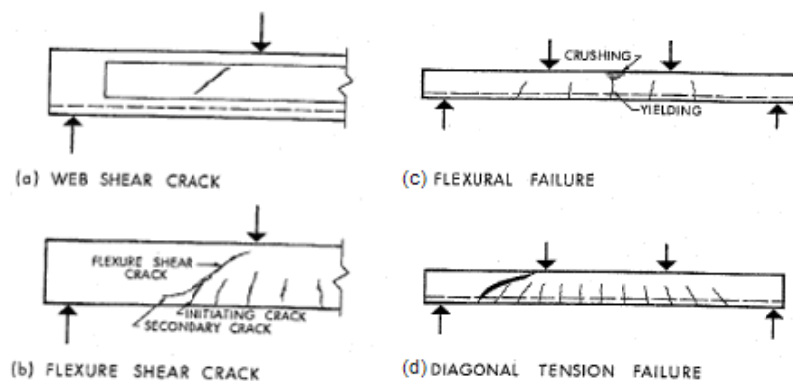


Fig. 3.9: Types of inclined cracks and failures of slender beams: (a) web shear crack; (b) flexure shear crack; (c) flexural failure; (d) diagonal tension failure. (ASCE-ACI committee 426, 1973).

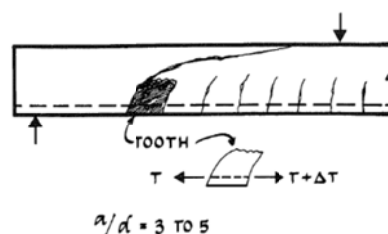


Fig. 3.10: Tooth failure cracking and diagonal tension failure. Bresler and MacGregor, 1967.

For beams with a short span ( $1 \leq a/d \leq 2.5$ ) the shear crack will form slower and result in a **shear-compression failure** (Fig. 3.11b) when combined with the crushing



of the concrete above the crack or in a **shear-tension failure** (Fig. 3.11a) when combined with the loss of bond and an anchorage failure (ACI-ASCE Committee 426,1973). In case of a shear-tension failure, a secondary crack will form which extends along the reinforcement for a short distance towards the support. This horizontal crack may be associated with either slip or dowel action of the reinforcement. According to Kotsovos (1984) the shear-compression type of failure is generally considered as a crushing mode of failure when the applied load increases to the level at which the diagonal crack that forms within the shear span at an earlier load stage penetrates into the compressive region towards the loading point. He suggested, however, that a crushing mode of failure in the region of the loading point is unlikely since the multi-axial compressive state of stress that exists which causes a local increase of the concrete strength. He proposes a failure mode in which the diagonal crack branches almost horizontally toward the compressive zone of the middle span of the beam in order to bypass this high-strength region, Fig. 3.12.

In a deep beam ( $0 \leq a/d \leq 1$ ) 4 types of failure can occur: flexural failure, shear failure, anchorage failure and bearing failure (Fig. 3.11c). A **flexural failure** occurs either when the concrete rib of the tied arch fails by crushing at the crown or when the tension tie ruptures. Full flexural capacity and ductility are achieved. The appearance is similar to the shear compression failure in short beams. A **shear failure** occurs through the destruction of the inclined strut that forms between the load point and the support. This failure mode involves little or no inelastic deformation (Manuel, 1973). The shearing stresses and vertical normal stresses require more consideration than the flexural stresses and significant compression and tension will be present in the section. The stress distribution becomes nonlinear with a concentration of tensile stresses towards the bottom of the beam (Cho, 2003). If the longitudinal reinforcement is high-performance steel, shear failure will occur before yielding of the reinforcement but with a nonlinear response of the reinforcement (Desalegne and Lubell, 2010).

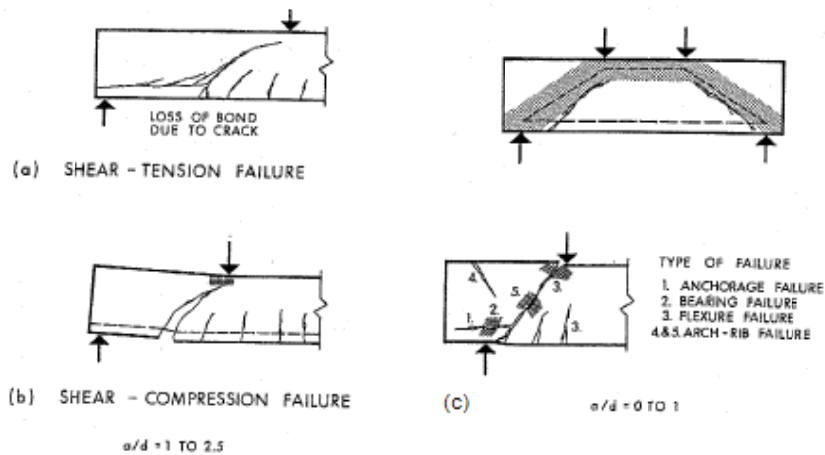


Fig. 3.11: Typical shear failures in short beams and deep beams: (a) shear tension failure; (b) shear compression failure; (c) modes of failure of deep beams. (ASCE-ACI committee 426, 1973). Originally by Bresler and MacGregor (1967).

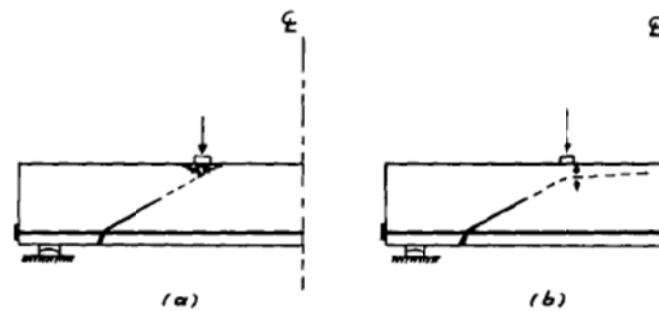


Fig. 3.12: (a) Generally accepted, and (b) postulated mode of failure of reinforced concrete beams with values of  $a/d$  between 1,0 and 2,5 (Kotsovos, 1984).

A frequently observed **secondary failure mode** is failure of the compression zone by instability. According to the shear study group (Barker et. al, 1969) it is caused by the development of the shear crack in such a way that the thrust line necessary for equilibrium with the external load falls outside the compressive zone over part of its length. According to Braestrup (2009), secondary buckling is a consequence of a hyperbolic yield line. The failure mechanism of Fig. 3.13 implies that the beam end rotates outwards about a center on the extension of the main reinforcement, which does not yield. Vaz Rodrigues (2007) explains this phenomenon based on a strut and tie model. When a strut is crossed by cracks (in this case the shear crack), only a limited amount of compression can be transmitted (Fig. 3.14c). As a result, the strut shifts towards the top edge of the beam. To maintain equilibrium, two additional ties are necessary to equilibrate the deviated strut (Fig. 3.14d). These ties will cause the decompression of the top fiber. Buckling of the compression zone then occurs when the tensile strength of concrete is reached on the tension tie near the concrete surface.

The same phenomenon is also observed in slab-column tests. The associated strut and tie models are shown in Fig. 3.15.

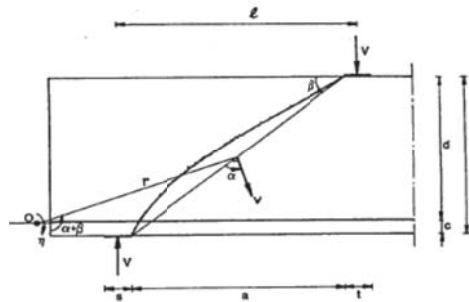


Fig. 3.13: Shear failure of reinforced concrete beam without stirrups (hyperbolic yield line) (Braestrup, 2009).

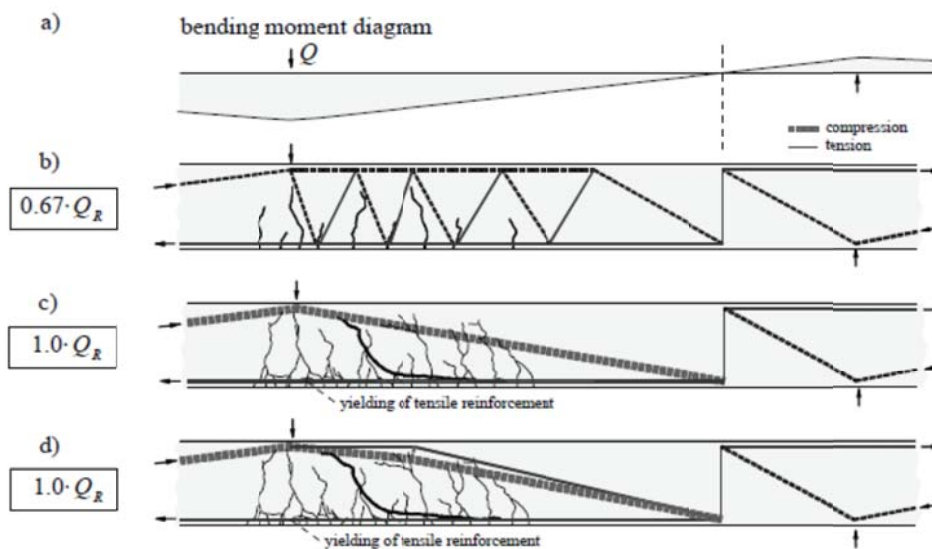


Fig. 3.14: Evolution of the load carrying mechanisms up to failure (Vaz Rodrigues, 2007).

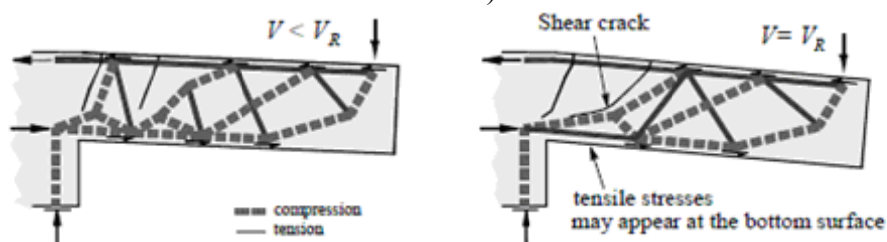


Fig. 3.15: Flow of inner forces prior to punching shear failure (Vaz Rodrigues, 2007).

Zararis and Papadakis (2001) divide the critical crack (leading to collapse) into two branches. The first branch is an inclined shear crack, which develops after nearby flexural cracking. The second branch initiates from the tip of the first branch and propagates towards the load point crossing the compression zone. Failure is induced by the second branch, typically failing in negative bending.

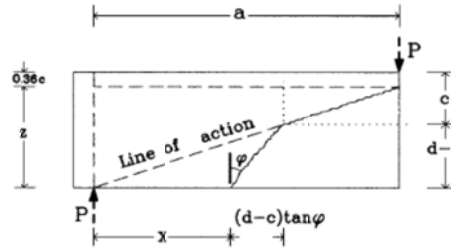


Fig. 3.16: Critical diagonal crack (Zararis and Papadakis, 2001).

### 3.1.2.3 The influence of arching action on the failure mode

After the formation of the critical diagonal tension crack, force redistribution will take place: the shearing and compressive forces in the concrete compression zone will increase, the tensile stress in the longitudinal reinforcement will increase and the transverse shear and local bending due to the resistance against transverse displacements in the longitudinal reinforcement will increase (Bresler and Scordelis, 1963; Moody et al, 1954). If this redistribution does not result in equilibrium, the beam will collapse upon the formation of the diagonal tension crack. In beams with short shear spans, a tied arch will form after inclined cracking. As not enough was known about the ability to reach equilibrium after force redistribution and the long-term behavior of a diagonally cracked beam, ACI-ASCE committee 326 (1962) decided that the load at which the critical diagonal tension crack forms should be taken as the maximum shear capacity. The design value of  $V_c$  from ACI 318-08 is still based on this assumption. The previous shows that the mode of failure is related to the  $a/d$  ratio for beams with concentrated loads, Fig. 3.17. A more general description is based on the  $\frac{M}{Vd}$  ratio. The TNO method (van den Beukel and Monnier, 1985) is

based on the  $\frac{M}{Vd}$  ratio and requires a calculation at a sufficient number of locations along the span of the member.

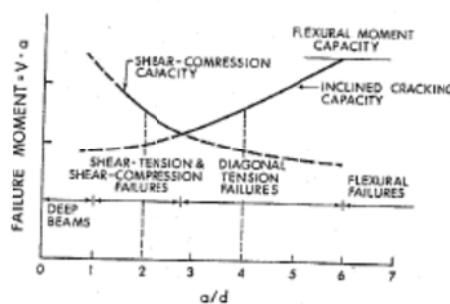


Fig. 3.17: Variation in shear capacity with  $a/d$  for rectangular beams, ASCE-ACI committee 426, 1973. Originally by Bresler and MacGregor, 1967.

### 3.1.3. The mechanisms of shear transfer

An overview of the mechanism contributing to shear transfer is given in Fig. 3.18 and Fig. 3.19:

- the force carried by the concrete compressive zone,  $V_c$  or  $V_{cz}$ ;
- the force carried by aggregate interlock  $T_f$  or  $V_a$  and
- the force carried by dowel action  $V_d$ .

The forces with their associated force polygon are shown in Fig. 3.20. The contribution of each of the mechanisms is shown in Fig. 3.21 and Fig. 3.22. The proportion of force carried by each of the mechanisms will vary as failure approaches, but if there is a breakdown in any of the mechanisms, there is typically insufficient capacity in the remaining mechanisms and collapse will result (Lubell, 2006; Fenwick and Paulay, 1968). Reineck (1997b) also identifies the clamping of the tooth into the compression zone. This mechanism is of transitory nature and can be neglected near failure. Taylor (1972) measured that up to the point at which the beam cracks, half of the shear is carried by the compression zone. This shear force is then parabolically distributed down the beam in accordance with the theory of elasticity, Fig. 3.23.

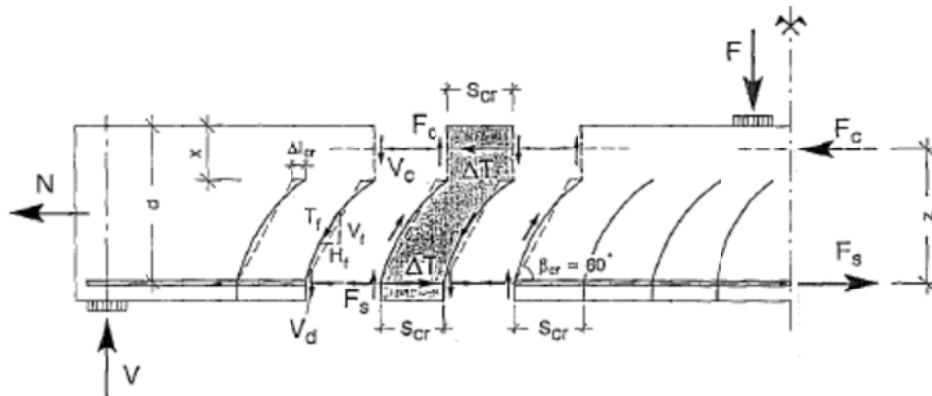


Fig. 3.18: Mechanisms of shear transfer (Reineck, 1997a).

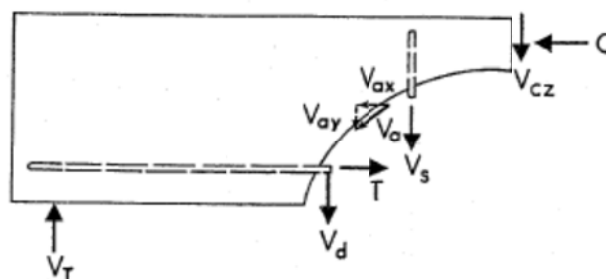


Fig. 3.19: Forces acting at inclined crack, ASCE-ACI committee 426 (1973).

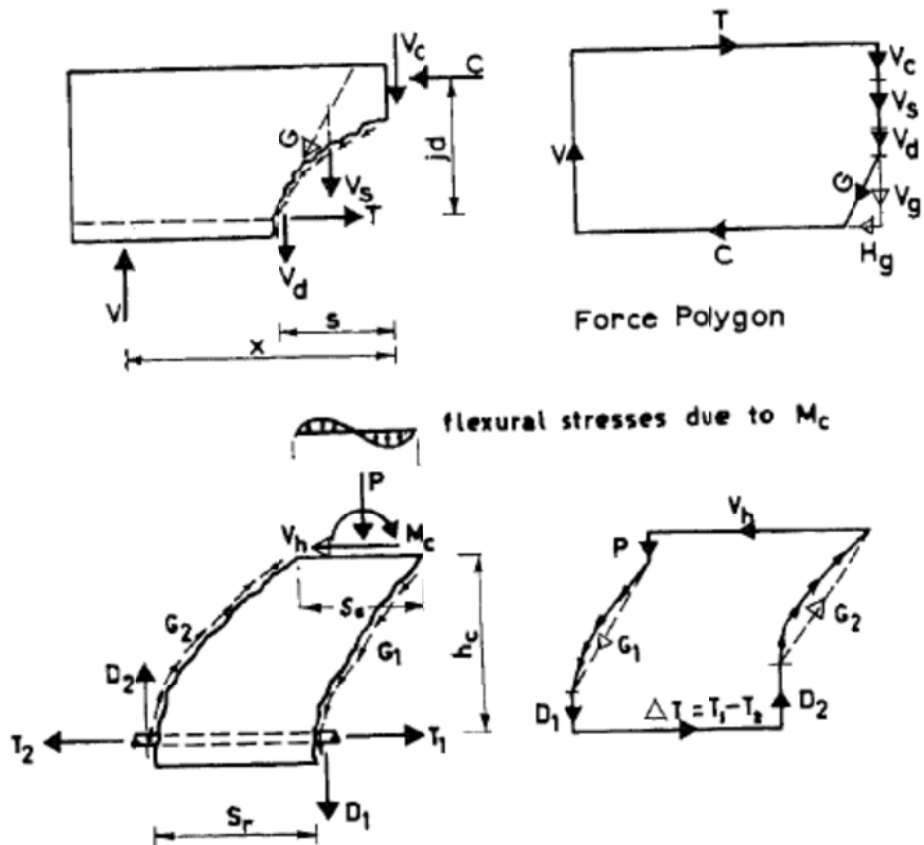


Fig. 3.20: Forces acting in shear span of a beam. (Fenwick and Paulay, 1968).

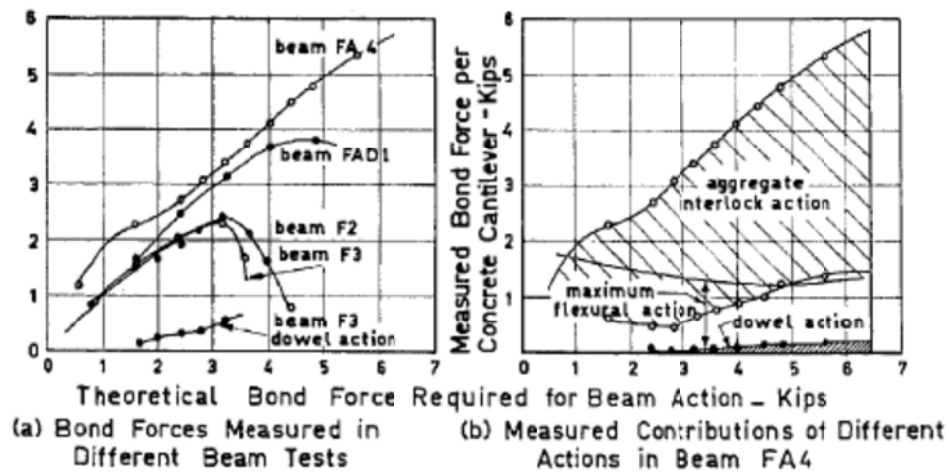


Fig. 3.21: Forces measured in test beam by Fenwick and Paulay (1968).

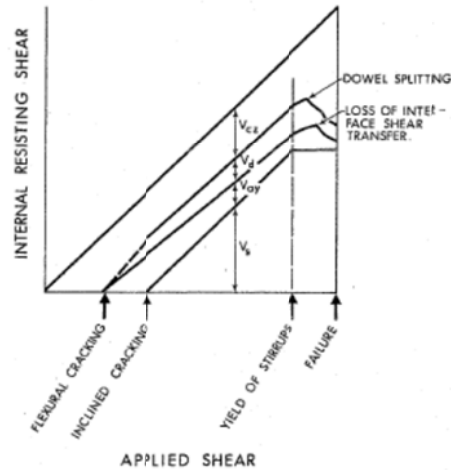


Fig. 3.22: Distribution of internal shears in beam with web reinforcement, ASCE-ACI committee 426, 1973.

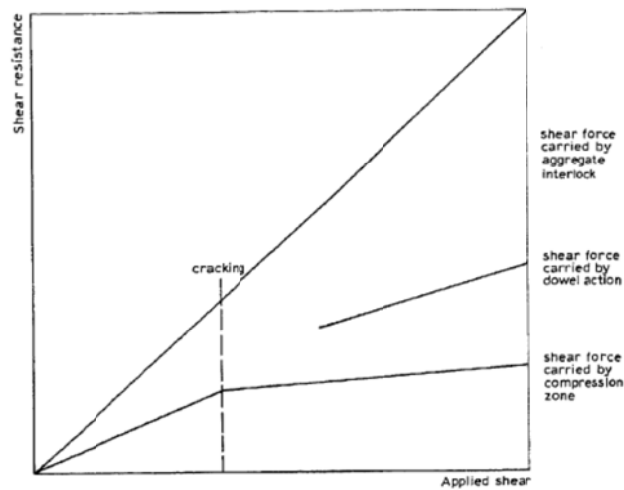


Fig. 3.23: Distribution of shear force in reinforced concrete beam without web reinforcement (Taylor, 1972).

A first attempt to describe the shear problem based on a critical crack, Fig. 3.24, was done by Bresler and MacGregor (1967). These authors gave a conceptual description of such a model, but pointed out that a bond-slip law must be formulated and that for a realistic determination of the stress a 3-dimensional model should be used.

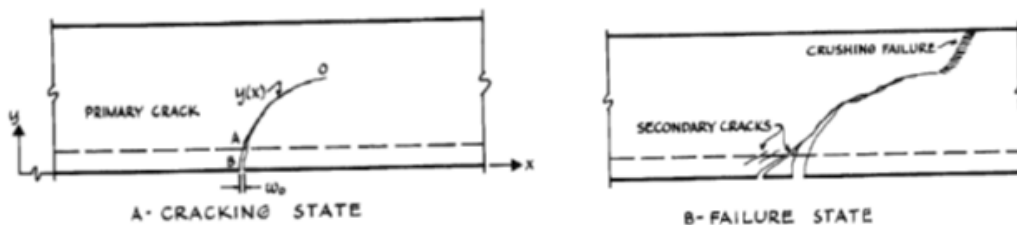


Fig. 3.24: Cracking and failure states, Bresler and MacGregor (1967).

Muttoni (2003) describes the shear transfer as first consisting of dowel action, cantilever action and aggregate interlock. These mechanisms can be represented by

strut and tie models (Muttoni and Schwartz, 1991), Fig. 3.25. For aggregate interlock, the concrete compressive forces are assumed to be transferred across the cracks. The dowel action can also be represented by a strut-and-tie model in which the longitudinal reinforcement also transmits forces in the transverse direction. After a critical point when several concrete ties break in the cantilever action, the crack will protrude horizontally, making the aggregate interlock impossible. At the same moment, the tie of the dowel action cracks and a new crack forms along the reinforcement. After formation of the critical shear crack, the mechanisms of shear transfer are arching action and strut and tie action with an elbow-shaped strut, Fig. 3.26. The resultant stress path can also be compared to a traditional frame model for the compressive force path. The failure load is very dependent upon the crack pattern.



Fig. 3.25: Mechanism of shear transfer without shear reinforcement: cantilever action, aggregate interlock and dowel action (Muttoni and Schwartz, 1991).

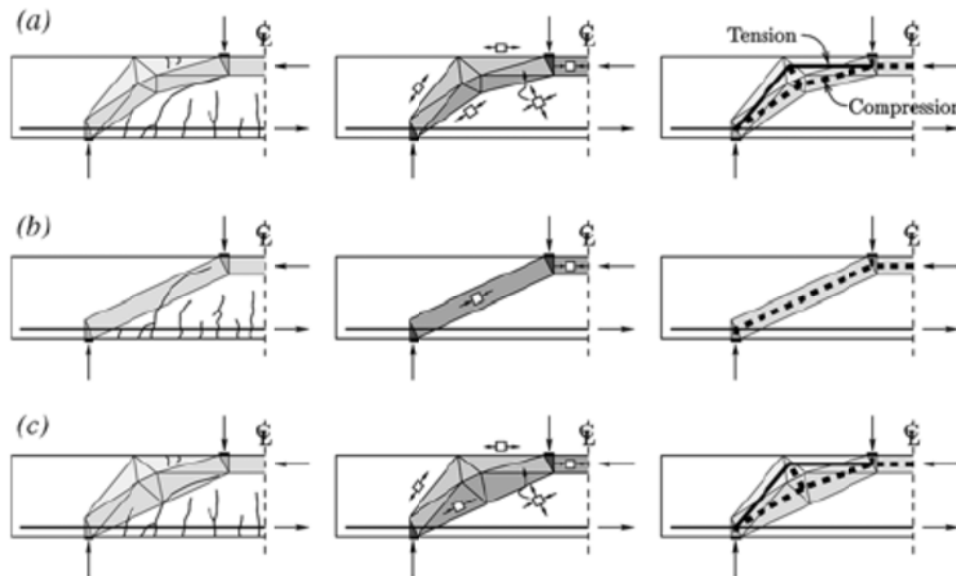


Fig. 3.26: Load-carrying capacity after development of the critical shear crack: (a) elbow-shaped strut; (b) straight strut (enabled by aggregate interlock); and (c) combined response, Muttoni and Fernández Ruiz, 2008.

Swamy and Andriopoulos (1973) argued that dowel action and aggregate interlock are interdependent and questioned the validity of simplified model tests to quantify the separate mechanisms of shear failure. The breakdown of dowel resistance results in a higher width of the diagonal crack, because the section is able to rotate more about the



head of the crack. The aggregate interlock forces depend on the crack width and crack rotation, and their contribution will thus be influenced by the action of the dowel forces. There is a time lag, in terms of the development of the diagonal crack, between the commencement of aggregate interlocking action and that of the dowel forces. In the initial stages of diagonal crack formation, the aggregate interlock action predominates while in the later stages of its development the influence of dowel forces predominates.

Although the shear resistance is typically found as the sum of the capacity of the concrete compression zone, the aggregate interlock, the dowel action and the residual tension over the crack, some models start from quite a different perspective. Ehmann (2006) based his model on the Zararis and Papadakis model (2001) in which a new and sudden shear crack crossing the previous cracks leads to collapse. This shear crack is caused by concrete splitting on the connecting line between the load and the support.

### 3.1.3.1 Concrete compression zone

#### 3.1.3.1.1 Models based on the capacity of the concrete compressive zone

The first models for shear attributed the shear carrying capacity of the concrete entirely to the capacity of the concrete compression zone (Shear study group – Barker et al., 1969; Kani, 1979). A few recent models (Khuntia and Stojadinovic, 2001, Zararis and Papadakis, 2001) also fully count on the capacity of the compression zone, arguing that dowel forces are not activated as the shear force of steel bars at a crack location is caused by pure shearing deformation and not due to kinking or a slip of the crack faces. Similarly, Kotsovos (1992) questions aggregate interlock and dowel action, and claims that the shear capacity is based solely on the capacity of the compressive force path, Fig. 3.27, tacitly combining it with arching action.



Fig. 3.27: Schematic representation of region of compressive force path (Kotsovos, 1992).



### 3.1.3.1.3 Contribution of concrete compressive zone to shear carrying capacity

An overview of the contribution to the shear carrying capacity that is attributed to the concrete compressive zone is given in Table 3.1

Table 3.1: Contribution of concrete compressive strength according to authors from literature.

Author(s)	year	%	comments
Fenwick and Paulay	1968	20%	based on measurements
Taylor	1972	20 – 40%	based on measurements
ACI-ASCE com. 426	1973	20 - 40%	
Sherwood, Bentz and Collins	2007	24%	measurement
		21%	calculation based on stress distribution from Mörsch
Kani	1979	40%	
Hamadi and Regan	1980	37%	calculated for beams with natural gravel aggregates
		40%	calculated for beams with expanded clay aggregates
Reineck	1990	30%	maximum, calculated from Eq. (3.7)

### 3.1.3.2 Residual tension over crack

As a shear crack is not a “clean break” and small pieces of concrete are bridging the crack, the residual tension over the crack contributes to the shear capacity. In fracture mechanics approaches to the shear capacity, these residual tensile stresses are seen as the primary shear transfer mechanism (ASCE-ACI committee 445, 1998), and it has also been implemented in finite element software (Reineck et al., 1997, Blaauwendraad and Walraven, 1992)

Reineck (1992) claims that residual tension can be neglected for practical ranges of beams, since the crack widths in the web become too large. Likewise, Rombach et al. (2009) point out that for beams with smaller effective depths, the contribution of the residual tension to the shear capacity is higher than for large beams.

Other models only consider the residual tension at the crack tip, for example by taking a characteristic length into account.

Pruijssers (1986) described the tensile capacity at the crack tip. The zone in which the tensile strain exceeds the fracturing strain is called the fracture zone (or tension-softening zone) and consists of concrete intersected by small micro-cracks, Fig. 3.29. The tension-softening zone contributes to the shear resistance by means of the (low) shear stiffness of the uncracked cross-sectional area and the mechanisms of aggregate

interlock of the cracked cross-sectional area. The mean shear stiffness of the tension-softening zone is approximately 40% of the shear stiffness of the compressive zone.

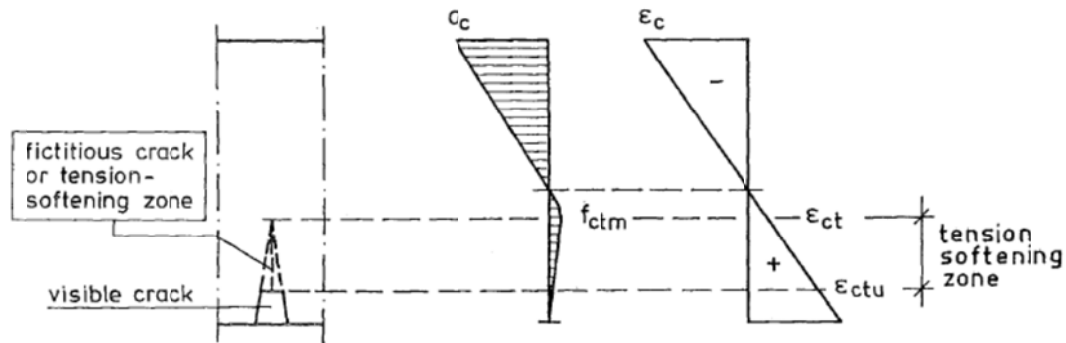


Fig. 3.29: The fracture zone. (Pruijssers, 1986).

Due to the development of micro-cracks the strain in this zone increases with a decreasing tensile stress, Fig. 3.30. The ultimate strain in the tension-softening zone is estimated as eleven times the cracking strain (equal to  $10^{-4}$ ):  $\epsilon_{ctu} = 1,1 \cdot 10^{-3}$ . For large shear deformations the contribution of the tension-softening zone to the shear transfer is considerable, Fig. 3.31. For the presented normal stresses the normal strain of the element  $\epsilon_{nn}$  is kept constant during the increase in the shear deformation  $\gamma$ . For increasing ratios of  $\gamma/\epsilon_{nn}$  the shear and normal stresses are shown.

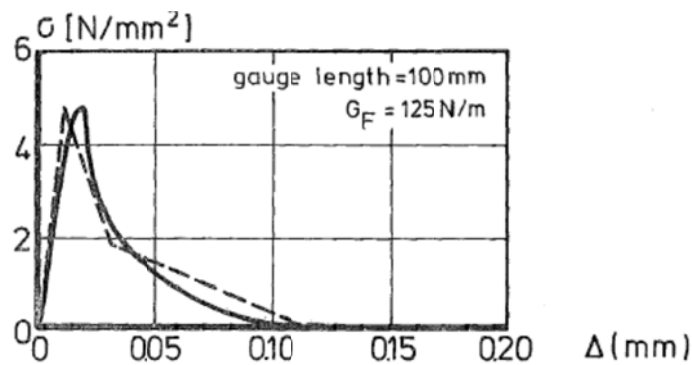
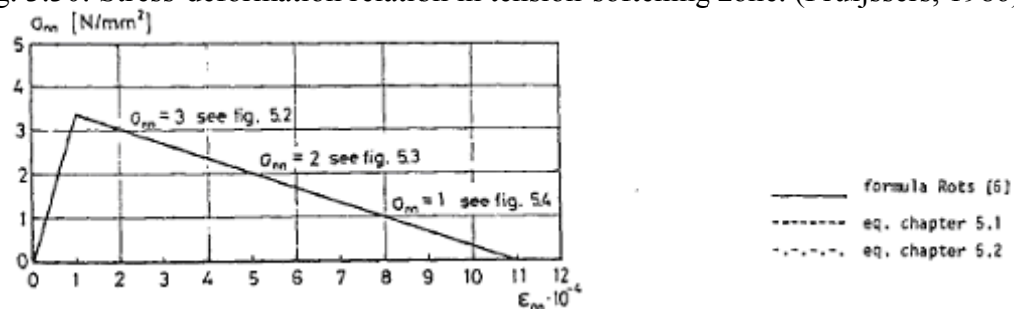


Fig. 3.30: Stress-deformation relation in tension-softening zone. (Pruijssers, 1986).



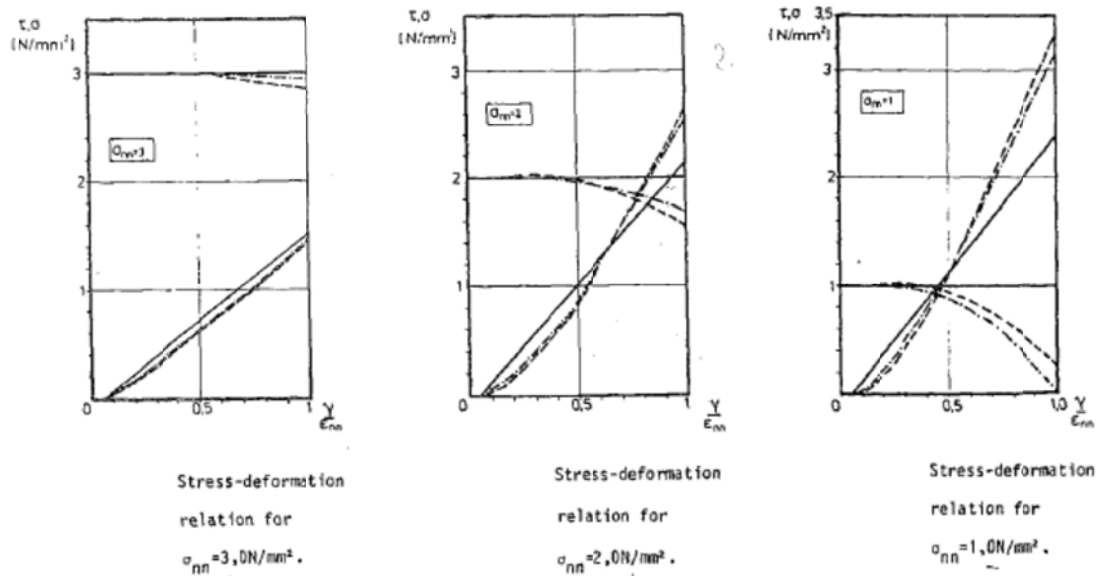


Fig. 3.31: Shear transfer in the tension-softening zone (Pruijssers, 1986).

### 3.1.3.3 Aggregate interlock

#### 3.1.3.3.1 What is aggregate interlock

The shear capacity from aggregate interlock is a result of the friction in a crack caused by its rough surface. Aggregate interlock is directly related to the way in which a crack is formed in concrete. Because the strength of the hardened cement paste in most concretes is lower than the strength of the aggregate particles, cracks intersect the cement paste along the edges of the aggregate particles. So the aggregate particles, extending from one of the crack faces, “interlock” with the opposite face and resist shear displacements (Walraven, 1980). Millard and Johnson (1984) concluded from the repeatability of their aggregate interlock tests that this mechanism does not depend upon the random path propagation of a tensile crack. According to Hamadi and Regan (1980), Bjuggren was the first author to point out the importance of aggregate interlock. Aggregate interlock forces are required to maintain the rotational equilibrium of the free body shown in Fig. 3.32 (a concrete tooth, Lubell, 2006).

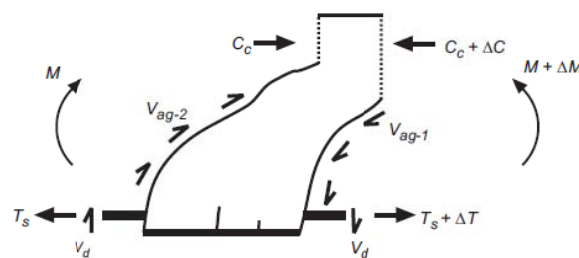


Fig. 3.32: Forces acting on a concrete tooth (Lubell, 2006).

The factors influencing the aggregate interlock capacity are: the concrete microstructure, the fracture energy of the concrete (Ghazavy-Khorasgany and Gopalaratnam, 1993), the aggregate size (Sherwood, Bentz and Collins, 2007) and the type of aggregate (Regan et al. 2005), with limestone and clay aggregates resulting in low aggregate interlock capacities. As the aggregate interlock capacity depends on the concrete microstructure and chosen mixture, several types of concrete with lower aggregate interlock capacities can be identified: self-consolidating concrete (Hassan, Hossain and Lachemi, 2010), lightweight concrete (Fig. 3.33 and Fig. 3.34, Taylor, 1973; Vaz Rodrigues, 2007) in which the shear crack crosses the aggregates because of their low strength and high strength concrete, where fracture of the aggregates leads to a smooth crack surface (Vintzileou, 1997). However, Khuntia and Stojadinovic (2001) do not see the smooth surface concept as a convincing explanation for the reduction in shear strength in high-strength concrete without stirrups. The shear capacity just before diagonal cracking (where aggregate friction has no role to play) is almost equal to that after formation of diagonal cracking. Khuntia and Stojadinovic (2001) consider the formation of longer flexural cracks (and thus a smaller effective shear depth) more appropriate as an explanation for the lower shear strength of high-strength concrete.



Fig. 3.33: Aggregate interlock in gravel concrete (intermediate or low strength) and lightweight concrete. (Walraven, 1980).

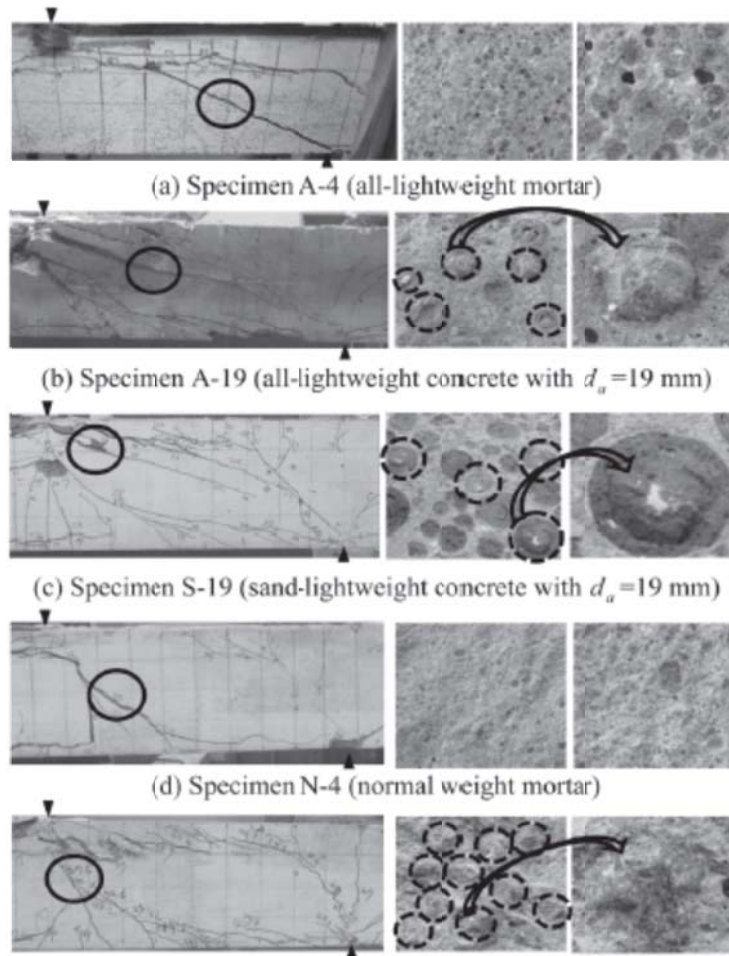


Fig. 3.34: Representative photographs for failure planes of tested beams. circles with perforated lines indicate unborken coarse aggregate particles (Yang et al. 2011).

In Fig. 3.35 the contribution of aggregate interlock and concrete in tension to the punching shear capacity of a slab are shown with respect to the crack width. Where limited crack widths develop (small depths, large amounts of flexural reinforcement) the punching strength is mostly governed by the tensile strength of the concrete, while for large crack widths aggregate interlocking becomes more dominant.

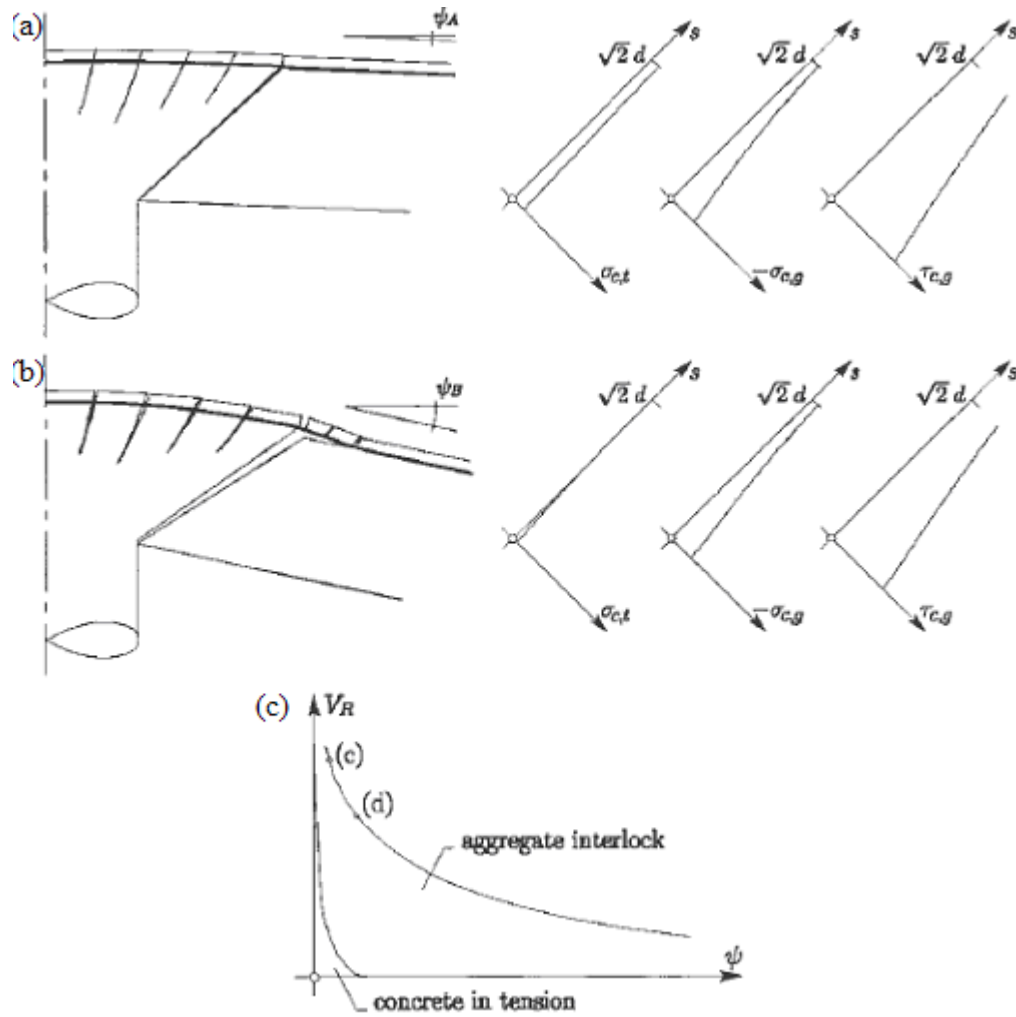


Fig. 3.35: Punching shear strength in critical shear crack theory (a) concrete in tension and aggregate interlock contributions for small rotations; (b) concrete in tension and aggregate interlock contributions for large rotations; and (c) punching shear strength and shear-carrying contributions of aggregate interlock and concrete in tension for cases (a) and (b) as a function of the rotation of the slab (Muttoni and Fernandez Ruiz, 2010).

### 3.1.3.3.2 Models

the first aggregate interlock models only related the interlock capacity to the crack width (Paulay and Loeber, 1973; Fenwick and Paulay, 1968).

Gambarova (1981) placed particular emphasis on the allowable paths in the displacement field when the crack starts opening, resulting in empirical relations between the interface stresses and the crack. This model (rough crack model) is based on the assumption that crack properties may be considered as a material property in the case of densely cracked plates. However, tests by Millard and Johnson (1984)



showed experimentally that the local/global roughness model does not yield to good results.

Walraven (1980, 1981) developed a model for aggregate interlock in which concrete is taken as a two-phase material consisting of stiff aggregate particles embedded in an ideally-plastic cement matrix. Earlier measurements on beams had shown that cracks do not open to their final width and shear then, but open and shear simultaneously. As a result, both the shear stress and the normal stress have to be taken into account as essential components. Assuming that the irregular faces of a crack can be deformed, both the shear stress  $\tau$  and the normal stress  $\sigma$  are functions of the crack width  $w$  and the shear displacement  $\Delta$ :

$$\begin{aligned}\tau &= f_t(w, \Delta) \\ \sigma &= f_n(w, \Delta)\end{aligned}\tag{3.8}$$

In (Walraven, 1981) a fundamental model is developed, based on a statistical analysis of the crack structure and the associated contact areas between the crack faces as a function of the displacements,  $w$  and  $\Delta$ , and the composition of the concrete mix. Two fundamental modes of behavior characterize the aggregate interlock: sliding at the contact area between particles and matrix at opposite sides of the crack (*overriding*) and irreversible deformation of the matrix by high contact stress. Considering concrete as a matrix and aggregate particles, and taking into account that the size of the particles is considerably greater than the crack width, the microroughness of the crack (aggregate particles projecting from the crack plane) is seen as dominant with respect to the macroroughness (the overall undulations of the crack plane), Fig. 3.36.

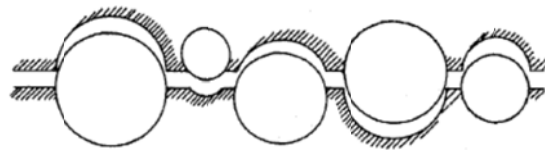


Fig. 3.36: Generally observed structure of crack plane (Walraven, 1981).

A flat crack plane (Fig. 3.37, Fig. 3.38) is thus used in the model. Initially during sliding, the contact area is reduced. This leads to high contact stresses, resulting in further plastic deformations until in the  $x$  and  $y$  direction equilibrium of forces is obtained. On the contact area, the stresses are resolved into a stress normal to the contact area  $\sigma_{pu}$  and tangential  $\tau_{pu}$ , Fig. 3.39. A rigid-plastic stress-strain relation for

the matrix is used, since it is expected that the plastic deformation will be significantly larger than the elastic deformation.



Fig. 3.37: Contact areas during sliding (Walraven, 1981).

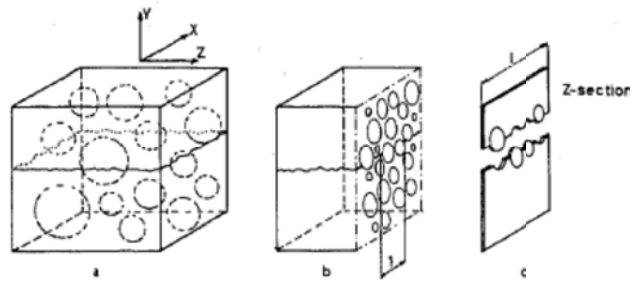


Fig. 3.38: (a) Cracked concrete body; (b) Z-plane of intersection; (c) Representative slice. (Walraven, 1981).

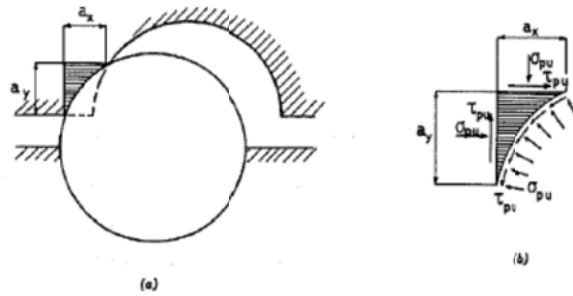


Fig. 3.39: (a) Contact area between matrix and aggregate; (b) stress conditions. (Walraven, 1981)

Under the condition that the contact areas are about to slide, the stresses are combined as

$$\tau_{pu} = \mu \cdot \sigma_{pu} \quad (3.9)$$

Equilibrium at a particle surface leads to the reactions:

$$\begin{aligned} F_y &= \sigma_{pu} \cdot a_x - \tau_{pu} \cdot a_y \\ F_x &= \sigma_{pu} \cdot a_y + \tau_{pu} \cdot a_x \end{aligned} \quad (3.10)$$

Considering all particles over a unit length of crack and taking  $\Sigma \bar{a}_x$ ,  $\Sigma \bar{a}_y$  as the most probable average projected contact lengths over the unit crack length leads to:

$$\begin{aligned}\Sigma F_y &= \sigma_{pu} \cdot \Sigma \bar{a}_x - \tau_{pu} \cdot \Sigma \bar{a}_y \\ \Sigma F_x &= \sigma_{pu} \cdot \Sigma \bar{a}_y - \tau_{pu} \cdot \Sigma \bar{a}_x\end{aligned}\quad (3.11)$$

Proceeding to areas with  $\bar{A}_x$  and  $\bar{A}_y$  as the most probable contact areas for a unit crack area and using equation (3.9), leads to:

$$\begin{aligned}\sigma &= \sigma_{pu} (\bar{A}_x - \mu \bar{A}_y) \\ \tau &= \sigma_{pu} (\bar{A}_y + \mu \bar{A}_x)\end{aligned}\quad (3.12)$$

The projected contact areas  $\bar{A}_x$  and  $\bar{A}_y$  are then calculated as follows:

1. The probability density function for an expected number of intersection circles with a diameter  $D_0$  which intersect also the unit crack length is constructed. The aggregate particles are assumed to be distributed according to the Fuller curve.
2. The contribution of the individual intersection circles to the contact area between the crack faces is determined.
3. Combining the previous results, leads to the total contact area for a unit crack area as a function of the displacements between the crack faces. The graphical representation of the resulting expressions is shown in Fig. 3.40.

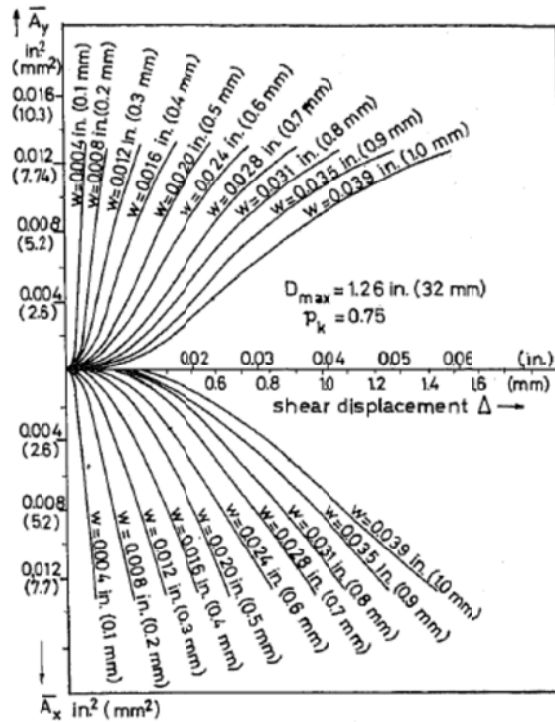


Fig. 3.40: Total projected contact areas  $\bar{A}_x$  and  $\bar{A}_y$  for 1 mm<sup>2</sup> crack plane, as function of crack width  $w$  and shear displacement  $\Delta$ . (Walraven, 1981).

Experimental results from push-off tests are then used to determine the matrix yielding stress  $\sigma_{pu}$  and the friction coefficient  $\mu$ . The best results are obtained for friction coefficients from  $\mu = 0,4$  (Walraven, 1981) to  $\mu = 0,5$  (Walraven, 1980) and  $\sigma_{pu}$  is found through fitting as  $\sigma_{pu} = 6,39 f_c'^{0,56}$  (Walraven, 1981) (N/mm<sup>2</sup>,  $f_c'$  the cube concrete compressive strength) or  $\sigma_{pu} = 5,83 f_{cc}'^{0,63}$  (Walraven, 1980) (N/mm<sup>2</sup>,  $f_{cc}'$  the uniaxial concrete strength). It must be noted that this is only a provisional, approximate relation since the relation between  $\sigma_{pu}$  and  $f_{cc}'$  is not unique. As expected, the matrix yielding strength is slightly higher than the strength of the concrete itself. Resulting relations are graphically presented in Fig. 3.41 (high strength concrete) and Fig. 3.42 (normal strength concrete). Simplified linear relations are developed for concrete with gravel aggregates, cube crushing strengths  $13 < f_c' < 59$  N/mm<sup>2</sup>,  $D_{max} = 16 - 32$  mm:

$$\tau = \frac{-f_c'}{30} + \left[ 1,8w^{-0,8} + (0,234w^{-0,707} - 0,20)f_c' \right] \Delta \quad (\tau > 0) \text{ (N, mm)} \quad (3.13)$$

$$\sigma = \frac{-f_c'}{20} + \left[ 1,35w^{-0,63} + (0,191w^{-0,522} - 0,15)f_c' \right] \Delta \quad (\sigma > 0) \text{ (N, mm)} \quad (3.14)$$

It was thus shown that for unreinforced cracks, there is a unique relationship between the stresses  $\tau$  and  $\sigma$  and the displacements  $w$  and  $\Delta$ . If two of these parameters are given, the two remaining ones are also known.

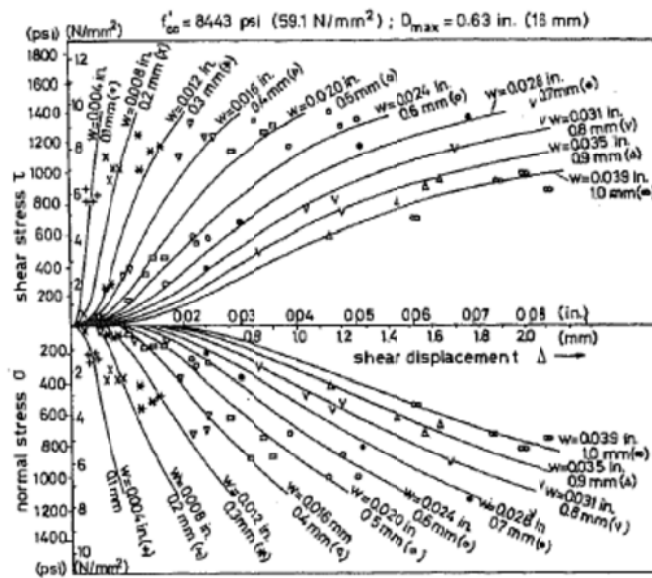


Fig. 3.41: Comparison between experimental values for concrete with  $f_{cc}' = 59$  N/mm<sup>2</sup>,  $D_{max} = 16$ mm,  $p_k = 0,75$  (ratio between total volume of aggregate and the concrete volume) and theoretical values, with  $\sigma_{pu} = 65$  N/mm<sup>2</sup> and  $\mu = 0,40$ . (Walraven, 1981).

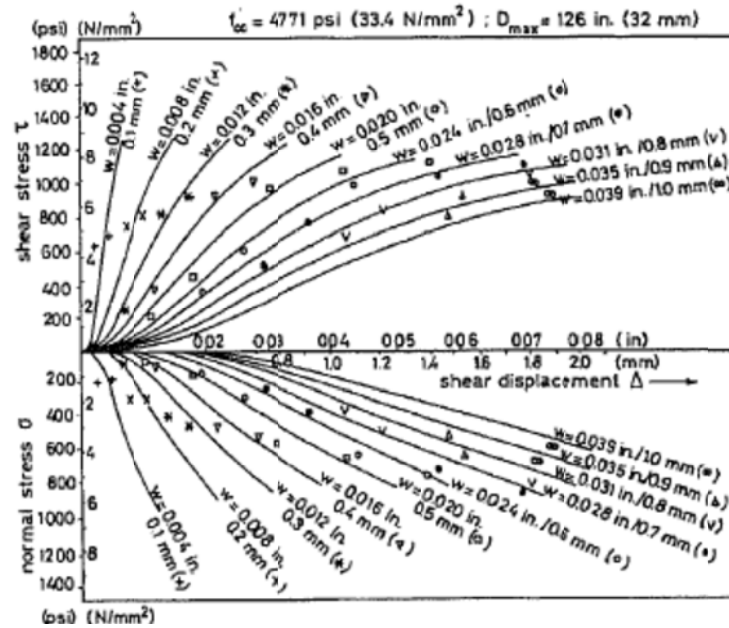


Fig. 3.42: Comparison between experimental values for concrete with  $f'_{cc} = 33,4$  N/mm<sup>2</sup>,  $D_{max} = 32$  mm,  $p_k = 0,75$  (ratio between total volume of aggregate and the concrete volume) and theoretical values, with  $\sigma_{pu} = 44$  N/mm<sup>2</sup> and  $\mu = 0,40$ . (Walraven, 1981).

Based on the theoretical model, parameter studies were carried out, leading to the conclusions:

1. A considerable part of the shear resistance is provided by friction. If friction is eliminated, more overriding of the particles and less deformation of the matrix occurs.
2. The small aggregate fractions loose importance if the crack width becomes greater.
3. The normal stress is not very sensitive for a variation of the maximum aggregate size. The shear stress is influenced: a smaller maximum aggregate size leads to a smaller maximum shear stress at a given crack width. The influence becomes larger for larger crack widths.
4. A grading curve with a higher proportion of sand particles leads to smaller maximum shear and normal stresses at a given crack width. The influence is largest on the shear stress and becomes larger for larger crack widths.
5. Aggregate interlock is mostly governed by the strength of the concrete.
6. The influence of the bar diameter is insignificant.

For reinforced concrete the mechanism works in a similar way (Walraven, 1981). The restraining force is now introduced internally by the reinforcement and depends on the

bond properties between reinforcement and concrete and the yield strength. The yield force in the reinforcement results in an equivalent normal stress on the crack,  $\omega f_{av}$ .

However, it was observed experimentally that the crack opening path does not seem to be significantly influenced by the reinforcement ratio. This is contrary to what had been observed in specimens with external restraint bars. Local disturbance of the crack structures was believed to be responsible for this difference. A different crack structure was also observed after testing. While crack faces of specimens with external restraint showed only a small amount of fine material torn off the crack face, specimens with reinforcing bars showed a considerable amount of loose particles and crater-shaped holes around the bars were visible. Assuming that the relationship between the shear stress  $\tau_u$  and the normal restraining stress  $\omega f_{av}$  in a reinforced crack is similar to the relation between  $\tau_u$  and  $\sigma$  in an unreinforced crack, leads to

$$\tau_u = C_1 (\omega f_{av})^{C_2} \quad (\text{N/mm}^2) \quad (3.15)$$

$$C_1 = (f'_c)^{0,36} \quad (\text{N/mm}^2) \quad (3.16)$$

$$C_2 = 0,09 (f'_c)^{0,46} \quad (\text{N/mm}^2) \quad (3.17)$$

A 5% fractile is obtained by multiplying equation (3.15) with 0,85 or 0,82 (Walraven et al., 1987). In case not a compressive but a tensile stress acts on the crack, equation (3.15) is multiplied by 0,8. Frenaij (1989) extended Walraven's model in order to account for the long term effects. Pruijssers (1986) indicates that the ratio between the crack widths and the shear slip of the crack at the bottom of the beam is approximately 3, Fig. 3.43.

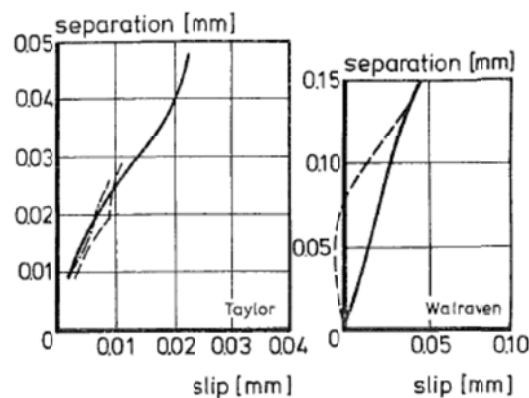


Fig. 3.43: Crack opening path in beams subjected to shear forces, Pruijssers (1986).

Millard and Johnson (1984) show experimentally that the two-phase model by Walraven (1980) should be used and not a local/global roughness model. However, the use of the two-phase model to predict the component of shear stiffness attributable to aggregate interlock in cracked reinforced concrete is not straightforward. When dowel action is eliminated, the local bond between reinforcement and concrete is also removed. In a reinforced concrete specimen, the axial stiffness restraining crack widening will be different from that when the bars are sleeved and will not remain constant during the test. This axial stiffness must be evaluated before the two-phase model can be used.

Vintzileou (1997) shows that when the constitutive laws of Fig. 3.44 are available, the shear transfer behavior at a reinforced interface can be predicted. For a certain shear slip, graph (b) gives the corresponding crack width. With curve (c), this crack width can be translated into a tensile stress in the reinforcement. The tensile force in the reinforcement equals the compression force on the interface, which gives the mean compressive stress at the interface when divided by the area of the crack. For this compressive stress value and for the given shear slip value, the curve in (a) allows for the calculation of the shear stress which is mobilized to resist the imposed slip. Repeating this procedure for different values of  $s$  leads to curve (d), which shows the behavior of a sheared interface.

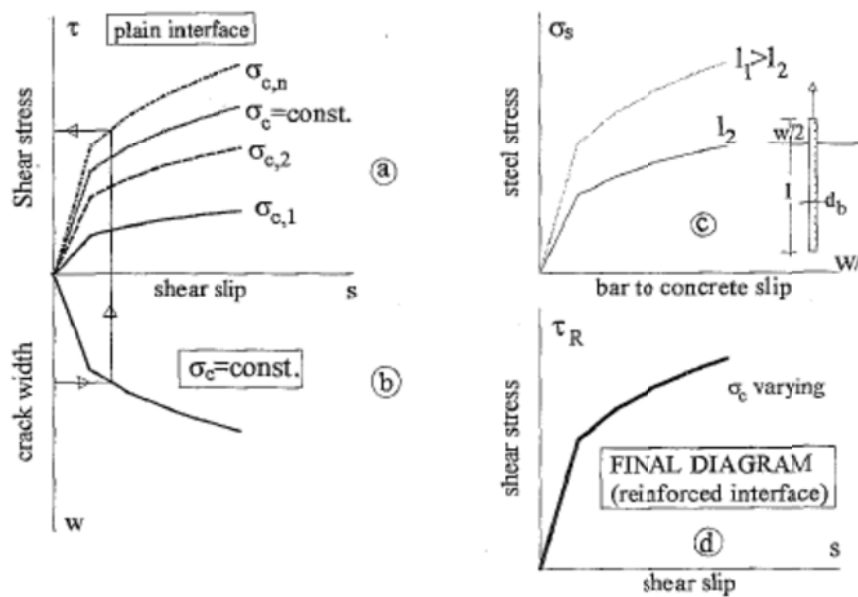


Fig. 3.44: Concrete to concrete friction; constitutive laws (schematic) (Vintzileou, 1997).

Vaz Rodrigues (2007) proved the necessity for a rounded crack based on a sensitivity analysis on the form of the critical shear crack, Fig. 3.45. In a straight crack, only opening but no sliding of the crack can occur, and thus a straight crack cannot carry any shear force.

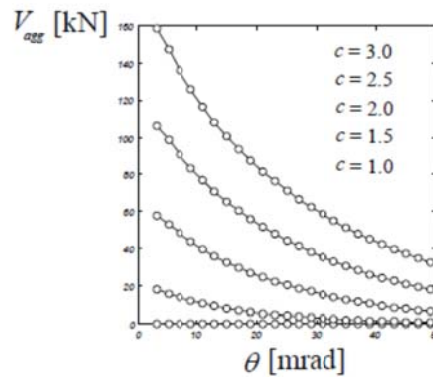


Fig. 3.45: Sensitivity analysis on the form of the critical shear crack (Vaz Rodrigues, 2007).

Reineck (1990) assumes that the maximum value of the friction stress  $\tau_{fu}$  is that without normal stresses perpendicular to the crack surface, Fig. 3.46, depending on the crack width  $\Delta n$ :

$$\tau_{fu} = 0,45 f_{ct} \left( 1 - \frac{\Delta n}{\Delta n_u} \right) \text{ with } \Delta n_u = 0,9 \text{ mm} \quad (3.18)$$

This maximum value for the friction stress is associated with a critical deformation state of the tooth; the corresponding slip is:

$$\Delta s_u = 0,336 \Delta n + 0,01 \text{ mm} \quad (3.19)$$

This method is valid up to crack widths of 0,5mm. However, Blaauwendraad and Walraven (1992) point out that Reineck's use of the concrete tensile strength and threshold value are rather dubious, since the fundamental model for aggregate interlock is based on shear and normal stresses.

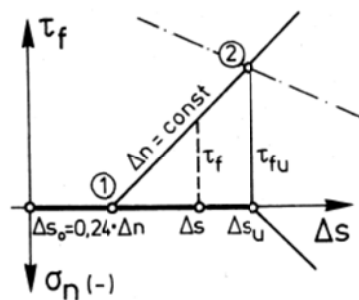


Fig. 3.46: Constitutive relation for friction along the crack shown for constant crack width (Reineck, 1990).



In finite element analysis (Voormeeren, 2011), the aggregate interlock can be best modeled by using a variable shear retention factor.

### **3.1.3.3.3 Contribution of aggregate interlock to shear carrying capacity**

An overview of the reported contribution of aggregate interlock to the total shear capacity as reported in the literature is given in Table 3.2.

Table 3.2: Contribution of aggregate interlock to shear capacity as reported in literature

Author(s)	Year	%	Comments
Fenwick and Paulay	1968	60	measured
Taylor	1972	33- 50%	measured
ACI-ASCE com. 426	1973	33 - 50%	after cracking
Sherwood, Bentz and Collins	2007	<70%	
Kani	1979	50 - 60%	
Hamadi and Regan	1980	44%	calculated for beams with natural gravel aggregates
		26%	calculated for beams with expanded clay aggregates
Swamy and Adriopoulos	1973	50 – 90%	see below

Swamy and Andriopoulos (1973) combined the amount of forces transferred through aggregate interlock and dowel action. They measured it to vary between almost 90% for a beam with 1,97% of tension steel and  $a/d = 2$  to about 50% for a beam with 3,95% of tension steel and  $a/d = 6$ .

Yang et al. (2011) point out that the reserve strength (ratio of ultimate shear strength to inclined cracking shear strength) is influenced by the maximum aggregate size, resulting in an increase in the ultimate shear strength for an increase in maximum aggregate size.

### **3.1.3.4 Dowel action**

#### **3.1.3.4.1 What is dowel action?**

Dowel action is the resistance of a reinforcing bar, crossing a crack, to shear displacement. The deflection of a bar, subjected to a dowel force, is partially a result of the deformation of the concrete around the bar and partially of the deformation of the steel over a free length (Walraven, 1980). Dowel action is typically small as the maximum shear stress to be carried by dowel action is limited by the tensile strength

of the concrete cover supporting the dowel. As a result of dowel action and deformation of the crack surface, the reinforcement bar will be pulled towards the concrete face. If this downward force exceeds the longitudinal splitting strength of the concrete, the cover can fail (Lubell, 2006). The dowel action contribution to the shear force is larger for large amounts of reinforcement (ASCE-ACI committee 445, 1998). Cope (1985) reported that dowel action in slabs is less significant than in beams because failing section lengths may not cross the entire member and because of the continuity provided by bars in two directions. Ghazavy-Khorasgany and Gopalaratnam (1993) on the other hand write that there is some evidence that dowel action is quite effective in slabs. Since this mechanism relies on shear deformations at the level of tension steel, bond characteristics and concrete stiffness around the bars play an important role.

#### **3.1.3.4.2 Models**

Fenwick and Paulay (1968) reported the results of their pioneering work regarding dowel action, Fig. 3.47. Their experimental results showed that the position of the bar in the concrete at the time of casting had a marked influence on the capacity and performance of the dowel. An attempt to quantify the force transferred through dowel action was based on a linear elastic stress distribution in the steel, Fig. 3.48. The maximum stress in the top bars was calculated as:

$$D_f = \frac{1}{3} b' s_r f_r \left( \frac{1}{1+R} \right) \quad (3.20)$$

and the corresponding expression for bottom bars is:

$$D_f = \frac{1}{3} b' s_r f_r \left( \frac{R}{1+R} \right) \quad (3.21)$$

in which:

$R$  the ratio of the displacements at the end of the dowel;

$s_r$  the length of the dowel in a test or the crack spacing in a beam.

The average value of  $R$  was found as 1,42 for top bars and 1,75 for bottom bars.

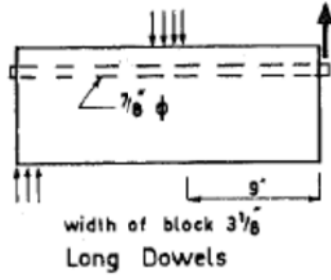


Fig. 3.47: Dowel action test. (Fenwick and Paulay, 1968).

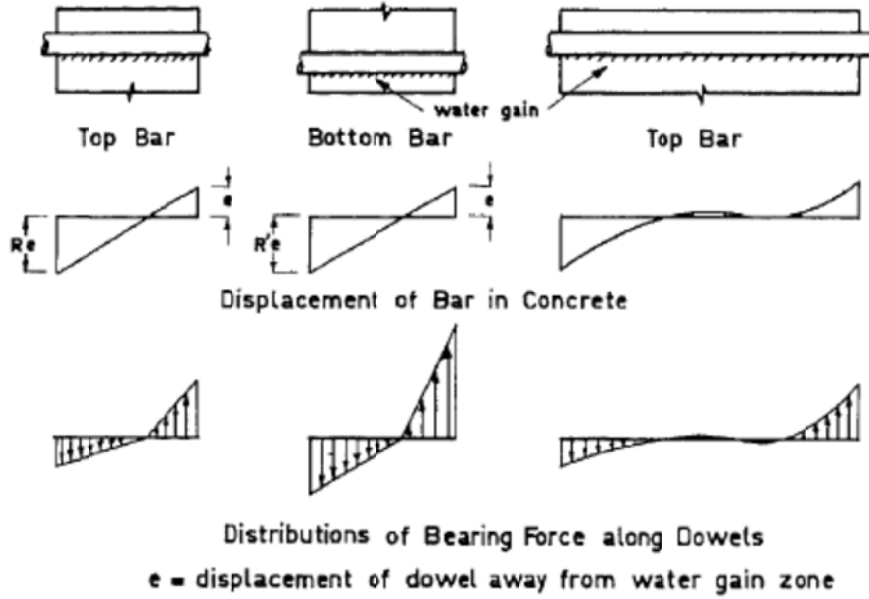


Fig. 3.48: Dowel action from long and short dowel. (Fenwick and Paulay, 1968).

Dulacska (1972) observed the dowel action to be almost ideally elasto-plastic. The probable and assumed system of forces on the steel are shown in Fig. 3.49. This results in the following expression for the dowel action:

$$V_{du} = 0,2d_b^2\rho f_{sy}(\sin\theta)\left(\sqrt{1+\frac{f_{cc}}{0,03\rho f_{sy}\sin^2\theta}}-1\right) \quad (3.22)$$

in which:

$d_b$  the diameter of the bar;  
 $f_{cc}$  the cube compressive strength of the concrete;  
 $\theta$  the angle between the bar and the shear crack;

$\rho = 1 - \left(\frac{N}{N_{sy}}\right)^2$  accounts for the axial bar force.

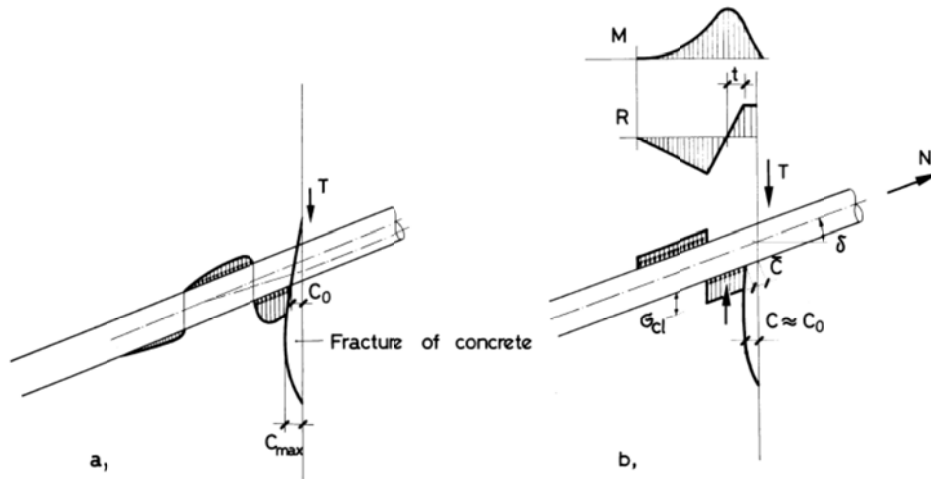


Fig. 3.49: (a) Probable system of forces; (b) assumed system of forces. Dulacska, 1972.

Chana (1988) developed a conceptual model for the dowel action based on the stress state in the reinforcement and the compression zone. The conceptual model is based on defining the distance  $s_d$  (the distance between the base of the inclined crack and the first crack) as  $s_d^*$  when the theoretical dowel force required to cause yielding  $V_y$  is equal to the dowel splitting force  $V_d$ . If  $s_d$  is greater than  $s_d^*$ , splitting failure takes place.  $V_y$  is taken as  $2m_p/s_d$  with  $m_p$  the plastic moment capacity of the reinforcing bar including the effect of axial tension. The plastic capacity is taken as:

$$m_p = \frac{4}{3} r^3 f_y \sin^3 \left( \frac{\theta}{2} \right) \quad (3.23)$$

in which

- $r$  the bar diameter;
- $f_y$  the yield strength of the bar;
- $\theta$  as shown in Fig. 3.51.

$V_d$  is based on a simplified stress distribution, Fig. 3.50.

$$V_d = 1,05 b_n \phi \sigma_t \quad (3.24)$$

in which

- $b_n$  the beam width minus the sum of the bar diameters;
- $\phi$  the bar diameter;
- $\sigma_t$  the tensile stress in the concrete, approximately taken as twice the splitting tensile strength attributable to the large strain gradient.

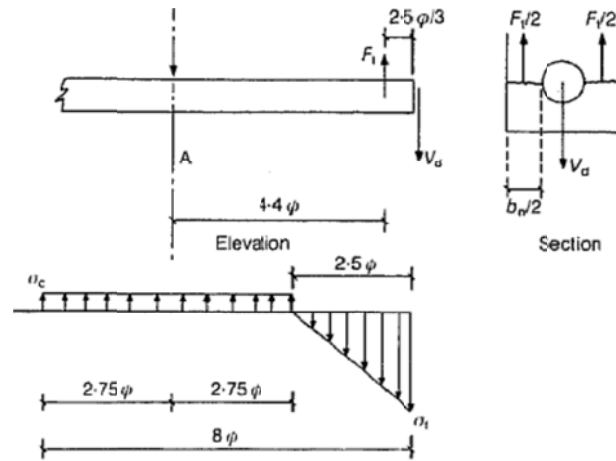


Fig. 3.50: Simplified stress distribution, Chana (1988).

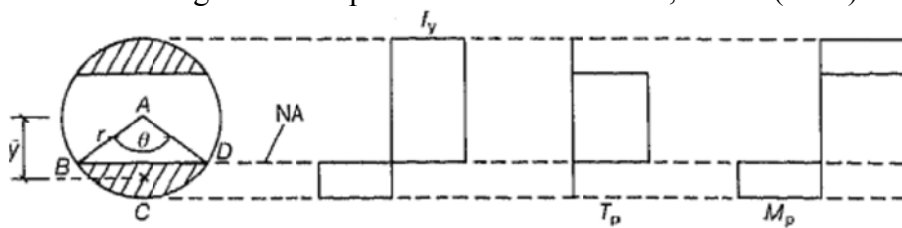


Fig. 3.51: Plastic analysis of circular section, Chana (1988).

Bhide and Collins (1989) considered the dowel to be an element in double curvature, limited by the plastic hinge capacity of the bar cross-section. Millard and Johnson (1984) showed that the shear stiffness associated with dowel action decreased as the axial force in the bar approached yield. The initial dowel stiffness was predicted well by the assumption of a beam on elastic foundation, and then decreased as the axial force increased. The ultimate load in dowel tests was predicted well by plasticity approaches. An axial tensile force in a bar reduces its dowel stiffness considerably. Taylor (1973) related the dowel split force to the side cover to the bars, the distance between the bars, the splitting tensile strength and the bar diameter.

Vintzileou (1997) show the 2 possible failure modes of dowel action, Fig. 3.52: splitting failure of the side or/and bottom concrete cover (mode I) or crushing of the concrete under the dowel and yielding of the bar (mode II). The stress distribution along the dowel and within a section is shown in Fig. 3.53. The stress distribution also shows that the maximum force to be transferred by means of dowel action will be decreased with increasing bar diameters.

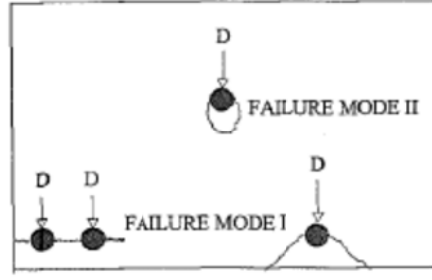


Fig. 3.52: Failure modes of dowel mechanism (Vintzileou, 1997).

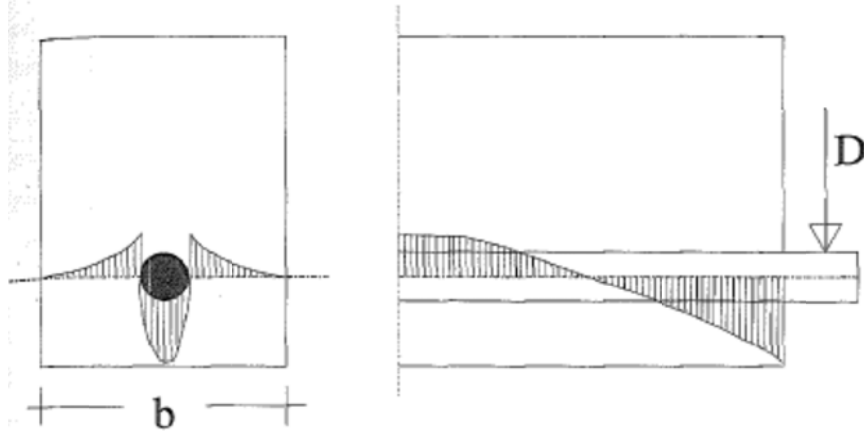


Fig. 3.53: Stress distribution along a dowel and within a section (schematic) (Vintzileou, 1997).

Reineck (1990) uses the following expression for the dowel action force:

$$V_{du} = \frac{6}{f_c^{1/3}} b_n d_b f_{ct} \quad \text{with } b_n = b_w - \sum d_b \quad (3.25)$$

and a lower limit:

$$\frac{V_{du}}{b_w d f_c} = 1, 4 \frac{\rho^{8/9}}{f_c^{2/3} d^{1/3}} \quad \text{with } \rho[1], f_c [\text{MPa}] \text{ and } d [\text{m}] \quad (3.26)$$

Near failure, these values are independent from the corresponding relative crack displacement within the considered range of application.

Fischer and König (1997) use the following expression for the dowel force:

$$H = 0,76 d_s b_n \sqrt[3]{12 f_{cm}} \quad (\text{in kN}) \quad (3.27)$$

with

$d_s$  the diameter of the reinforcement bars in mm,

$b_n$  the width of the cross-section in mm,

$f_{cm}$  the cylinder concrete compressive strength in  $\text{N/mm}^2$ .

#### 3.1.3.4.3 Contribution of dowel action to shear carrying capacity

The load-transfer capacity after the peak load of the beam would thus be mainly caused by the dowel action of the longitudinal reinforcement (Yang, 2010).

An overview of the contribution of dowel action to the overall shear capacity as reported in the literature is shown in Table 3.3.

Table 3.3: Contribution of dowel action to total shear capacity.

Author(s)	Year	%	Comments
Fenwick and Paulay	1968	20%	measured
Taylor	1972	15 - 25%	measured
ACI-ASCE com. 426	1973	15 - 25%	more important after cracking
Barker et al.	1969	33 – 82%	see below
Hamadi and Regan	1980	19%	calculated for beams with natural gravel aggregates
		34%	calculated for beams with expanded clay aggregates
Long	1975	30%	for punching in slabs

The shear study group (Barker et al., 1969) mentions Ashdown's model which includes dowel action and carries between 33% and 82% of the shear force. However, the shear study group claims that: "..., but it is generally agreed that it is safer to ignore dowel action as a contribution to shear resistance. To ignore dowel action is to assume that failure has taken place before the tearing begins, which is a wise assumption since a tearing failure is sudden and dangerous." Bresler and Scordelis (1963) on the other hand attribute the higher tested shear capacities than calculated by large to the effect of dowel action.

### 3.1.3.5 Arch action

#### 3.1.3.5.1 What is arch action?

Arch action enables load to be transferred from its point of application towards the support by means of a compressive strut. In members with plain reinforcement, arch action is the main shear transfer mechanism after the collapse of beam action (Feldman and Bartlett, 2005; Feldman and Bartlett, 2008). According to Elzanaty et al. (1986), arch action is not a shear transfer mechanism, in the sense that it does not transmit a tangential force to a nearby parallel plane, but permits the transfer of a vertical concentrated force to a reaction and thereby reduces the demand on other types of load transfer. The principle of internal arches can be based on a study of stress trajectories, Fig. 3.54 and Fig. 3.55 (Kani, 1969).

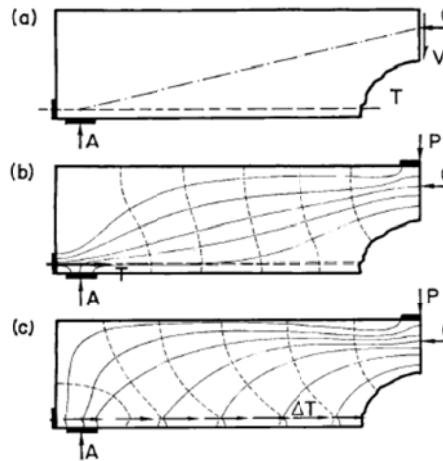


Fig. 3.54: Forces and trajectories in the shear span (Kani, 1969).

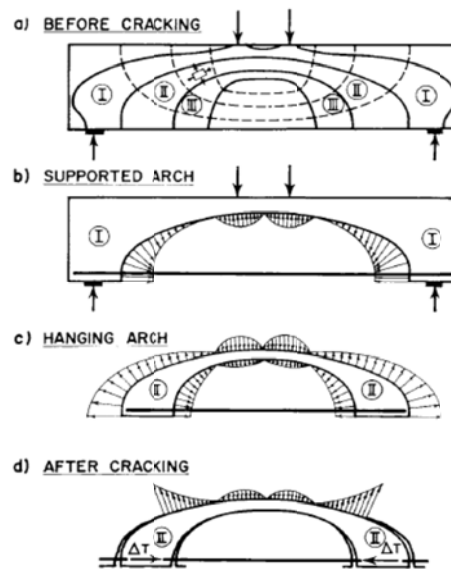


Fig. 3.55: Internal arches in a reinforced concrete beam (Kani, 1969).



Fig. 3.56: Cracking pattern of beam that failed due to the breakdown of the arching mechanism (Sneed and Ramirez, 2010).

Kim et al. (1999) developed an empirical method based on strain readings to predict the arching action capacity. The arch action capacity is taken as proportional to the beam action capacity – these components are shown in Eq. (3.3). Leonhardt and Walther (1962) point out that the arch action is clearly manifested in the pattern presented by the shear cracks, which take on a very flat slope at the top under the arch. In more slender beams, the portion of the beam situated above the arch suddenly



fractures off at the end, so that the arch loses its bearing, Fig. 3.57 (Zararis and Papadakis, 2001).

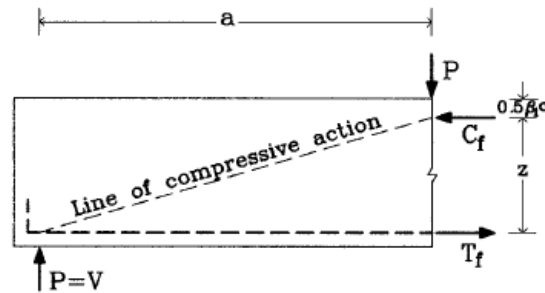


Fig. 3.57: Line of diagonal compressive action (Zararis and Papadakis, 2001).

The parameters influencing arching action are: the layout of the reinforcement, with layering resulting in a smaller depth for arching action, the anchorage of the tie (Rafla, 1971; Ghazavy-Khorasgany and Gopalaratnam, 1993), the crack shape (influenced by the  $a/d$  ratio) that defines the remaining uncracked compression zone (Reineck, 1997) and the type of reinforcement - with plain bars facilitating arching action more than ribbed bars in which the force in the tension chord decreases due to bond (Reineck, 1990).

However, Adebar (2000) claims that the development of a compression strut is unreliable and that it depends on the exact diagonal crack orientation.

### 3.1.3.5.2 Experiments

Olonisakin and Alexander (1999) measured beam and arch action in wide beam shear tests, Fig. 3.58. Yielding of the reinforcement was found to shift the forces from beam action to arching action. They also pointed out that the concept of a limiting nominal shear stress is more consistent with beam action than with arching action and that it is conceptually incorrect to assign all load to beam action.

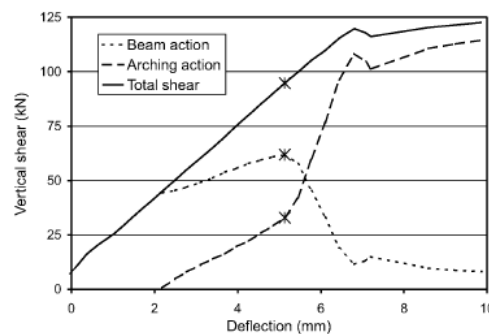


Fig. 3.58: Measured beam and arch action in test RB1 (Olonisakin and Alexander, 1999).

### 3.1.3.5.3 Models

Fenwick and Paulay (1968) studied the arch action in a beam, Fig. 3.59. Two points worth noting emerged from their study:

- (1) Substantial translational displacements develop when arch action occurs. The maximum slip for the model beam studied, is of the same order as the total elongation of the reinforcement in the shear span; and
- (2) in the vicinity of the load point, the line of thrust and the position of the neutral axis rise well above their respective positions predicted by conventional flexural theory.

The authors determined the arching index  $= \frac{v - v_t}{v}$  in which  $v = \frac{V}{bjd}$  as the normal shearing stress and  $v_t$  the average horizontal shear stress in the tension zone of the beam, found from the bond forces which act on the concrete cantilevers. An arching index of unity would indicate that the whole of the external shear is resisted by arch action. Towards the ultimate, the arching index increases, as wide diagonal cracks appear in the shear span.

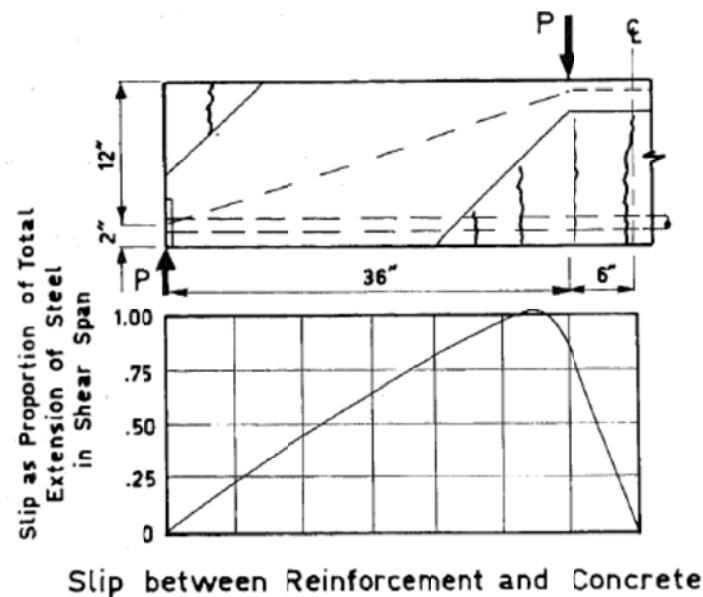


Fig. 3.59: Arch action in beam without bond. (Fenwick and Paulay, 1968)

Kim and Jeong (2011) decoupled arch and beam action for shear in beams. A section (a tooth) is idealized as a tied arch having a shear element inside, Fig. 3.60, in which the lever arm  $z$  varies along the span. Combining the definition of  $\alpha V = C \frac{dz}{dx}$  and

$C = V \frac{x}{z}$  leads to the expression  $\alpha = \frac{xdz}{zdx}$ . The value of  $\alpha$  is assumed to remain

constant throughout the shear span of a given member. With boundary conditions of  $z = z_0$  at  $x = a$  the expression for the compressive force paths (Fig. 3.61) becomes:

$$z_{(x)} = z_0 \left( \frac{x}{a} \right)^\alpha = z_0 R_{(x)}^\alpha \quad (3.28)$$

with  $z_0$  the lever arm calculated by the beam theory at the maximum moment section ( $x = a$ ). All models of the compressive force paths can be modeled: from Bernoulli beam theory with  $\alpha = 0$  to a simple strut-and-tie model with  $\alpha = 1$ , Fig. 3.61

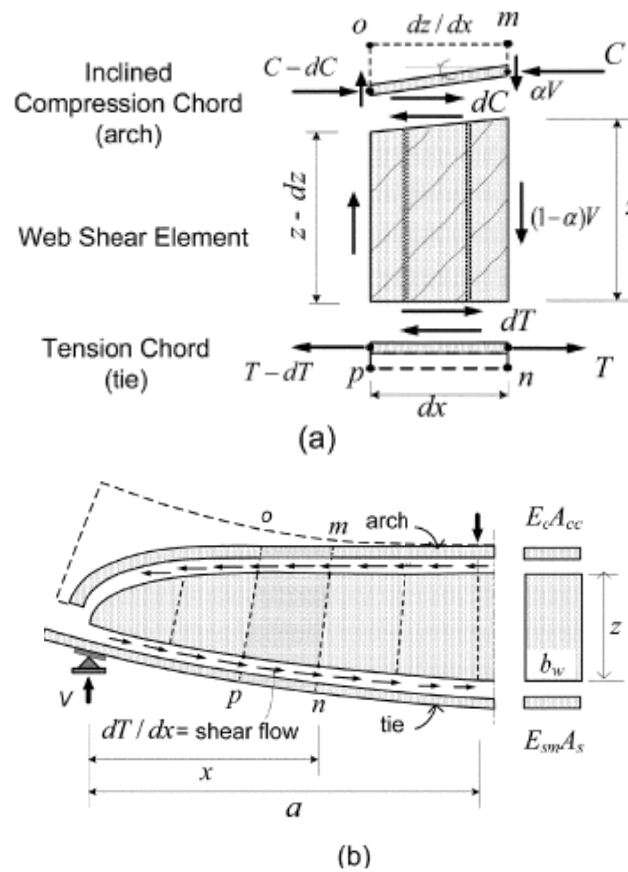


Fig. 3.60: Smeared truss idealization with inclined compression chord (Kim and Jeong, 2011).

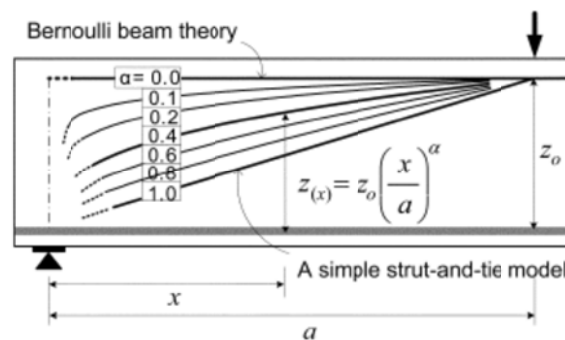


Fig. 3.61: Simplified compression force paths in a point-loaded simple beam (Kim and Jeong, 2011).

The internal distribution of shear force mainly depends on the relative ratio between the axial stiffness of the chords and the shear stiffness of the web. The beams with smaller slenderness ratios show greater shear resistance by the concrete compression zone (Kim and Jeong, 2011).

#### ***3.1.3.5.4 Contribution of arch action to shear carrying capacity***

In T-beams the contribution of arch action to the overall shear carrying capacity is found to be larger than for rectangular beams (Kim and Jeong, 2011). At the ultimate, Kim and Jeong (2011) found that 26 to 55% of the ultimate load is resisted by arching. Leonhardt (1962) stated that 15 to 25% of the total shear was carried by the inclined compression chord in the beams. As the compression zone is now assumed to be inclined, the contribution also takes into account the contribution of the compression zone on the shear carrying capacity.

#### **3.1.4. The size effect**

The size effect in shear is the relative decrease in shear capacity for an increasing effective depth. Recently, more attention has been given to the size effect in shear. Researchers have uttered their concern about the validity of the current code provisions empirically derived from small beam shear tests. The failure of the Shelby Warehouse, which was originally contributed to the combination of shear and axial tension (Anderson, 1957) and later to a lack of longitudinal reinforcement (Bhide and Collins, 1989) is now believed to have failed due to the size effect, Fig. 3.62.



Fig. 3.62: Shear failure of 900mm deep beams in the Air Force Warehouse, Shelby, OH (Lubell, et al. 2004).

The size effect in concrete is not limited to shear only (Morita et al., 1993) but includes:

- the effect of the cylinder size on plain concrete in compression and tension,
- the bar size effect in bond at the interface between steel and concrete, and
- the effect of strength reduction for increasing size of reinforced concrete elements in flexure and shear under monotonic and reversed cyclic loading.

An example of a large beam failing in shear is shown in Fig. 3.63.



Fig. 3.63: Large beam failing in shear (Lubell et al., 2004).

#### 3.1.4.1 Observations related to size effect

As early as 1948, Richart experimentally observed that: “The maximum shearing stresses, computed on the conventional critical section varied considerably with the effective depth of the footing, being larger for the thinner footings.” In 1967, Kani wrote: “To date (1966), the majority of reinforced concrete beams which have been tested to failure range in depth from 10 to 15in (25 to 38 cm). Essentially, these are the beams on which all our design practices and safety factors are based. The immediate aim of the test program described in this paper was to answer the question: How representative are the test results derived from such relatively small beams for the safety factors of large beams?” Based on his rational theory, Kani had stated: “All other factors being equal, the safety factor decreases as the depth of the beam increases.” The results reported by Kani (1967) show indeed a decrease in relative beam strength due to increasing depth. He assumed the differences in the crack pattern, Fig. 3.64, which dictates the shape of concrete teeth, to be the main reason. MacGregor suggested in the discussion to Kani’s paper (1967) that part of the reduction in shear strength with depth can be explained by the reduction in modulus of rupture with increasing depth. Leonhardt and Walther (1962) attributed Kani’s

observations to the varying bond resulting from complete similarity in his experiments.

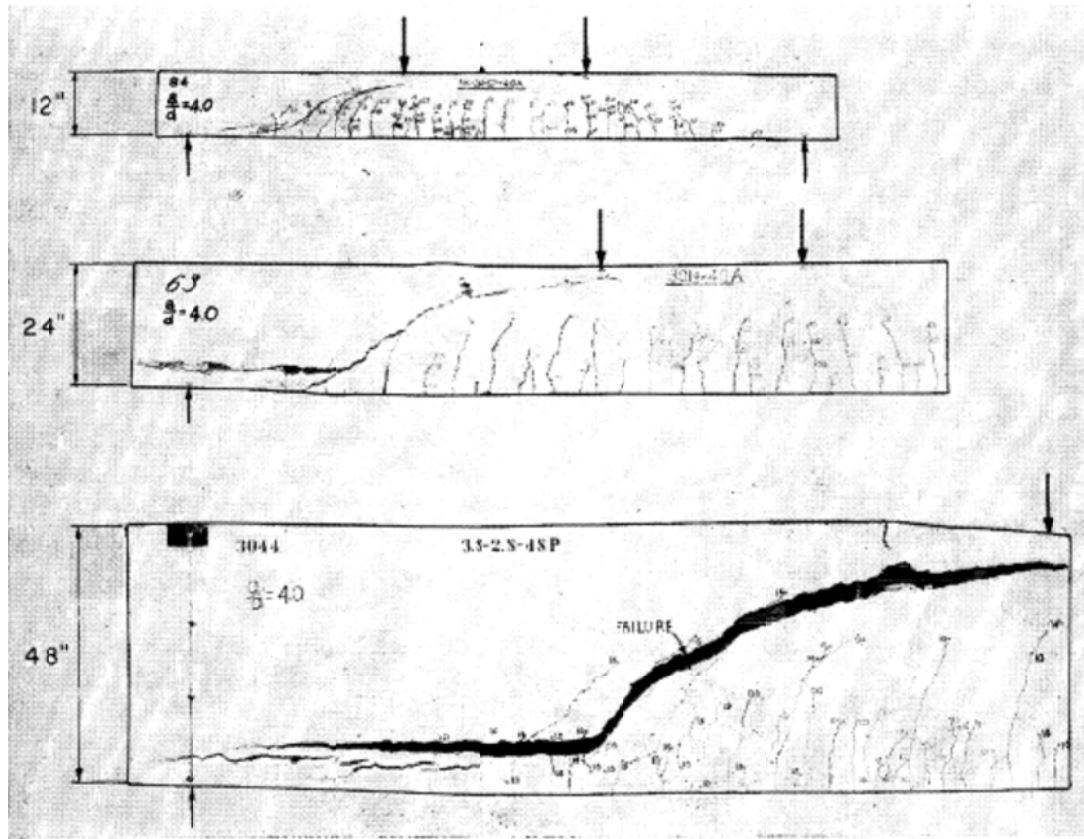


Fig. 3.64: Differences in crack patterns among beams of different depths (Kani, 1967).

Morita et al. (1993) observed experimentally much larger crack widths for full-scale specimens, not allowing stress transfer across the crack, while in the half and quarter-scale specimens the cracks remained in the tension softening zone.

Bažant et al. (2007) show that the failure probability of a 200mm deep beam is about  $P_f \approx 10^{-6}$  while the failure probability for a 1m deep beam is  $P_f \approx 10^{-3}$ , Fig. 3.65. As a result, the safety factors used in design and the expected (mean) design strength should not be considered as size independent (Bažant and Pang, 2006).

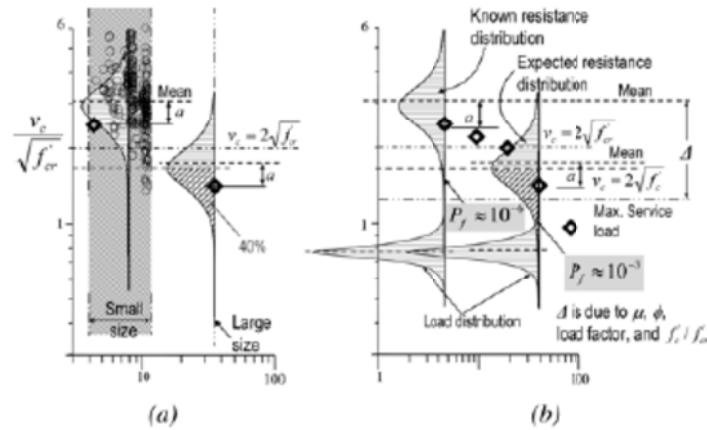


Fig. 3.65: (a) Probability distribution of shear strength of beams from 10 to 30cm deep, based on ACI committee 326 (1962) database, compared with Toronto data; and (b) failure probability for small beam and 1m deep beam.

Bažant (2004) shows that very little test data are available to support a theory for size effect, Fig. 3.66, with too many tests on small, heavily reinforced beams, leading to statistical bias (Bažant and Yu, 2008).

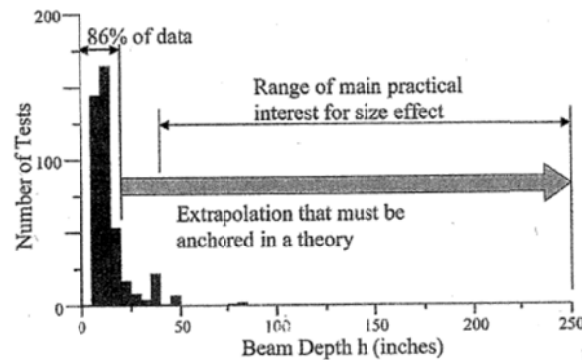


Fig. 3.66: Histogram of the number of tests in ACI 445 database as a function of beam depth  $d$ , demonstrating the necessity of extrapolating on the basis of a sound theory. (Bažant, 2004).

Bažant and Kazemi (1991) use a fracture mechanics based approach in which the size effect is attributed to brittleness, based on a series of experiments. These experiments, however, turned out not to be repeatable (Bentz and Buckley, 2005). The repeat tests had shear capacities of 31 to 70% higher of the original 1991 series. As shown in Fig. 3.67, there is large scatter on the test data as compared to most size effect laws (not all shown). While the size effect as of now stands undisputed, the size effect law to use is still under discussion.

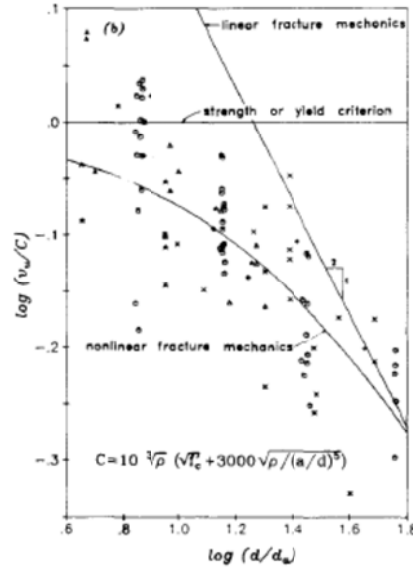


Fig. 3.67: Comparison with existing test data for beams of different sizes (Bažant and Kim, 1984).

Iguero et al. (1984) and Shioya et al. (1989) tested a series of beams with effective depths up to 3m to investigate the size effect in shear. A 4<sup>th</sup> root of effective depth size law was developed and it was noted that the ultimate compressive strain in the concrete  $\varepsilon_u$  became lower due to the size effect.

Additional tests by Niwa et al. (1987) confirmed the findings of the test series by Iguero et al. (1984). Brown et al. (2006) argue that Shioya's beams might have failed due to the effects of anchorage and bar cutoff and did not produce a genuine shear failure.

The size effect is also observed in slab-column tests (Guandalini, Burdet and Muttoni, 2009). Birkle and Dilger (2008) suggest that for slabs with a thickness larger than 260mm the size effect should be taken into account and that the reduction is larger for slabs without shear reinforcement, Fig. 3.68. Uzel et al. (2011) showed that in the case of direct strut action, the size effect is smaller.

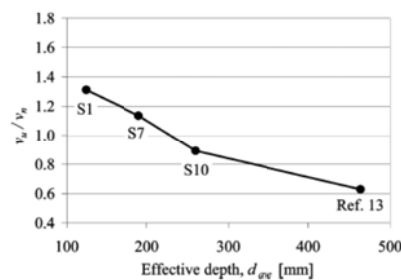


Fig. 3.68: Influence of slab thickness of failure stress in slabs without shear reinforcement (Birkle and Dilger, 2008).



According to Sundquist (2005), no good analysis method has been presented to date that can really explain the size effect for punching shear. A model developed by Hallgren (1996) was cited, based on fracture mechanics that incorporated the aggregate size. This led to the formula:

$$\varepsilon_{cTu} = \frac{3,6}{1,4} \frac{G_{F0}}{x} \quad (3.29)$$

where

- $\varepsilon_{cTu}$  the ultimate tangential strain,
- $x$  the depth of the compression zone in mm,
- $G_{F0}$  the fracture energy equal to 0,025; 0,030; 0,038 for aggregate size  $d_a = 8$  mm, 16 mm, 32 mm respectively.

With the ultimate tangential strain, the stress distribution in a section at a given location in the critical zone can be calculated. Then the forces are found and the maximum punching force is calculated. Hallgren and Bjerke (2002), however, stated that the influence of tensile strength and fracture energy has been found significant for the size effect in earlier research, but in their research based on non-linear finite element analysis of footings, no significant influence was found.

In 1939, Weibull introduced the statistical concept of the weakest link. In the context of size effect, the strength size effect comes from the probability to meet the most dangerous defect (depending on its size and orientation), which obviously increases with increasing structural size, thus providing the strength reduction (Carpentieri et al., 1993). The strength of the specimen is inversely proportional to the volume of the specimen, to the inverse power of the Weibull parameter  $m$ :  $f_v \sim V^{-1/m}$ . The parameter  $m$  is governed by the scatter in strength. The basic assumptions within the Weibull theory are that the ultimate structural failure occurs as soon as a stress criterion is reached anywhere within the structure, and that the material is not able to expose any gradual softening (Gustaffson and Hillerborg, 1988). These assumptions are not valid for shear failure. Weibull's model only gives realistic results if no redistribution of stresses is possible (Walraven, 1993).

Other possible contributions to the size effect in shear are unintended out-of-plane actions such as nonsymmetrical cracking (Kotsovos, 2006), the decrease in concrete strength in the upper layers of the section when concrete is cast in deep members in

practical construction and the possible change in critical section location with increasing beam size (Khuntia and Stojadinovic, 2001). Sabnis (1993) also points out that significant structural size effects can be obtained due to the diffusion process of drying of concrete in structures, the conduction of heat produced by hydration and the non-uniformities of creep produced by differences in temperature and moisture content throughout the structures. He also mentions the “wall effect” which could be a source of the size effect. This effect is caused by the fact that a boundary layer near the surface of concrete inevitably has a different composition and strength than the interior of the concrete structure. This layer contains a lower percentage of large aggregates and a higher percentage of mortar.

### **3.1.4.2 Size effect explained by aggregate interlock**

A possible reason for the size effect is that larger crack widths occur in larger members, leading to a reduced aggregate interlock (Taylor, 1972, 1973). The crack widths increase nearly linearly both with tensile strain in the reinforcement and spacing between the cracks. For the same reinforcement strain, doubling the depth of the beam will double the crack widths at mid-depth (Lubell et al. 2004). Taylor (1972) and Leonhardt (1978) as a result concluded that if the maximum size of the aggregates used in the concrete is scaled correctly, the loss of strength is smaller. The larger the size effect, the smaller the influence of aggregate interlock and the smaller the bending stiffness of the concrete teeth. However, it was shown by Walraven (1980) that aggregate interlock is not responsible for the size effect. If aggregate interlock were the main cause of the size effect, the implication would be that, in lightweight concrete beams, scarcely any size effect could occur (Walraven and Lehwalter, 1994). The experimental results proved this hypothesis wrong, as a very pronounced size effect was observed in lightweight beams. Blaauwendraad and Walraven (1992) discuss the hypothesis that size effect is caused by aggregate interlock by pointing out the following arguments:

1. the size effect does not disappear in lightweight concrete members in spite of their smaller aggregate interlock capacity;
2. in tests with plastic sheets to reduce the aggregate interlock capacity, the residual tension in the concrete was eliminated as well.

After testing a 3m high beam, Shioya et al. (1989) (Fig. 3.69) contribute the size effect to two factors: (1) reduced aggregate interlock due to larger crack widths and (2)

the size effect on the flexural tensile strength of concrete (Shioya and Akiyama, 1993). The first contribution affects the shear strength of a beam of  $d \leq 1\text{m}$ , Fig. 3.70.

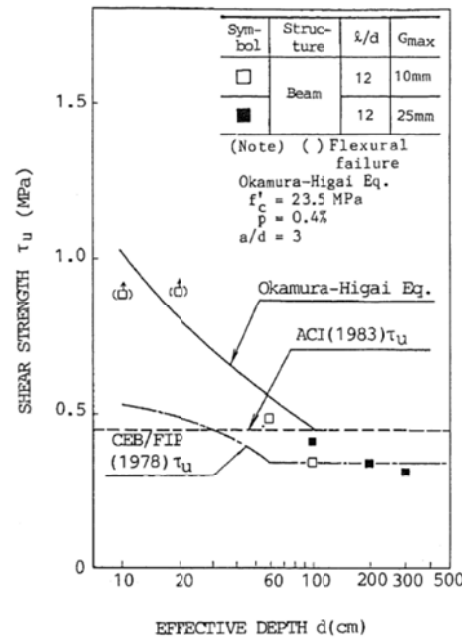


Fig. 3.69: Effect of the depth (Shioya et al., 1989).

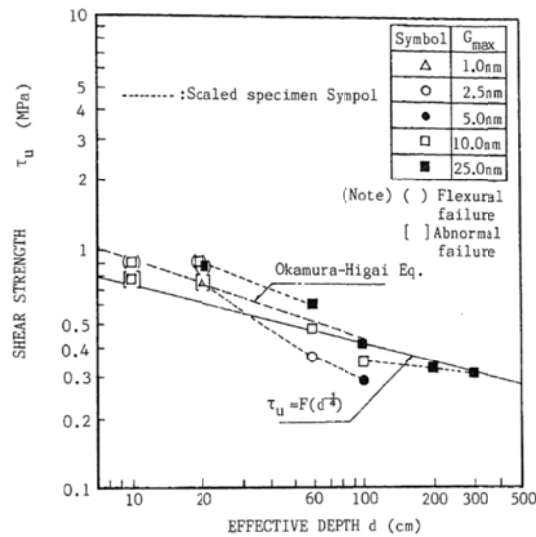


Fig. 3.70: Effect of maximum aggregate size. (Shioya et al., 1989).

### 3.1.4.3 Size effect explained by fracture mechanics

Ozbolt and Elighausen (1997) attribute the main reason for size effect to concrete cracking and the related structural energy release. There is a relation between the rate of crack propagation and the size of the member. This phenomenon is a consequence of the energy-release rate, which is larger for larger structures. In large beams, the cracking pattern develops significantly faster than in small beams (Walraven and

Lehwalter, 1994). The so-called softening behavior of concrete at crack opening is the key to the solution of the size problem. In small beams the cracks have small widths so that over the crack faces, substantial tensile stresses can be transmitted, whereas in large beams with the same crack pattern but larger crack widths, the contribution of stresses across the cracks to the shear capacity is much smaller.

The dimensional disparity between tensile stress  $([F][L]^{-2})$  and stress-intensity factor  $([F][L]^{-3/2})$  causes a constant slope equal to -0,5 in the nominal strength versus structural size bilogarithmic diagram, Fig. 3.71 (Carpinteri et al., 1993). This approached results in the linear elastic fracture mechanics size effect law.

Two major theoretical scaling laws exist for concrete structures (Ozbolt and Elighausen, 1997). The first type of scaling laws is based on linear elastic fracture mechanics (LEFM), nonlinear fracture mechanics, cohesive crack models or a simple energy balance consideration between the structural energy release and the concrete energy consumption capacity. These approaches are based on a single crack and an assumption of proportionally scaled initial flow. With the assumption of crack length proportionality at peak load and the size of the concrete fracture process zone Bažant's size effect law, Fig. 3.71, can be found, based on an energy criterion of failure (Bažant and Kim, 1984; Bažant and Kazemi, 1991):

$$\sigma_N = Bf_t(1 + \beta)^{-\frac{1}{2}} \quad (3.30)$$

with:

$\beta = \frac{d}{d_0}$  the brittleness number;

$\sigma_N$  the nominal strength, the ultimate load divided by the characteristic area;

$d$  the structural size (beam depth, embedment depth, ...);

$f_t$  the concrete tensile strength;

$B, d_0$  two constants, to be determined experimentally or by a more sophisticated analysis.

Eq. (3.30) is based on 4 hypotheses:

1. Fracture propagation requires an approximately constant energy supply per unit length and width of fracture.
2. The potential energy released from the structure due to fracture growth is a function of both the fracture length and the area of the cracking zone.

3. At the ultimate load, the fracture shapes and lengths in geometrically similar structures of different sizes are also geometrically similar.
4. The structure does not fail at crack initiation.

For propagating failures in which the fracture process is not concentrated at a point, but takes place within a finite zone ahead of the fracture front, the size effect is transitional between plasticity and linear elastic fracture mechanics. The dissipated energy depends on: (1) length of the fracture or cracking zone and (2) its area. If only the first part of the hypothesis is made, the size effect of linear elastic fracture mechanics results, and if only the second part of the hypothesis is made, there is no size effect as in plasticity (Bažant and Kazemi, 1991). As shown in Fig. 3.71, for small depths the strength criterion dominates and for large depths the fracture mechanics aspect of failure dominates (Bažant and Kim, 1984). The strength reserve due to stable crack growth becomes smaller as the size increases and vanishes when a certain size is exceeded.

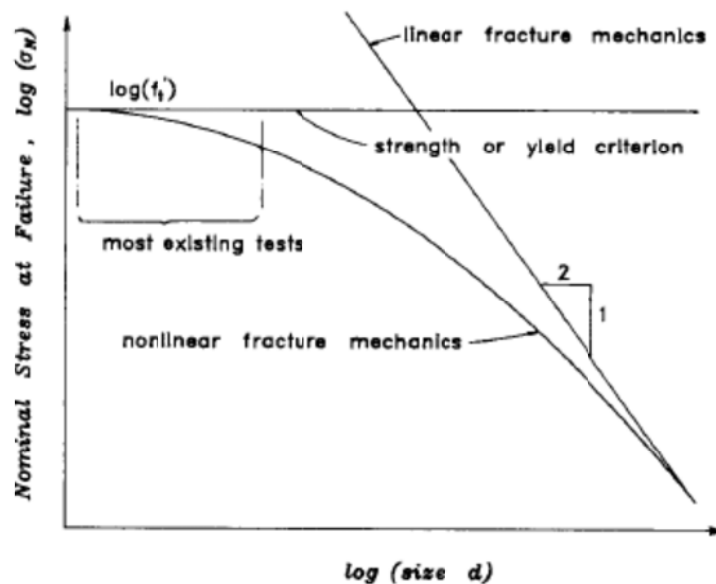


Fig. 3.71: Illustration of size effect according to various theories (Bažant and Kim, 1984).

Especially in large structures, the hypothesis of crack similarity and its proportionality at peak load is generally not fulfilled. According to Ozbolt and Elighausen (1997), the validity of Bažant's size effect law is limited. Carpenteri et al. (1993) also point out that several experimental results indicate that even the largest members without initial cracks resist some stress, contrarily to Bažant's size effect law. Some theoretical

explanations of the inadequacy of Bažant's size effect law have also been provided. A main point of criticism is that Bažant obtained his formulation only for notched specimens and assuming that the notch size, responsible for the stress singularity, was scaled proportionally to the structural size. When applying the size effect law to unnotched specimens, the hypothesis merely falls, since in disordered material the size  $a$  of the characteristic flaw, which is responsible for the crack propagation, should be independent of the specimen size.

The second type of scaling laws is based on multifractal aspects of damage and multifractality of crack surfaces. The concept is based on the homogeneity of the material. In a small concrete structure the aggregate size is large relative to the structure size. Therefore, the inhomogeneity is maximal and the size effect is strong. In large structures, the aggregate size is small relative to the structure size (perfect homogeneity) and the size effect disappears. This is expressed by:

$$\sigma_N = \left(A + \frac{B}{d}\right)^{\frac{1}{2}} \quad (3.31)$$

in which  $A$  and  $B$  are two constants obtained by fitting of experimental data, Fig. 3.72. Since the microstructural morphology of a disordered material is obviously the same, independently of the macroscopic specimen dimensions, the influence of disorder on the mechanical properties of the material strictly depends on the ratio of the size of the largest heterogeneities (here: aggregates) to the macroscopic size of the specimen (Carpinteri et al., 1993).

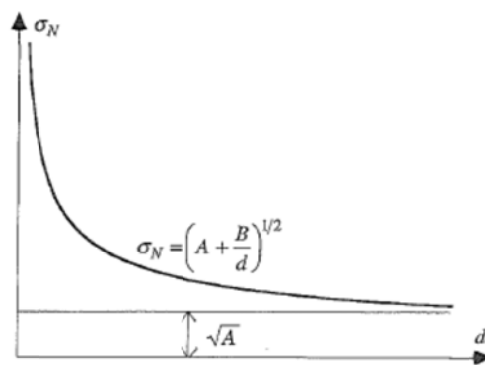


Fig. 3.72: Multifractal scaling law (Carpinteri et al., 1993)

For size effect, it can be said that in large structures the microstructures is somehow homogenized, i.e., behaves macroscopically as an ordered microstructure. Therefore the scale effect should vanish in the limit of structural size  $d$  tending to infinite. For small specimens, the effect of the disordered microstructures becomes progressively

more important, and the strength increases with decreasing size, ideally tending to infinity as the size tends to zero, Fig. 3.73.

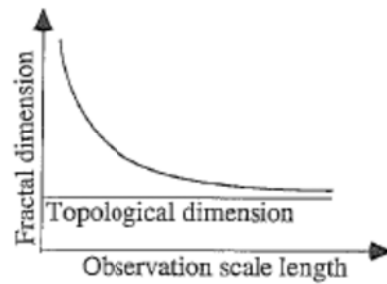


Fig. 3.73: Geometrical multifractality (Carpinteri et al., 1993)

Contrarily to Bažant's size effect law, in multifractal scaling law (MFSL), limit analysis governs only in correspondence with the homogeneous regimes, when the disordered microstructures has been homogenized at the larger scales. On the other hand, according to MFSL, the linear elastic fracture mechanism is supposed to govern the collapse mechanism of an unnotched material when the characteristic flaw size  $a$  becomes comparable with the macroscopic dimensions or, when the disorder comes essentially into play, Fig. 3.74. A comparison between MFSL and Bažant's size effect law is shown in Fig. 3.75.

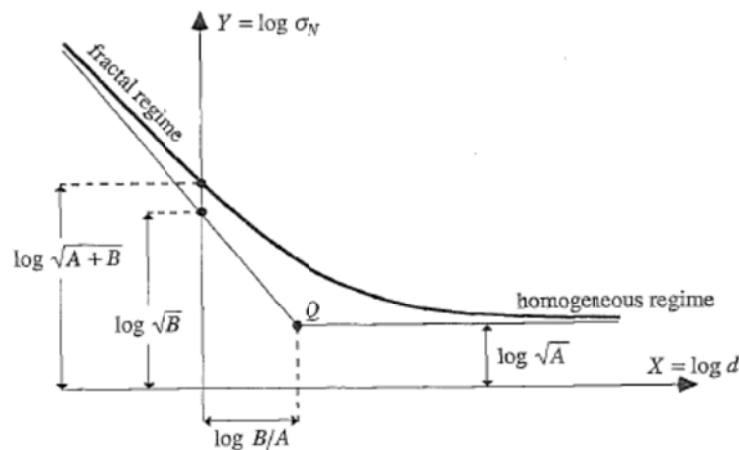


Fig. 3.74: Multifractal scaling law: bilogarithmic diagram (Carpinteri et al., 1993).

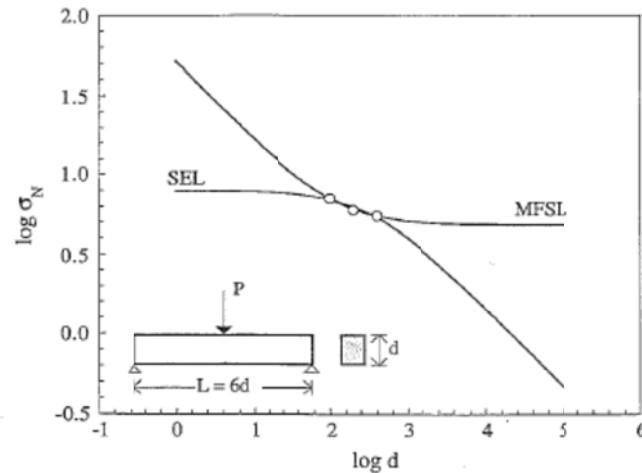


Fig. 3.75: Multifractal scaling law as compared to the size effect law and test data (Carpinteri et al., 1993).

Criticism on this procedure is based on the fact that in larger structures the material inhomogeneity disappears but the inhomogeneity of the strain field generally does not disappear.

Ozbolt and Elighausen (1997) show with a parametric study that for small beams the concrete fracture energy significantly contributes to the shear strength while for large beams, the ultimate load is mainly controlled by concrete tensile strength. By comparing experimental data, they found that the size effect is significant up to depths of 1m. For large beams the shear strength is constant and size independent. When the flexural reinforcement ratio increases, the shear strength increases as well and the size effect is present in a smaller size range. They conclude by pointing out that from a LEFM point of view there are two types of geometries:

1. Geometries which exhibit stable crack growth before the ultimate load is reached.
2. Geometries for which the ultimate load coincides with crack initiation.

The first type shows a strong size effect in a broad range, while the second only shows a size effect in a limited size range. As a result, there is no general size effect law.

#### 3.1.4.4 Size effect related to type of shear failure

Different opinions on the influence of the slenderness of the member on its vulnerability to the size effect exist.

Yang (2010) postulated that the size effect becomes more significant in beams that have a smaller shear span-depth ratio because the failure of concrete struts joining the



loading and support points show more brittle behavior with the decrease of shear span-depth ratio. Similarly, Yu and Bažant (2011) wrote that “If the deep beam fails by compression crushing of concrete, the compressive strength of the “strut” exhibits a strong size effect.” Experimental work by Walraven and Lehwalter (1994), Fig. 3.76, showed that the load at which inclined cracking occurs in deep beams is hardly size-dependent, while the final bearing capacity shows strong size dependence. The size effect in short members was found to be similar to that in slender members, in spite of the different types of failure.

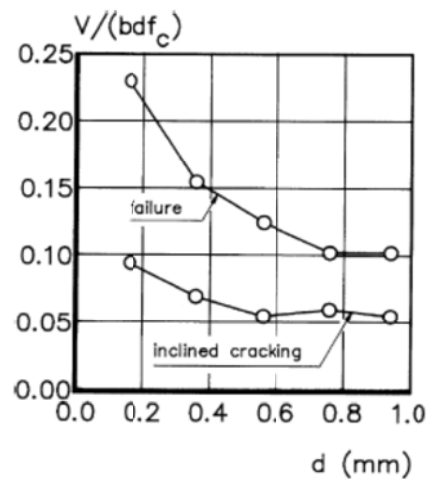


Fig. 3.76: Relative shear stresses at inclined cracking and failure for short members with  $a/d = 1$  but different absolute dimensions. (Walraven and Lehwalter, 1994).

Contrarily, Reineck (1992) says that, since the crack widths are reduced if  $a/d$  decreases, the size effect becomes less important in members with short shear spans. Adebar (2000) states that the size effect reduction is only needed when  $a/d \geq 2$ .

## 3.2. One-way and two-way shear

### 3.2.1. Distinction

When a slab under a point load fails as a wide beam with a distinct shear crack on the side, the failure mode is denoted as “one-way shear”. When a slab under a point load fails like a slab-column connection with a circular failure face, the failure mode is denoted as punching or “two-way shear”, Fig. 3.77. Fig. 3.78 shows the distribution of cracking due to the occurring moment in a slab-column connection. The radial moment  $M_r$  decreases at a rapid rate with the distance from the loaded area. It causes yielding to develop first at the perimeter of the loaded area. Meanwhile, a tangential moment  $M_\theta$  will restrain any rotation at the inclined crack (ASCE-ACI Committee

426, 1974).  $M_\theta$  leads to cracks on lines radiating from the center of the loaded area and dividing the slab into sectors.  $M_r$  leads to inclined cone-shaped internal cracks. Models for punching shear can be divided into four categories: models based on shear stress, strut and tie models, beam analogy models and plate analysis models (solved by using finite elements methods) (Lantsoght, 2009).

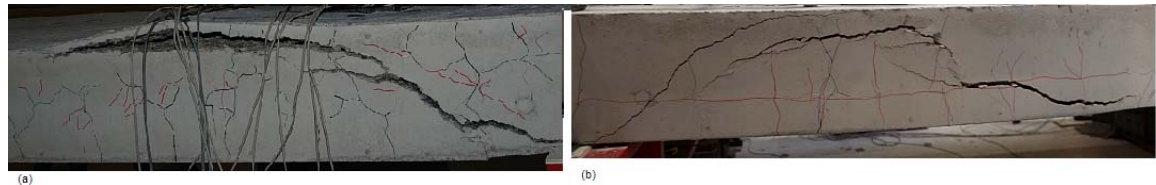


Fig. 3.77: (a) one-way shear, (b) two-way shear.

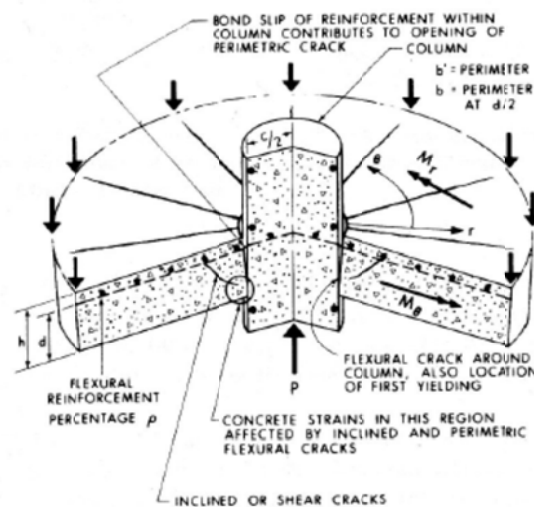


Fig. 3.78: Crack formation in column area of slab (ASCE-ACI Committee 426, 1974).

Hawkins and Mitchell (1979) differentiate between wide beam shear failure and punching shear failure based on the influence of flexure on the failure mode. For wide beam shear failure the shear strength is independent of the stiffness and therefore of the flexural strength of the slab. Contrarily, for a punching failure the shear strength decreases as the stiffness of the connection decreases. Inclined cracking develops at about the same shear stress for either a wide beam or punching shear failure.

However, for the punching situation those cracks cannot open until there is a marked decrease in the tangential stiffness of the slab. A two-way reinforcement pattern or in-plane restraints will maintain stiffness and permit development of an ultimate capacity considerably greater than the wide beam capacity.

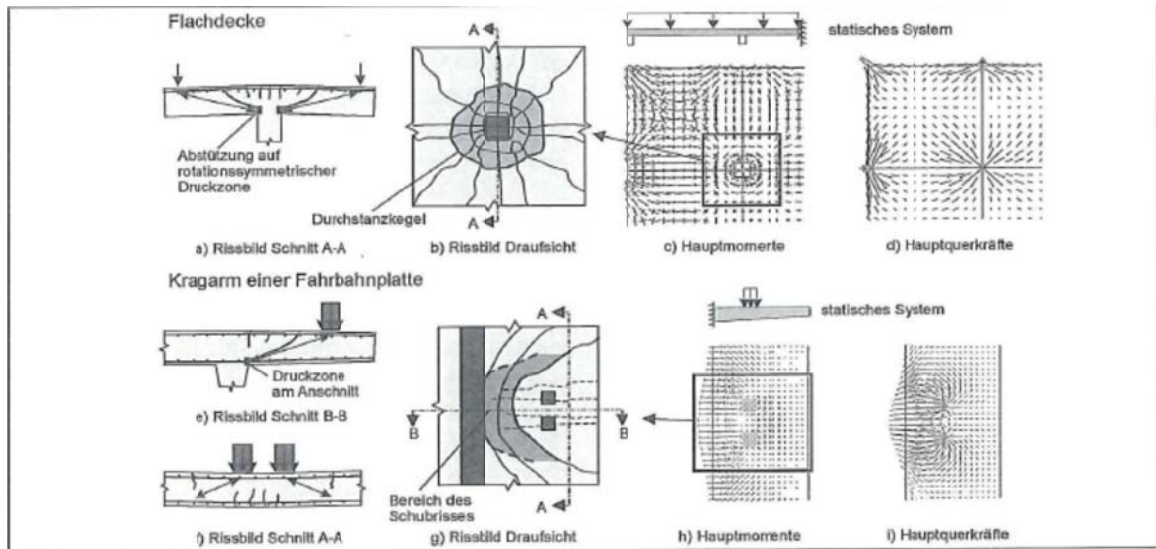


Fig. 3.79: Bearing behavior and crack pattern at a column supporting a floor slab as well as for a cantilevering bridge deck slab under concentrated loads (Rombach et al. 2009)

According to Reineck (1992) the crack pattern and kinematic behavior of punching is very different from beam shear, and additional load-carrying mechanisms may occur. Rombach et al. (2009) note the difference between flat floor slabs and bridge deck slabs under concentrated loads: the principal shears and moments are rotational symmetric around the load in flat floor slabs, while in bridge deck slabs a different force distribution occurs. Due to the line supports in bridge deck slabs, and the eccentricity of the loading, the flow of shear stresses is influenced and is not rotational symmetric anymore.

Cope and Clark (1984) point out that it is not clear whether the same shear strength as attributed to beams can be applied to slabs in more general circumstances than building slabs, when the support conditions and/or the loading are non-uniform. An additional problem occurs when the flexural reinforcement is not perpendicular to the planes of the principal shear forces, because it is not obvious what area of reinforcement should be used to calculate the shear capacity. It is not certain whether this can be ignored in complex slabs, such as bridge slabs, where large principal shear forces can act at large angles to the flexural reinforcement directions. It should also be noted that shear forces in slabs subjected to concentrated loads can vary rapidly across the slab width. A decision then has to be made as to whether to design against the peak shear force or against a value averaged over a pre-determined width.

Based on measurements on a one-way slabs under a concentrated load (Hegger and Reißer 2011), the principal stresses and directions are determined. It is shown that the

tangential concrete compressive stress is significantly larger than the radial concrete compressive stress, as typical for punching problems, Fig. 3.80.

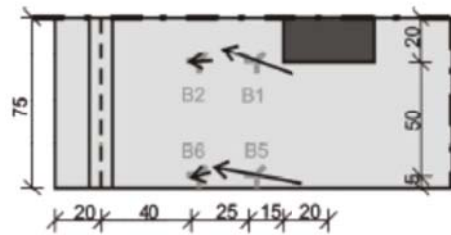


Fig. 3.80: Directions of principal compressive stresses from measurements on  $b = 150\text{cm}$  (Hegger and Reîßen 2011).

Criswell and Hawkins (1973) point out the differences between one-way shear and two-way shear:

- The inclined crack location: for punching, the inclined crack is confined to a region immediately adjacent to the perimeter of the loaded area. The crack is less free to develop at the weakest section than in a slender beam. It is likely that inclined cracking develops first in regions of high shear stress. The use of the ultimate rather than the initial cracking load can be safely considered as the usable strength.
- The stress conditions at the apex of the inclined crack: in a slab under a concentrate load, the concrete at the apex of the inclined crack is subjected to complex triaxial stress conditions. The biaxial bending moments in the slab create orthogonal compressive stresses in a horizontal plane and the concentrated load causes compressive stresses in the vertical plane.
- The lack of symmetry, resulting in variations in the loads for cracking and inelasticity at different locations around the loaded area.
- Distribution of moments: the relative magnitudes of the radial and tangential moments vary with the pattern of cracking and yielding in a slab. Also, the stiffness of the slab in the  $\theta$  direction helps to control the opening of the inclined cracks.
- Limitations of static considerations, as shown in Fig. 3.81. Statics cannot provide a unique value for the compressive force  $C_l$  acting above the inclined crack.  $C_l$  depends on compatibility conditions in the column region, and it need not equal the tension force  $T_l$ .
- Dowel forces: dowel action carries a larger amount of the total shear force in slabs than in beams.

The ability of a slab to resist higher unit shear stresses diminishes as the size of the loaded area increases relative to the slab thickness. For large rectangular loaded areas, the slab near the corners of the load is effectively point loaded while at the center of the load the action is more like a wide beam. The rate of decrease in shear strength is slow if the maximum principal moment acts about the long side so that there is essentially one-way slab action. However if that moment acts about the short side, a rapid transition from slab to beam behavior begins when the aspect ratio for both sides exceeds two.

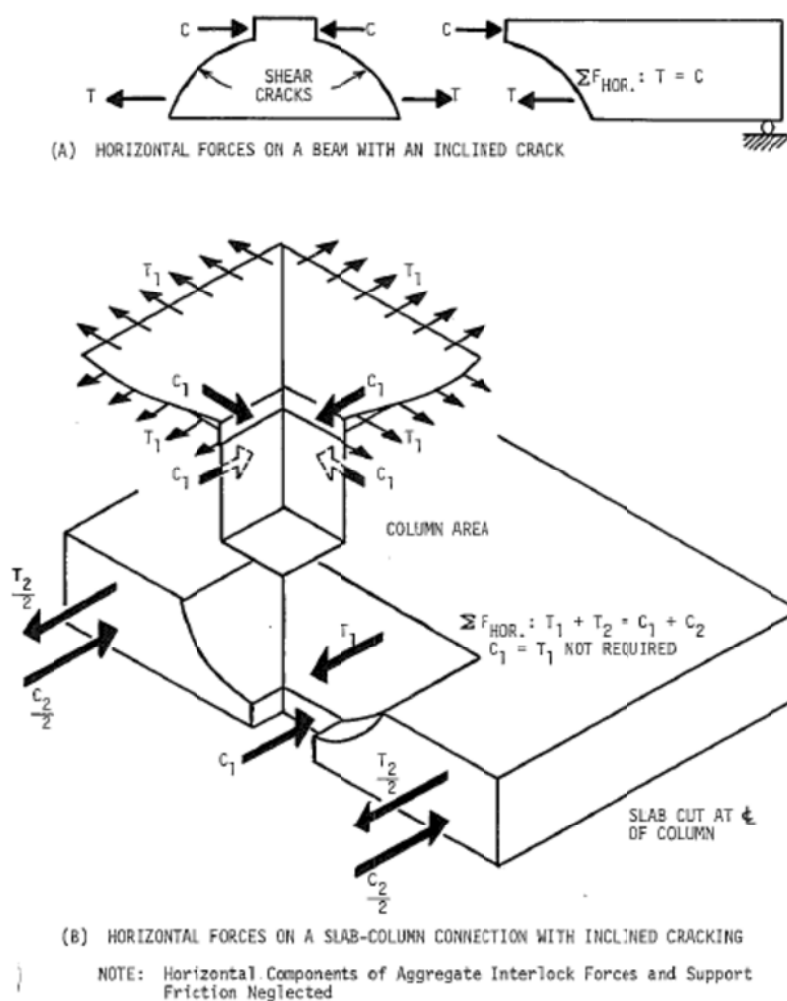


Fig. 3.81: Horizontal forces on sections near inclined cracks (Criswell and Hawkins, 1973).

### 3.2.2. Similarities and transition zone

Vaz Rodrigues (2007) argues that one-way shear and two-way shear are confusing terms, as shear is inherently unidirectional as a mechanical quantity (it can be

represented as a vector). At any location, shear equilibrium is ensured by two components ( $v_x$  and  $v_y$ ). As a result, there is only one direction for principal shear, and not two directions as for moments, which are a tensorial quantity of a higher level, and have at each location two principal directions. Shear is thus exclusively carried in the direction of the principal shear, with no perpendicular shear transfer. In that sense, two-way shear is a physical impossibility. Based on the flow of shear forces, however, the concept of one-way and two-way shear can be explained. Zones in which one-way shear is acting are the areas where the principal shear lines run parallel to one another. Zones in which two-way shear is acting are those in which the principal shear lines are not running in parallel, for example around the point of introduction of the concentrated load. The compressive and tensile force paths for a slab in two-way shear are shown in Fig. 3.84. Four modes of failing are distinguished in punching failures. The “yield” failure mode governs for low values of  $\rho f_y/f_c'$ . As the value for  $\rho f_y/f_c'$  increases, the “shear and yield”, “shear” and “compression” failure modes will govern. The force flow in another practical model is shown in Fig. 3.83.

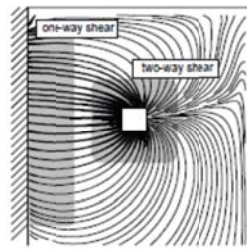


Fig. 3.82: Shear flow in a slab: zones of one-way and two-way shear (Vaz Rodrigues, 2007).

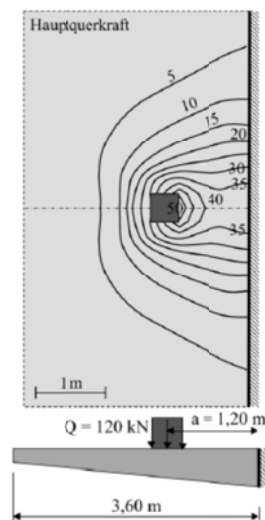


Fig. 3.83: Contour plot of main shear force  $v = \sqrt{v_x^2 + v_y^2}$  (plane model) (Rombach and Velasco, 2005).

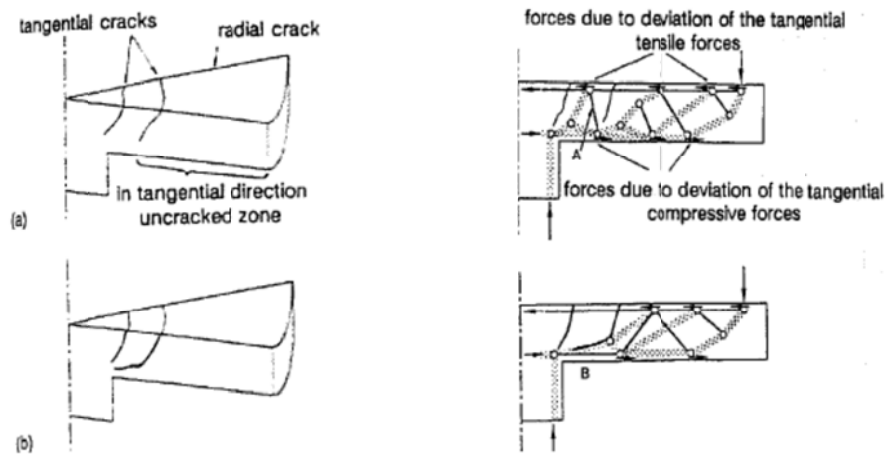


Fig. 3.84: Structural behavior in the cracked state (Muttoni and Schwartz, 1991).

Close to the support, the sections for one-way shear and two-way shear interact. Fig. 3.85 shows the situation when the load is not close to the support. Moving the load closer to the support would cause the sections for one-way and two-way shear to overlap and interact, starting at  $a_v = 2d$ . The three-dimensional force flow of the punching mechanism is thus interacting with the force flow from the one-way shear approximation and the modes cannot be treated independently (Lubell, 2006). For a footing, this transition is shown in Fig. 3.86.

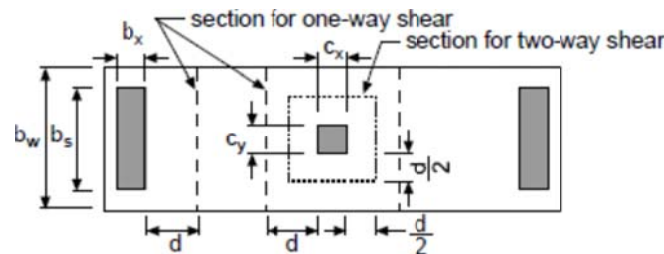


Fig. 3.85: Critical sections for shear (Lubell, Bentz and Collins, 2008).

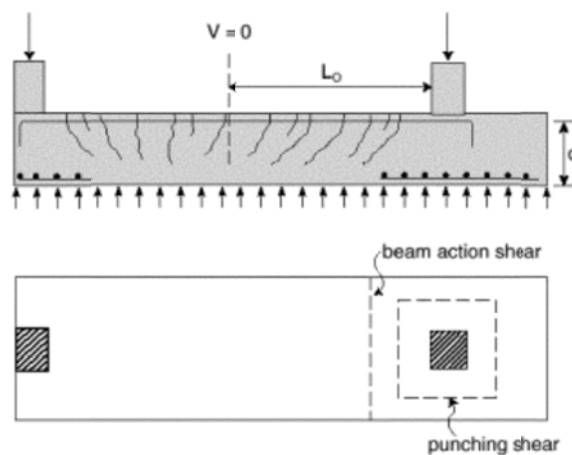


Fig. 3.86: Example of two-way and one-way shear in footing (Uzel et al., 2011).

Lubell (2006) calculated for each thickness the member  $b_w/d$  ratio that would represent the transition from one-way to two-way shear failure modes, for a range of loaded width to member width ratios. A parameter  $\kappa$  was introduced to represent the more severe difference in width:

$$\kappa = \min \left\{ \begin{array}{l} \frac{c_y}{b_w} \\ \frac{b_s}{b_w} \end{array} \right. \quad (3.32)$$

in which:

$c_y$  the width of the loaded area;  
 $b_w$  the member width;  
 $b_s$  the support width.

For very large values of  $\kappa$ , greater than about 0,8, the punching crack at 45 degrees would intercept the edge of the member. In this case, a continuous punching perimeter cannot form around the loaded area and a one-way shear mechanism will govern. The calculations are based on the Canadian Code (Fig. 3.87).

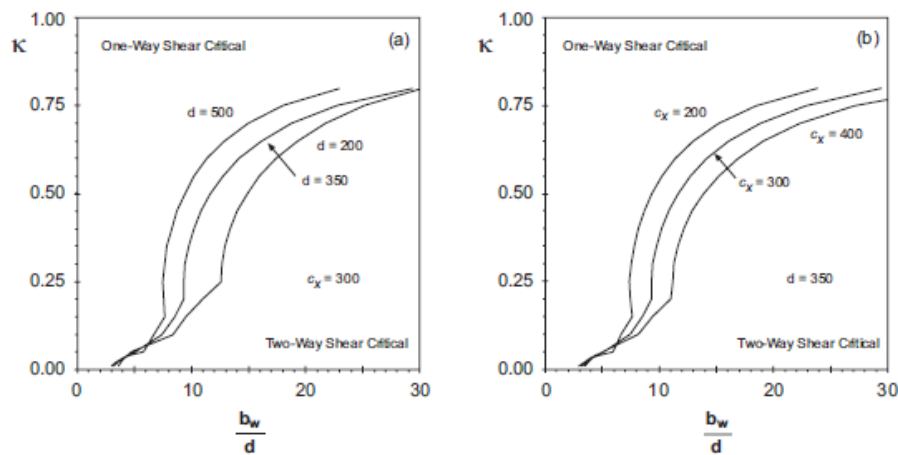


Fig. 3.87: Failure mode prediction for  $\kappa$  values (Lubell, 2006).

Hawkins and Mitchell (1979) studied one-way shear action in slabs. These results suggest that the beam shear formula is not appropriate for slabs and that the variation in shear capacity with reinforcement ratio is small for slabs. All specimens had depths of 178mm or less. It could be argued, however, that these results lie within the scatter observed for beams, Fig. 5.7, and that not enough test data are presented to conclude this.



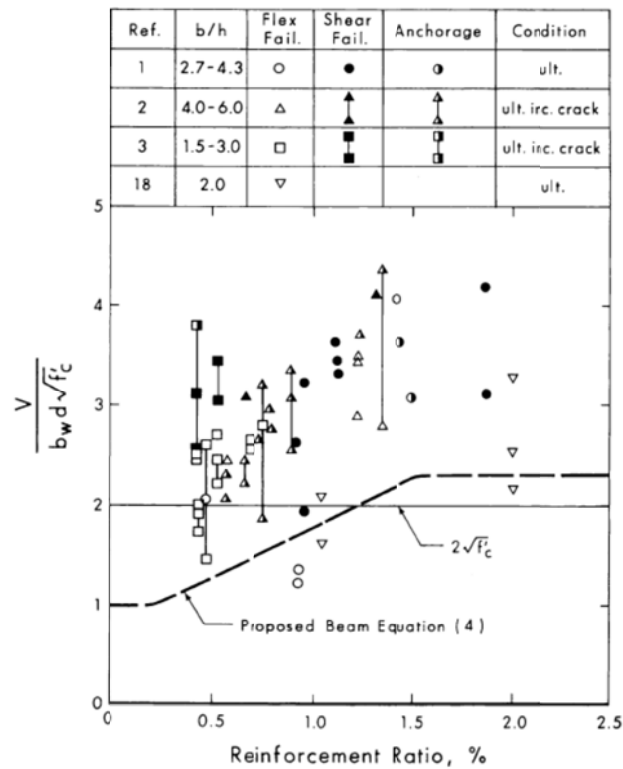


Fig. 3.88: Wide beam shear capacity of slabs (in US units), Hawkins and Mitchell (1979).

Olonisakin and Alexander (1999) measured the force gradient in one-way and two-way slabs and found that the values are very similar. According to the authors, this suggests that there ought to be a fundamental link between one- and two-way shear. Fernandez Ruiz et al. (2009) suggest using a modified punching perimeter for cases in between one-way and two-way shear, Fig. 3.89.

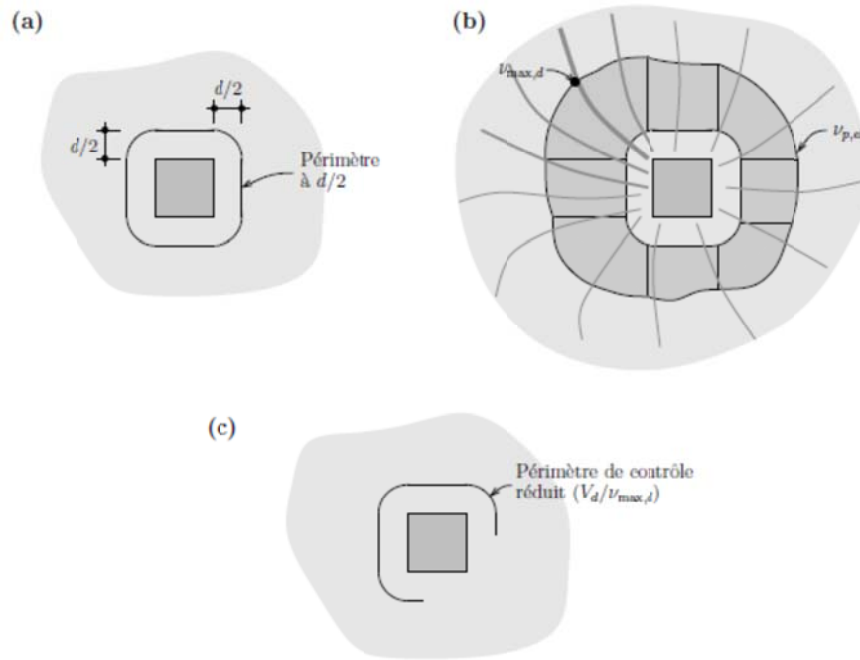


Fig. 3.89: Determination of the length of the control perimeter based on a linear elastic shear field: (a) reference control perimeter; (b) field of shear force and redistribution of the shear force perpendicularly to the reference perimeter and the maximum value; (c) suggested reduced control perimeter. (Fernandez Ruiz et al., 2009).

An example of a punching failure with some one-way shear distress is shown in Fig. 3.90.

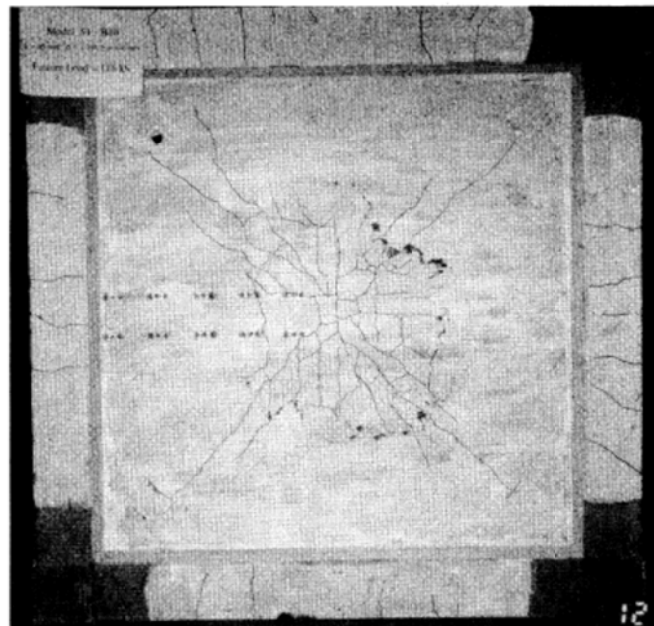


Fig. 3.90: Slab tested by Kuang and Morley (1992).

### 3.2.3. Effective width in wide beams

Typically, the effective width is determined from the stress distribution in the slab (Goldbeck and Smith, 1916; Goldbeck, 1917). For flexure, the effective width is defined such that the resisting moment due to the total maximum fiber stress uniformly distributed over this width equals the resisting moment due to the variable fiber stresses over the whole slab, Fig. 3.91.

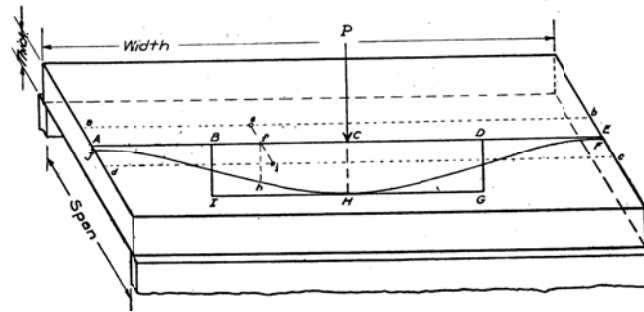


Fig. 3.91: Diagram showing the assumed conditions in slab under load, Goldbeck (1917).

The moment distribution can be approached in different ways, with elastic conditions usually on the safe side (Ferguson, Breen and Jirsa, 1988). Elastic solutions for the moments in the center of a slab due to a wheel load at any location were developed by Westergaard, 1930 and serve as a basis for the AASHTO effective widths. Amer, Arockiasamy and Shahawy (1999) developed a simplified formula based on the flexural capacity to calculate the effective width for slab bridges under a concentrated wheel load:

$$E = 2,10 + 0,23L \leq \frac{W}{N_L} \quad (3.33)$$

in which:

- $E$  the equivalent width over which the truck load is assumed to be uniformly distributed (m);
- $L$  the span length (m);
- $W$  the physical edge-to-edge width of the bridge
- $N_L$  the number of design lanes.

For shear, however, comparable approaches are not available.

### 3.2.3.1 Observations and measurements with regard to effective width

Zokaie (1992) writes: "..., very little has been reported on shear distribution factors or distribution factors for bridges other than beam-and-slab." For slab bridges, it only reads: "According to the AASHTO specifications, slab bridges are adequate for shear if they are designed for moment." Ferguson, Breen and Jirsa (1988) wrote: "The effective width for shear would call for the concentrated load near the support that would give less slab deflection and a much reduced effective width... Although there are limited data about reaction distribution, it is difficult to imagine a diagonal tension failure that would involve less than a width of four to five times the slab thickness." The load spreading is three-dimensionally shown in Fig. 3.92 (Lubell, 2006).

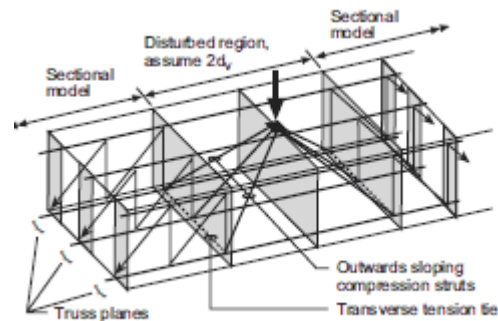


Fig. 3.92: Load spreading from point load (Lubell, 2006).

Leonhardt and Walther (1964) tested a series of 500mm wide slab strips under 4-point bending. One of the applied loads was a line load across the full member width, while the other represented a concentrated load through a plate approximately 16% of the specimen width. Both supports were across the full specimen width. It is noted that 7 of the 9 specimens that were reported to fail in shear did so on the side with the concentrated load. This suggests that the shear capacity decreased as the loaded width to specimen width ( $c_y/b_w$ ) ratio decreased, but the influence was, according to Lubell, (2006) not much more than typical laboratory scatter.

Zheng et al. (2010) developed an expression for the effective slab width subjected to arching forces based on non-linear finite elements calculations. The effective depth (position of reinforcement), depth of bridge deck, the concrete compressive strength and the loading styles were found not to influence the effective width. The main influence was found to be the size of the loaded area:  $c_x$  and  $c_y$  as shown in Fig. 3.93. The  $a/d$  ratio used for these calculations was  $\approx 9$ .

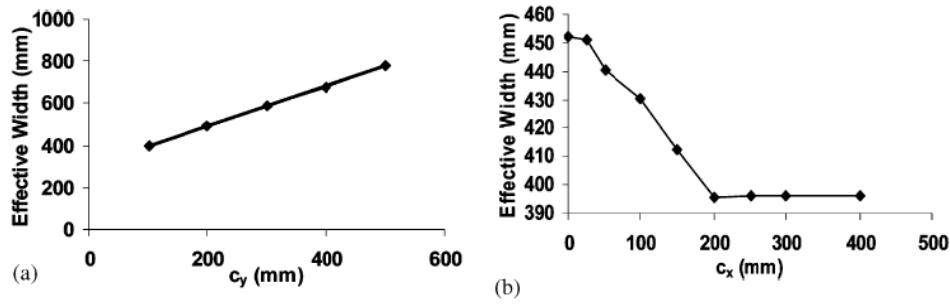


Fig. 3.93: Influence of  $c_x$  and  $c_y$  of the loaded area on the effective width (Zheng et al., 2010).

Lubell, Bentz and Collins (2008) tested slabs on narrow supports and concluded that the shear capacity is reduced when the support or load width is narrower than the width of the specimen. A reduction factor  $\beta_L$  was introduced:

$$\beta_L = 0,7 + 0,3\kappa$$

$$\kappa = \min\left(\frac{b_{load}}{b_w}, \frac{b_{sup}}{b_w}\right) \quad (3.34)$$

in which

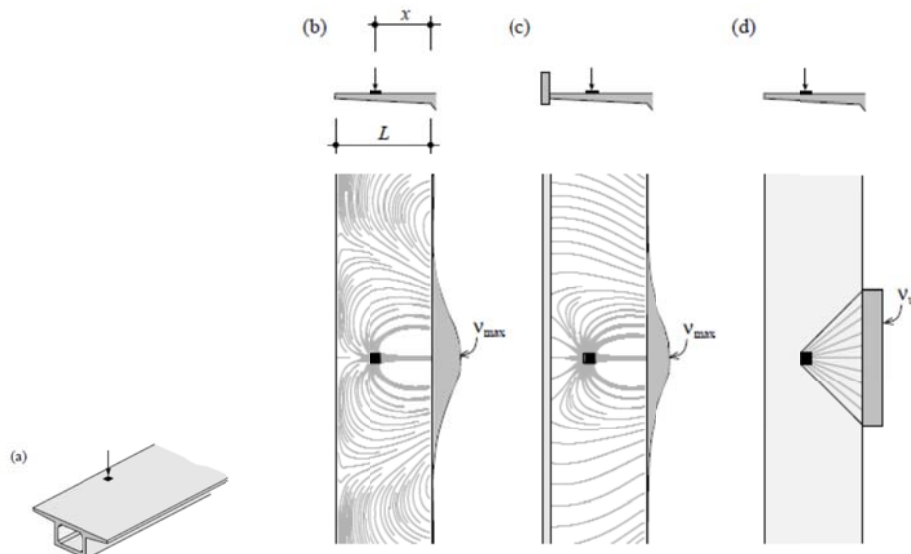
$b_{load}$  the width of the load;

$b_w$  the total width;

$b_{sup}$  the width of the support.

Fernandez Ruiz et al. (2009) show how the shear flow and thus the effective width can be influenced by conditions such as the presence of a parapet, Fig. 3.94.

Calculations for this case in Fig. 3.94(e) also showed that the 45° load spreading method underestimates the shear force at the fixed end (governing value for design).



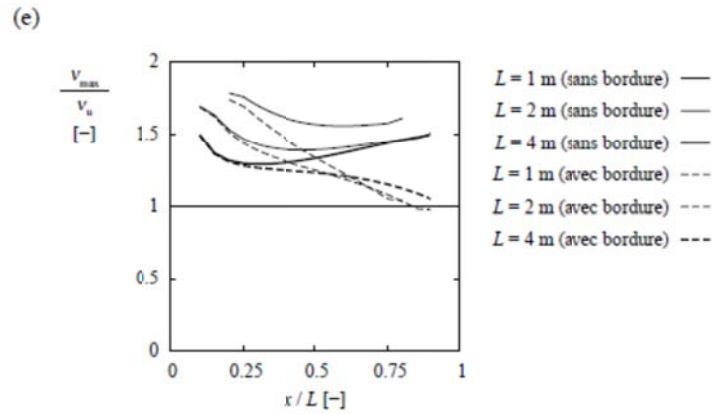


Fig. 3.94: Shear force transfer for a road slab under concentrated load: (a) considered case, (b) principal directions of the shear force in a cantilever without parapet; (c) with parapet (0,9m x 0,3m); (d) force transfer assuming a 45° load spreading; (e) comparison of shear forces for cases b, c, and d. (Fernandez Ruiz et al., 2009).

Hegger and Reißer (2011) calculated the effective width based on the measured strains in the direction of the width of the slab, which leads to a lower bound for the effective width. The results for the effective width are given in Table 3.4. The authors give two possible reasons why the effective width for  $b = 350\text{cm}$  is larger than the effective width for  $b = 250\text{cm}$ : (1) the possible scatter in the concrete strength, and (2) larger effect of the confining action of the neighboring material in the widest slab.

Table 3.4: Determination of effective width (Hegger and Reißer 2011).

Versuch		$\max \sigma_{s,SL2}$	$m_{SL2}$	$F_{m,SL2}$	$M_{calc,SL2}$	$b_{eff,M}$
$b$ [cm]		N/mm <sup>2</sup>	kNm/m	kN	kNm	m
50	2. TV	427,7	218,1	194	116	0,53
50_W	1. TV	492,7	251,3	183	130	0,52
	2. TV	475,9	242,7	215	129	0,53
150	1. TV	488,3	249,0	543	387	1,55
	2. TV	470,6	240,0	638	383	1,60
250	1. TV	400,0	204,0	658	469	2,30
	2. TV	477,8	243,7	780	468	1,92
350	1. TV	454,6	231,8	881	628	2,71
	2. TV	423,3	215,9	980	588	2,72

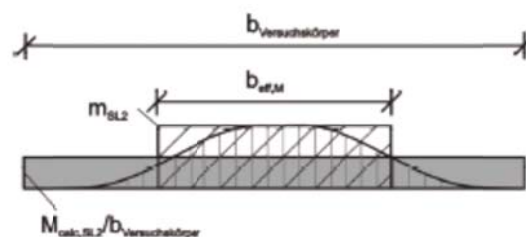


Fig. 3.95: Calculation of the effective width (Hegger and Reißer 2011).

It was observed during testing that the slabs of  $b = 50\text{cm}$  and  $150\text{cm}$  showed straight cracks on the bottom while the slabs of  $b = 250\text{cm}$  and  $350\text{cm}$  showed cracks inclining towards the support, indicating two-way action, as shown in Fig. 3.96. For  $b = 50\text{cm}$  and  $150\text{cm}$  the reported failure modes are beam shear failure. For  $b = 250\text{cm}$  the shear crack developed at the inside of the slab, and was only visible at the side faces of the slab after attaining the maximum load and was categorized by the authors as a secondary failure. It was also remarked that the shear crack crossed the flexural cracks and could not have developed at the side face as a flexure-shear crack. For  $b = 350\text{cm}$  no shear crack was visible at the side and the critical shear crack had developed fully at the inside of the slab. The authors quantify  $b_{eff}$  to be smaller than  $250\text{cm}$  since for this width inclined cracks at the bottom face were visible. However, for  $b = 250\text{cm}$  a shear crack was still visible at the side face and between  $b = 250\text{cm}$  and  $b = 350\text{cm}$  an increase in ultimate load was still observed. The authors also point out that the shear capacity of slabs  $q$  (in  $\text{kN/m}$ ) is smaller than for beams. The authors, however, used the entire width of the specimen to calculate  $q$ . The transition of beam-to-slab bearing behaviour is assumed to be between  $1,5\text{m}$  and  $2,5\text{m}$ , indicated by the failure behavior, the crack development, the load-deformation behavior and the principal stresses on the top surface.

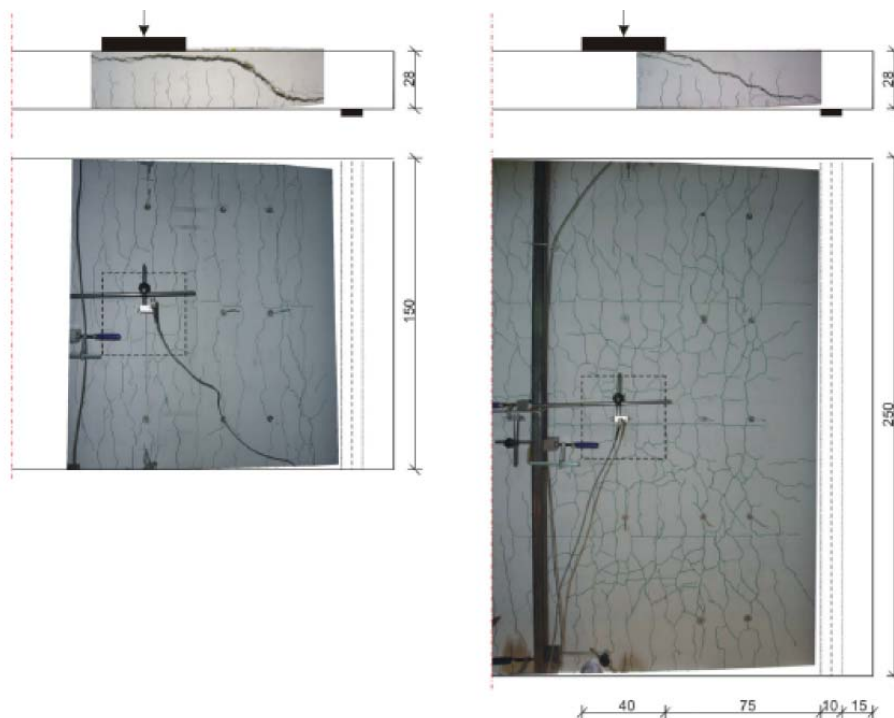


Fig. 3.96: Cracking patterns of  $b = 150$ , 2.TV and  $b = 250$ , 2.TV (Hegger and Reißer 2011).

To determine the effective width in an experiment, Hegger and Reißen (2011) defined  $b_{eq,exp}$  which is the experimental equivalent width:

$$b_{eq,exp} = \frac{V_{F,u} - V_{G,l}}{v_{Rm,ct} - v_g} \quad (3.35)$$

With

$V_{F,u}$  the experimental maximum shear force

$V_{G,l}$  the dead weight of the loading plate

$v_{Rm,ct}$  the mean value of the shear resistance according to EN 1992-1-1:2005 divided by the full specimen width

$v_g$  the shear forces over the width due to the dead load of the specimen.

For increasing specimen widths, the results of  $b_{eq,exp}$  are shown in Fig. 3.97, which indicated the full activation of the width respectively a beam-bearing behavior when  $b \leq 1,5\text{m}$ . In contrary, the equivalent width of the specimens with width  $b \geq 2,5\text{m}$  is smaller than the actual slab width indicating that not the full width of the specimens has been activated to carry the loads.

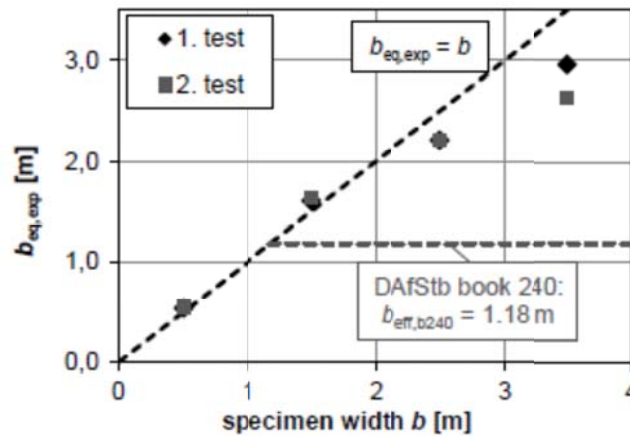


Fig. 3.97: Experimental equivalent widths  $b_{eq,exp}$  dependent on the specimen width.

The equivalent width and thus the shear resistance increase with an increasing slab width, span and transverse reinforcement ratio in the tension zone due to the higher potential for load redistribution, and it decreases with increasing shear span to depth ratio due to the decreasing influence of the direct compression strut. The equivalent width was then described as:

$$b_{eq} = b \cdot \lambda_b \cdot \lambda_{pQ} \cdot \lambda_l \cdot \lambda_{a/d} \quad (3.36)$$

with

$\lambda_b$  a factor to consider the slab width  $b$ , according to Table 3.5,



$\lambda_{pQ}$  a factor to consider the transverse reinforcement ratio in the tension zone according to Table 3.6,

$\lambda_l$  a factor to consider the span length according to Table 3.6,

$\lambda_{a/d}$  a factor to consider the shear span to depth ratio:

$$\lambda_{a/d} = 1,8 - 0,19 \frac{a}{d} \text{ for } 2,91 \leq \frac{a}{d} \leq 5,41 \quad (3.37)$$

Table 3.5: Factor  $\lambda_b$  due to variation of slab width  $b$

$b$	$\leq 1.5$	2.5	3.5	4.5	5.5	6.5	7.5	$\geq 8.5$
$\lambda_b$	1.0	0.92	0.79	0.65	0.56	0.48	0.42	$3.2/b$

Table 3.6: Factors  $\lambda_{pQ}$  and  $\lambda_l$  due to variation of transverse reinforcement ratio in the tension zone and span.

transverse reinforcement ratio $\rho_Q$	$\lambda_{pQ}$	span $l$	$\lambda_l$
%	-	m	-
0	0.74	2	0.89
0.115	0.87	3	0.96
0.23	0.95	4	1
0.47	1.0	5	1.03
0.7	1.04	$\geq 6$	1.04

In a series of computer models, the effective width was determined over several sections between the concentrated load and the support,

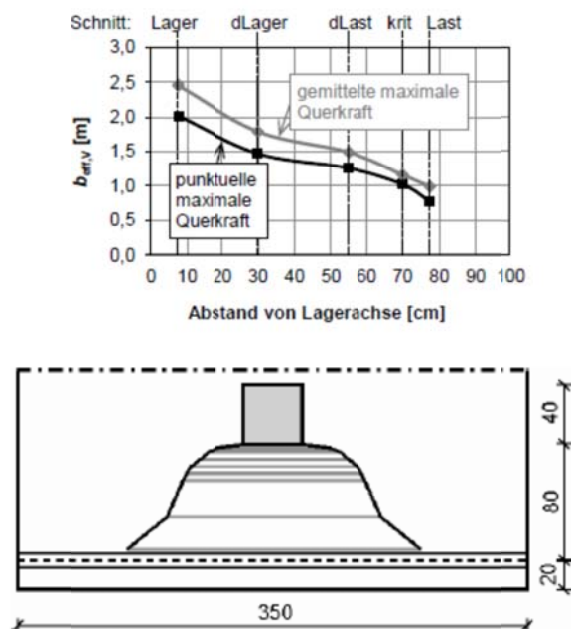


Fig. 3.98: Effective width for a case with  $b = 350\text{cm}$ , C30/37 as a function of the considered cross-section and top view.

### 3.2.3.2 Design methods for effective width

In Dutch practice, a  $45^\circ$  load spreading is used (Fig. 3.99(a)) and in French practice the load spreading is taken from the farthest end of the load (Fig. 3.99(b)).

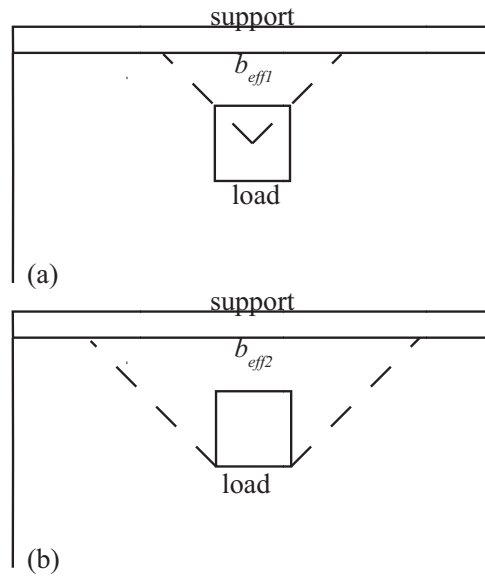


Fig. 3.99: (a) Load spreading under  $45^\circ$  as used in Dutch practice, (b) Load spreading as used in French practice, Chauvel et al. (2007).

In German practice (DAfStB Heft 240), the theoretical effective width for a slab as:

$$b_{eff,V} = t_y + 0,5x \leq b \quad (3.38)$$

$$\text{valid for } \begin{cases} 0 < x < l \\ t_y \leq 0,8l \text{ with } t_y = b_0 + 2h_1 + h \\ t_x \leq l \end{cases}$$

and for a cantilever:

$$b_{eff,V} = t_y + 0,3x \leq b \quad (3.39)$$

$$\text{valid for } \begin{cases} 0,2l_k < x < l_k \\ 0,2l_k < t_y < 0,4l_k \text{ with } t_y = b_0 + 2h_1 + h \\ t_x \leq 0,2l_k \end{cases}$$

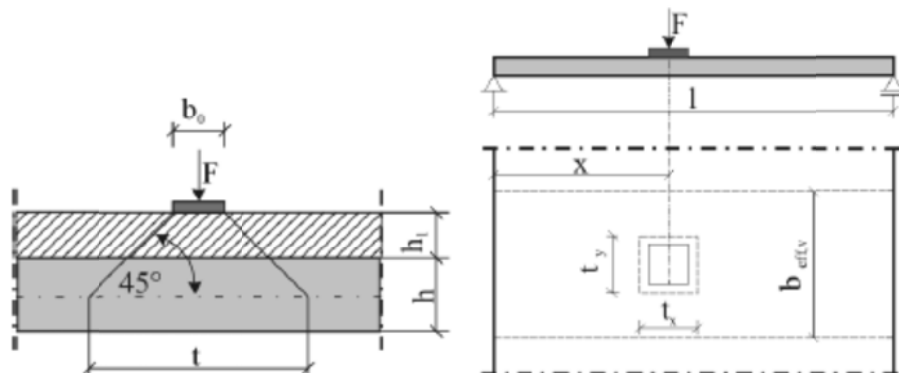


Fig. 3.100: Definition of width  $t$  for load transfer and effective width  $b_{eff,V}$  for single span beams (Reißen and Hegger, 2011).

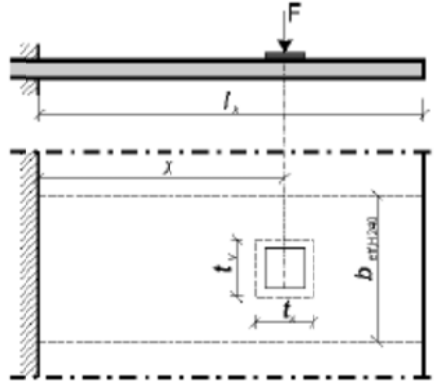


Fig. 3.101: Definitions of width  $t$  for load transfer and effective width  $b_{eff,V}$  for cantilever (Reißen and Hegger, 2011).

Taylor, Rankin and Cleland (2003) take the effective width as a measure for the region in which the arching force is present  $b_{eff} = L_e + h = a_v + h$  ( $L_e$  = the effective span =  $a_v$ ;  $h$  = the depth of the slab), while the outside region is assumed to attribute to the external restraint, Fig. 3.102.

Zheng et al. (2010) determined the effective width to be:

$$b_{eff} = c_y + L(1 - r_{cp}) \tan(\Phi) \quad (3.40)$$

$$\Phi = 23,3r_{cp} + 35,1$$

in which

$r_{cp}$  the ratio of  $c_x$  and the span of the bridge deck  
 $= 0,4$  when  $r_{cp} > 0,4$ .

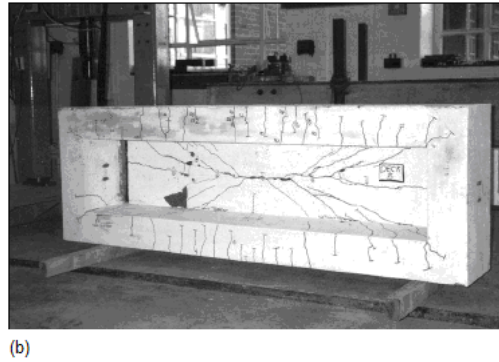
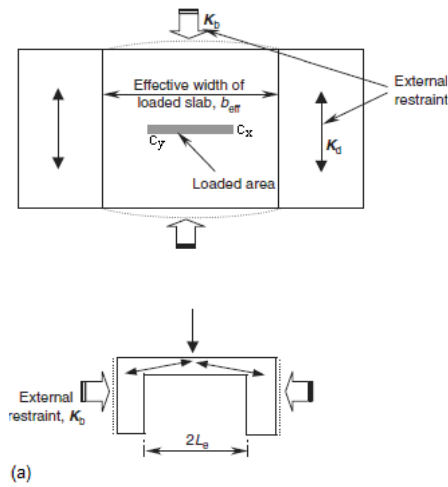


Fig. 3.102: (a) Typical restraint model; (b) Typical crack pattern in experiment (modified from Taylor, Rankin and Cleland, 2003).

Diaz de Cossio (in a discussion on the ACI-ASCE Committee 326, 1962) calculated the effective width  $s'$  as half the perimeter of a critical section taken at a certain distance from the load plate (optimal results were obtained for a distance  $0,75d$ ), not exceeding the total slab width, Fig. 3.103. According to Lubell (2006) however, there is an insufficient range of data to determine whether using the enlarged perimeter or simply  $b_w d$  captures the relevant influence.

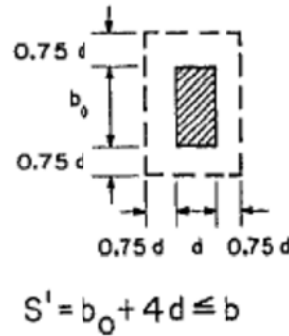


Fig. 3.103: Determination of effective width by Diaz de Cossio, 1962.

The Swedish Code BBK79 includes specific recommendations for the effective widths of slab to be used in calculating wide beam shear strengths at concentrated loads. The greater of the following two values is used as effective width:

$$\begin{aligned} b_{eff1} &= c_l + 7d_l \\ b_{eff2} &= 0,65(c_l + c_t) + 10,65d_l \end{aligned} \quad (3.41)$$

in which:

- $c_l$  dimension of the loaded area parallel to the span of the slab;
- $c_t$  dimension of the loaded area perpendicular to the span of the slab;
- $d_l$  effective depth of longitudinal bars.

Graf (1933) suggests an effective width  $b_{eff} = 5d$  and Regan and Rezai-Jorabi (1988) suggest an effective width  $b_{eff} = 3,5a$  with  $a$  the shear span from the center of the load to the center of the support.

Rombach and Velasco (2005) developed the following formula for the effective width of a cantilever deck assuming a 400mm x 400mm wheel load:

$$b_{eff,v} = 0,60 + 0,95h + 1,15a \quad (3.42)$$

This formula is extended for the case of a load which is not 400mm x 400mm:

$$b_{eff,v} = 0,20 + b_{0,y} + 0,95h + 1,15a + 0,09 \cdot \frac{m_{VK,L}}{z_{VK,L} f_{ck}} \quad (3.43)$$

with

$b_{0,y}$  the width of the loading plate perpendicular to the main span direction

$h$  slab depth in the middle of the load

$m_{VK,L}$  the moment at the front side of the load as a result of all loads except for the concentrated load,

$z_{VK,L} = 0,9 \cdot d_{VK,L}$

A comparison between Eq. (3.42), German practice and the 45° load spreading is shown in Fig. 3.104.

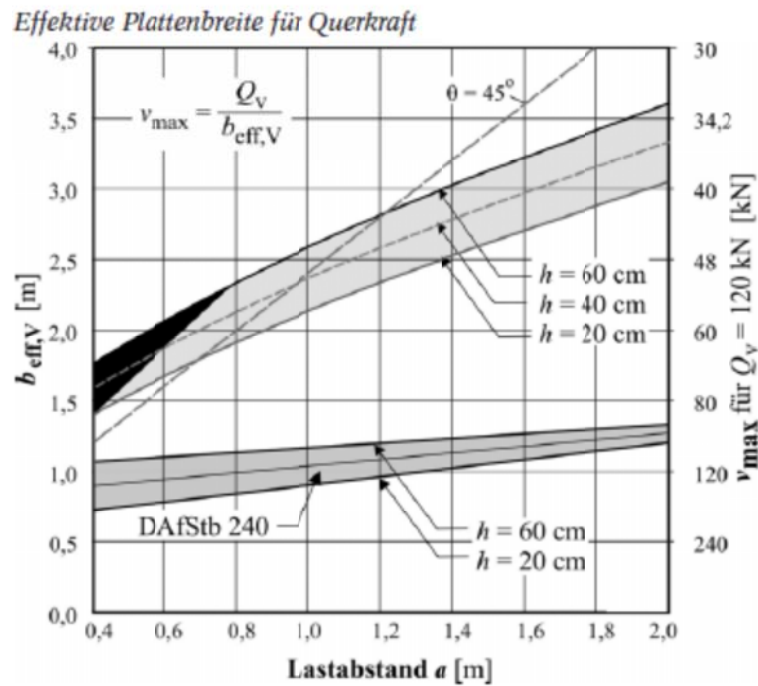


Fig. 3.104: Effective width  $b_{eff}$  and greatest shear force  $v_{max}$  for a wheel load of  $Q_v = 120\text{kN}$  (rombach and Velasco, 2005).

Based on experimental results, Hegger and Reißer (2011) suggested the following equation for the effective width of a cantilever deck:

$$b_{effv,R,H} = 0,2 + b_{0,y} + 0,95h + 1,15a + 0,09 \frac{m_{fl}}{z_{fl} \cdot f_{ck}} \quad (3.44)$$

with

$b_{0,y}$  the width of the loading plate perpendicular to the main load-bearing direction of the cantilever slab [m],

$h$  the height of the slab at the center of the load,

$a$  the distance between the center of the load and the clamped edge of the cantilever slab [m],

$m_{f,l}$	the moment at the front edge of the load plate due to all loads except the considered single load [kNm/m],
$z_{f,l}$	the inner leverarm at the front edge of the load plate with $z_{f,l} = 0,9d_{f,l}$ ,
$f_{ck}$	the characteristic compression strength.

### 3.3. Models for shear

#### 3.3.1. Compression field theory models

##### 3.3.1.1 Development of the compression field theory

Compression field approaches are inspired by the tension field theory from aerospace engineering developed by Wagner in 1929 to study the post-buckling shear resistance of thin webbed metal beams. After buckling the metal cannot resist compression and that shear stresses are carried by a field of diagonal tension. The angle of the diagonal tensile stresses should equal the principal tensile strain from deformations.

The diagonal compression field theory was originally developed for concrete in pure torsion (no warping) by Mitchell and Collins (1974). After cracking, the theory of elasticity is no longer applicable, requiring a model for cracked concrete. In the original compression field theory the shear stress was used to find the stresses in the steel and the concrete (inclined at a certain angle  $\theta$  or  $\alpha$ ), which were combined to stress-strain relationships for cracked concrete. After cracking the concrete was assumed not to carry tension, resulting in a field of diagonal compression. The angle of diagonal compression  $\theta$  (or  $\alpha$ ) was found with an energy criterion: the internal energy will be a minimum if the external work done, and hence for a given load the external displacement, is a minimum. The crack pattern is idealized as a series of parallel cracks all occurring at an angle  $\theta$  (or  $\alpha$ ) to the longitudinal direction.

These principles were then applied to reinforced concrete members in shear with shear reinforcement (Collins, 1978). The strains were analyzed with Mohr's circle, Fig. 3.106, and the stresses were analyzed with Mohr's circle in pure compression, Fig. 3.105. The method uses a relation between *average* strains and *average* stresses. These average strains are measured over a base length that is several times the crack spacing. The relations between the strains are based on compatibility requirements. For the diagonally cracked concrete it was assumed that the direction subjected to the largest average compressive stress will coincide with the direction subjected to the largest average compressive strain. When studying stress-strain distributions, it is

observed that while the average longitudinal concrete stress must be compressive, the average longitudinal strain may be tensile. Thus it is not possible to directly relate the average concrete stress in this direction by means of the usual stress-strain relationship for uncracked concrete. The procedure initially was carried out in the following way:

1. Estimate the angle of diagonal compression.
2. Calculate the shear stress  $v$  from the known loads.
3. Find the transverse compression in the concrete.
4. Find the tensile strains in the transverse steel.
5. Use the stress-strain relations for steel.
6. Find the transverse strain in the steel.
7. Similarly, find the longitudinal strain and the principal compressive strain in the steel.
8. Find the angle of inclination of the principal compressive strain and compare to the estimate.

The ultimate shear capacity could be found by fixing the maximum possible stress to the point of yield of the longitudinal steel. Alternatively, the limiting concrete compressive strength (which does not equal the uniaxial concrete compressive strength) may be reached. It should be kept in mind that this compressive stress must be transmitted across cracked and severely deformed concrete (Collins and Mitchell, 1980).

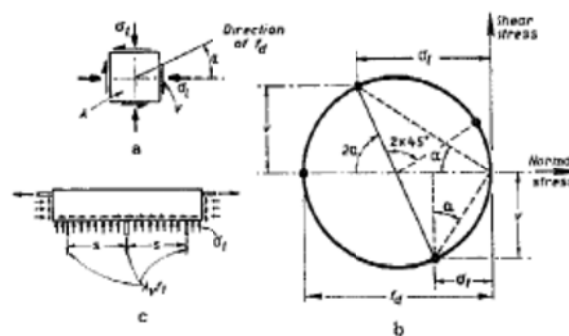


Fig. 3.105: Equilibrium conditions for average stresses in concrete (Collins, 1978).

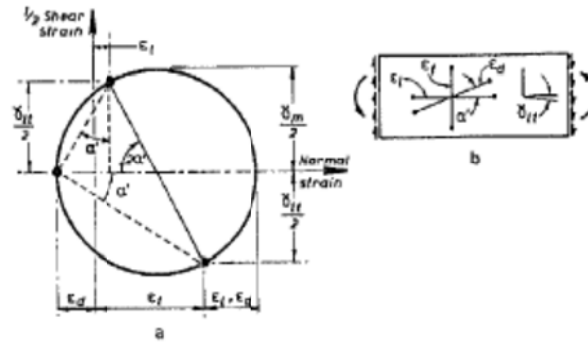


Fig. 3.106: Compatibility conditions for average strains in concrete (Collins, 1978).

When it was found that the tensile stresses between the cracks after cracking contribute to the shear capacity, the Modified Compression Field Theory (Vecchio and Collins, 1986) was developed. It is based on the response of rectangular reinforced concrete elements (“panels”) subjected to in-plane shear and axial stresses. Vecchio and Collins (1986) reported the results for a number of reinforced concrete panels tested under direct shear, and combinations of shear and axial stress. The tests showed that the initial shear cracking was related to the external load ratios and could be predicted by a Mohr’s circle type of analysis. Additional load increments result in a rotation of the angle of principal stress to reflect the relative stiffness provided by the reinforcement in each direction, with new cracks forming parallel to the new angle of principal compression. When reinforcement in one direction yielded at a crack, the changing relative stiffness would cause further rotation of the principal stress directions. The theory is based on the following assumptions:

1. For each strain state there exists only one corresponding stress state; situations in which the influence of loading history is significant cannot be treated.
2. Stresses and strains can be considered in terms of average values when taken over areas or distances large enough to include several cracks.
3. The concrete and reinforcement are perfectly bonded together at the boundaries of the element.
4. The longitudinal and transverse reinforcing bars are uniformly distributed over the element.

In reality, cracked reinforced concrete transmits load in a relatively complex manner involving opening or closing of pre-existing cracks, formation of new cracks, interface shear transfer at rough crack surfaces and significant variation of the stresses in reinforcing bars due to bond, with the higher steel stresses occurring at crack locations. The studied strains and stresses are shown in Fig. 3.107 and Fig. 3.108.



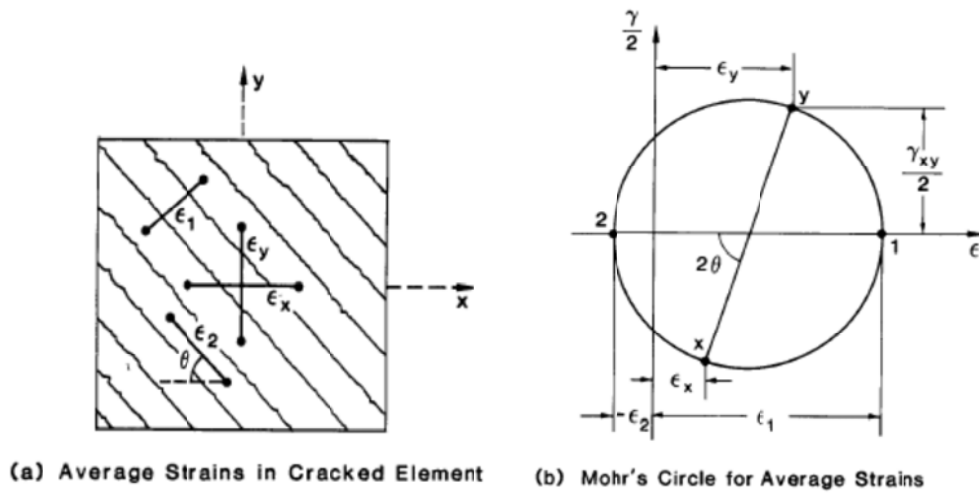


Fig. 3.107: Compatibility conditions for cracked element (Vecchio and Collins, 1986).

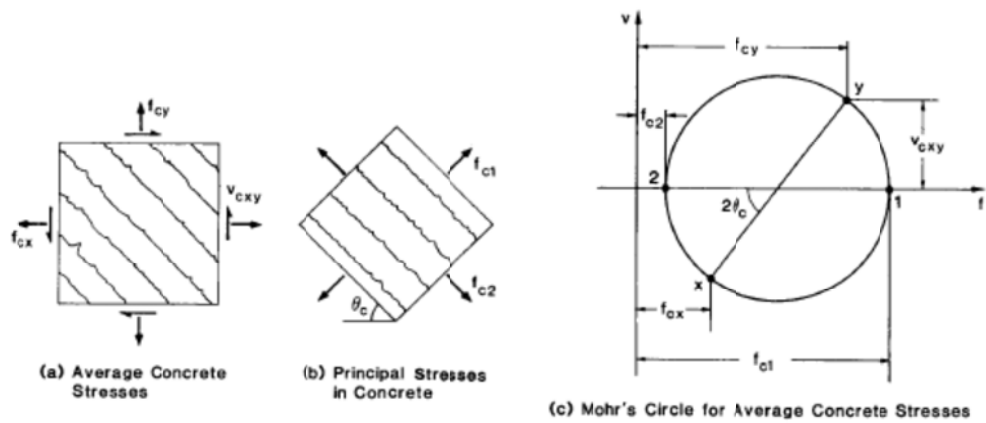
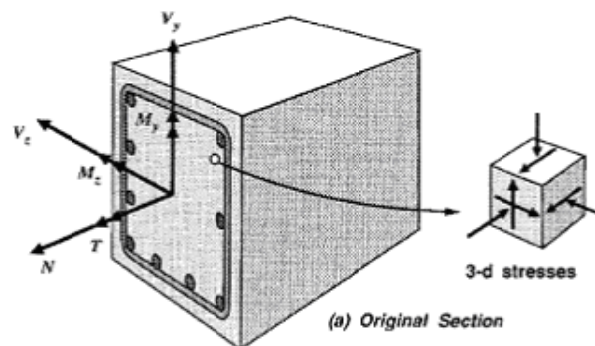


Fig. 3.108: Stresses in cracked concrete (Vecchio and Collins, 1986).

Bhide and Collins (1989) tested panels with only longitudinal reinforcement and formulated requirements for the longitudinal reinforcement to carry the increased stresses due to shear. These insights were applied to combined shear and torsion with a strut and tie model by Rahal and Collins (1995), Fig. 3.109.



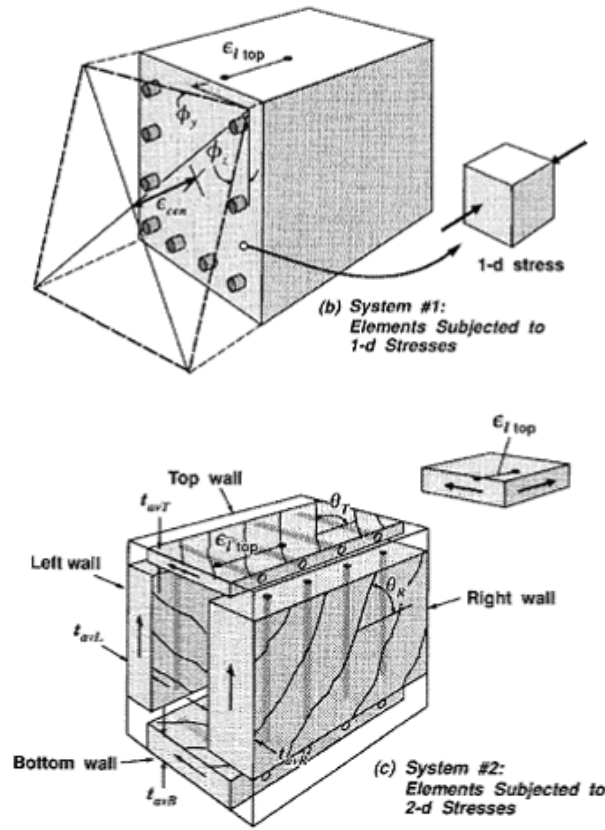


Fig. 3.109: Combined shear and torsion (Rahal and Collins, 1995).

Consequently, Adebar and Collins (1996) used the MCFT to determine the shear strength of members without transverse reinforcement by introducing concrete tension ties perpendicular to concrete compression struts. The modified compression field theory can be seen as a variable angle truss model that includes a contribution from the tensile stresses in cracked concrete. The total shear capacity can then be written as the sum of a stirrup contribution and a concrete contribution. The principal compressive stress is given by

$$f_2 = v \cot \alpha = v \cot \frac{\theta}{2} \quad (3.45)$$

and, although there can be no tension stress normal to the crack plane, a principal tensile stress

$$f_1 = v \tan \alpha = v \tan \frac{\theta}{2} \quad (3.46)$$

does exist in the concrete at an inclination of  $\theta/2$  from the normal to the crack plane. The shear stress on the crack plane (interface) is independent of the diagonal crack

inclination and is equal to the shear stress on the vertical and horizontal planes. Thus the concrete contribution can be expressed independently of the crack angle as:

$$V_c = v_{ci} b_v d_v \quad (3.47)$$

where  $v_{ci}$  is the shear stress resisted by the crack interface. The modified compression field theory, which attributes the concrete contribution  $V_c$  to the shear that can be transmitted across diagonal cracks by aggregate interlock, captures the influences of the longitudinal reinforcement.

The average principal tensile strain  $\varepsilon_I$  in the cracked concrete is used as a “damage indicator” (Collins et al., 1996). This strain controls the average tensile stress  $f_I$  in the cracked concrete, indicating the ability of the diagonally cracked concrete to carry compressive stresses  $f_2$  and the shear stress  $v_{ci}$  that can be transmitted across a crack. The principal compressive stress in the concrete  $f_2$  is related to both the principal compressive strain  $\varepsilon_2$  and the principal tensile strain  $\varepsilon_I$  in the following manner:

$$f_2 = f_{2\max} \left( \frac{2\varepsilon_2'}{\varepsilon_c'} - \left( \frac{\varepsilon_2'}{\varepsilon_c'} \right)^2 \right) \quad (3.48)$$

where

$$f_{2\max} = \frac{f_c'}{0,8 + 170\varepsilon_1} \leq f_c' \quad (3.49)$$

$$\varepsilon_2 = -0,002 \left( 1 - \sqrt{1 - \frac{f_2}{f_{2\max}}} \right) \quad (3.50)$$

and  $\varepsilon_c'$  is taken as 0,002. After cracking, the principal tensile stress in the concrete  $f_I$  is related to the principal tensile strain  $\varepsilon_I$  as follows:

$$f_I = \frac{f_{cr}}{1 + \sqrt{500\varepsilon_1}} \quad (3.51)$$

where the cracking stress  $f_{cr}$  can be taken as  $0,33\sqrt{f_c'}$ . For large values of  $\varepsilon_I$  the cracks will become wide and the magnitude of  $f_I$  will be controlled by the yielding of the reinforcement at the crack and by the ability to transmit shear stresses  $v_{ci}$  across the cracked interface.

For members without stirrups, the ability of the cracked concrete to transmit shear is primarily governed by the width of the diagonal cracks. Hence, for a given value of  $\varepsilon_I$  the shear strength will be a function of the crack spacing, with more widely spaced

cracks resulting in lower shear capacities. The stresses carried across a crack (Fig. 3.110) are based on Walraven's work (1981), resulting in the following relationship:

$$v_{ci} = 0,18v_{ci\max} + 1,64f_{ci} - 0,82\frac{f_{ci}^2}{v_{ci\max}} \quad (3.52)$$

with

$$v_{ci\max} = \frac{\sqrt{-f_c'}}{0,31 + 24\frac{w}{a + 16}} \quad (3.53)$$

in which  $a$  is the maximum aggregate size in mm and the stresses are in MPa. The crack width to be used in Eq. (3.53) should be the average crack width over the crack surface. It can be taken as the product of the principal tensile strain and the crack spacing  $s_\theta$ :

$$w = \varepsilon_1 s_\theta \quad \text{with} \quad s_\theta = \frac{1}{\frac{\sin \theta}{s_{mx}} + \frac{\cos \theta}{s_{my}}} \quad (3.54)$$

in which  $s_{mx}$  and  $s_{my}$  are the indicators of the crack control characteristics of the x-reinforcement and the y-reinforcement respectively. The crack spacing can be estimated as (Bhinde and Collins, 1989):

$$s_m = s \left( c + \frac{s}{10} \right) + 0,1 \frac{d_b}{\rho} \quad (3.55)$$

with  $s$  the spacing between bars.

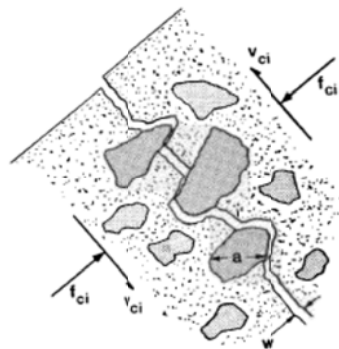


Fig. 3.110: Transmitting shear stresses across crack by aggregate interlock (Vecchio and Collins, 1986).

As the tensile straining of the concrete increases, the shear that can be resisted by tensile stresses in the concrete  $V_c$  decreases. The resulting compression softening and the tension softening are shown in Fig. 3.111.

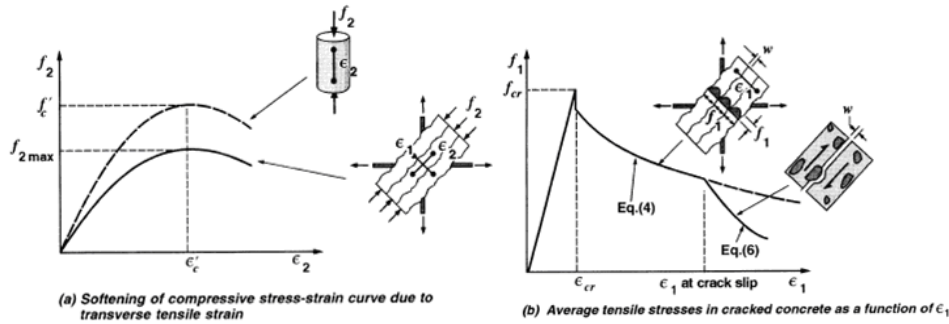


Fig. 3.111: Stress-strain relationships for cracked concrete (Collins et al., 1996).

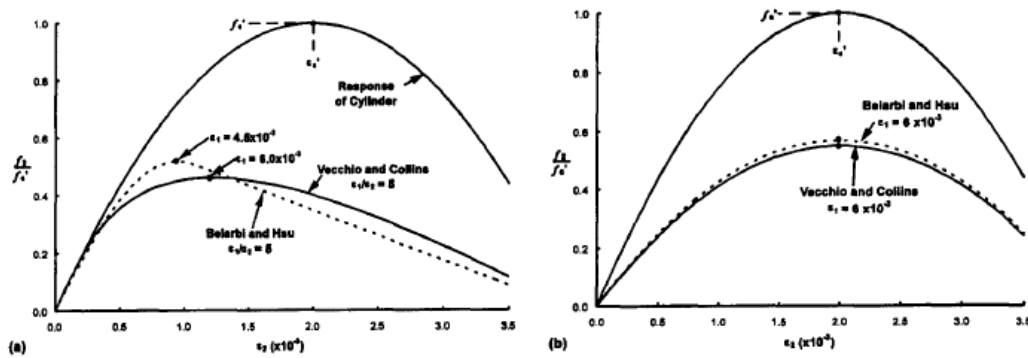


Fig. 3.112: Compressive stress – compressive strain relationships for diagonally cracked concrete: (a) proportional loading  $\epsilon_1$  and  $\epsilon_2$  increased simultaneously; (b) sequential loading,  $\epsilon_1$  applied first, then  $\epsilon_2$  increased. (ACI-ASCE Committee 426, 1998).

Softened concrete behavior is also described by Hsu et al. (1987). A three-dimensional panel tester has been developed at the University of Houston and currently the softening behavior of concrete under triaxial loading is studied (Labib et al., 2009), to expand the scope of smeared crack models to account for three-dimensional load effects.

### 3.3.1.2 Design method: modified compression field theory

The Modified Compression Field Theory (MCFT) is used for one-way shear only. It is the basis for the provisions of CSA and AASHTO and is described as a design method, for example, in Collins, Mitchell and Bentz (2008). The MCFT considers cracked reinforced concrete as a new material, with constitutive properties reflecting tension stiffening of the average concrete response in the principal tension direction and compression softening of the peak compressive resistance in the principal direction due to the parallel tension cracks. The design equations of this method are based on equilibrium equations, geometric equations and a stress-strain relationship, Fig. 3.113. The design method based on the MCFT is the Simplified Modified

Compression Field Theory (Bentz and Collins, 2006; Bentz et al., 2006). Dowel action is not taken into account. Three main parameters are used in this method:

1. the normalized applied shear stress  $\left(\frac{v}{f'_c}\right)$ ;
2. the longitudinal strain  $\varepsilon_x$ ; and
3. the effective crack spacing  $s_{ze}$ .

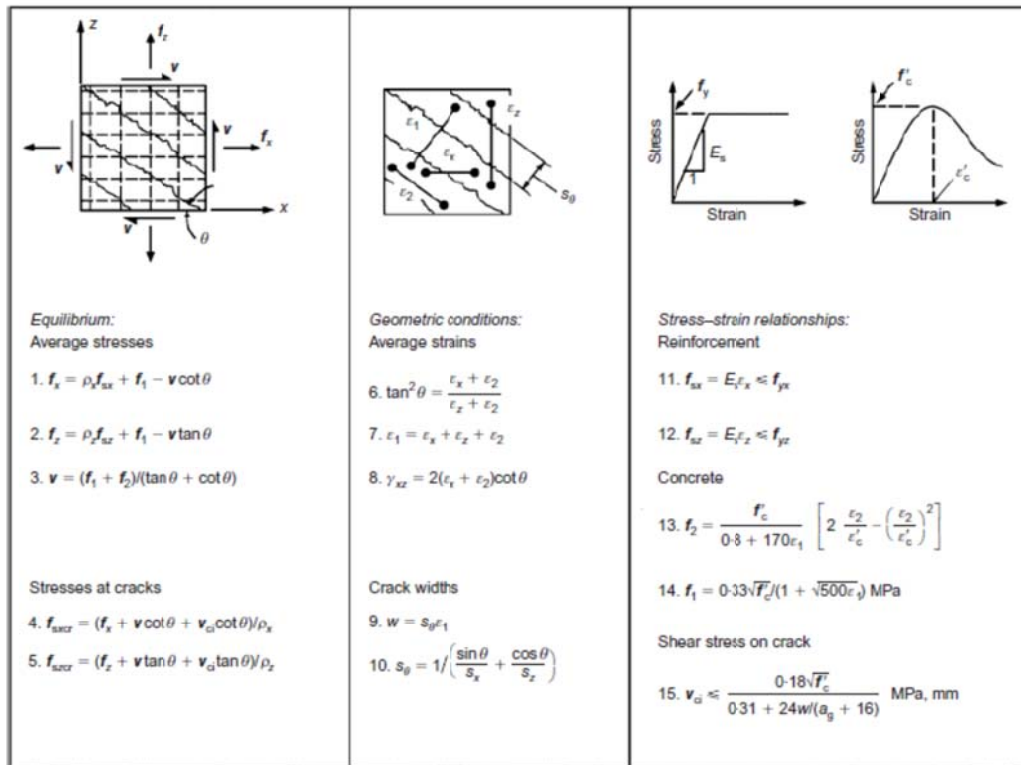


Fig. 3.113: Overview of the MCFT equations, Collins et al.(2008).

To calculate the ultimate shear capacity of a beam, the design method uses a different approach for D-regions and B-regions. In D-regions a strut and tie model is used and in B-regions the formulas are based on parameters such as the crack spacing.

In B-regions, the unfactored failure shear stress is calculated as:

$$v_n = \beta \sqrt{f'_c} + \rho_z f_y \cot \theta \leq 0.25 f'_c \quad \text{with} \quad \sqrt{f'_c} \leq 8 \text{ MPa} \quad (3.56)$$

in which the first term represents the concrete contribution and the second term the contribution of the stirrups.

The following factors are used in formula (3.56):

- $\beta$  the aggregate interlock parameter;
- $f'_c$  the concrete compressive strength in MPa;

Values for  $\beta$  and  $\theta$  for design are given in Table 3.7.

Table 3.7: Design values of  $\beta$  and  $\theta$  for members without transverse reinforcement (Rahal and Collins, 1999).

$s_x$ (mm)		Longitudinal strain, $\epsilon_x \times 1000$					
		$\leq 0.0$	$\leq 0.25$	$\leq 0.5$	$\leq 1.0$	$\leq 1.5$	$\leq 2.0$
$\leq 125$	$\beta$	0.406	0.309	0.263	0.214	0.183	0.161
	$\theta$	27°	29°	32°	34°	36°	38°
$\leq 250$	$\beta$	0.384	0.283	0.235	0.183	0.156	0.138
	$\theta$	30°	34°	37°	41°	43°	45°
$\leq 500$	$\beta$	0.359	0.248	0.201	0.153	0.127	0.108
	$\theta$	34°	39°	43°	48°	51°	54°
$\leq 1000$	$\beta$	0.335	0.212	0.163	0.118	0.095	0.080
	$\theta$	37°	45°	51°	56°	60°	63°
$\leq 2000$	$\beta$	0.306	0.171	0.126	0.084	0.064	0.052
	$\theta$	41°	53°	59°	66°	69°	72°

The aggregate interlock parameter  $\beta$  depends on the width of the cracks and the size of aggregate  $a_g$ , and consists of a strain term and a crack spacing term (also called the size effect term).

$$\beta = \frac{0,4}{1+1500\epsilon_x} \cdot \frac{1300}{1000+s_{xe}} \quad (3.57)$$

where

$\epsilon_x$  the longitudinal strain at mid-depth;

$s_{xe}$  the crack spacing.

Assuming that there is no axial load or prestressing, the longitudinal strain at mid-depth is

$$\epsilon_x = v_n \frac{1 + \frac{M}{V \cdot d_v}}{2E_s \rho_l} \quad (3.58)$$

with

$M/V$  the ratio of bending moment to shear at the section being considered;

$v_n$  the unfactored failure shear stress;

$d_v$  the flexural lever arm which can be taken as  $0,9d$ ;

$E_s$  the modulus of elasticity of the reinforcement steel;

$\rho_l$  the geometric ratio of the area of longitudinal flexural tension reinforcement to the shear area:  $\rho_l = \frac{A_s}{b_w d_v}$ ;

$b_w$  the width of the web.

The effective crack spacing is taken as

$$s_{xe} = \frac{35s_x}{15+a_g} \geq 0,85s_x \quad (3.59)$$

with

$a_g$  the aggregate size in mm;

$s_x$  the spacing of the vertical cracks near mid-depth of the member,

$$s_x = 0,9d .$$

For high strength concrete the cracks will go through the aggregate rather than around the aggregate particles leading to smoother crack surfaces with less aggregate interlock capacity. To account for this,  $a_g$  in Eq. (3.59) is taken as zero if  $f'_c$  exceeds 70 MPa and is linearly reduced to zero as  $f'_c$  goes from 60 MPa to 70 MPa.

In D-regions, for example in regions close to concentrated loads, a strut and tie model is used. The principal tensile strain  $\varepsilon_1$  in the concrete strut is

$$\varepsilon_1 = \varepsilon_s + (\varepsilon_s + 0,002) \cot^2 \theta_s \quad (3.60)$$

$\varepsilon_s$  the tensile strain in the reinforcing steel tension tie;

$\theta_s$  the angle between the strut and tie.

The crushing strength of the strut  $f_{cu}$  is then given by:

$$f_{cu} = \frac{f'_c}{0,8 + 170\varepsilon_1} \leq 0,85 f'_c \quad (3.61)$$

Wei et al. (2011) developed an improvement for the MCFT based on a linear crack width expression over the depth of the beam, leading to a size effect factor similar to Bažant and Kazemi (1991). The MCFT assumes that the aggregate interlock resistance of the complex crack geometry can be estimated at only one depth in the beam. This means that the shear strength of the section in the flexural region of a beam may be modeled by an element loaded in shear combined with axial stress. As a result, parameters such as shear stress, tension stress, compression stress, aggregate interlock stress, the angle of inclination of the compression struts and the strains corresponding to these stresses over the depth of the beam are all uniform. In reality, the crack width profile is a complex function of material properties and geometrical parameters such as the effect of the shear stresses transmitted across the crack, the presence of longitudinal steels crossing the crack and the size effect on the crack shape.

Wei et al. (2011) assumed that the shear crack width is a linear function of the depth, with zero opening at the tip and maximum opening at the bottom:

$$w(y) = w_{\max} \frac{y}{d_v} = s_{\theta} \varepsilon_{1\max} \frac{y}{d_v} = k d_v \varepsilon_{1\max} \frac{y}{d_v} = k \varepsilon_{1\max} y \quad (3.62)$$



The average aggregate interlock stress  $v_{ci}$  along the crack surface can be derived by integrating this stress along the depth and taking the average value:

$$v_{ci} = \frac{1}{d_v} \int_0^{d_v} \frac{0,18\sqrt{f_c'}}{0,31+0,686w(y)} dy = \frac{0,18\sqrt{f_c'}}{k_1 d_v} \ln \left( 1 + \frac{k_1 d_v}{0,31} \right) \quad (3.63)$$

with

$$k_1 = 0,686k \frac{\varepsilon_{sx} (1 + \cot^2 \theta) + (4 \cdot 10^{-5} \cot^4 \theta)}{1 + 0,0034 \cot^4 \theta} \quad (3.64)$$

To obtain a consistent result with that of the classic MCFT,  $k = 2,5$  is taken in Eq. (3.64). For design purposes, a simplified formula was sought. The best fit to the numerical results was found in the format of:

$$\beta = \frac{a}{\sqrt{1 + b\varepsilon_{sx} d_v}} \quad (3.65)$$

with  $a = 0,4$  and  $b = 6,25$ . This expression is similar to the size effect expression of Bažant and Kazemi (1991), leading to a simple expression for the shear capacity of beams without stirrups:

$$V = v b d_v = \frac{0,4\sqrt{f_c'} b d_v}{\sqrt{1 + 6,25\varepsilon_{sx} d_v}} \quad (3.66)$$

### 3.3.1.3 Methods based on a compression field

A similar method considering the properties of cracked concrete is the fixed-angle softened truss model (FA-STM) (Fig. 3.114), which is based on the observation that concrete struts in membrane elements under shear and normal stress remain parallel to the initial cracks. Softened equilibrium equations and compatibility equations are used. The fixed angle  $\alpha_2$  lies between the 2-axis and l-axis, Fig. 3.115. After initial cracking, the change in direction of the subsequent cracks are due to changes in the direction of the principal tensile stresses in the concrete, which, in turn, are dependent on the relative amount of steel in the longitudinal and transverse directions (Hsu, 1996). A fixed-angle softened-truss model is the only model capable of predicting the concrete contribution.

A simpler method is the rotating-angle softened-truss model (RA-STM), which is very similar to a compression field approach. The rotating angle stands for the fact that the angle of diagonal tensile stresses becomes smaller as the shear force goes up. The angle between the  $d$ -axis and the  $l$ -axis is called the rotating angle  $\alpha$ , because this

angle continues to rotate away from the fixed angle  $\alpha_2$ , Fig. 3.115. The actual angle of each new crack is observed to lie between  $\alpha$  and  $\alpha_2$ . The equilibrium equation is based on average stresses, and through compatibility average strains are obtained in combination with a softened stress-strain relationship and the correct stress-strain relationship for possible yielding at the crack. Both the RA-STM and the FA-STM adjust the average stress-average strain relationships of the reinforcement to account for increased demand on the reinforcement at the crack and bond issues between the reinforcement and the surrounding concrete (Sun and Kuchma, 2007).

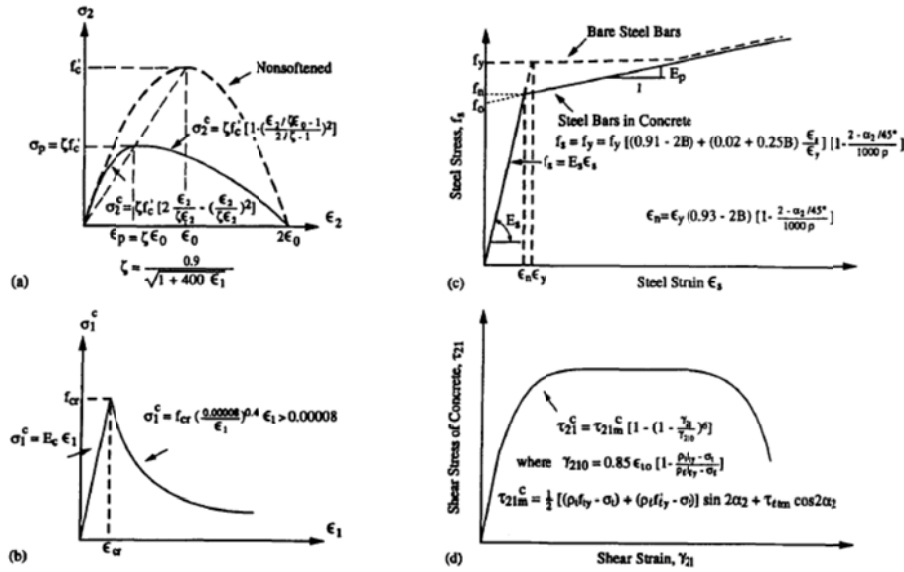


Fig. 3.114: Constitutive laws of concrete and steel for fixed-angle softened truss model: (a) softened stress-strain curve of concrete in compression; (b) average stress-strain curve of concrete in tension; (c) average stress-strain curve of steel bars in concrete; (d) average stress-strain curve of concrete in shear (ASCE-ACI committee 445, 1998).

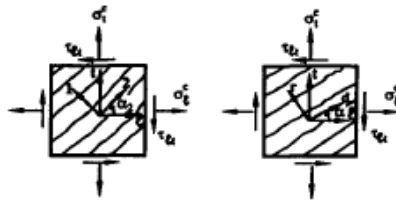


Fig. 3.115: Assumed crack direction in fixed-angle model and assumed crack direction in rotation-angle mode. (Hsu, 1996).

The cracked membrane model (Kaufmann and Marti, 1998) is another model for cracked, orthogonally reinforced concrete panels subjected to in-plane stresses. Crack faces are assumed to be stress free, able to rotate, and perpendicular to the principal tensile direction of the average strains. Tensions stiffening effects are taken into account by extending the basic concepts of the tension chord model to cracked panels.

The cracked membrane model considers maximum stresses at the crack, whereas the modified compression field approach considers average stresses in the concrete between the cracks. The experimental evidence also suggests a more drastic softening for high-strength concrete; hence  $f_c$  is supposed to be proportional to  $(f'_c)^{\frac{2}{3}}$  rather than to  $f'_c$ . Extension of the tension chord model to cracked panels eliminates the need for constitutive equations relating average stresses and average strains in tension. Thus, contrary to the modified compression field approach, crack spacing and tensile stresses in the concrete and in the reinforcing bars between the cracks can be determined from equilibrium conditions and bond shear stress-slip relationships. Concrete tensile stresses enhance the stiffness but they do not directly affect the ultimate strength; thus, the cracked membrane model reintroduces the link to limit analysis that had been lost with the modified compression field approach. As compared to the MCFT, the cracked membrane model more accurately takes tension stiffening into account, but similarly simplified the treatment of cracks.

The sandwich model for transverse shear in reinforced concrete slabs (Marti, 1990 and Jaeger, 2002) consists of a reinforcement cover and a concrete core. The covers are assumed to carry moments and membrane forces, while the transverse shear forces are assigned to the core, Fig. 3.116. The twisting moment is divided into a couple of forces that are added to the shear force. The core is considered uncracked as long as the nominal shear stress due to the principal shear force does not exceed  $0,17\sqrt{f'_c}$  ( $f'_c$  in MPa). When this value is exceeded, a diagonal compression field is considered in the cracked core, Fig. 3.117. Additional membrane forces are consecutively added to the cover elements, Fig. 3.118. In the vicinity of concentrated loads or reactions, fan-shaped stress fields should be used.

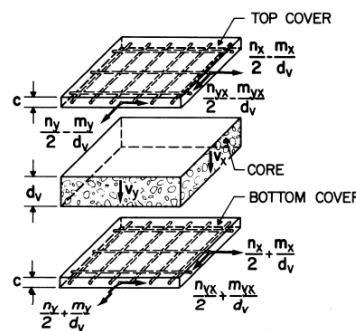


Fig. 3.116: Sandwich model consisting of cover parts and core, Marti (1990).

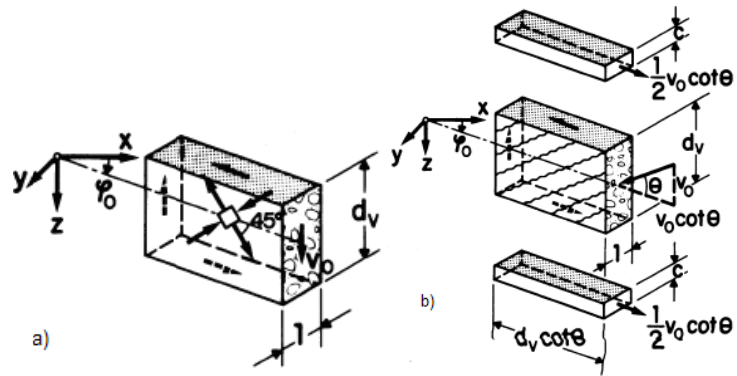


Fig. 3.117: a) Pure shear in uncracked core, b) Diagonal compression field in cracked core, Marti (1990).

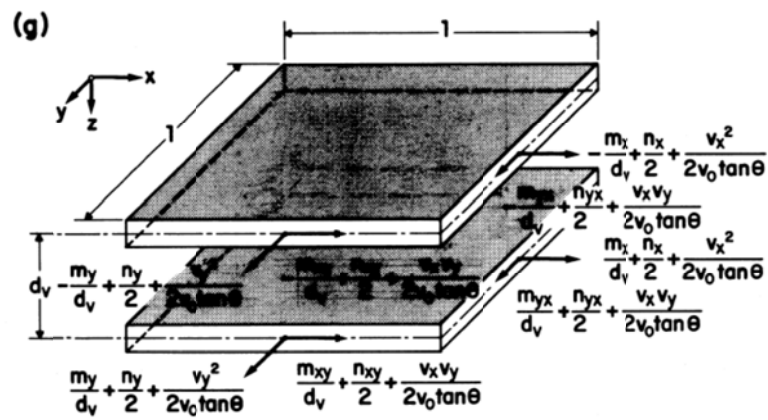


Fig. 3.118: Forces acting on cover elements (Marti, 1990).

#### **3.3.1.4 Discussion of compression field theory models**

The link between compression field models and plasticity models is found in the redistribution capacity in shear for the mechanisms transferring shear across the crack (Hsu et al., 1987).

The main deficiencies of the MCFT are (Sun and Kuchma, 2007):

1. The restriction in coincidence of principal directions of average stress and average strain. The observed tendency is for the principal stress direction to lag behind the change in the principal strain direction.
2. Reorientation of the crack direction: the MCFT is a fully rotating crack model in which a gradual reorientation occurs in the direction of cracks. However, crack patterns in girder tests have shown that crack directions remained fixed in the direction of first cracking.
3. Exclusion of shear slip: shear slip together with crack opening contributes to the most component parts of average strain in compatibility.
4. Inaccuracy in the crack spacing estimation: the assumed crack spacing was found not to correspond with experimental results.
5. Perfect bond without stress variation in the reinforcement: in reality, the distribution of stress in the reinforcement between cracks is like a parabolic curve with the highest values at the crack points and the lowest at the middle point.

Hawkins and Kuchma (2009) compared measurements to the strain distributions as calculated with the MCFT and found some inconsistencies. The principal stress direction was found to lag behind the principal strain direction.

Sun and Kuchma (2007) developed a model (Crack Displacement Field Theory) in which bond between reinforcement and concrete is based on the MC90 local bond-slip relation. Aggregate interlock is based on the rough crack model by Bažant and Gambarova (1980). Since the model captures the discrete displacement due to crack opening and slip, the restriction that principal directions of average strain and average stress must coincide is removed.

Gurley (2011) points out that placing skin reinforcement is not aimed at countering the size effect, but ensures sufficient ductility for applying a plastic method like the MCFT. Another two areas of improvement of the MCFT include;

1. members containing heavy amounts of reinforcement in both directions, members subjected to high biaxial compression in addition to shear, or members where the reinforcement and loading conditions are such that there is no rotation of the principal stress or strain conditions, for example panels where the principal loading directions are coincident with the reinforcement directions and hence, no reorientation of the stress-strain fields occurs.
2. Shear strength and stiffness are generally overestimated for uniaxially reinforced panels or for panels containing very light reinforcement in the transverse direction.

Reduced accuracy is also observed in shear-critical beams containing very little or no transverse reinforcement. Hsu (1996) questions the possibility of transmitting forces across cracks when combining concrete struts with a crack shear stress and criticizes the combination of an average stress-strain diagram of concrete in tension with a local stress-strain curve of the steel bars rather than an average stress-strain curve of steel bars embedded in concrete.

Vecchio (2000) developed the Disturbed Stress Field Model which is a hybrid formulation between a fully rotating crack model and a fixed crack model. A new approach to the reorientation of concrete stress and strain fields, removing the restriction that they be coincident as well as an improved treatment of shear stresses on crack surfaces were developed. With rotating crack models it is assumed that a gradual reorientation occurs in the direction of cracks, as dictated by the loading or material response. Vecchio (2000) points out that it is the assumption of coaxiality of stresses and strains which, in large part, leads to the inaccuracies of the MCFT. Also, MCFT allows no actual shear slip along the crack. The Disturbed Stress Field Model takes local disturbances by cracks into account, Fig. 3.119. The concrete tensile stresses  $f_{c1}$  will approach zero at the crack locations, but will be greater than zero between the cracks due to tension stiffening and other mechanisms. The concrete compressive stresses  $f_{c2}$  will be increased somewhat near cracks due to aggregate interlock mechanisms and equilibrium requirements. The internal force resisting mechanism is expressed in terms of average stress fields, but recognizing that these fields are disturbed by the presence of cracks. The localized deformation must be considered in addition to the average (smeared) strain

resulting from the constitutive response of the concrete of the average stresses. The element equilibrium condition becomes then:

$$[\sigma] = [D_c][\varepsilon_c] + \sum_{i=1}^n [D_s]_i [\varepsilon_s]_i \quad (3.67)$$

where

$n$  the number of reinforcement components;

$[D_c]$ ,  $[D_s]_i$  the concrete and reinforcement stiffness matrices, respectively;

$[\varepsilon_c]$ ,  $[\varepsilon_s]_i$  the net strains in the concrete and reinforcement components.

Crack interfaces are considered planes of weakness. The component of the concrete principal tensile stresses due to tension stiffening is assumed to be zero at the crack location. The combination of the smeared and local strains is shown in Fig. 3.120. The apparent total strains will be the summation of the continuum stress-induced strains, the shear slip strains, and the elastic and plastic offset strains (both typically taken as equal to zero).

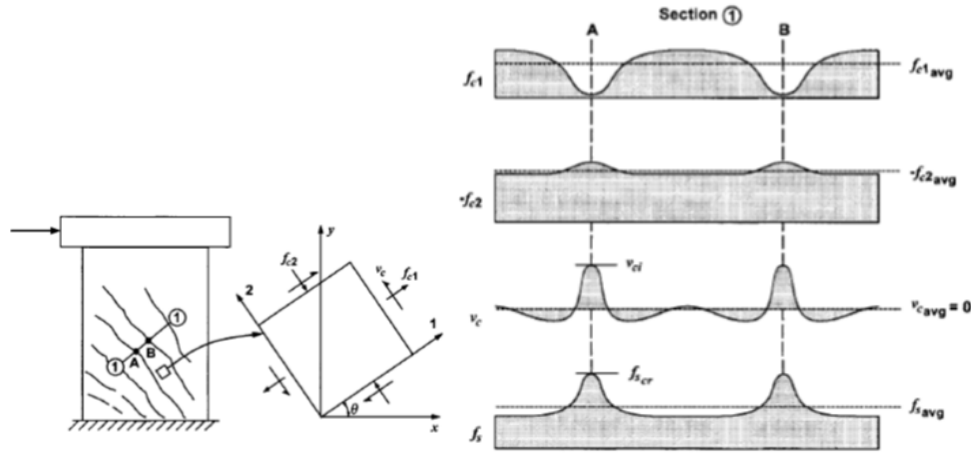
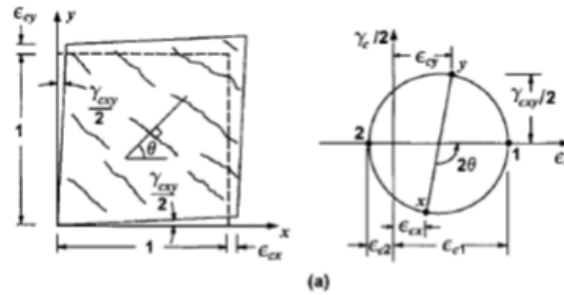


Fig. 3.119: Nature of disturbed stress fields in cracked reinforced concrete (Vecchio, 2000).



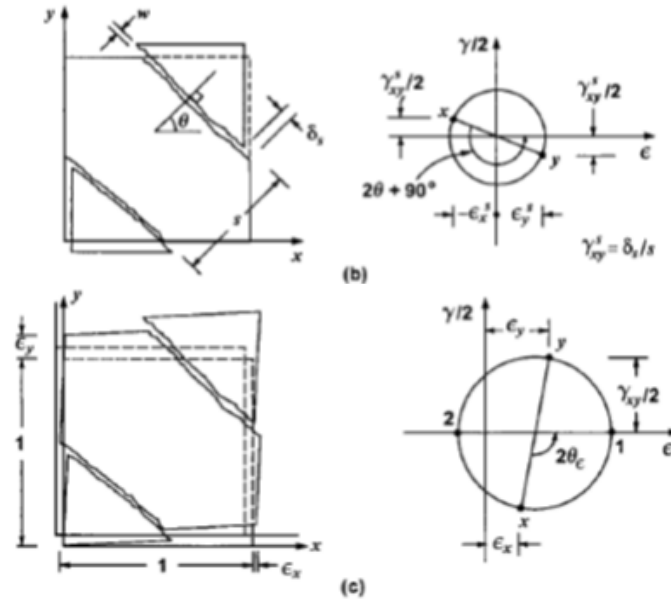


Fig. 3.120: Compatibility Conditions: (a) Deformations due to Average (Smeared) Constitutive Response; (b) Deformations due to Local Rigid Body Slip along Crack; (c) Combined Deformations. (Vecchio, 2000).

### 3.3.2. Critical shear crack theory

#### 3.3.2.1 Development of CSCT

The Critical Shear Crack Theory (CSCT) has been developed since 1985 in order to estimate the ultimate beam shear capacity and the ultimate punching shear capacity. The theory is treated in more detail in Muttoni and Fernández Ruiz (2008a, b) and Muttoni (2003). The basic assumption of this theory is that the shear strength of members without transverse reinforcement is governed by the width and roughness of a shear crack which develops through the inclined compression strut carrying the shear.

#### 3.3.2.2 Design procedure based on CSCT

The critical zone is estimated at a cross section located at  $0,5d$  from the point of introduction of the load and at  $0,6d$  from the extreme compression fiber. The width of the critical shear crack  $w$  is proportional to the strain  $\epsilon$  in a control depth for one-way members and to the slab rotation  $\psi$  for two-way members (Muttoni, 2008). The width  $w$  is also influenced by the aggregate size and the spacing between the layers of reinforcement. Based on these assumptions, the following failure criteria have been developed for members without stirrups:



$$\frac{V_R}{b_0 d \sqrt{f_c}} = \frac{1/3}{1 + 120 \frac{\varepsilon d}{d_{g0} + d_g}} \quad (3.68)$$

for one-way shear (units: MPa, mm)

$$\frac{V_R}{b_0 d \sqrt{f_c}} = \frac{3/4}{1 + 15 \frac{\psi d}{d_{g0} + d_g}} \quad (3.69)$$

for two-way shear (units: MPa, mm)

in which

- $V_R$  the shear strength;
- $b_0$  a control perimeter, equal to the width of the member  $b$  in beams and set at  $d/2$  of the border of the loaded area for punching shear;
- $d$  the effective depth of the member;
- $f_c$  the average cylinder compressive strength of the concrete;
- $\varepsilon$  the strain in a control depth for one-way members;
- $\psi$  the slab rotation for two-way members;
- $d_g$  the aggregate size;
- $d_{g0}$  the reference aggregate size equal to 16mm.

For one-way shear the strain in the control depth is taken as:

$$\varepsilon = \frac{M}{d \rho E_s \left( d - \frac{x}{3} \right)} \frac{0,6d - x}{d - x} \quad (3.70)$$

$$x = d \rho \frac{E_s}{E_c} \left( \sqrt{1 + \frac{2E_c}{\rho E_s}} - 1 \right)$$

in which

- $x$  the depth of the compression zone;
- $M$  the bending moment at the critical cross section;
- $\rho$  the reinforcement ratio for the longitudinal steel;
- $E_s$  Young's modulus of steel;
- $E_c$  Young's modulus of concrete.

For two-way shear the rotation can be assumed as:

$$\psi = 1,5 \frac{r_s}{d} \frac{f_y}{E_s} \left( \frac{V}{V_{flex}} \right)^{3/2} \quad (3.71)$$

in which

$r_s$  radius of circular isolated slab element,

$f_y$  yield strength of the reinforcement,

$V_{flex}$  the flexural strength  $V_{flex} = 2\pi m_R \frac{r_s}{r_q - r_c}$ ,

$m_R$  the radial moment per unit width  $m_R = \rho f_y d^2 \left( 1 - \frac{\rho f_y}{2f_c} \right)$

$r_q$  the radius of the load introduction at the perimenter,

$r_c$  the radius of a circular column.

The CSCT can be used in the case of deck slabs of bridges, where the shear field and developed rotations around the wheel loads differ from residential flat slabs support by columns. For critical existing bridges, it is advised to calculate the nonlinear load-rotation relationship by integrating the moment-curvature behavior of the slab, Fig. 3.121.

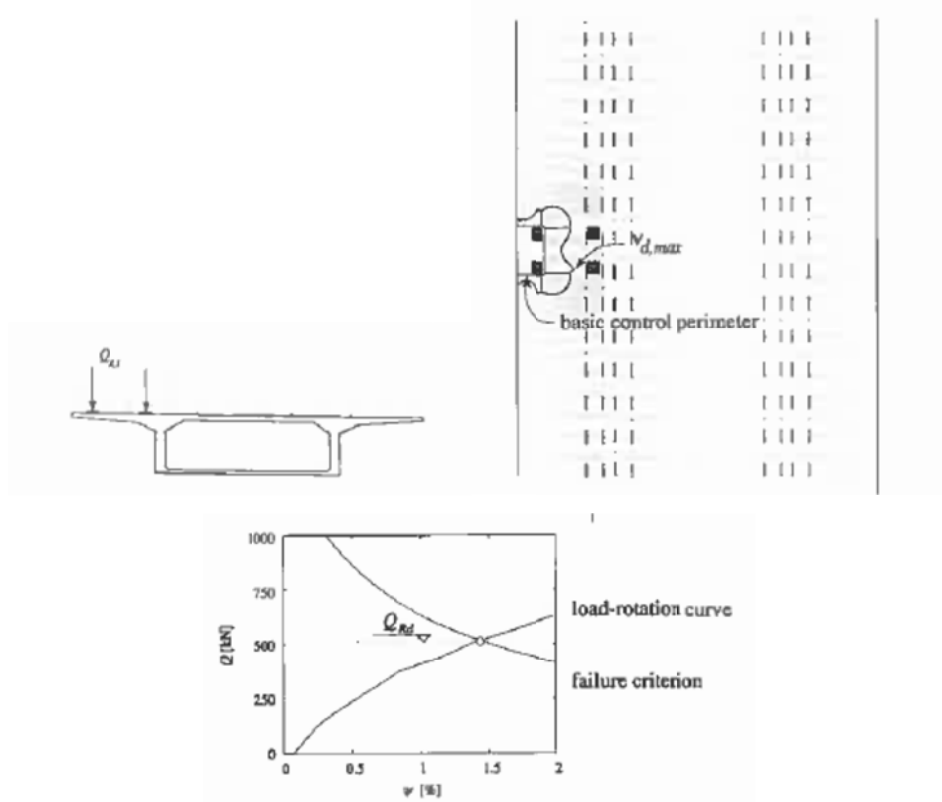


Fig. 3.121: Application of the CSCT to estimate the shear strength of the cantilever deck slab of an existing bridge: shear field trajectories and calculation of punching strength on the basis of the nonlinear load-rotation curve of the cantilever (Vaz Rodrigues 2007)

### 3.3.2.3 Non-axis-symmetrical punching based on CSCT

For non-axis-symmetrical punching, as shown in Fig. 3.122, a method based on the CSCT is developed (Sagasetta et al., 2011). Non-axis-symmetry in slabs can be due to loading, slab and column geometry and reinforcement layout. The presented method focuses mainly on cases where  $\rho_x$  and  $\rho_y$  are significantly different, Fig. 3.123. It was experimentally observed that the slope of the failure cone was steeper at the sides with maximum rotations, than in the other, stiffer, direction. This observation suggests that punching shear in slabs with  $\rho_x \neq \rho_y$  can be treated considering the  $x$  and  $y$  directions individually.

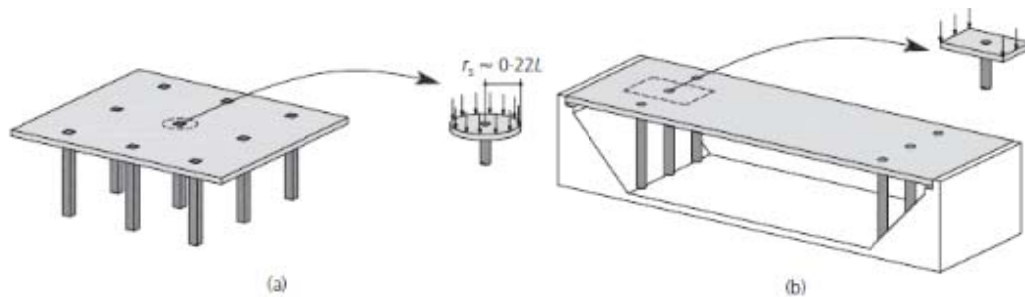


Fig. 3.122: Punching shear in (a) flat slabs with square bays (axis-symmetrical conditions) and (b) slab bridges (non-axis-symmetrical conditions).

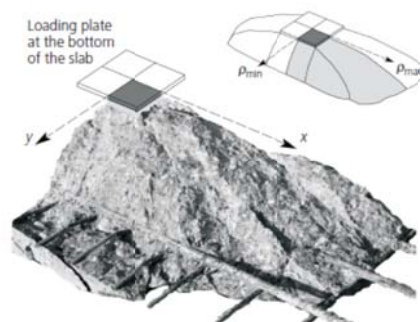


Fig. 3.123: Punching shear tests at EPFL with non-symmetrical reinforcement ( $\rho_x/\rho_y \approx 0,80/0,35\%$ ): failure cone after testing (specimen PT23) (Note only one quadrant of the cone is shown; steep face corresponds to the weak reinforced direction). (Sagasetta et al., 2011).

The nominal punching strength  $v_R(s)$  in non-axis-symmetrical slabs is non-uniform along the control perimeter since the slab rotation  $\psi(s)$  depends on the direction, Fig. 3.124.

Some parts of the perimeter will reach their ultimate strength, whereas others will still have a potential strength capacity. When assuming a constant nominal strength  $v_{Rmax}$  this additional strength is neglected. In reality, once the nominal shear stresses reach the nominal strength  $v_{Rmax}$ , a softening of shear will occur at segments with the largest slab rotations (segment A in Fig. 3.125). The failure criterion from the CSCT is used, accompanied by an increase of shear at segments of the perimeter with higher nominal strength (segment B in Fig. 3.125). The redistribution of shear stresses from A to B results in higher punching shear strengths and slab rotations than the initially estimated values of  $V_{R0}$  and  $\psi_{R0}$ . This is true provided that the increase in shear at B shown in Fig. 3.125 balances the softening in shear at A.

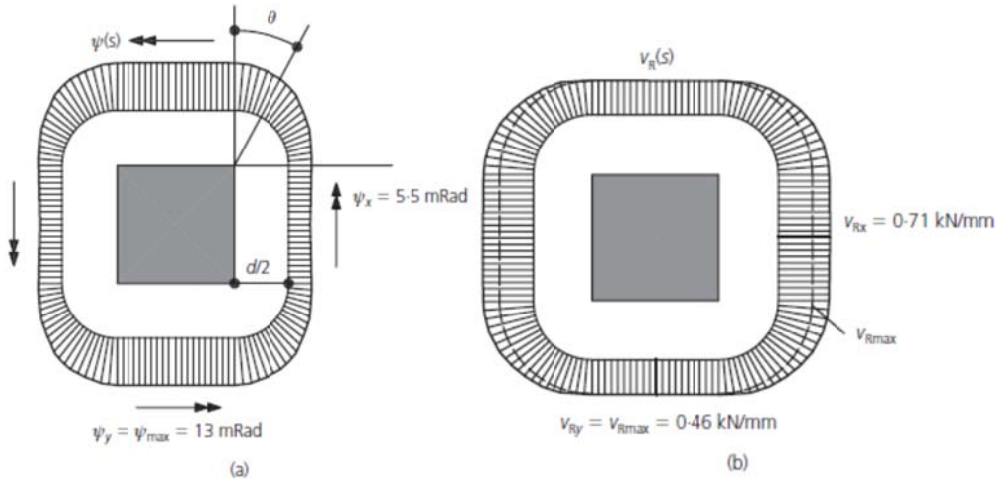


Fig. 3.124: Non-uniform distribution along the control perimeter of (a) slab rotations (NLFEA predictions for PT34 at 800kN) and (b) corresponding nominal strengths according to the CSCT (Sagasetta et al., 2011).

In general, the punching strength can be determined by integrating the nominal strength along the control perimeter:

$$V_R = \oint_{cp} v_R(s) ds \quad (3.72)$$

$$v_R(s) = \frac{\frac{3}{4} d \sqrt{f_c}}{1 + 15 \left( \psi(s) \frac{d}{d_g + d_{g,0}} \right)} \quad (3.73)$$

The assumed relationship  $\psi(s)$  should be validated experimentally, although predictions from FEA or similar approaches can provide useful information. The rotations  $\psi(s)$  can be assumed to be constant along the straight segments of the control perimeter in slabs supported on square columns. The transition between  $\psi_y$  and  $\psi_x$  is assumed to take place at the corners primarily, leading to:

$$V_R = \oint_{cp} v_R(s) ds = 2c(v_{Rx} + v_{Ry}) + V_{R, corners} \quad (3.74)$$

$$v_{Rx} = \frac{\frac{3}{4}d\sqrt{f_c}}{1 + 15\left(\frac{\psi_x d}{d_g + d_{g,0}}\right)} \quad (3.75)$$

$$v_{Ry} = \frac{\frac{3}{4}d\sqrt{f_c}}{1 + 15\left(\frac{\psi_y d}{d_g + d_{g,0}}\right)} \quad (3.76)$$

$$V_{R, corners} = 4 \int_0^{\frac{\pi}{2}} v_R(\theta) \frac{d}{2} d\theta \quad (3.77)$$

where  $V_{R, corners}$  is the total strength corresponding to the four corners. The angle  $\theta$  varies between 0 and  $\pi/2$  (Fig. 3.124) and  $v_R(\theta)$  is the nominal strength corresponding to the rotation  $\psi(\theta)$  according to Eq. (3.73).

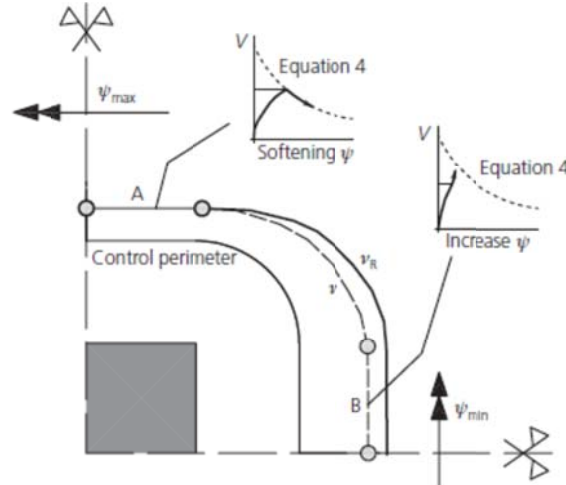


Fig. 3.125: Shear stress redistribution from segments of the control perimeter with largest slab rotations (shear softening) to segments with lowest slab rotations (increase in shear). (Sagasetta et al., 2011).

To estimate  $\psi(s)$ , the control perimeter can be subdivided into segments and with the use of a NLFEA program, the rotation  $\psi_i$  and the nominal strength  $v_{Ri}$  can be assessed for each segment. Carrying out such a routine for a test specimen showed that: (a) the rotations were fairly constant along the straight sides of the perimeter, as assumed, and (b) the rotations  $\psi(\theta)$  at the corners followed an approximately parabolic relationship, which is consistent with experimental evidence.

This general approach can be simplified by dividing the control perimeter into four segments, as shown in Fig. 3.126. The slab rotations  $\psi_x - \psi_y$  and nominal strengths  $v_{Rx} - v_{Ry}$  are assumed to be constant along  $b_x - b_y$ , leading to:

$$V_R = v_{Rx} b_x + v_{Ry} b_y = \frac{V_{Rx}}{b_0} b_x + \frac{V_{Ry}}{b_0} b_y \quad (3.78)$$

This approach assumes that  $V_{Rx}$  and  $V_{Ry}$  are completely uncoupled, which seems less realistic than the method with shear redistribution.

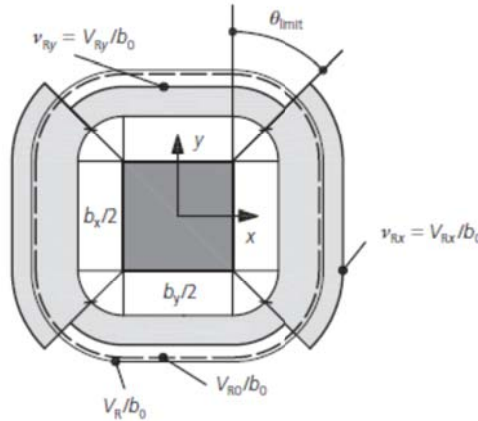


Fig. 3.126: Simplified discretization of control perimeter into x-y segments; distribution of nominal shear strength and general notation. (Sagasetta et al., 2011).

### 3.3.2.4 Discussion of CSCT

Muttoni and Fernandez Ruiz (2010) point out that an additional advantage of the CSCT is that it allows one to calculate not only the punching strength but also to estimate the

deformation capacity (rotation) at failure, providing valuable information to the designer on the behavior of the structure (ductility, brittleness).

Windisch (2011, in a discussion to Vaz Rodrigues et al., 2010) questions the possibility of the shear crack to penetrate the compressive strut. The detrimental development of the critical shear crack is assumed along the theoretical compression strut that leads to the failure of the inclined compression strut and that of the member. This compression strut is “prestressed” by the compressive force in it; and therefore it might be questionable that the shear crack can penetrate this strut. In this way, the critical shear crack model contradicts both the variable angle stress field and the MCFT. According to the discussor, however, this could actually be considered an advantage of the CSCT model.

### **3.3.3. Strut and tie models and truss models**

#### **3.3.3.1 Development of strut and tie models**

Strut and tie models are mechanical models representing the force flow in a concrete member by compressive struts and tension ties. The tensile ties can be reinforcing bars, prestressing tendons or concrete tensile stress fields (Schlaich et al, 1987). Strut-and-tie models also incorporate the major elements of detailing. The lower bound theorem of plasticity is used. For slabs in which the state of stress is not predominantly plane, as for example in the case of concentrated loads, three-dimensional strut-and-tie models should be developed. The direction of struts can be taken in accordance with the mean direction of principal compressive stresses. Since loads follow the path which requires the least forces and deformations, and reinforced ties are much more deformable than concrete struts, the model with the least and shortest ties is the best (principle of minimum strain energy for linear elastic behavior of the struts and ties after cracking). Three types of strut and ties are used:  $C_c$  (concrete struts in compression, two or three-dimensional stress field),  $T_c$  (concrete ties in tension without reinforcement, two or three-dimensional stress field) and  $T_s$  (ties in tension with reinforcement, linear, one-dimensional element).

Depending on the combination of struts and ties, 4 types of nodes are possible: CCC, CCT, CTT and TTT. Since  $C_c$  and  $T_c$  are stress fields, these tend to spread in between two adjacent nodes. Three types of compression fields are used: the fan, the bottle and the prism, Fig. 3.127. In case of bottle-shaped stress fields, force distribution leading to a

biaxial or triaxial compression state close to the load and the transverse tensile stresses in the strut need to be taken into account. The failure criterion for the compression fields or within the nodes depends on the concrete compressive strengths, which is by large influenced by the multi-axial state of stress and the disturbances from cracks and reinforcement. Transverse compression is favorable, while transverse tension and cracks which are not parallel to the compressive stresses are detrimental.

It must be noted that the structure adapts itself to the assumed internal structural system (Schlaich et al., 1987). The resulting models are quite often kinematic, which means that equilibrium in a given model is possible only for the specific load case. Relevant examples of strut-and-tie models are shown in Fig. 3.128 and Fig. 3.129. A strut and tie model which takes the size effect into account is discussed by Yang (2010).

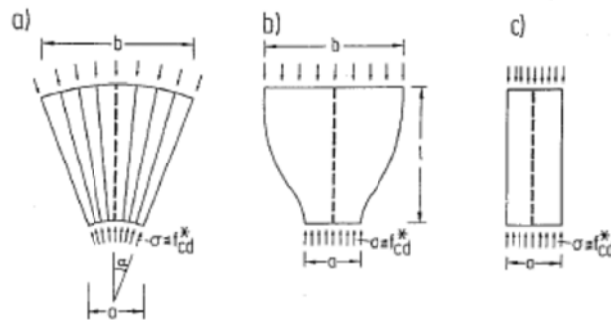


Fig. 3.127: The basic compression fields: (a) the fan, (b) the bottle and (c) the prism (Schlaich et al., 1987).

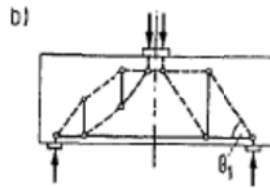


Fig. 3.128: Strut-and-tie model for beam with small  $a/d$  ratio. Left: refined model and right: simplified model (Schlaich et al., 1987).

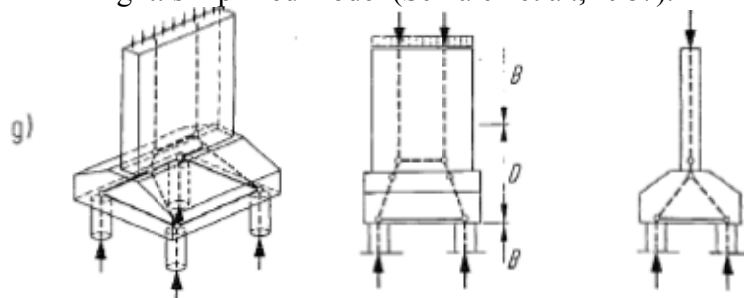


Fig. 3.129: 3-D strut-and-tie model for pier of a pile cap (Schlaich et al., 1987)



### 3.3.3.2 Truss with concrete tensile contribution

The traditional truss model as first introduced by Ritter (1899) assumes concrete compression struts and steel tension ties. More recent approaches (ASCE-ACI committee 445, 1998) take the tensile stresses transverse to the struts and the shear stresses across the inclined crack by aggregate interlock or shear friction into account. Both mechanisms are interrelated and result in:

- the angle of the principal compression stress to be smaller than the crack angle and,
- a vertical component of the force along the crack contributing to the shear strength of the member.

Schlaich et al. (1987) showed that for example slabs use stress fields  $T_c$  to transfer tension in the concrete. Redistribution of stresses avoiding cracking may be possible if at any part of the stress field a cracked failure zone with an area  $\Delta A_c$  can be assumed. Stress peaks can be smoothed out over  $5\text{cm} < 3d_g$  ( $d_g$  is the maximum aggregate size). A certain fraction of the tensile strength is used for carrying loads and another fraction is used by restraint stresses. If the tensile stress field is crossed by a compression field, the reduced biaxial strength must be considered.

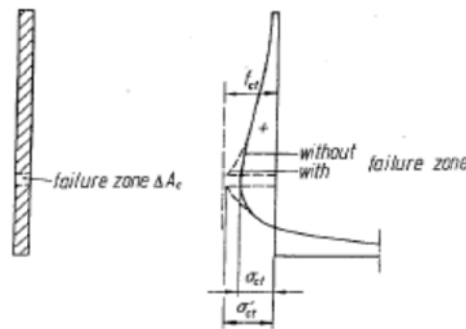


Fig. 3.130: Assumption of a failure zone for the check of the tensile strength of a concrete tension tie  $T_c$  (Schlaich et al., 1987).

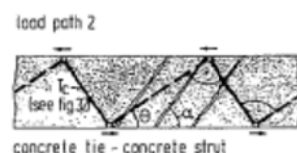


Fig. 3.131: Load path of beam in shear using concrete tie (Schlaich et al., 1987).

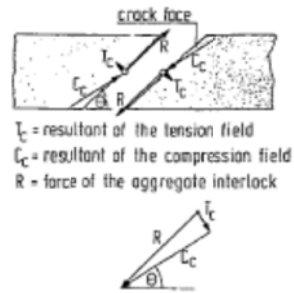


Fig. 3.132: Aggregate interlock force  $R$  and corresponding compression  $C_c$  and tension  $T_c$  in the concrete (Schlaich et al., 1987).

A newer development is the use of discontinuous stress fields that more adequately represent the ultimate limit state behavior of panel elements subject to in-plane loading (Cho, 2003).

### 3.3.3.3 3D strut and tie model

A 3D strut and tie model was developed by Alexander and Simmonds (1986, 1987), initially to model punching of edge columns. The model consisted of two types of compression struts: in-plane or anchoring struts (parallel to the slab) and out-of plane or shear struts (at some angle ( $\alpha$ ) to the plane of the slab). It is based on the principle that cases of unbalanced load have a combined failure mode. Typical failures are shown in Fig. 3.133. Alexander and Simmonds (1987) argue that it is unlikely that a punching failure is the result of shear stress on some vertical plane, since this requires a diagonal tension field in the concrete. However, diagonal cracking at a relatively early load stage should preclude this tension field, according to the authors.

Two problems arise when developing a strut-and-tie model. Firstly, estimating the actual stress within each strut and the critical failure stress to compare with requires effective strengths. Secondly, the limits for the inclination of the compressive struts need to be found.

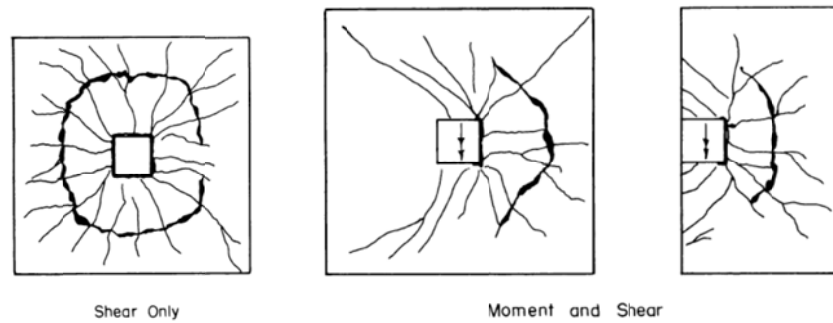


Fig. 3.133: Typical punching failures (Alexander and Simmonds, 1987).

The anchoring, in-plane struts are presented in Fig. 3.134a. Each is equilibrated by two mutually perpendicular reinforcing bars: one passing through the loaded zone and the other at some distance from the loaded zone. This mechanism gives an explanation for the influence of the flexural reinforcement on the shearing strength: bars at some distance from the loaded zone are able to exert flexural moment. An out-of-plane or shear strut is similar to the force diagram used in corbel design (Fig. 3.134b). However, there are two differences between the shear struts for slabs and the struts in corbel design. First, the point of load application does not coincide with the junction of the tensile and compressive force, and as a result the angle of inclination of the shear strut,  $\alpha$ , is not preset. The second difference is that the vertical component of the compression strut is no longer equilibrated at the junction by the applied load. There exists a force component out of the plane of the slab which must be balanced by some form of tension field within the concrete, resulting in a three-dimensional truss (Fig. 3.135 and Fig. 3.136).

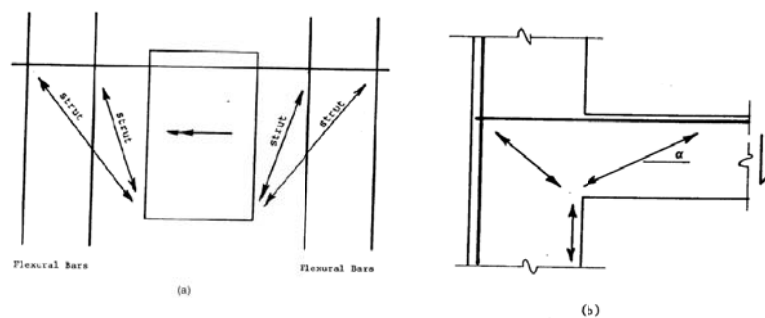


Fig. 3.134: (a) In-plane or anchoring struts, (b) out-of-plane or shear strut (Alexander and Simmonds, 1986).

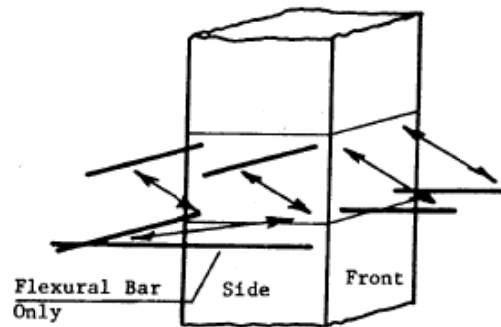


Fig. 3.135: 3D strut and tie model (Alexander and Simmonds, 1986)

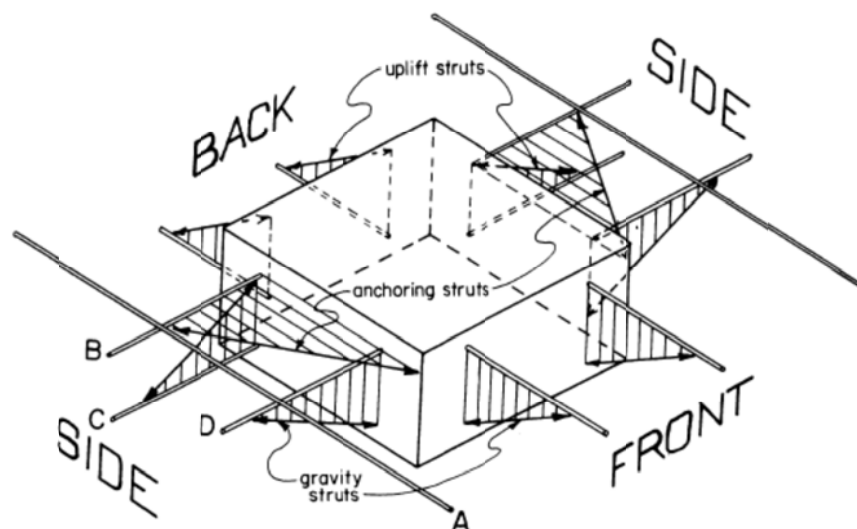


Fig. 3.136: 3D strut and tie model (Alexander and Simmonds, 1987).

In a slab, the amount of steel participating in the tension ties (called “shear steel”) is not clearly defined. Alexander and Simmonds (1986) assumed that all steel aligned through the loaded zone participates in the tension tie, plus some fraction of the steel within a distance  $d_s$  (the effective depth) of the face of the loaded zone. This fraction decreases linearly from 1 at the face of the loaded zone to 0 at a distance  $d_s$  from the face of the loaded zone. The shear steel is assumed to yield at failure. Three conditions can lead to failure in the strut and tie model of Alexander and Simmonds (1986): failure of the tension tie, failure of the compression strut, and failure when the out-of-plane component of the compression strut exceeds the confining strength of the slab.

The ultimate capacity of an in-plane bar-strut unit is limited by the yield of the reinforcing bars. Therefore, the model requires that the steel reaches yield. To define the

ultimate capacity, the bar force at yield and the angle of the compression strut ( $\alpha$ ) need to reach a critical value. The parameters which are likely to affect  $\alpha$  are assembled in a non-dimensional empirical term. From geometric considerations,  $\tan(\alpha)$  equals the ratio of the out-of-plane component (defined by the ability of the slab to confine the bar, function of tributary width of each bar ( $s$ ), cover ( $d'$ ) and concrete strength) to the in-plane component (yield force in steel). These observations led to the expression:

$$\tan \alpha = \frac{P_{failure}}{A_{SV}^{top} f_y} K$$

$$K = \frac{s_{eff} \cdot d' \cdot \sqrt{f_c'}}{A_{bar} \cdot f_y \cdot (c / d_s)^{0.25}} \quad (3.79)$$

where

$P_{failure}$	the failure load;
$A_{SV}^{top}$	the top mat shear steel;
$f_y$	the yield strength of the steel;
$s_{eff}$	the maximum of $s$ or $3d'$ ;
$d'$	the cover of the reinforcement measured to the near side of the slab;
$d_s$	the cover of the reinforcement measured to the far side of the slab;
$c$	the column dimension perpendicular to the bar being considered;
$f_c'$	the concrete strength;
$A_{bar}$	the area of a single reinforcing bar.

Based on these theoretical considerations, a design equation for  $\alpha$  was determined from test results:

$$\tan \alpha = 1,0 - e^{-2,25K} \quad (\text{SI units}) \quad (3.80)$$

### 3.3.3.4 Discussion of strut and tie models

Strut and tie models are based on the principle of an inclined compression field in the concrete. Not only does this mechanism provide a load path for shear forces in the presence of diagonal cracking, it explains the role that flexural reinforcement plays in determining shear strength, according to Alexander and Simmonds (1986).

As a result of the multi-axial stress state, simplified strength values of the concrete compressive design strength need to be used, which could be seen as a disadvantage

(Schlaich et al, 1987). Reineck (1990) connects the subdivision in B- and D-regions by Schlaich et al. (1987) to Kani's valley (1964) by pointing out that in order to have a B-region develop in a beam, the load should be at a distance greater than  $2h$  from the support axis, which corresponds with the minimum of Kani's valley around  $a/d = 2,5$ . Marti (1999) points out that strut and tie models include strain compatibility and an effective concrete compressive strength  $f_c$  just like compression field approaches, and that they also provide a theoretical framework with experimental evidence.

Gastebled and May (2001) argue that a different approach is needed to capture the shear failure of slender members without stirrups, for which the failure mechanism differs significantly from those assumed in the truss models.

In his discussion to the 1987 ACI paper by Alexander and Simmonds, Braestrup (1988) denotes the strut-and-tie model as an example of the lower bound method of plastic analysis. He criticizes the assumption that all steel is yielding, since the typical slab-column tests might not be able to describe adequately the conditions in prototype structures. The same remark is made by Rangan (1988), regarding the angle  $\alpha$ . Braestrup further argues that it may be desirable to preclude concrete failure, but this requires an adequate design which can only be based upon a description of the failure which is to be avoided. Windisch (1988) states that the model does not meet the equilibrium conditions:

1. At the bar-strut junction there exists a force component out of the plane of the slab that is not equilibrated directly by the applied load, which must be balanced by some form of tension field in the concrete. This concrete tension field, which is not treated further in the paper, is incompatible with the assumptions of the truss model.
2. The anchoring struts deliver considerable in-plane compressive forces that are not balanced by any other truss member. The inclination of these anchoring struts hardly depends on the pure geometrical conditions.
3. A gravity strut should belong to the strut steel of bar A in Fig. 3.136. The tensile force in the reinforcing bar is not equilibrated in the cross section of the plate parallel to the front side of the column.

4. An anchoring strut with all corresponding steel struts should be placed at the level of the bottom reinforcement as well.

In the closure, Alexander and Simmonds (1988) explain that the figures only show the orientation of the compression struts and attendant reinforcing bars acting in the slab. Equilibrium is provided by forces in the slab and column not shown. Bar A is located further than  $d_s$  from the face of the column and is not serving as strut steel nor associated with a gravity strut and interacts with the column only through the anchoring strut mechanism. The tension in bar A at any cross section in front of the column is equilibrated by a flexural compression zone in the slab. The reaction to the anchoring strut is provided by shear and compression in the column. Regarding the tension field the authors reply: “The truss model describes conditions at ultimate in a localized area round the column. This area is surrounded by a flexural plate. In the region where these two areas overlap, equilibrium requires a tension field to resist the out-of-plane force in the concrete since there is no other mechanism available.” By basing the punching shear resistance upon the reinforcement exclusively, the authors do not imply that the punching capacity of the slab vanishes in the absence of flexural reinforcement; only the strut and tie mechanism vanishes.

### 3.3.4. Mechanical models

#### 3.3.4.1 Tooth model

A first idea for a tooth model was shown by Mörsch (1922) by showing the zone between two flexural cracks, the force in the concrete compressive zone and the force in the steel, Fig. 3.137.

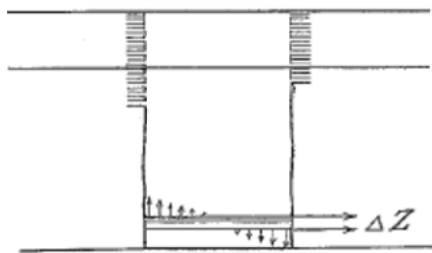


Fig. 3.137: First idea of tooth model by Mörsch, 1922.

The tooth model was introduced as an explanation for the riddle of shear failure by Kani (1964). Kani's tooth model (Fig. 3.139) consists of free cantilevers fixed in the compression zone and loaded by horizontal shear forces resulting from the bonded reinforcement. Kani (1964) correctly linked the beam shear capacity (the capacity of the concrete teeth) and the capacity of the remaining arch to the experimentally observed valley of diagonal failure, Fig. 2.18. The bond force between the deformed bars and the concrete was expressed as a distributed load, Fig. 3.138. The concrete teeth were calculated as short vertical cantilevers anchored in the compression zone, Fig. 3.139. Kani (1964) also measured the transformation into a concrete arch by registering the increase in compressive strain at the neutral axis, Fig. 3.140. Assumptions concerning the inclination and spacing of the discrete cracks (the factor  $\frac{\Delta x}{s}$  in Fig. 3.139) were made and remain a source of discussion (Brock et al., 1964). MacGregor and Walters (1967) used a programming routine to calculate stresses. Several values of crack spacing  $\Delta x$  were assumed to study the effect of crack spacing on the computed inclined cracking load. The computed strengths depended on the crack spacing to some extent, but were not nearly as strongly affected as predicted by Kani. The reason for this appeared that the more flexible, narrow teeth deflected laterally under load and thus the steel stress on each side of them tended to approach the same value. In addition, the larger lateral deflections led to large friction and doweling shear forces between the teeth which tended to reduce the tooth stresses. Reineck (1997) estimates the crack spacing as  $s_{cr} = 0,70(d - x)$  with  $x$  the depth of the compression zone, which mainly depends on the reinforcement ratio. The shear strength in Kani's tooth model is expressed as  $V_R = r_u M_y / a$  where  $M_y$  is the yielding moment,  $r_u$  the reduction factor as shown in Fig. 2.18 and  $a$  the shear span. The problem of "shear strength" has thus become an investigation, and search for, the type and quantity of web reinforcement required to increase the reduction factor  $r_u$  to 1 (Kani, 1966).

The assumed force distribution versus the later measured force distribution is shown in Fig. 3.141.



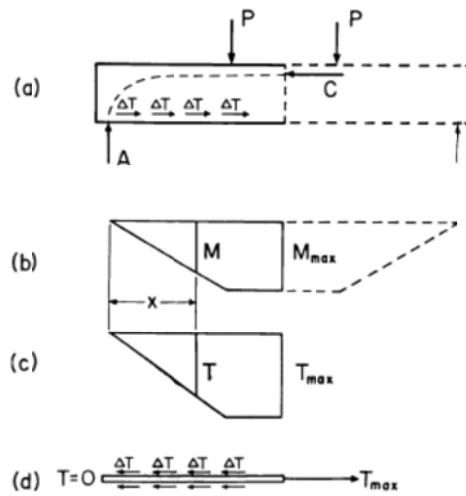


Fig. 3.138: Internal forces of a reinforced concrete beam with bond (Kani, 1964).

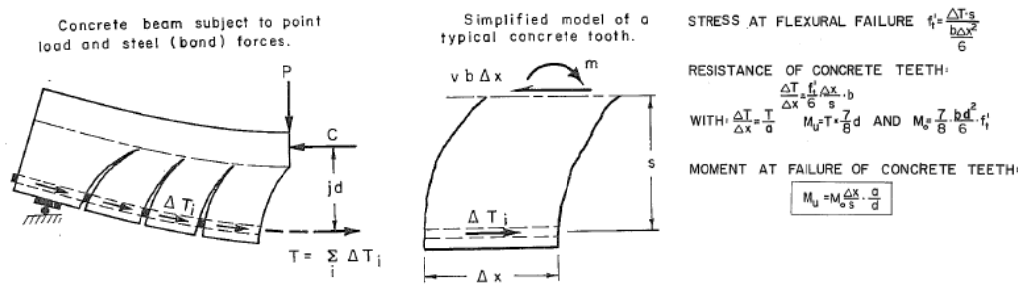


Fig. 3.139: Kani's tooth model (Kani, 1979).

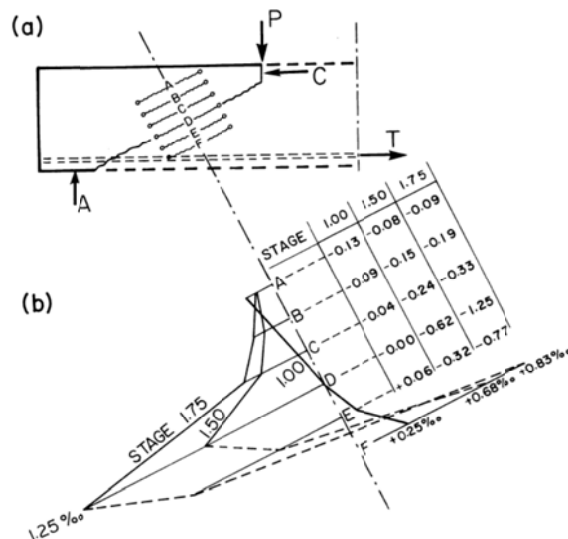


Fig. 3.140: Transformation of a beam into an arch as measured on a specimen (Kani, 1964).

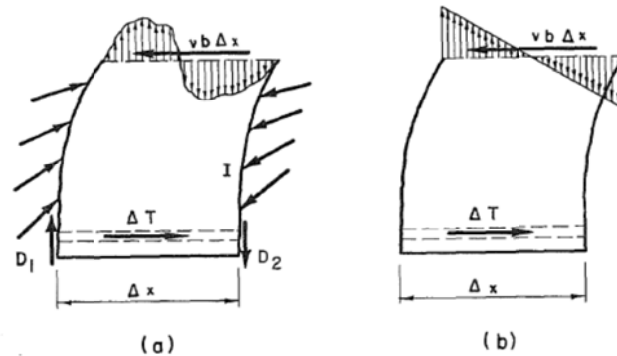


Fig. 3.141: (a) Possible forces existing in the vicinity of the tooth; (b) Assumed force distribution at root of tooth (Kani, 1979).

While Kani (1964) assumed that the distribution of the stress in the remaining arch is almost the same as it is in the original compressive zone, Puijssers (1986) assumed that due to the separation of the teeth the remaining arch is no longer forced to rotate under the flexural moment. As a result, there is a system of centrally loaded compressive and tensile zone, Fig. 3.142.

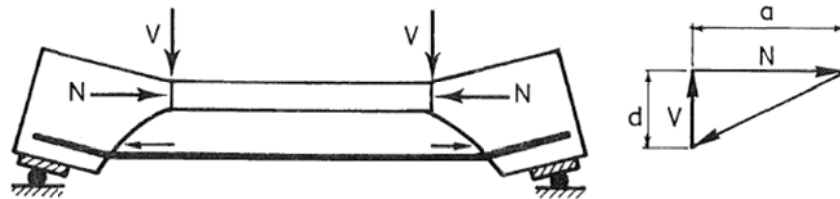


Fig. 3.142: System of centrally loaded compressive and tensile zone. (Puijssers, 1986).

Regan (1969) used a similar tooth model to Kani's model to develop design charts. Hamadi and Regan (1980) point out that the comb-like structure of the concrete "teeth" between flexural cracks is naturally better developed in the longer shear spans. Russo et al. (1991) have expanded Kani's tooth model into a flexure-shear interaction model.

Reineck (1990, 1997) developed a model in which the dowel action and aggregate interlock are calculated with strut-and-tie models and the equilibrium of all mechanisms contributing to the shear transfer is studied on a tooth. These mechanisms (Fig. 3.143) are:

- friction in cracks,
- dowel force,

- cantilevering action of the tooth from the compression zone, and
- a shear force component in the compression chord.

Reineck's model is based on strut-and-tie models representing the principal stress fields in a concrete tooth. The dowel forces are equilibrated by friction stresses along the crack, so that the bending stresses in the tooth due to the dowel forces superimpose with a biaxial tension – compression stress field as before. The friction stresses are assumed to be a superposition of a constant friction part and a parabolic part related to the dowel action. The dowel action causes a negative slip in the lower part of the tooth and thus reduces the possible friction transfer over the crack, which results in the parabolic shape of the friction stresses. Equilibrium and the condition of equal shear stresses for an element at the neutral axis lead to:

$$\tau_{f2} = 2v_{n,d} \text{ with } v_{n,d} = \frac{V_d}{b_w(d-c)} \quad (3.81)$$

This leads to a statically admissible and consistently described stress-field in the tension zone. The resulting stress fields are visualized through a strut-and-tie model, Fig. 3.145. Some bending occurs at the lower part of the tooth, but the inclined tension and compression field prevails. The maximum shear force is then

$$V = b_w z \tau_f + \frac{3}{4} \frac{z}{d-c} V_d \quad (3.82)$$

The stress field is completely known. At the crack tip zone, the crack opens without any slip so that no friction stresses can be activated. It is shown by Reineck (1990) that the assumed stress field near the neutral axis can be transferred by a combination of friction and tensile stresses in this fracture zone. The stress field is then represented by a simple truss model, Fig. 3.146, which shows that the tensile strength of the concrete is utilized in members without transverse reinforcement such as slabs.

This model requires the constitutive laws to be formulated for all the considered mechanisms of shear transfer (Reineck, 1997a). Reineck (2010) explains the ultimate capacity not by the concrete ties attaining the concrete tensile strength, but by the limited capacity of friction along the cracks and the dowel action.

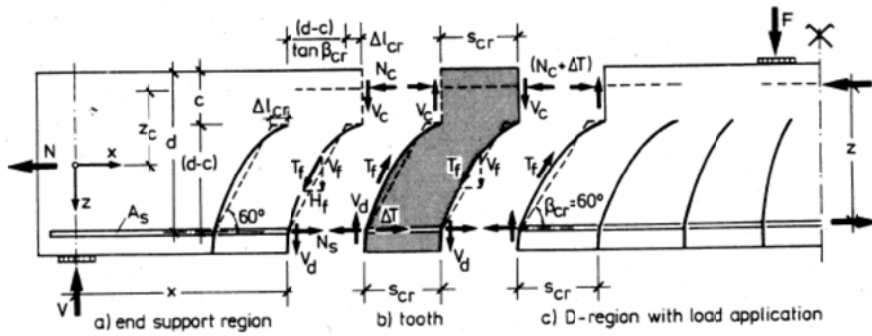


Fig. 3.143: Reinforced concrete member with tooth-element and its forces in B-region (Reineck, 1990).

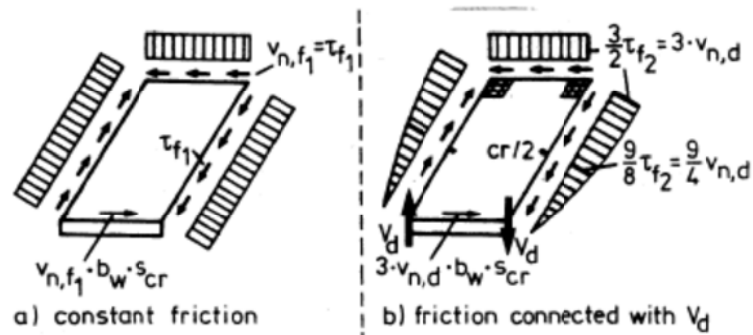


Fig. 3.144: Assumed shear stress distribution due to friction along cracks (Reineck, 1990).

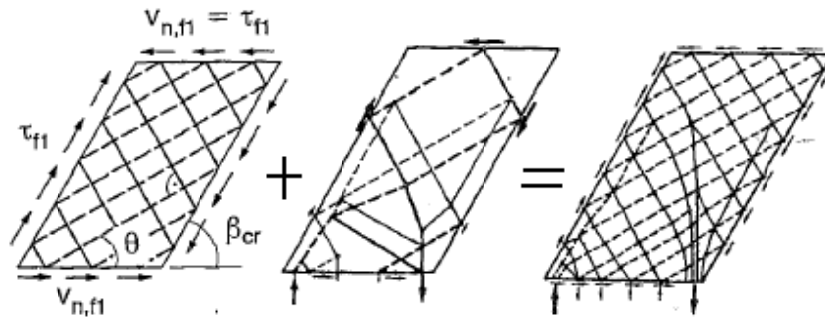


Fig. 3.145: Strut-and-tie model representing the principal stress fields in tooth: stress field due to constant part of friction stresses plus strut-and-tie model due to dowel forces (Reineck, 1997a).

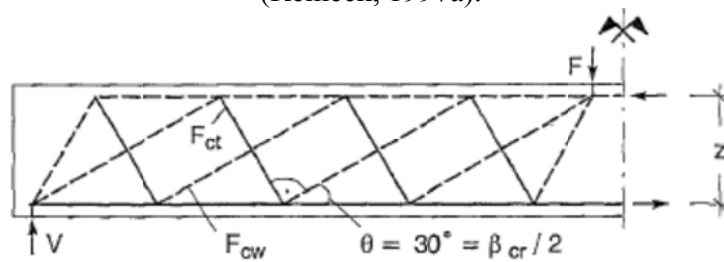


Fig. 3.146: Truss model with biaxial tension-compression stress field in concrete of web (Reineck, 1990).

Reineck (2002) points out that failure mechanism approaches have a common feature with fracture mechanics approaches, where the localization of the failure zone either in tension or compression plays the major role. When the friction in the concrete is correctly modeled, a truss model with crack friction can be developed. In such a method, the shape and the geometry (inclination) of the crack is modeled and also the spacing. This approach is in principle different from the smeared approaches such as the shear-compression field theory (MCFT, Collins 1978) and the rotating-angle softened truss model (Hsu, 1999). In these methods, the crack angle and the angle of the compression field are equal, such that no slip occurs and the friction cannot be checked correctly. In fact, friction forces can not be transferred at cracks which are assumed parallel to the compression field. Although refined tooth models and the MCFT approach the problem from different directions, the end result is very similar. Both methods consider that the ability of diagonal cracks to transfer interface shear stress is most important in determining the shear strength of members without transverse reinforcement (ASCE-ACI committee 445, 1998).

The tooth model method was illustrated with test results by Mihaylov et al. (2010). The shaded area of concrete in the LS3 crack diagram (Fig. 3.147) can be viewed as a cantilever fixed at the top part of the beam, which Kani et al. (1979) called a “tooth.” The bond forces between the bottom reinforcement and the concrete tend to bend the cantilever toward midspan, while the aggregate interlock (AI) and dowel action (DA) resist this bending. Both of these resisting mechanisms degrade as cracks widen; and by LS4 (Fig. 3.147), this cantilever had failed as shown by the now nearly uniform stress in longitudinal reinforcement over the width of the tooth. In deep beams, the loss of the teeth does not result in an immediate collapse of the beam. It resulted in almost constant tension in the bottom reinforcement, showing that the load-bearing mechanism has switched from beam action to almost pure arch action, as suggested by Kani (1964).

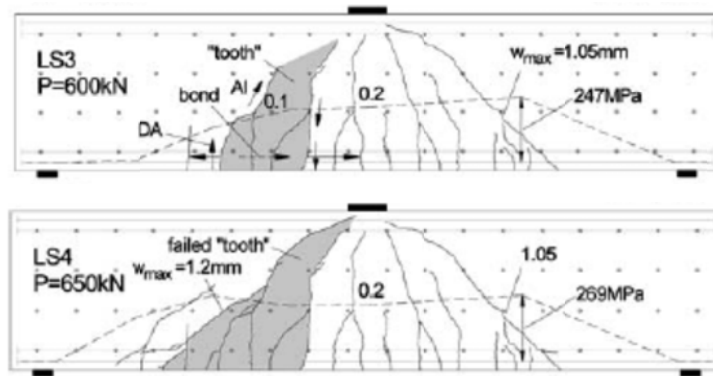


Fig. 3.147: Illustration of Kani's tooth model with test results (Mihaylov et al., 2010).

### 3.3.4.2 Bond model

Alexander and Simmonds (1992) developed a bond model in which radial arching action and the concept of a critical shear stress on a critical section are combined. The bond strength of the reinforcement is the significant factor. The model gives a simple lower bound estimate of the ultimate slab shear strength. Tests showed that the radial compression struts (as assumed in the 3D strut-and-tie model by Alexander and Simmonds, 1986) are actually curved and parallel to the reinforcement in plan, which changes the mechanics of the truss model. The bond model combines features of the truss model with the concept of a limiting shear stress. The basis of the method is the following expression of the shear force:

$$V = \frac{d(Tjd)}{dx} = \frac{d(T)}{dx} jd + \frac{d(jd)}{dx} T \quad (3.83)$$

in which the first part is carried by beam action (requiring strong bond forces) and the second part by arching action (requiring only remote anchorage of the reinforcement).

In equation (3.83) the following parameters are used:

- $T$  the steel tension force;
- $jd$  the effective moment arm.

The geometry of the curved arch (which replaced the compression strut) is not governed by conditions at the intersection of the arch and the reinforcement tying the arch, but rather by the interaction between the arch and the adjacent quadrants of the slab. The radial strips (Fig. 3.148) extend from the loaded zone, up to a "remote end", which is a position of zero shear. The shear carried in the radial compression arch varies from a

maximum near the loaded zone where the slope of the arch is large, to a minimum at the intersection of the arch and the reinforcing bar, where the slope is small. The shear carried by a radial strip needs to be dissipated some distance away from the loaded area, depending on the curvature of the arch. Fig. 3.149 describes the radial strip as a cantilever beam. The length  $l$  is called the loaded area, and  $w$  the uniformly distributed load. For four radial strips extending from the loaded area, a lower bound of the shear capacity is expressed as:

$$P = 8\sqrt{M_s w} \quad (3.84)$$

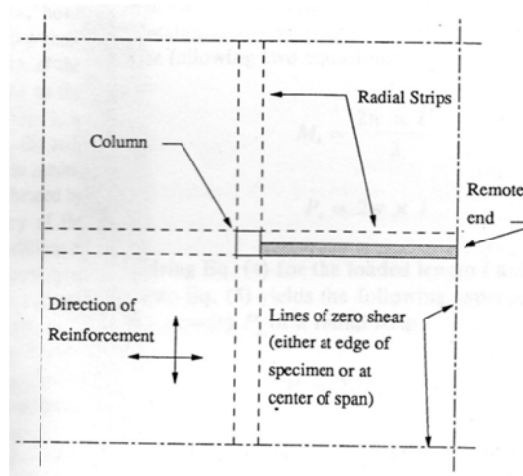


Fig. 3.148: Layout of radial strips, Alexander and Simmonds (1992).

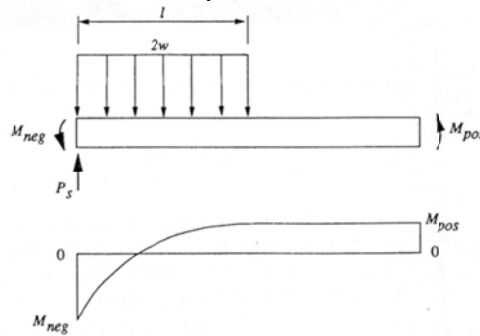


Fig. 3.149: Equilibrium of radial strip, Alexander and Simmonds (1992). The flexural capacity of the strip  $M_s$  and the loading term  $w$  are consequently defined to meet two conditions:

- the equilibrium of the strip has to be satisfied, and
- both the flexural capacity and shear capacity of the strip may not be exceeded at any point in the strip.

The flexural capacity depends upon the amount of reinforcement that effectively acts within the strip and is composed of the negative and positive moment capacity.

$$M_{neg} = \rho_{neg} f_y j d^2 c \quad (3.85)$$

$$M_{pos} = k_r \rho_{neg} f_y j d^2 c \quad (3.86)$$

In these equations, the following symbols are used:

$\rho_{neg} = \frac{A_{sT}}{bd}$  the negative effective reinforcing ratio;

$\rho_{pos} = \frac{A_{sB}}{bd}$  the positive effective reinforcing ratio;

$A_{sT}$  the total cross-sectional area of top steel within the radial strip plus half the area of the first top bar on either side of the strip;

$A_{sB}$  the total cross-sectional area of bottom steel within the radial strip plus half the area of the first top bar on either side of the strip;

$b$  the total distance between the first reinforcing bars on either side of the radial strip;

$d$  the effective depth;

$jd$  the internal moment arm;

$c$  the width of the radial strip;

$f_y$  the yield stress of the reinforcement;

$k_r$  a factor which accounts for the proportion of the bottom steel that can be developed by the rotational restraint at the remote end of the strip. This is zero if the remote end is simply supported.

The loading term  $w$  represents a lower bound estimate of the maximum shear load that may be delivered to one side of a radial strip by the adjacent quadrant of the slab.

The maximum value of the loading term  $w$  is based on the maximum value of beam action shear

$$w_{ACI} = 0.166d\sqrt{f'_c} \quad (3.87)$$

The bond model also explains how load may be carried in the presence of diagonal cracking. Test results have shown that diagonal cracking occurs at 50 to 70% of the ultimate load.



### 3.3.5. Plasticity-based models

#### 3.3.5.1 Failure criteria

This section focuses on the failure criteria used in plasticity-based models. The concrete material strengths are the effective uniaxial tensile  $f_t$  and compressive  $f_c$  strengths, as opposed to the actual measured uniaxial tensile and compressive strengths. Typically, effectiveness factors need to be applied to the measured concrete material strengths.

##### 3.3.5.1.1 Coulomb's hypothesis and the modified Coulomb criterion

In 1776, Coulomb advanced the frictional hypothesis, based on the observation that failure often occurs along certain sliding planes or yield planes. These yield planes are determined by:

- their resistance: the cohesion, and
- an internal friction, the magnitude of which depends on the normal stress in the sliding plane.

Mohr (Fig. 3.150) generalized this theory and assumed that failure occurs when the stresses in a section satisfy the condition  $f(\sigma, \tau) = 0$  which gives a failure envelope in a  $(\sigma, \tau)$  coordinate system.

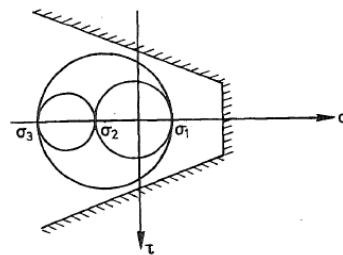


Fig. 3.150: Mohr's circles of principal stresses. (Nielsen, 1984).

Combining Coulomb's hypothesis with an extra limitation on the greatest principal stress  $\sigma_I$  (a tension cutoff), the modified Coulomb criterion is obtained (Nielsen, 1984). By combining Coulomb's criterion with a limit on the tensile stress, two failure modes can be distinguished:

- sliding failure (characterized by cohesion  $c$  and internal friction which is a fraction  $\mu$  of the normal stress), or
- separation failure (characterized by the separation resistance  $f_A$ ).

The condition for sliding failure is given as:

$$|\tau| = c - \mu\sigma \quad (3.88)$$

The condition for separation failure is:

$$\sigma = f_A \quad (3.89)$$

In a  $(\sigma, \tau)$  coordinate system this is represented by Fig. 3.151.

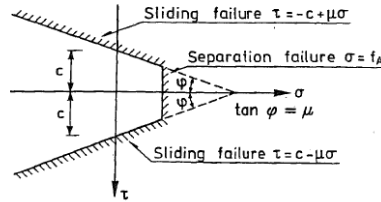


Fig. 3.151: Failure criterion for a modified Coulomb material. (Nielsen, 1984).

Transforming this into relations between the principal stresses  $\sigma_1$  and  $\sigma_3$ , this becomes:

$$\frac{1}{2}(\sigma_1 - \sigma_3) = c \cos \varphi - \frac{1}{2}(\sigma_1 + \sigma_3) \sin \varphi \quad (3.90)$$

With  $\mu = \tan \varphi$ , Eq. (3.90) becomes:

$$\left(\mu + \sqrt{1 + \mu^2}\right)^2 \sigma_1 - \sigma_3 = 2c \left(\mu + \sqrt{1 + \mu^2}\right) \quad (3.91)$$

Using  $k = \left(\mu + \sqrt{1 + \mu^2}\right)^2$ , the condition for sliding failure becomes:

$$k\sigma_1 - \sigma_3 = 2c\sqrt{k} \quad (3.92)$$

and the condition for separation failure is still represented by Eq. (3.89).

For a plane stress field, this is graphically represented in Fig. 3.152.

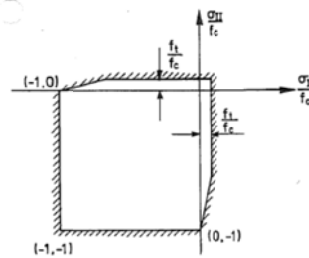


Fig. 3.152: Failure criteria for concrete as a modified Coulomb material at plane stress (Nielsen, 1984).

In Fig. 3.152, the relation between the principal stresses is:

$$\sigma_2 = f_{ctm} - \frac{f_{ctm}}{f_{ccm}} \sigma_1 \quad (3.93)$$

According to the theory of Mohr, the principal stresses can be written as a function of the actual stresses:

$$\begin{aligned} \sigma_1 &= \frac{\sigma_c}{2} - \frac{1}{2} \sqrt{\sigma_c^2 + 4\tau_c^2} \\ \sigma_2 &= \frac{\sigma_c}{2} + \frac{1}{2} \sqrt{\sigma_c^2 + 4\tau_c^2} \end{aligned} \quad (3.94)$$

Substituting (3.94) in (3.93) yields:

$$\sqrt{\sigma_c^2 + 4\tau_c^2} \left( 1 + \frac{f_{ccm}}{f_{ctm}} \right) + \sigma_c \left( 1 - \frac{f_{ccm}}{f_{ctm}} \right) - 2f_{ccm} = 0 \quad (3.95)$$

Solving for  $\tau_c$  gives:

$$\tau_c = \sqrt{\frac{1}{4} A f_{ccm}^2 + B f_{ccm} + C} \quad (3.96)$$

with

$$\begin{aligned} A &= \frac{f_{ccm} - f_{ctm}}{f_{ccm} + f_{ctm}} \\ B &= \frac{(f_{ccm} - f_{ctm}) f_{ccm} f_{ctm}}{(f_{ccm} + f_{ctm})^2} \\ C &= \frac{(f_{ccm} f_{ctm})^2}{(f_{ccm} + f_{ctm})^2} \end{aligned}$$

This is represented in Fig. 3.153.

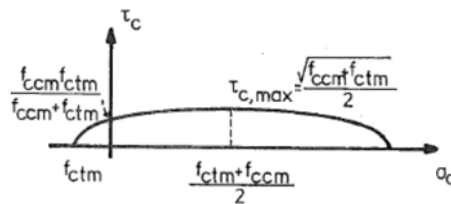


Fig. 3.153: The relation between the normal stress and the shear stress (Pruijssers, 1986).

Strictly speaking, concrete cannot be treated as an isotropic material, but must be treated as a material with load induced anisotropy. However, according to Nielsen (1984) applying a simple isotropic failure condition like the modified Coulomb criterion is a

reasonable approximation. Typically, for concrete  $\mu = 0,75$ ; the angle of friction  $\varphi = 37^\circ$  and  $c = \frac{1}{4} f_c$ . Comparison of the criterion with test results is shown in Fig. 3.154.

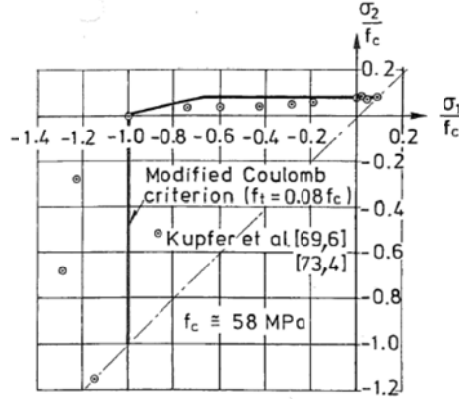


Fig. 3.154: Test results for concrete in biaxial stresses compared to the failure criterion for a modified Coulomb material (Nielsen, 1984)

### 3.3.5.1.2 Parabolic Mohr failure criterion

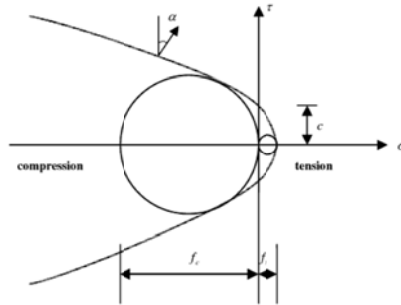


Fig. 3.155: Parabolic Mohr-failure criterion for concrete (Salim and Sebastian, 2002).

The parabolic Mohr failure criterion (Fig. 3.155) is expressed as:

$$\left( \frac{\tau}{c_k f_t} \right)^2 + \frac{\sigma}{f_t} = 1 \quad (3.97)$$

where  $\tau$  and  $\sigma$  are shear and normal stresses on an arbitrary plane and  $c_k$ :

$$c_k = \sqrt{1 + \frac{f_c}{f_t}} - 1 \quad (3.98)$$

The shear and normal stresses in the parabolic Mohr failure envelope can be given as functions of the parameter  $\alpha$  defined in Fig. 3.155:

$$\tau = f_t \frac{c_k^2}{2} \cot \alpha \quad (3.99)$$

$$\sigma = f_t \left( 1 - \frac{c_k^2}{4} \cot^2 \alpha \right) \quad (3.100)$$

The maximum and minimum principal stresses are:

$$\sigma_1 = f_t \left( 1 - \frac{c_k^2}{4} (\csc \alpha - 1)^2 \right) \quad (3.101)$$

$$\sigma_3 = f_t \left( 1 - \frac{c_k^2}{4} (\csc \alpha + 1)^2 \right) \quad (3.102)$$

The yield loci for the cases of plane stress and plane strain are shown in Fig. 3.156.

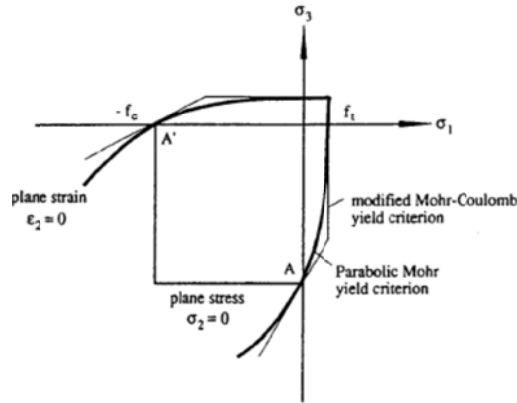


Fig. 3.156: Yield loci in cases of plane stress and plane strain (Salim and Sebastian, 2002).

### 3.3.5.2 Plasticity models

#### 3.3.5.2.1 Introduction

For shear failure, the modified Coulomb criterion can be applied to the narrow plastic zone in between two rigid zones (Fig. 3.157 and Fig. 3.158).



Fig. 3.157: Discontinuities in shear failures (Cope and Clark, 1984).

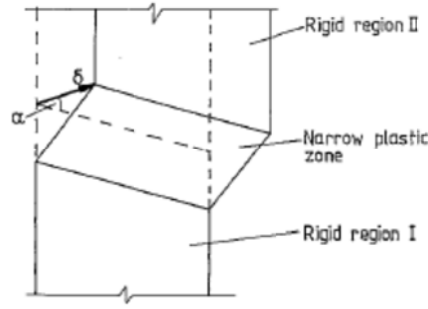


Fig. 3.158: Relative displacement of rigid zones (Cope and Clark, 1984).

The cohesion  $c$  equals  $c = \frac{f_e(1 - \sin \phi)}{2 \cos \phi}$  with  $f_e$  the effective uniaxial compressive strength. The yield criterion consists again of a sliding criterion and a separation criterion. If a region II moves in a given direction relative to a rigid region I, then the normal and shear displacements in the narrow plastic zone can be determined. The work per unit area dissipated in the narrow plastic zone can be evaluated. For a displacement  $\delta$  at an angle  $\alpha$  to the discontinuity, as shown in Fig. 3.158, the work equations are:

*Plane strain:*

$$W = \delta \left( \frac{f_e}{2} (1 - \sin \alpha) + \frac{(\sin \alpha - \sin \phi)}{(1 - \sin \phi)} f_{te} \right) \text{ for } \phi \leq \alpha \leq \pi/2 \quad (3.103)$$

At the limits Eq. (3.103) reduces to:

$$W = \delta f_e \frac{(1 - \sin \phi)}{2} \text{ for } \alpha = \phi \text{ (sliding)} \quad (3.104)$$

$$W = \delta f_{te} \text{ for } \alpha = \pi/2 \text{ (separation)} \quad (3.105)$$

Failure in the narrow plastic zone cannot occur for  $\alpha < \phi$ .

*Plane stress:*

Eq. (3.103) is applicable for  $\phi \leq \alpha \leq \pi/2$

$$W = \delta f_e \frac{(1 - \sin \alpha)}{2} \text{ for } -\pi/2 \leq \alpha \leq \phi \quad (3.106)$$

### 3.3.5.2.2 Shear capacity explained by plasticity models

Walther developed a generalized design theory using Mohr circles, Fig. 3.159, in which line (1) represents Mohr's envelope curve, (2) is the stress Mohr circle ( $\sigma_y = 0$ ) and (3) is the failure criterion of a biaxial stress state with  $\sigma_y = 0$  (Balazs, 2010).

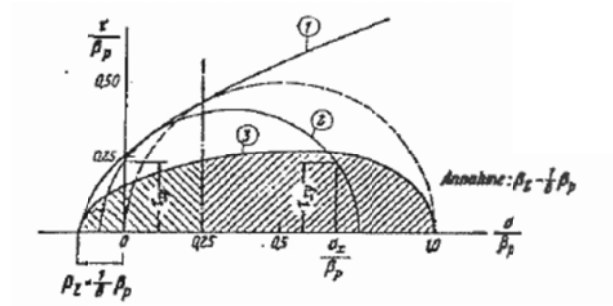


Fig. 3.159: Background of the model by Walther, ( $\beta_z = f_{ct}$ ,  $\beta_p = f_{c,pr}$ ), (Balazs, 2010)

A lower bound plasticity solution requires a statically admissible, safe stress field to be constructed, which can only exist in certain simple cases.

An example of a lower bound solution for a beam in shear without web reinforcement is shown in Fig. 3.160. The beam is assumed to act as an arch, with region ABDE in uniaxial compression and regions AEF and BCD under biaxial hydrostatic pressure.

Geometric considerations give  $BC = x_0 = \frac{1}{2} \left( \sqrt{a^2 + h^2} - a \right)$ , which leads to the lower bound solution:

$$P = bx_0 f_c \quad (3.107)$$

which can also be written as:

$$\frac{\tau}{f_c} = \frac{P}{bh f_c} = \frac{x_0}{h} = \frac{1}{2} \left( \sqrt{1 + \left( \frac{a}{h} \right)^2} - \frac{a}{h} \right) \quad (3.108)$$

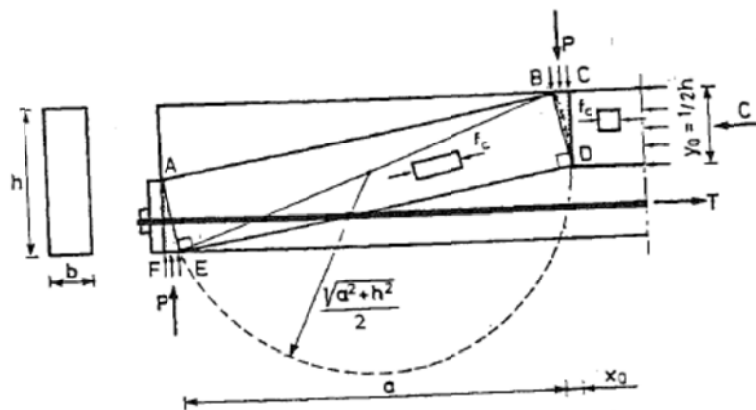


Fig. 3.160: Lower bound solution for a beam without shear reinforcement (Nielsen, 1984).

An upper bound approach based on the critical crack as a yield line leads to the same solution. Eq. (3.108) is thus exact, Fig. 3.161.

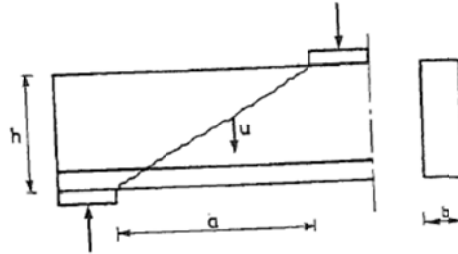


Fig. 3.161: Failure mechanism for a beam without shear reinforcement. (Nielsen, 1984).

Fernandez Ruiz and Muttoni (2007) suggested the use of stress fields to decide which strut-and-tie model to select. Stress fields are developed as a direct application of the theory of plasticity. The presented method shows an approach how to develop stress fields and truss models based on the finite element method. A different stress-strain law is used for stress fields (Fig. 3.162(b)) as compared to regular strut-and-tie models, Fig. 3.162(a). Vecchio and Collins' (1986) approach of the MCFT for compression fields including the effect of transverse strains of concrete is used to account for the effect of cracking. A Mohr-Coulomb yield surface is used with a tension cut-off and an associative flow rule, where the effect of the transverse strains  $\eta(\epsilon_i)$  can be interpreted as a contraction in the yield surface with increasing positive transverse strains, Fig. 3.163. An example of a stress field approach is shown in Fig. 3.164 and Fig. 3.165 while the classic solution through a strut-and-tie model is shown in Fig. 3.166. Unusual cases can be systematically investigated with stress fields, considering the actual reinforcement layout and the nonlinear behavior of the concrete.

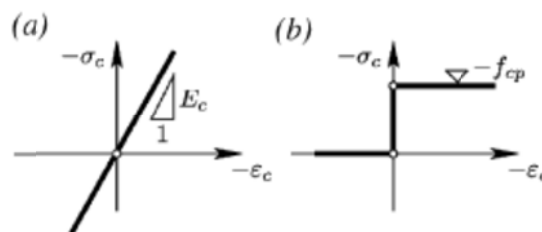


Fig. 3.162: Comparison of uniaxial stress-strain laws for concrete: (a) linear elastic (with tensile strength); and (b) rigid-plastic without tensile strength. (Fernandez Ruiz and Muttoni, 2007).



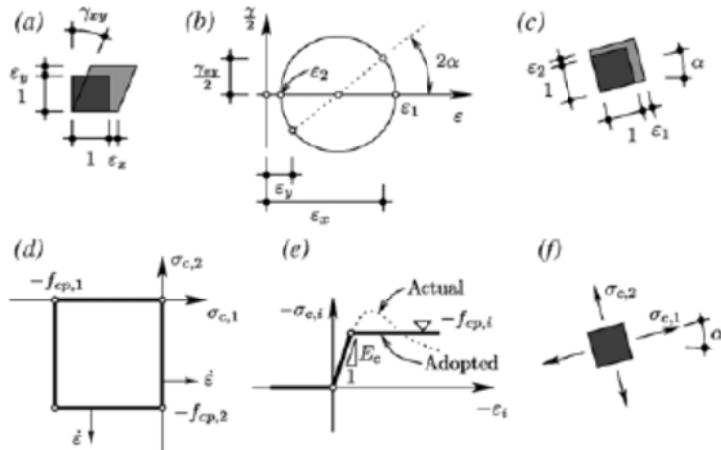


Fig. 3.163: Concrete modeling: (a) strains; (b) Mohr's circle and principal strains; (c) directions of principal strain; (d) adopted yield surface for plane stress and associative flow rule; (e) actual and adopted (elastic-perfectly plastic) stress-strain response; and (f) assumed directions for principal stresses. (Fernandez Ruiz and Muttoni, 2007).

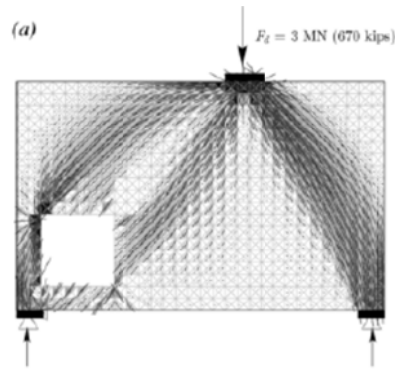
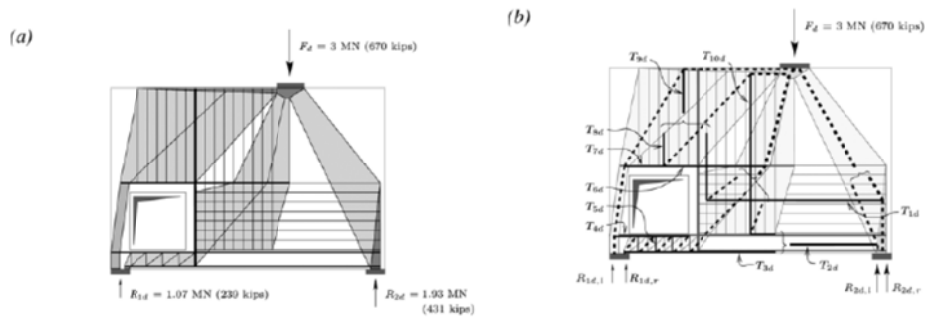


Fig. 3.164: Nonlinear FE model results for deep beam with opening: plot of concrete principal compressive stress directions. (Fernandez Ruiz and Muttoni, 2007).



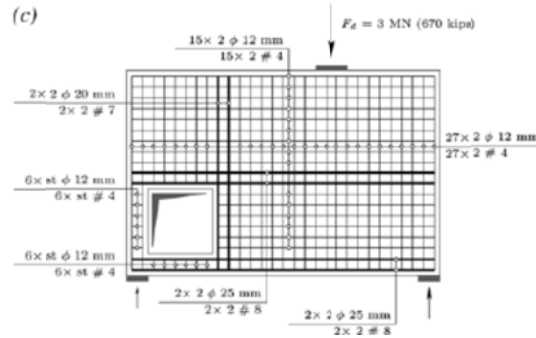


Fig. 3.165: Dimensions of a deep beam according to FE results: (a) adopted stress field; (b) resulting truss model and main values; and (c) proposed reinforcement layout. (Fernandez Ruiz and Muttoni, 2007).

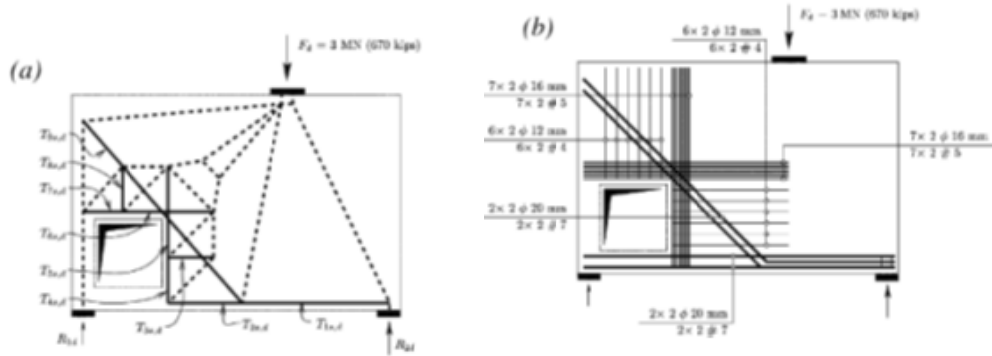


Fig. 3.166: Dimensioning of deep beam according to Schlaich et al. (1987): (a) adopted truss model and main values; and (b) reinforcement layout. (Fernandez Ruiz and Muttoni, 2007).

Cho (2003) uses a plasticity model to describe the shear behavior of short beams taking crack sliding into account. A modified Coulomb failure criterion with zero tension cutoff is used. Reinforcement is assumed to resist forces in the axial direction only with the yield stress  $f_y$ . The effective compressive strength of uncracked or cracked concrete is taken as

$$f_c = \nu_0 \nu_s f_c' \quad (3.109)$$

with:

- $f_c'$  the cylinder compressive strength,
- $\nu_0$  the effectiveness factor for uncracked or microcracked concrete, and
- $\nu_s$  the sliding resistance reduction factor to account for macrocracking.

### 3.3.5.2.3 Punching shear capacity explained by plasticity models

A plasticity-based model for punching shear was developed by Kinnunen and Nylander (1960). The theory was based on the assumption that the slab portion outside the shear crack, which is bounded by this crack, by radial cracks, and by the circumference of the slab, can be regarded as a rigid body, which is turned under load action around a centre of rotation located at the root of the shear crack.

The considered failure modes were:

- failure in shear under the plane of flexural reinforcement,
- failure of the concrete cone between the shear crack and the column,
- failure in compression of the concrete in a tangential direction.

Kuang and Morley (1993) used a two-phase approach in a plasticity model to describe the punching capacity of slabs taking the compressive membrane action into account. A parabolic Mohr failure criterion was used.

Salim and Sebastian (2002) used rigid plastic theory to analyze punching shear based on a parabolic Mohr failure criterion, Fig. 3.155. The upper-bound theorem of plasticity states that if, for any assumed failure mechanism, the external rate of work is equated to the rate of dissipation of internal energy, then an upper-bound for the collapse load of the structure can be found. Salim and Sebastian (2002) used a parabolic and linear failure generatrix to describe the punching cone. Comparison to experimental results gave high coefficients of variation.

#### ***3.3.5.2.4 Discussion of plasticity models***

The main points of criticism of the plasticity models are the following:

1. The location of the crack is based on simplifications. When the crack is transformed into a yield line, there will be a displacement component parallel to the crack. The cracking moment is derived from simplifications, a fracture mechanics approach could lead to an improved quantification of the cracking load (Nielsen, 1984).
2. Plasticity models require a certain amount of redistribution and ductility which is not always available in the case of a brittle shear failure (Lubell 2006,
3. The effectiveness factors need to be determined empirically. These factors are not the same for all load cases and cannot be physically explained in a satisfactory way (Walraven 1980). Salim and Sebastian (2002), however, see it as an

advantage that only effectiveness factors relating concrete compressive and tensile strengths need to be determined through the calibration of theoretical results against experimental results. Nielsen (1984) explains that finding the effectiveness factor is straightforward for beams with web reinforcement, but becomes complicated and dependent on  $a/h$  for elements without web reinforcement.

4. The size effect is not modeled correctly. According to Bažant and Kim (1984), this is not surprising, since the stress-strain relation of concrete has no yield plateau and exhibits strain softening, which causes that the limit stress state cannot exist along some postulated failure surface, as required by plastic limit analysis, but is reached successively at various points of the failure surface.

### **3.3.6. Fracture mechanics models**

#### **3.3.6.1 Introduction to fracture mechanics models**

Fracture mechanics approaches were first applied to the problem of shear in concrete in the late 1970s. The field of fracture mechanics provides tensile stress-crack opening relations further to stress-strain relations, making it possible to better describe the behavior of structures, especially those which exhibit a brittle failure behavior. The fracture energy, as a function of the concrete compressive strength and the maximum aggregate size, is used in these expressions (Walraven, 2007).

Fracture mechanics models (ASCE-ACI committee 445, 1998) study the peak tensile stress near the crack and the reduced tensile stress (the so-called softening) in the cracked zone. Shear cracks are supposed to have the Mode II (shear) fracture energy. However, Mode II fracture energy can be neglected and replaced by mode I fracture energy if the crack plane is properly modeled (McCabe and Niwa, 1993). Normal and shear stresses on a crack plane correspond to modes I and II respectively (Reinhardt, 1986). Shear failure is related to the critical stress intensity factor of the material. Fracture mechanics approaches do not treat fracture as a point phenomenon, but recognize that in a brittle heterogeneous material such as concrete, the fracture propagates with a relatively large fracture process zone ahead of the crack tip in which progressive microcracking gradually reduces the tensile stress to zero (Mihashi and Nomura, 1993). Most approaches are

based on nonlinear fracture mechanics (Bažant and Kim, 1984). The propagation nature of failure gives rise to size effect unless the failure occurs at the first initiation of fracture (Bažant and Kazemi, 1991; Ghazavy-Khorasgany and Gopalaratnam, 1993).

### 3.3.6.2 Modeling material behavior

McCabe (1997) highlights that under the right conditions, concrete can develop widespread micro-cracking even under nominal loading. The challenge is to determine how this complex material behaves as these cracks coalesce and grow into structural cracks. To incorporate fracture mechanics into a finite element solution, two approaches are possible:

1. The discrete crack model: the actual geometry of the crack is modeled. The finite element mesh must be modified to include the actual crack as it propagates through the material.
2. The smeared crack model: the stiffness properties of the element are changed to capture the effects of cracking.

An example of the smeared crack formulation is the fictitious crack model, which describes the stress versus deformation properties of materials in tension (Gustafsson and Hillerborg, 1988). Before peak stress, the deformation of a specimen in uniform tension is assumed to be uniform along the length of a specimen and may be described as a strain  $\epsilon$ , Fig. 3.167a,b.

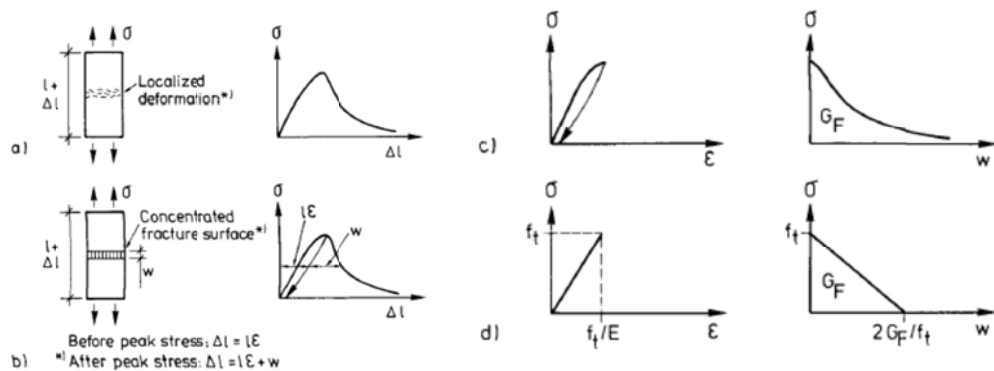


Fig. 3.167: Fictitious crack model description of tensile fracture: (a) Realistic structural behavior; (b) model of structural behavior; (c) model for description of properties of material; and (d) presently assumed simplified properties of material (Gustafsson and Hillerborg, 1988).

At peak stress, a localized fracture zone, or a concentrated damage zone, is assumed to develop. This strain localization is a result of strain instability. As the total elongation of the specimen increases further, the stress within the specimen decreases gradually. During this decrease in stress, the strain outside the concentrated fracture zone decreases (unloading) while the additional deformation or elongation  $w$  within the fracture zone increases (softening). The fictitious crack model uses tension softening to go from the initiation of micro-cracks in concrete under tension to the development of major macroscopic cracks (Niwa, 1997). Tension softening means that once the tensile stress reaches the tensile strength of the concrete, the stress decreases as the fictitious crack increases in width. This behavior is represented by a tension softening curve, Fig. 3.168; simplified models in Fig. 3.169 and Fig. 3.170. The properties of the material are thus described by one stress-strain ( $\sigma - \varepsilon$ ) diagram valid for the material outside the fracture zone, and by one stress-elongation ( $\sigma - w$ ) diagram, valid for the additional deformation of the material within the fracture zone, Fig. 3.167c, schematized in Fig. 3.167d. Three parameters are required for defining the material properties and thus the magnitude of stress, strain and elongation. These parameters can be chosen as  $f_t$  (tensile strength),  $E$  and  $G_F$  (fracture energy). The area enclosed by the tension softening curve is the fracture energy of the concrete,  $G_F$ . The fracture energy is defined as the energy required to create a fully cracked unit surface of concrete across which the tensile stress cannot be transferred. The main drawback of the fictitious crack model is that the crack plane must be modeled before analysis (McCabe, 1997). The fictitious crack model also cannot provide analytical expressions which could be used in a design formula (Reinhardt, 1986). The local fracture energy  $g_f$  increases as the crack grows and then turns almost constant if the ligament lengths are sufficiently long.

$$G_F = \int_0^{w_0} \sigma dw \quad (3.110)$$

The influence of the fictitious crack on the overall behavior of a structural element is large when the element is small and the influence diminishes as the element becomes larger (Reinhardt, 1986). The characteristic, or intrinsic length can be defined as:

$$l_{ch} = \frac{EG_F}{f_t^2} \quad (3.111)$$

This length gives a general measure of the ratio between the steepness of the  $(\sigma - \varepsilon)$  curve and the  $(\sigma - w)$  curve. In the case of pure bending,  $\sqrt{EG_F}$  approaches  $K_c$  if the depth of the unreinforced beam is about 20 times  $l_{ch}$ . Typically,  $l_{ch}$  is in the order of 0,25 to 0,40m which shows that the usual civil structures are too small for linear elastic fracture mechanics. Values of  $l_{ch}$  between 80 and 1300mm have been reported (Gustaffson and Hillerborg, 1988).

Gustaffson and Hillerborg (1988) suggest that the normalized shear strength  $f_v/f_t$  of geometrically similar beams is governed by the dimensionless ratio between absolute structure size  $d$  and the characteristic length of the material  $l_{ch}$ . The ratio  $d/l_{ch}$  can be regarded as a measure of the brittleness of structures sensitive to tensile stress-induced fracture.

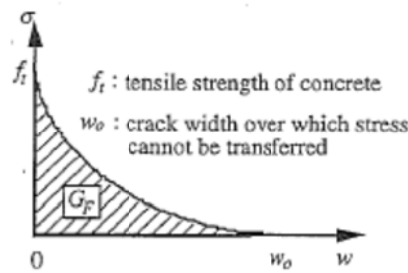


Fig. 3.168: Tension softening curve (Niwa, 1997).

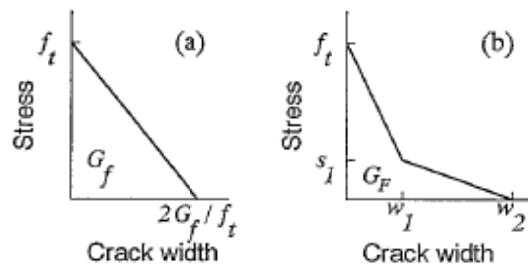


Fig. 3.169: Simplified softening diagrams (Mihashi and Nomura, 1993)

Gustaffson and Hillerborg (1988) studied the sensitivity of the shear strength  $f_v$  with regard to changes in the parameters  $d$ ,  $E$ ,  $G_F$  and  $f_t$ . While the effect of the fracture energy  $G_F$  becomes more significant, the contribution of the strength  $f_t$  decreases.

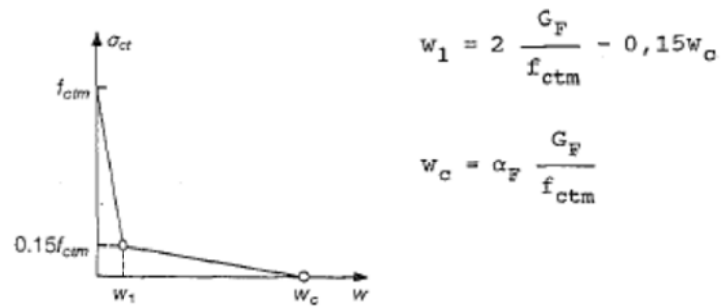


Fig. 3.170: Stress versus crack opening relation according to CEB-FIP model code 1990 (Walraven, 1993).

A decrease of the maximum particle diameter leads to an increase of the fracture energy, Table 3.8, due to a larger dispersion of the microcracks, Fig. 3.171. Within the band of microcracks, “crack bridging” occurs: this phenomenon is the mechanism behind the residual stresses transmitted across the crack faces during crack widening.

Table 3.8: Fracture energy  $G_F$  from Model Code 1990 (Walraven, 1993).

max. aggregate size $d_{\max}$ (mm)	$G_F$ (N/mm <sup>2</sup> )			
	C20	C40	C60	C80
8	50	70	95	115
16	60	90	115	135
32	80	115	145	175

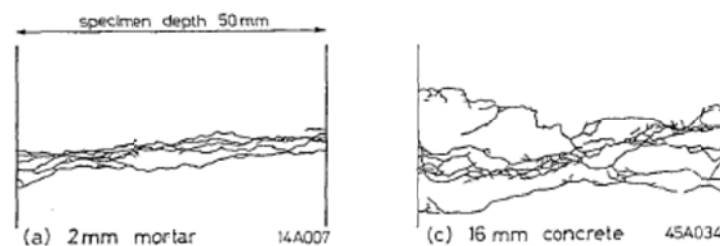


Fig. 3.171: Influence of maximum particle diameter on crack band width (Walraven, 1993)

In Model Code 2010, the fracture energy is determined as:

$$G_f = 73 f_{cm}^{0.18} \quad (3.112)$$

with



$f_{cm}$  the mean concrete compressive strength.

Voormeeren (2011) varied the crack bandwidth in nonlinear finite element analysis to model a reinforced concrete slab under a concentrated load close to the support. The assumption of a band width  $h = \sqrt[3]{V}$  seemed to simple, since the crack bandwidth is greatly depending on the mesh shape and the inclination of the crack in brick elements. In case of a higher fracture energy the structure shows a stiffer response and a higher peak load, and more ductile behavior. An increase in the crack bandwidth  $h$  to  $h = 1,5\sqrt[3]{V}$  implies a reduction of the fracture energy  $G_f/h$ , which in turn results in a lower ultimate strain  $\varepsilon_u$  (ductility) of the concrete. Three reasons are given for this reduction of the fracture energy:

1. The assumption that cracks in rectangular solid element meshes do not always run along the meshing lines. Especially in the case of the slab subjected to a concentrated load, the shear crack propagation is expected in an inclined direction.
2. The adopted linear softening curve: in case of exponential softening, the negative slope after reaching the tensile strength is steeper than in case of linear tension softening. Therefore, one normally reduces the adopted amount of tensile fracture energy by a factor  $(1/3 - 1/2)$  to simulate the slope of the real exponential softening curve of concrete.
3. An overestimation of the fracture energy by the guidelines is also a possibility.

### 3.3.6.3 Fracture mechanics models for shear

Gustaffson and Hillerborg (1988) used a semi-empirical approach to show that the shear

strength of concrete is proportional to  $\left(\frac{EG_f f_c'}{d}\right)^{\frac{1}{4}}$  with  $E$  the elastic modulus and  $G_f$  the fracture energy of concrete.

Pruijssers (1986) altered Kani's tooth model (1964) to account for the shear carried by residual tension at the crack tip, Fig. 3.172. He described that at the onset of shear failure, the crack propagates into the compression zone, decreasing the effective depth of the uncracked area. The concrete teeth are shown in detail in Fig. 3.173. The concrete teeth deform due to the bond between the concrete and the longitudinal reinforcing bars. At the

root of the teeth the tensile strain is reached and another tension-softening zone develops. Due to this softening the teeth will slide over each other close to the root, where the crack width is very small. The micro cracks in zone I (Fig. 3.173) undergo a shear deformation. Aggregate interlock can be used to describe the shear stiffness of the tension softening zone.

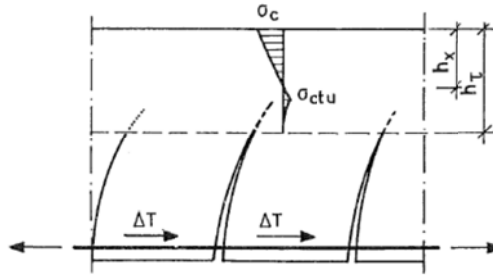


Fig. 3.172: Concrete teeth and stress distribution (Pruijssers, 1986).

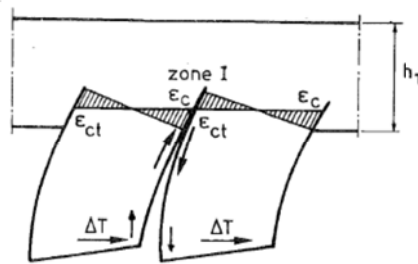


Fig. 3.173: Concrete teeth (Pruijssers, 1986).

Due to the fact that the tension softening zone transfers shear stress, the depth of the arch is not the depth  $h_x$  of the uncracked compressive zone, but equals the so-called effective shear depth  $h_t$ , Fig. 3.174. The shear resistance can then be based on a simple equation:

$$V_{cu} = \frac{2}{3} \alpha \tau_o b h_t \quad (3.113)$$

in which:

$\alpha$  a parameter representing the effectiveness of the tension-softening zone in transferring shear stress.

A final expression is then obtained by using the Mohr-Coulomb failure criterion for the maximum shear stress.

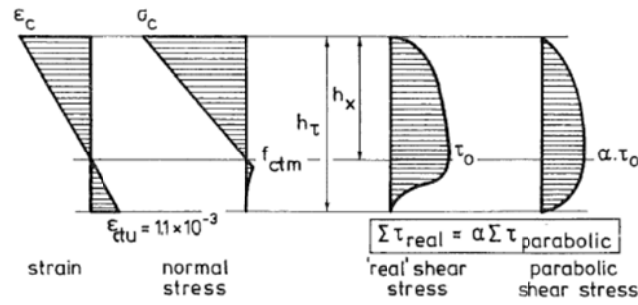


Fig. 3.174: Representation of the effective shear depth  $h_\tau$ . (Pruijssers, 1986).

The model by Fischer and König (1997), is related to the fracture energy. The maximum shear force is determined by:

$$V = \frac{(12G_f + 523)bd^2 + H\sqrt{3}d + Z3/4d}{(x_s + \sqrt{3}d)} \quad (3.114)$$

$$G_f = 65 \ln \left( 1 + \frac{f_{cm}}{10} \right) \quad (3.115)$$

$$H = 0,76d_s b_n^3 \sqrt{12f_{cm}} \quad (3.116)$$

$$Z = A_s \sigma_s = A_s \sqrt{\frac{0,215 \tau_{sm} E_s}{d_s}} \quad (3.117)$$

$$x_s = \frac{3}{4} \frac{a}{d} \sqrt[3]{\frac{a/d}{21,9}} d \quad (3.118)$$

with

$f_{cm}$  the concrete compressive strength,

$d_s$  the diameter of the reinforcement bars.

Gastbled and May (2001) developed a model based on the assumption that the release of the main reinforcement by splitting controls the opening and the extension of the diagonal crack. Once splitting has begun, the steel bar is released from its concrete encasement. The drastically reduced stiffness in tension allows for the diagonal crack to open and extend, while a rotation about the tip of the diagonal crack occurs, Fig. 3.175. The axial and shear force in the steel bar crossing the diagonal crack can be linked to the angle of rotation  $\theta$  using the elastic properties of the bar and the geometry of the deformation mechanism. Assuming the angle of the diagonal crack  $\varphi$  to be  $45^\circ$ :

$$F_s = \frac{E_s A_s}{\delta_s} \Delta u_s = \frac{E_s A_s}{\delta_s} y \theta \quad (3.119)$$

$$V_d = \frac{G_s \Sigma_s}{\delta_s} \Delta v_s = \frac{9}{26} \frac{E_s A_s}{\delta_s} y \theta \quad (3.120)$$

with

$G_s$  the shear modulus of steel,  
 $\Sigma_s$  the reduced cross section of the bar  
 $\delta_s$  the unbonded length of the reinforcement.

In Eq (3.120) the principles from beam theory for a circular cross section are used:

$$\Sigma_s = 0,9 A_s$$

$$G_s = \frac{E_s}{2(1+\nu_s)} = \frac{9}{26} E_s$$

Moment equilibrium around the free body as shown in Fig. 3.176 and assuming the diagonal crack extent  $y$  and the internal moment arm  $jd$  to be proportional to the height of the beam  $H$  ( $y=\beta H$  and  $jd=\gamma H$ ) leads to a formula for the rotational stiffness:

$$V a_c = \beta \left( \frac{9}{26} \beta + \gamma \right) \frac{E_s A_s}{\delta_s} H^2 \theta \quad (3.121)$$

Differentiating this expression about the unbonded length  $\delta_s$  yields:

$$\delta \theta = \delta \left( a_c \frac{\delta_s}{A_s E_s} \frac{V}{\beta \left( \frac{9}{26} \beta + \gamma \right) H^2} \right) = \frac{a_c}{A_s E_s} \frac{V}{\beta \left( \frac{9}{26} \beta + \gamma \right) H^2} \delta e \quad (3.122)$$

with

$\delta e$  the variation of the unbonded length, that is, the variation of the extent of the splitting crack.

It is now possible to write the fundamental relation of fracture mechanics as a criterion for splitting failure:

$$\delta W_{ext} = 2 \delta G \quad (3.123)$$

$$a_c V_{cr} \delta \theta = 2 \Gamma \cdot \delta e \quad (3.124)$$

with

$\Gamma$  the fracture energy necessary to extend the splitting crack by unit length.

Substituting the Eq. (3.122) into Eq. (3.124) gives the expression for the critical shear load:

$$V_{cr}^2 = \left( \frac{\beta H}{a_c} \right)^2 \left( \frac{9}{13} + 2 \frac{\gamma}{\beta} \right) A_s E_s \Gamma \quad (3.125)$$

$$V_{cr} = \sqrt{\frac{9}{13} + 2 \frac{\gamma}{\beta}} \frac{\beta H}{a_c} \sqrt{A_s E_s \Gamma} \quad (3.126)$$

To simplify this formula, the following assumptions can be made:

$$jd = \gamma H = 0,9H \quad (3.127)$$

$$y = \beta H = 0,8H \quad (3.128)$$

$$d_{agg} = 20\text{mm}$$

For the assessment of the fracture energy, the formula from CEB-FIP Model Code (1990) was used:

$$G_f = (0,0469d_{agg} - 0,5d_{agg} + 26) \left( \frac{f_c}{10} \right)^{0,7} \text{ in Nm/m}^2 \quad (3.129)$$

If failure occurs without further increase in load, then only the fracture energy from the splitting crack is required to estimate the failure load. It is then possible to simplify Eq. (3.126):

$$V_{cr} = 4,517 \frac{H}{a_c} f_c^{0,35} \sqrt{A_s E_s b} \quad (3.130)$$

It remains difficult to determine the position of the critical diagonal crack  $a_c$ . The point of first shear cracking can be obtained by assuming that the diagonal crack initiates from a flexural crack when the tensile strength of the concrete is reached due to bond stress concentration at the steel bar level, near the flexural crack. First, the load required for a flexural crack to exist is given as:

$$V_{fl} = \frac{M_{cr}}{a_c} = k_1 \frac{\sqrt{\rho_s f_c} b d^2}{a_c} \quad (3.131)$$

with  $k_1$  an empirical factor. Secondly, the load at which the bond stress reaches the tensile strength of concrete is given:

$$V_b = k_2 \left( 1 - \sqrt{\rho_s} \right) \sqrt{\frac{f_c a_c}{a_s}} b d \quad (3.132)$$

with  $k_2$  an empirical factor. When both loads are equal, diagonal cracking occurs and  $a_c$  can be found as:

$$a_c = k_3 a_2 \left( \frac{\rho_s \left( \frac{d}{a_s} \right)^2}{(1 - \sqrt{\rho_s})^2} \right)^{1/3} \quad (3.133)$$

The suggested value for  $k_3$  is 3,3. Substituting Eq. (3.133) into Eq. (3.130) provides a predictive analytical formula for the flexural-shear capacity:

$$V_{cr} = \frac{1,109}{\sqrt{H}} \left( \frac{H}{a_s} \right)^{1/3} (1 - \sqrt{\rho})^{2/3} \rho_s^{1/6} f_c^{0,35} \sqrt{E_s} b H \quad (3.134)$$

The first term corresponds to the size effect, the second takes into account the slenderness of the beam, the third and fourth terms reflect the reinforcement ratio influence and the fifth term the influence of the concrete strength.

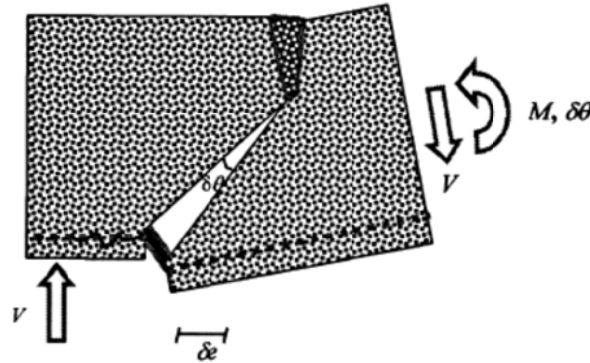


Fig. 3.175: Failure mechanism by flexure-shear failure by splitting (Gastebled and May, 2001).

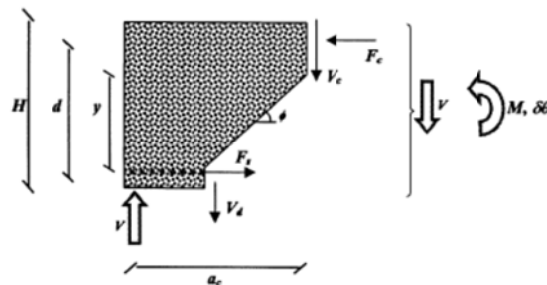


Fig. 3.176: Free body diagram and notation definition (Gastebeld and May, 2001).

A new approach (Xu and Reinhardt, 2005) focuses on using the mode II fracture toughness  $K_{IIc}$  and mode II fracture energy  $G_{IIF}$  of concrete materials. A method to determine these properties experimentally is described. The authors argue that the bond fracture as described by Gasteble and May (2001) is a mode II fracture case and not a mode I fracture. Therefore the mode II fracture properties should be used, replacing Eq. (3.125) by

$$V_c^2 = \left( \frac{qH}{a_c} \right)^2 \left( \frac{9}{13} + \frac{2r}{q} \right) A_s E_s G_{IIF} b \quad (3.135)$$

Assuming  $q = 0,8$  and  $r = 0,9$  as done by Gasteble and May (2001), the following expression is obtained:

$$V_c = 1,372 \frac{H}{a_c} \sqrt{b G_{IIF} A_s E_s} \quad (3.136)$$

The same assumptions for  $a_c$  as in Eq. (3.136) are used and  $d = 0,9H$  is introduced, which leads to the shear capacity of reinforced concrete beams without stirrups to be:

$$V_c = \frac{0,446}{\sqrt{H}} \left( \frac{H}{a_s} \right)^{1/3} \rho^{1/6} (1 - \sqrt{\rho})^{2/3} \sqrt{E_s} \sqrt{G_{IIF}} b H \quad (3.137)$$

Using a basic fundament of linear elastic fracture mechanics there is a relationship of  $K_{IIc} = \sqrt{G_{IIF} E_c}$  Eq. (3.137) could then be expressed as:

$$V_c = 1,372 \sqrt{\frac{E_s}{E_c}} \frac{1}{a_c} \sqrt{\rho H} K_{IIc} b H \quad (3.138)$$

In terms of mode II fracture toughness, the expression for  $V_c$  then becomes:

$$V_c = \frac{0,446}{\sqrt{H}} \sqrt{\frac{E_s}{E_c}} \left( \frac{H}{a_s} \right)^{1/3} \rho^{1/6} (1 - \sqrt{\rho})^{2/3} K_{IIc} b H \quad (3.139)$$

### 3.3.6.4 Discussion of fracture mechanics models

Reineck (1990) points out that fracture mechanics considerations are needed in the case of a relatively brittle failure, wherein a discrete crack propagates into the compression zone. However, before a refined failure criterion can be applied, there must be an explanation of how the shear force is transferred and how the stresses and forces in the member are calculated.

### 3.3.7. Empirical models

As the mechanics of the shear problem are still not fully understood, many empirical models have been developed. These models have been developed based on laboratory tests on beams under point loads (for one-way shear: for example Zsutty, 1971; Tureyen and Frosch, 2004) or slab-column connections (for two-way shear). The code formulations which are discussed in section 5 are also based on experimental results. Of all empirical methods which are available in the literature, Regan's formula (Regan, 1982) is of most interest as it is developed for slabs under concentrated loads near to supports.

#### 3.3.7.1 Regan's formula for concentrated loads close to supports

Based on a series of small-scale tests, Regan (1982) developed a method to calculate the shear capacity of slabs under concentrated loads close to the support. The basis for this method is the punching shear formula from the British code CP110. The critical perimeter is calculated depending on the clear shear span,  $a_v$ . The critical perimeter is subdivided and the longitudinal and transverse slab properties are taken according to the part of the perimeter under consideration as shown in Fig. 3.177.

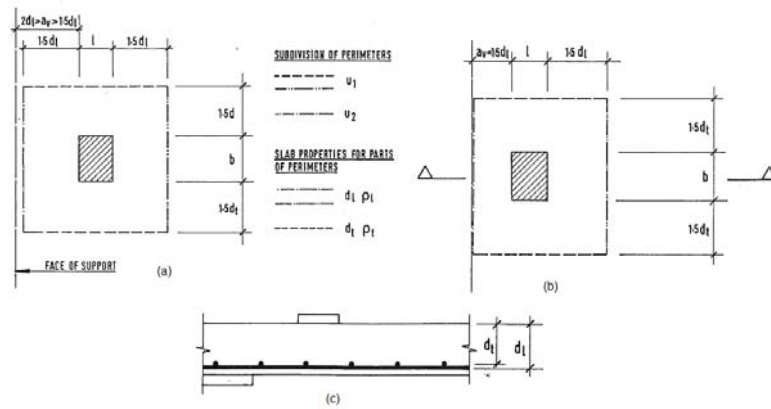


Fig. 3.177: Illustration of design method as proposed by Regan: (a) critical perimeter and slab properties for parts of the perimeter for  $2d_l > a_v > 1.5d_l$ ; (b) critical perimeter and slab properties for parts of the perimeter for  $a_v < 1.5d_l$ ; (c) slab properties. (Regan, 1982)

The resistance of the part of the perimeter parallel to the support is calculated as:

$$P_{R2} = \left( \frac{2d}{a_v} \right) \xi_s v_c u_2 d < \frac{\sqrt{f_{cu}}}{\gamma_m} u_2 d \quad (3.140)$$

with

$a_v$  the clear distance between the load and support;



$$\xi_s \quad \text{a depth factor } \xi_s = \sqrt[4]{\frac{500}{d(mm)}}; \quad (3.141)$$

$$v_c \quad \text{the shear stress (resistance) } v_c = \frac{0,27}{\gamma_m} \sqrt[3]{100\rho f_{cu}}; \quad (3.142)$$

$\gamma_m$  the partial safety factor for materials;

$u_2$  the length of the part of the perimeter under consideration, Fig. 3.177;

$f_{cu}$  the cube crushing strength of the concrete.

The resistance of the remainder ( $\Sigma u = u_l$ ) of the perimeter is calculated as:

$$P_{R1} = \sum \xi_s v_c u d \quad (3.143)$$

The total shear resistance is then:

$$P_R = P_{R1} + P_{R2} \quad (3.144)$$

Each part of the calculation should use the local values of the ratio of flexural reinforcement  $\rho$  ( $\rho_t$  and  $\rho_l$ ) and the effective depth  $d$  ( $d_t$  and  $d_l$ ) as indicated in Fig. 3.177c.

At a continuous support, the total resistance to punching is multiplied with a factor  $\alpha$ :

$$\alpha = \sqrt{\frac{M_1 + M_2}{M_1}} \quad (3.145)$$

in which

$M_1$  the larger moment at the end of the shear span;

$M_2$  the smaller moment at the end of the shear span.



		CS	100 x 100	80	2,16	180	P
<b>3</b>	35,4	SS	100 x 100	40	2,46	195	P
		CS	100 x 100	40	1,68	250	WB
<b>4</b>	41,3	SS	100 x 100	20	1,98	230	P
<b>5</b>	35,7	SS	200 x 100	80	1,44	190	P
<b>6</b>	32,4	SS	100 x 200	80	2,16	160	WB
		CS	100 x 200	80	2,75	160	WB
<b>7</b>	43,2	SS	200 x 100	40	3,05	200	P
		CS	200 x 100	80	1,68	230	P

Regan and Rezai-Jorabi (1988) reported a series of tests on one-way slabs under concentrated loads at larger distances from the support and leading to either wide beam shear failure or punching shear failure. The test setup is shown in Fig. 4.2. The specimens were reinforced with Swedish steel type Ks60s. The 10mm longitudinal bars had a yield strength of 670MPa and an ultimate strength of 955MPa. The maximum aggregate size was 10mm for slabs 1-6 & 24-26 and 20mm for the other slabs. The results of the tests are given in Table 4.2, in which

$c_t$  the dimension of the loaded area transverse to the span of the slab;

$c_l$  the dimension of the loaded area parallel to the span of the slab;

$a$  the shear span;

$\rho_l$  the amount of longitudinal reinforcement;

$f_c'$  the concrete cube compressive strength.

The failure modes are denoted WB for wide beam, P for punching, P/WB for a combination of punching shear and wide beam shear failure and P2 for punching around both concentrated loads.

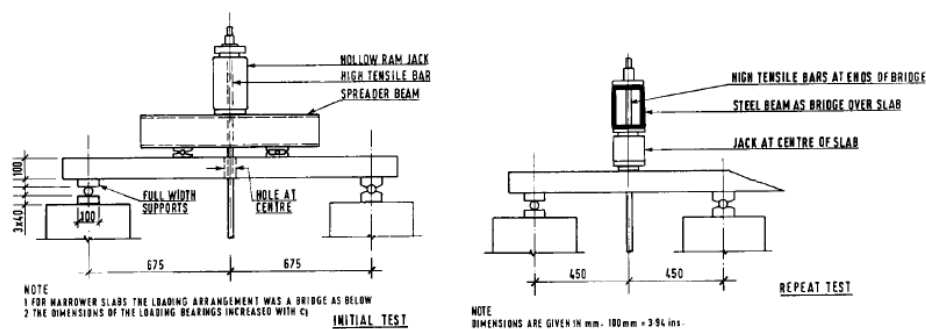


Fig. 4.2: Test arrangements, Regan and Rezai-Jorabi (1988).

Table 4.2: Summary of data for slabs loaded with two symmetrical loads and with single central loads (denoted R), Regan and Rezai-Jorabi (1988).

Test No.	$f_c'$ (MPa)	$\rho_l$ (%)	$d_l$ (mm)	$a$ (mm)	$a/d$	$b$ (mm)	$c_t$ (mm)	$c_l$ (mm)	$V_u$ (kN)	Mode
1	37,8	1,66	83	450	5,42	400	75	75	62,5	WB
2	37,8	1,58	83	450	5,42	600	75	75	85	WB
3	37,8	1,54	83	450	5,42	800	75	75	97,5	WB
4	28,1	1,66	83	450	5,42	400	400	100	54,5	WB
5	28,1	1,58	83	450	5,42	600	600	100	80,0	WB
6	28,1	1,54	83	450	5,42	800	600	100	96,5	WB
10	33,4	1,66	83	450	5,42	400	150	100	52,5	WB
11	33,4	1,66	83	450	5,42	400	300	100	55,0	WB
12	33,4	1,58	83	450	5,42	600	150	100	76,0	WB
13	33,4	1,58	83	450	5,42	600	300	100	79,5	WB
14	31,0	1,54	83	450	5,42	800	150	100	92,5	WB
15	30,8	1,54	83	550	6,63	800	150	100	85,0	WB
16	31,2	1,54	83	450	5,42	800	800	100	108,0	WB
17	31,0	1,51	83	450	5,42	1000	100	75	90,0	WB
18	31,2	1,51	83	450	5,42	1000	300	100	120,0	WB
19	29,0	1,51	83	450	5,42	1000	150	100	111,0	WB
20	30,8	1,51	83	450	5,42	1000	1000	100	122,5	WB
21	38,2	1,64	80	450	5,63	1200	70	100	117,5	P
22	37,0	1,64	80	450	5,63	1200	150	100	121,5	P/WB
23	35,4	1,64	80	450	5,63	1200	300	100	125,0	WB
24	38,6	1,64	80	450	5,63	1200	100	300	150,0	WB
25	30,3	1,64	80	550	6,88	1200	150	100	105,8	P2
26	29,7	1,64	80	350	4,38	1200	150	100	137,5	WB
14R	31,0	1,54	83	450	5,42	800	75	100	77,0	P
15R	30,8	1,54	83	450	5,42	800	150	100	86,0	P
16R	31,2	1,54	83	450	5,42	800	600	100	116,5	WB
17R	31,0	1,51	83	450	5,42	1000	600	100	137,5	WB
19R	29,0	1,51	83	450	5,42	1000	150	100	85,0	P
20R	30,8	1,51	83	450	5,42	1000	300	100	132,5	P

#### 4.2. Test data by Furuuchi et al.

Furuuchi, Takahashi, Ueda and Kakuta (1998) tested the shear capacity of structural elements in between beams and slabs, with small shear span to depth ratios, which they called “deep slabs”. The goal of this series of experiments is to determine which effective width has to be taken when using the shear capacity equation for deep beams. The reinforcement is 9 $\phi$ 16mm for  $b_w = 500$ mm and 12 $\phi$ 16mm for  $b_w = 650$ mm. The effective depth is 160mm. For the loading and supporting plates the width and depth are 50mm and 10mm respectively. The longitudinal bars have a yield strength of 345MPa and the stirrups 295MPa. Stirrups of  $\phi$ 10mm with 50mm spacing are used outside of the

supporting points, Fig. 4.3. The maximum aggregate size is not given. The target concrete strengths are 24,5MPa for specimens A and B and 30,0MPa for specimens C and D. The experiments are carried out at an age of 7 days. The test results are given in Table 4.3.

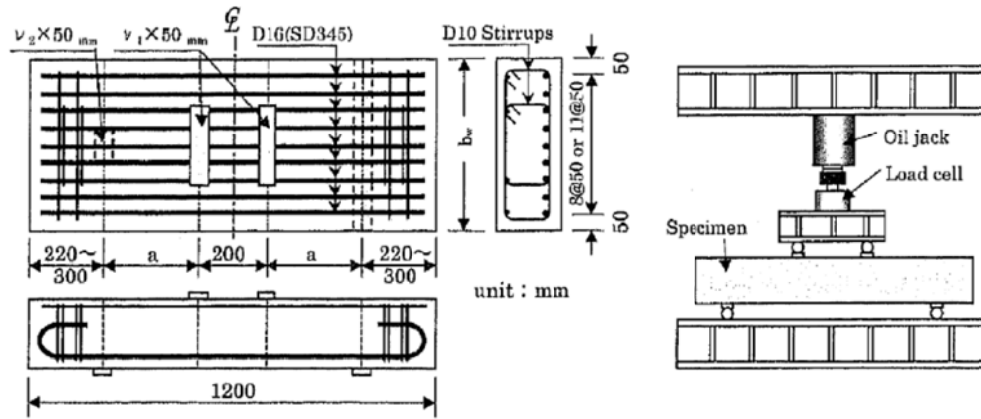


Fig. 4.3: Specimen and loading system, Furuuchi et al. (1998).

Table 4.3: Test data from Furuuchi et al. (1998).

Name	$a$ (cm)	$b_w$ (cm)	$d$ (cm)	$p$ (%)	$v_1$ (cm)	$v_2$ (cm)	$f'_c$ (MPa)	$P_b$ (kN)
A-10-10	28	50	16	2,23	10	10	26,1	294
A-10-20	28	50	16	2,23	10	20	20,2	294
A-10-30	28	50	16	2,23	10	30	23,8	333
A-20-10	28	50	16	2,23	20	10	19,6	340
A-30-10	28	50	16	2,23	30	10	23,8	450
B-10-10	28	65	16	2,29	10	10	29,4	368
C-10-10	20	50	16	2,23	10	10	34,6	480
C-20-10	20	50	16	2,23	20	10	32,1	525
C-30-10	20	50	16	2,23	30	10	31,5	626
C-50-10	20	50	16	2,23	50	10	34,9	811
C-10-20	20	50	16	2,23	10	20	36,4	483
C-10-30	20	50	16	2,23	10	30	30,7	520
D-10-10	36	50	16	2,23	10	10	35,2	294

#### 4.3. Test data from University of Toronto

Sherwood, Lubell, Bentz and Collins (2006) reported a series of tests on thick slabs and wide beams. Details of these experiments can be found in Sherwood (2008). The properties of specimen AT-1 are given in Fig. 4.4. The results are given in Table 4.4. To investigate the influence of the member width, a test series AT-2 is carried out, Fig. 4.5. Steel reinforcement types 15M ( $f_y = 452\text{MPa}$ ,  $f_u = 595\text{MPa}$ ) and 25M ( $f_y = 465\text{MPa}$ ,  $f_u =$

618MPa) are used. The size of the load plates is 152mm x 152mm and the  $a/d$  ratio is 2.77. The test results are given in Table 4.5, in which

- $\rho_w$  the amount of longitudinal reinforcement;  
 $\rho_{s+t}$  the amount of shrinkage and temperature reinforcement;  
 $f_c'$  the cylinder compressive strength of concrete.

From these observations, Sherwood et al. (2006) concluded that the member width does not affect the shear capacity. Another series (AT-3) was designed to study the effect of shrinkage and temperature reinforcement. The specimen lay-out and test setup is shown in Fig. 4.6 and the test results are given in Table 4.6. The specimens are loaded with a line load. From these results Sherwood et al. (2006) concluded that temperature and shrinkage reinforcement does not influence the shear capacity of one-way spanning members. All three series have a maximum aggregate size of 10mm.

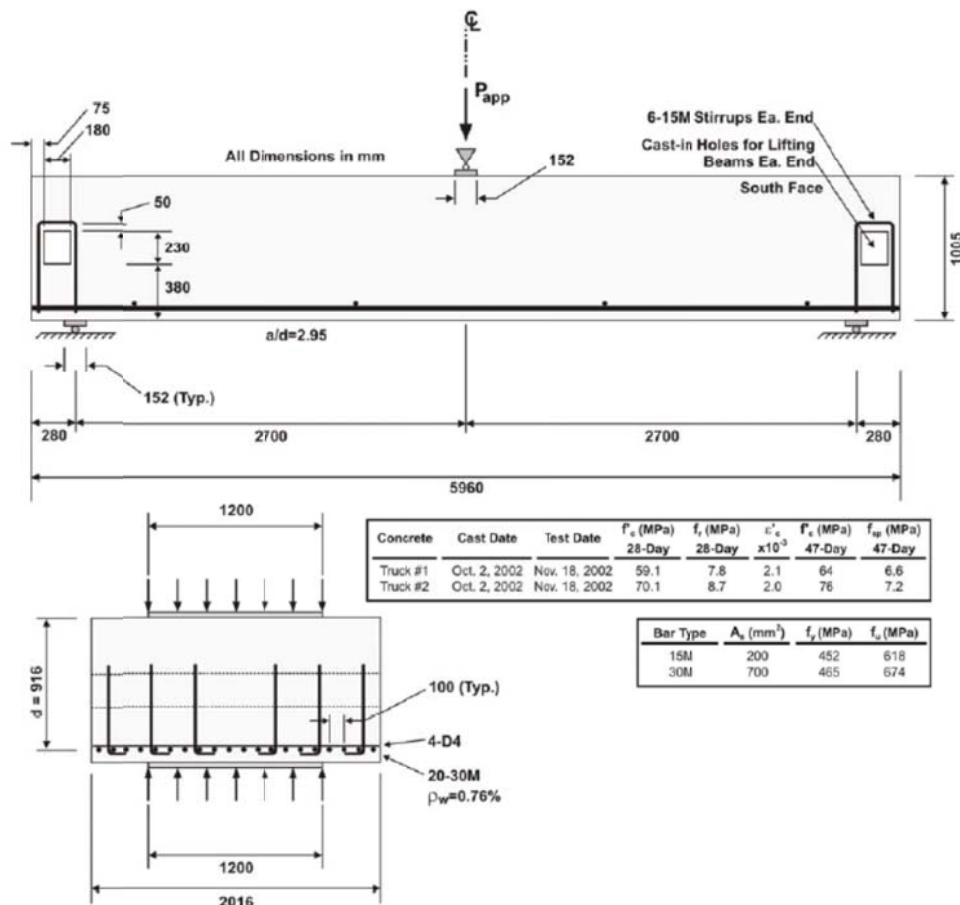


Fig. 4.4: Test specimen AT-1 (Sherwood, 2008).

Table 4.4: Experimental results AT-1 (Sherwood, 2008).

Specimen	$h$ (mm)	$d$ (mm)	$b_w$ (mm)	$L$ (mm)	$\rho_w$ (%)	$f_c'$ (MPa)	$P_{exp}$ (kN)
AT-1-East	1005	916	2016	5400	0,76	64	2266
AT-1-West							2441

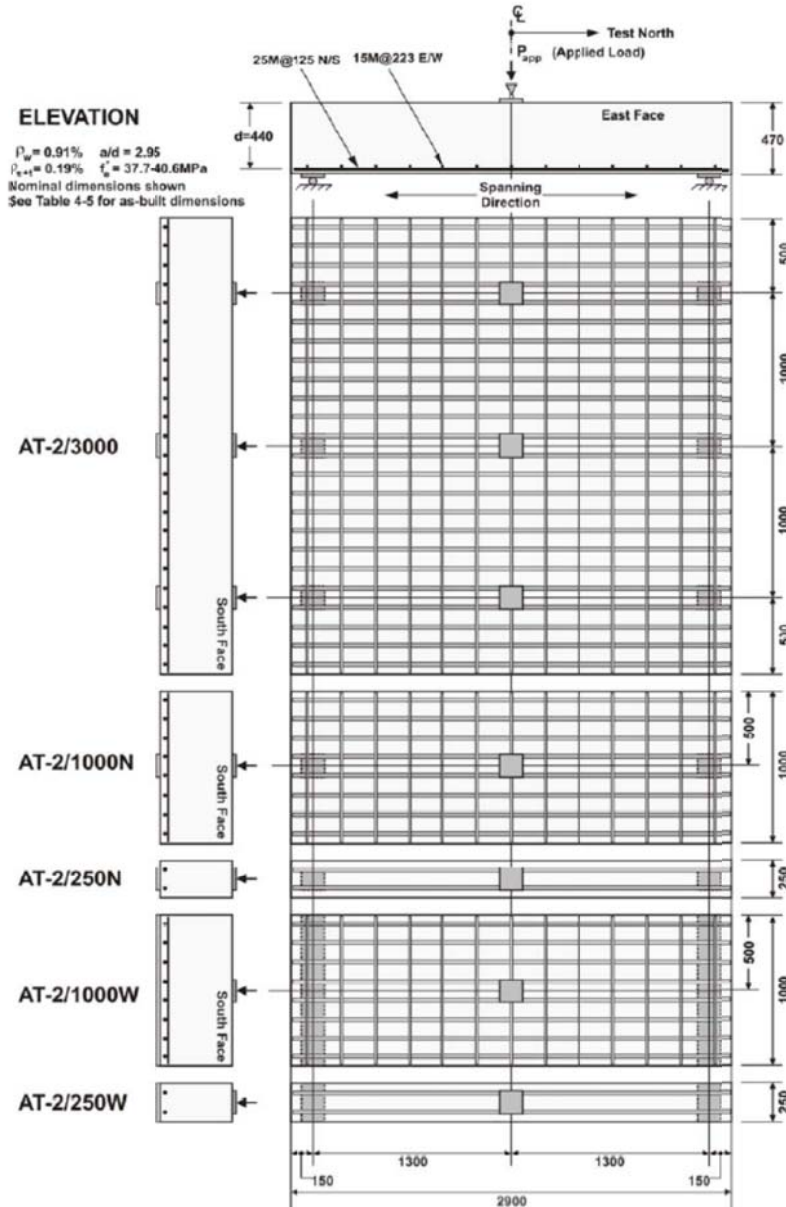


Fig. 4.5: Design of AT-2 series of test specimens (Sherwood, 2008).

Table 4.5: As-built properties and experimental observations AT-2 series (Sherwood, 2008).

Specimen	$h$ (mm)	$d$ (mm)	$b_w$ (mm)	Support size ( $w \times L$ , mm)	$\rho_w$ (%)	$\rho_{s+t}$ (%)	$f_c'$ (MPa)	$P_{exp}$ (kN)
AT-2/250N	469	437	250	152 x 152	0,915	--	37,7	229
AT-2/250W	471	439	252	252 x 152	0,904	--	38,5	224

<b>AT-2/1000N</b>	470	438	1002	152 x 152	0,911	0,191	37,9	880
<b>AT-2/1000W</b>	471	439	1002	1002 x 152	0,909	0,190	39,0	942
<b>AT-2/3000</b>	472	440	3005	152 x 152	0,908	0,190	40,6	2564

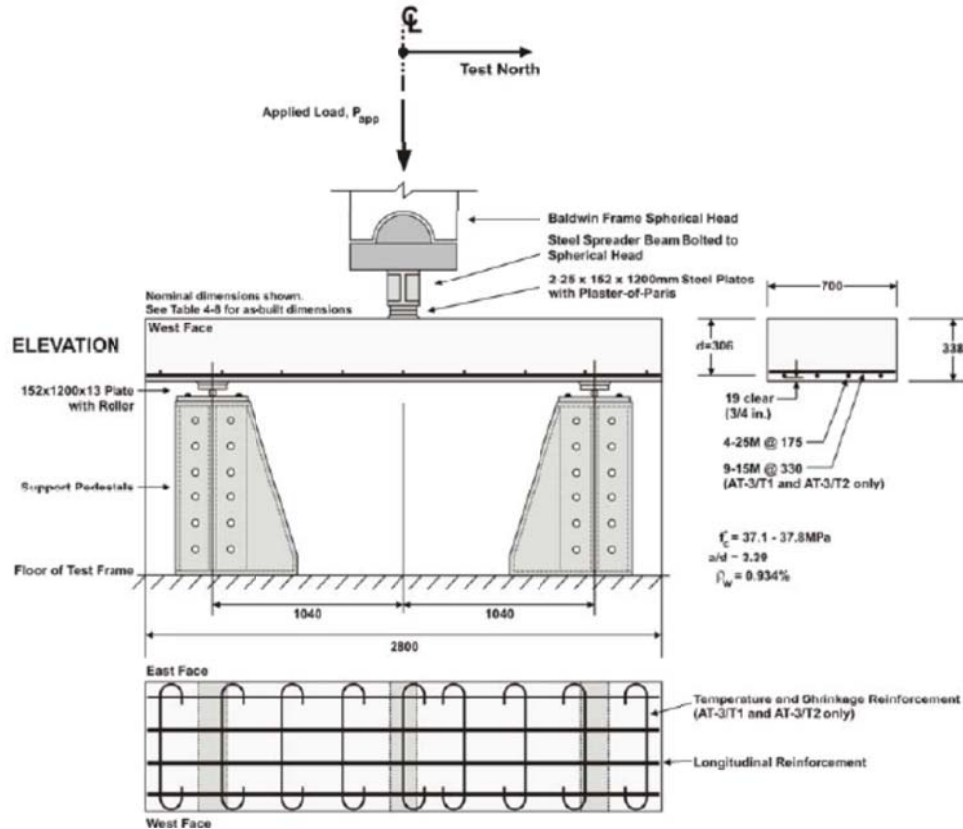


Fig. 4.6: Specimen design and test setup, AT-3 series, (Sherwood, 2008).

Table 4.6: As-built properties and experimental observations AT-3 series, (Sherwood, 2008).

Specimen	$h$ (mm)	$d$ (mm)	$b_w$ (mm)	$L$ (mm)	$\rho_w$ (%)	$\rho_{s+t}$ (%)	$f'_c$ (MPa)	$P_{exp}$ (kN)
<b>AT-3/N1</b>	339	307	697	2080	0,93	0	37,5	475
<b>AT-3/N2</b>	339	306	706	2080	0,93	0	37,1	517
<b>AT-3/T1</b>	338	306	700	2080	0,93	0,19	37,8	506
<b>AT-3/T2</b>	339	307	706	2080	0,93	0,19	37,1	497

Lubell, Bentz and Collins (2009a) experimentally investigated the influence of the longitudinal reinforcement on one-way shear in slabs and wide beams. The test specimens are shown in Fig. 4.7. Specimen AY1 contains 15mm diameter high strength deformed reinforcement provided by Dywidag and spiral reinforcement (D6 deformed wire) at the end of each Dywidag bar. The specimen properties and test results are shown



in Table 4.7. The data from specimen AW8 are taken from Lubell, Bentz and Collins (2009b). All specimens had a maximum aggregate size of 10mm.

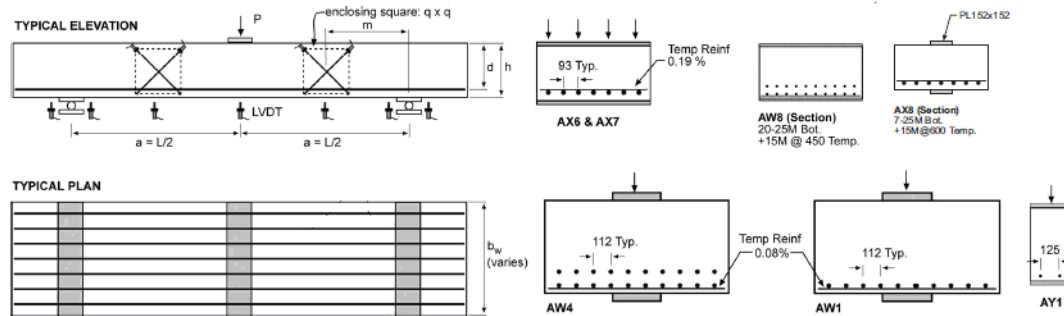


Fig. 4.7: Typical configuration of test specimens, Lubell (2006) and Lubell et al. (2009a and 2009b).

Table 4.7: Specimens properties and test results, Lubell et al. (2009).

Specimen	$b_w$ (mm)	$d$ (mm)	$h$ (mm)	$L$ (mm)	$a/d$	$\rho$ (%)	$f_c'$ (MPa)	Bearing plates (mm x mm)	$V_u$ (kN)
AY1	249	434	467	2600	3,00	0,328	40,7	152 x 249	85
AX7	704	287	335	2080	3,62	1,04	41,0	152 x 704	249
AX6	703	288	338	2080	3,61	1,73	41,0	152 x 703	281
AX8	705	289	339	2080	3,60	1,72	41,0	152 x 152	272
AW1	1170	538	590	3700	3,44	0,79	36,9	305 x 305	585
AW4	1168	506	590	3700	3,66	1,69	39,9	305 x 305	716
AW8	1169	507	591	3700	3,65	1,69	39,4	152 x 1170	800

#### 4.4. Test data from EPFL

Vaz Rodrigues, Muttoni and Olivier (2006) tested two  $\frac{3}{4}$  models of a bridge slab cantilever. Loading was applied according to the traffic loads from EN 1991-2. The dimensions of the tested cantilever are 2,78m span and 10,0m length. The  $a/d$  ratio for the concentrated load  $Q$  (test DR1c and test DR2-c) is  $a/d = 4,66$  based on the value of  $d = 278$  mm at the position of the load. The concrete cover is 30mm. The hot rolled reinforcement steel has a yield strength of 515 MPa for bars with 16 mm and 22 mm diameter, and 535 MPa for bars with 12 mm diameter. For DR1, the top reinforcement of the top layer at the fixed end consists of 16mm diameter bars at 75mm spacing ( $\rho = 0,79\%$ ). For DR2, the top reinforcement of the top layer at the fixed end consists of 14mm diameter bars at 75mm spacing ( $\rho = 0,6\%$ ). The results are given in Table 4.8, in which:

$E_c$  the modulus of elasticity of the concrete;

$a_g$  the maximum aggregate size.

The cracking patterns are shown in Fig. 4.9 and Fig. 4.10. The size of the load plate was 300mm x 300mm x 30mm. The total force in the prestressing bars is 7MN. The observed failure is reported as between beam shear and punching. The measurements made of the slab thickness in the zone of shear failure indicate possible redistributions of the internal shear flow, with the progressive formation of shear cracks until equilibrium is no longer possible, Fig. 4.11.

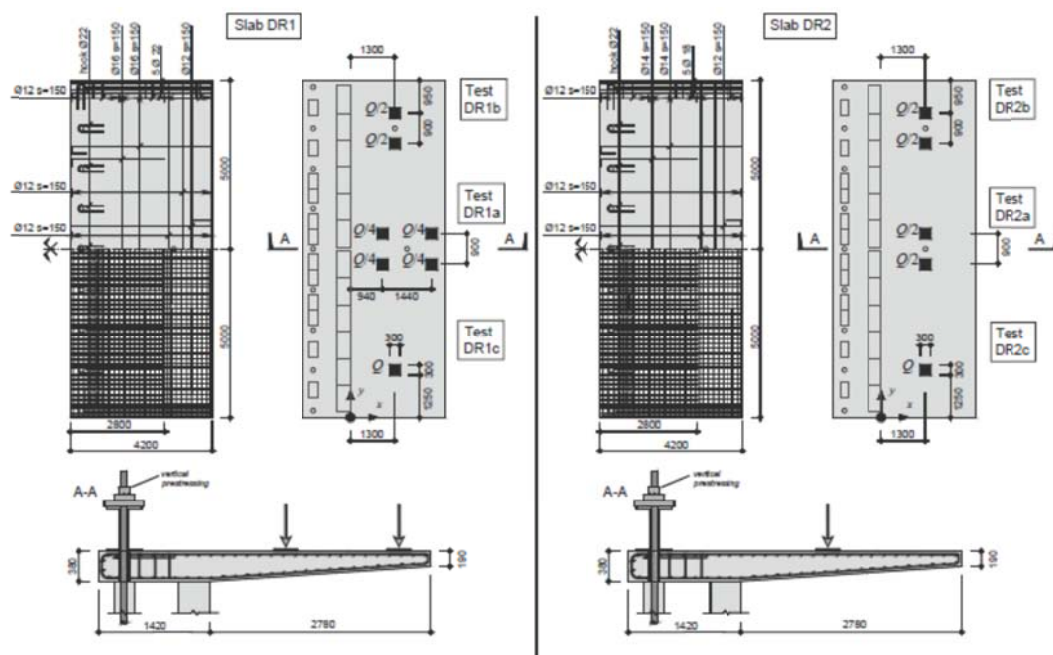


Fig. 4.8: Slab dimensions, reinforcement layout and applied loads for the tests, dimensions in mm (Vaz Rodrigues, 2007).

Table 4.8: Experimental results, Vaz Rodriguez et al. (2006)

Test	$f_c$ (MPa)	$E_c$ (MPa)	$\rho$ (%)	$a_g$ (mm)	Failure Load $Q_R$ (kN)
DR1a	39,1	36000	0,78	16	1397
DR1b	39,9	36100	0,78	16	1025
DR1c	40,8	36200	0,79	16	910
DR2a	38,9	36300	0,60	16	961
DR2b	42,0	37400	0,60	16	857
DR2c	40	36000	0,6	16	719

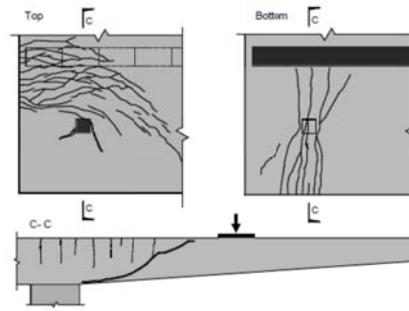
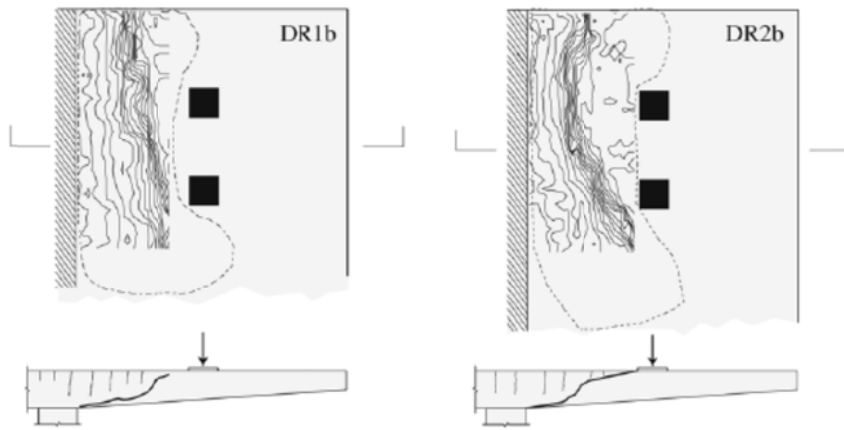


Fig. 4.9: Crack pattern on the top and bottom surfaces for test DR1c, Vaz Rodrigues et al. (2006).



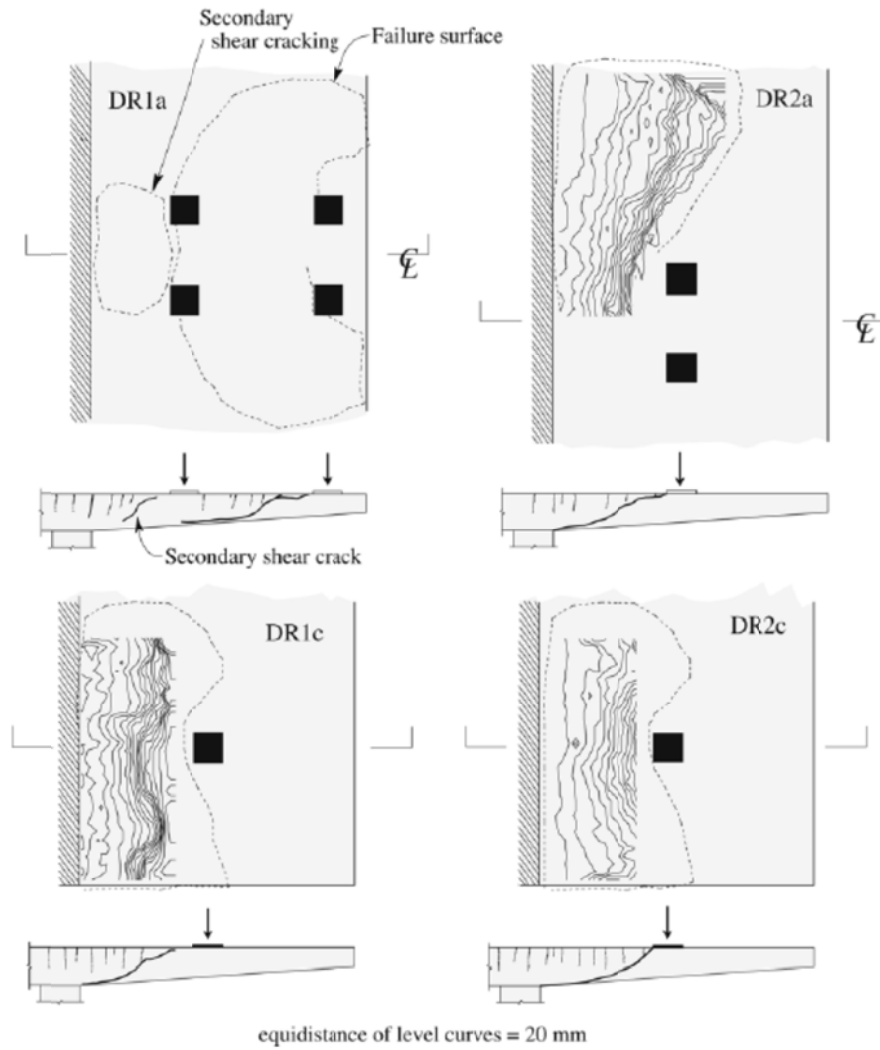


Fig. 4.10: Failure surfaces after cutting of the slab (Vaz Rodrigues et al., 2008).

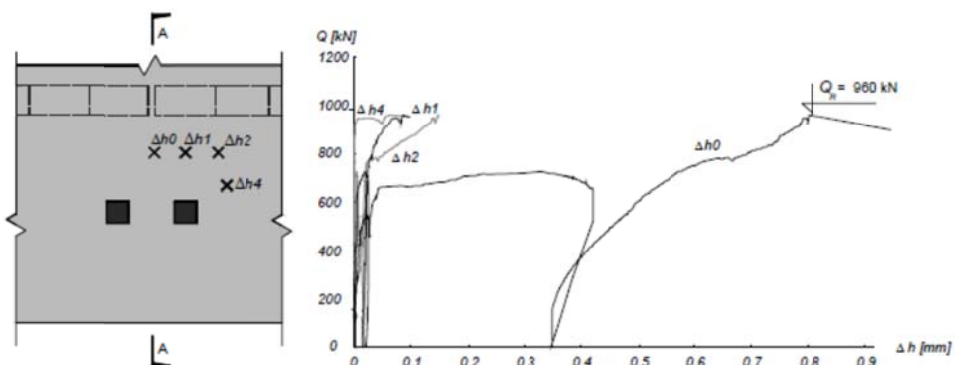


Fig. 4.11: Measurement of the variation of slab thickness (test DR2a). (Vaz Rodrigues, 2008)

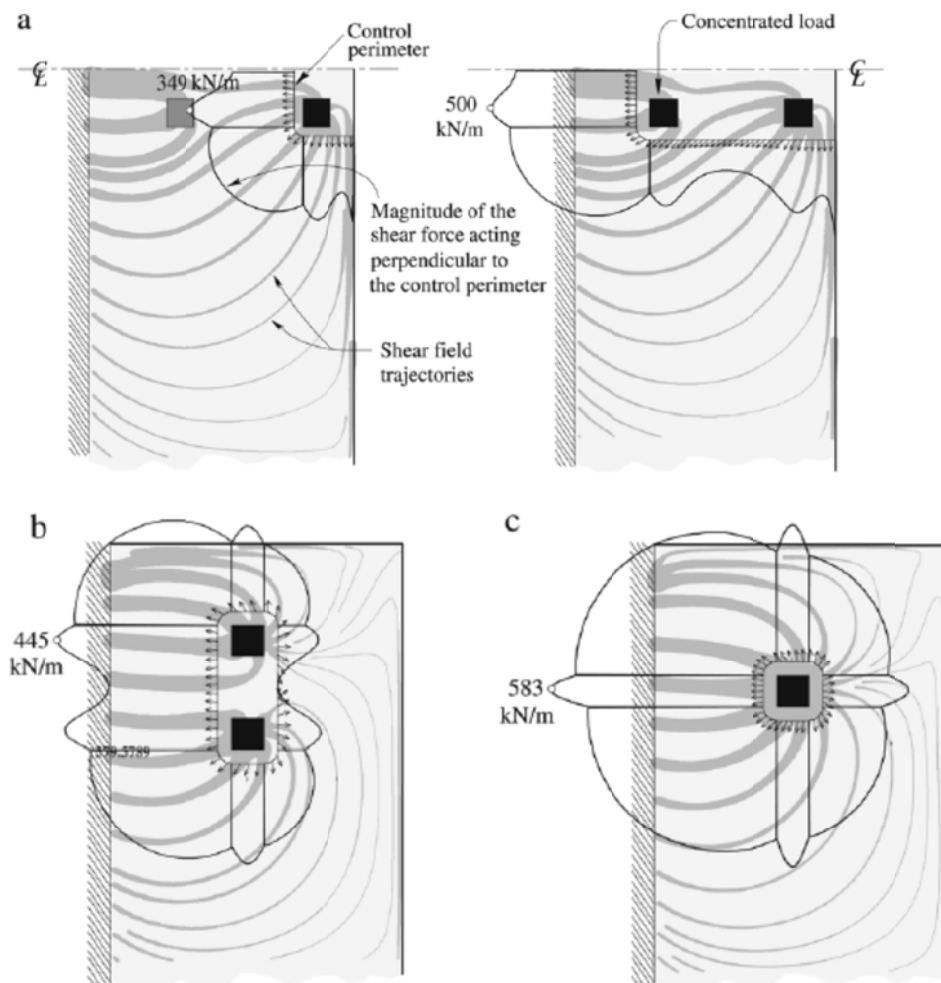


Fig. 4.12: linear elastic distribution of shear forces in kN/m, including self-weight along control perimeters at  $d/2$  of the applied loads: (a) test DR1-a; (b) test DR2-b and (c) test DR2-c. (Vaz Rodrigues, 2008)

Vaz Rodrigues et al. (2008) suggest the use of a three-sided control perimeter in the case of combined one-way and two-way shear action, as found in cantilevering cross sections, Fig. 4.13.

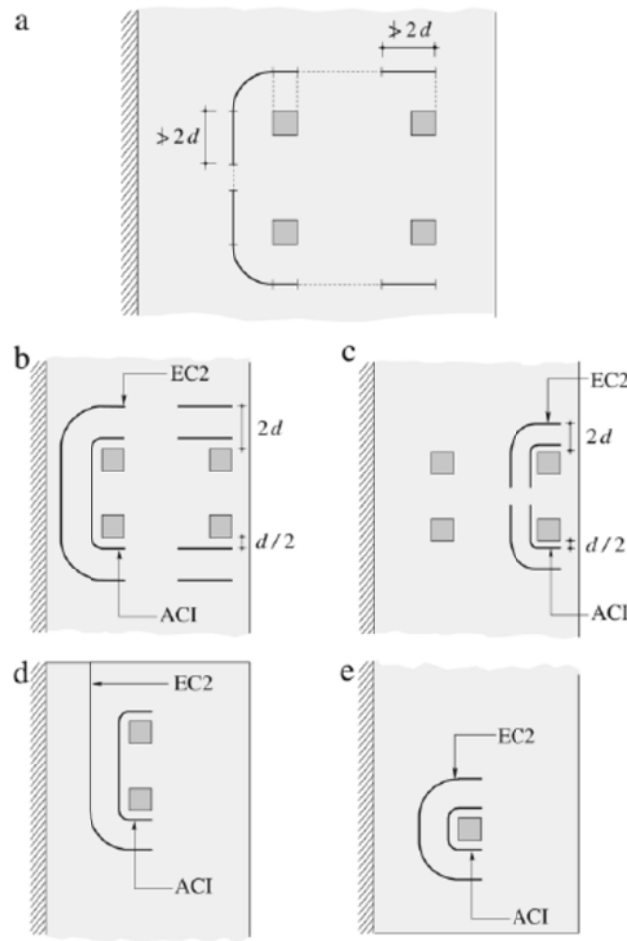


Fig. 4.13: Three-sided control perimeters used with ACI 318-05 and EC2 2004: (a) generic perimeter; (b) perimeter for test DR1-a considering the four concentrated loads; (c) perimeter for test DR1-a around the concentrated loads near the tip of the cantilever and for test DR2-a; (d) perimeter for tests DR1-b and DR2-b and (e) perimeter for tests DR1-c and DR2-c. (Vaz Rodrigues et al, 2008.)

Rombach et al. (2009) explain the observed bearing capacity as follows: the shear crack occurs early during the test, after which stress redistribution can occur, leading to a higher failure load. They also point out that distance between the edge and the loading plate (400mm) is very small, and not possible in real bridge deck slabs.

#### 4.5. Test data from ETH

A test program of 30 shear tests on 15 reinforced concrete slabs with shear span to overall depth ratios  $a/h$  of 3,2 and overall depths  $h$  ranging from 200 to 800mm is carried out and described by Jaeger (2002, 2005, 2007). These experiments (Jaeger, 2002) aimed at:

- quantifying the size effect for the shear strength of thick slabs with and without transverse reinforcement,
- the influence of angle between the span direction and the reinforcement direction, and
- the influence of the in-plane reinforcement ratio  $\rho_x$  and  $\rho_y$  on the shear strength of reinforced concrete slabs.

The specimens without shear reinforcement failed in shear without yielding of the flexural reinforcement. The results of four slabs are used for a prediction competition (Jaeger and Marti, 2009; discussion by Pujol et al., 2010). Test 1 slab C (B1V1 in Jaeger (2005, 2007)) and test 1 slab D (B3V1 in Jaeger (2005, 2007)) do not contain stirrups, Fig. 4.14 and Fig. 4.18. The load  $w$  is applied at the cantilevering end of the slab. The maximum aggregate size is 16mm. The load is placed over the entire width and has dimensions 800mm x 100mm. The relevant test results from this test series (Jaeger and Marti, 2009 and Jaeger, 2005, 2007) are given in Table 4.9.

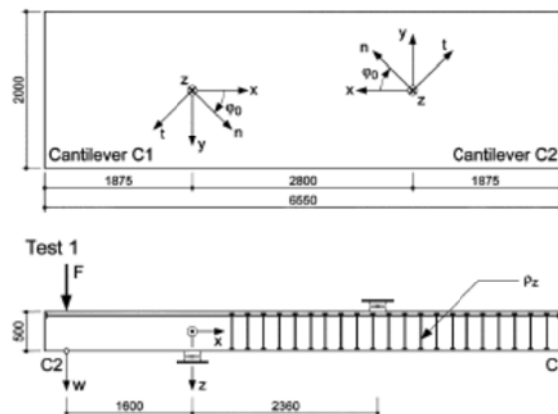
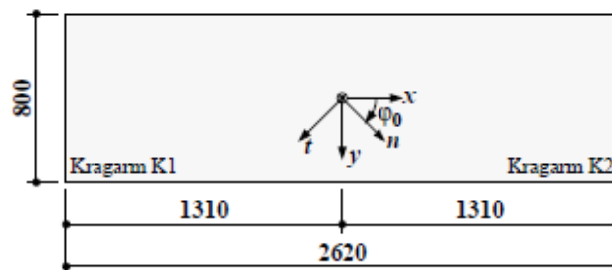


Fig. 4.14: Test concept for slabs C (B1) and D (B3), test concept for B-series, dimensions in mm. (Jaeger and Marti, 2009)



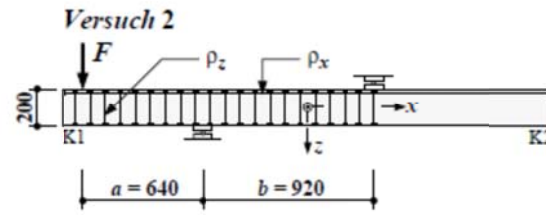


Fig. 4.15: Test concept for A-series, dimensions in mm(Jaeger, 2005).

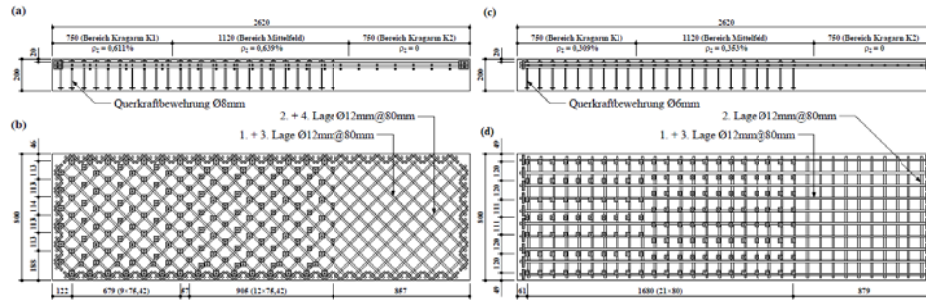


Fig. 4.16: a) Longitudinal section of reinforcement of A1; b) Plan of reinforcement of slab A1; c) Longitudinal reinforcement of A3; d) Plan of reinforcement of A3, Jaeger (2005).

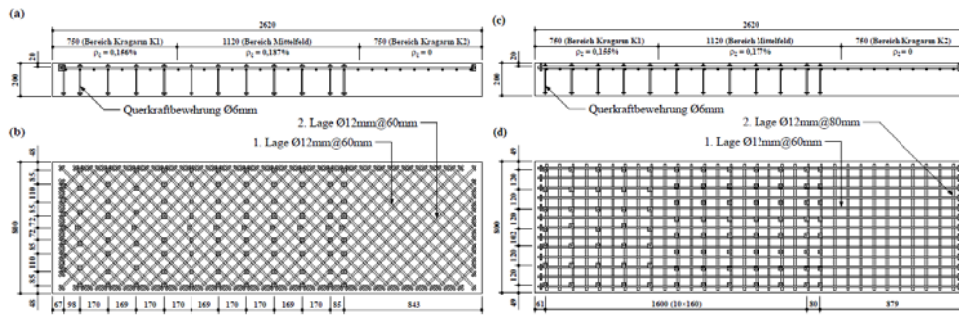


Fig. 4.17: a) Longitudinal section of reinforcement of A4; b) Plan of reinforcement of A4; c) Longitudinal reinforcement of A5; d) Plan of reinforcement of A5, Jaeger (2005).

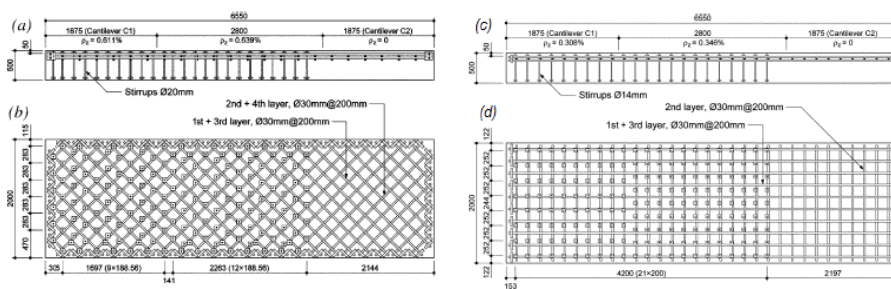


Fig. 4.18: a) Longitudinal section of reinforcement of slab C/B1; b) Plan of reinforcement of slab C/B1; c) Longitudinal reinforcement of slab D/B3; d) Plan of reinforcement of slab D/B3, Jaeger and Marti (2009).



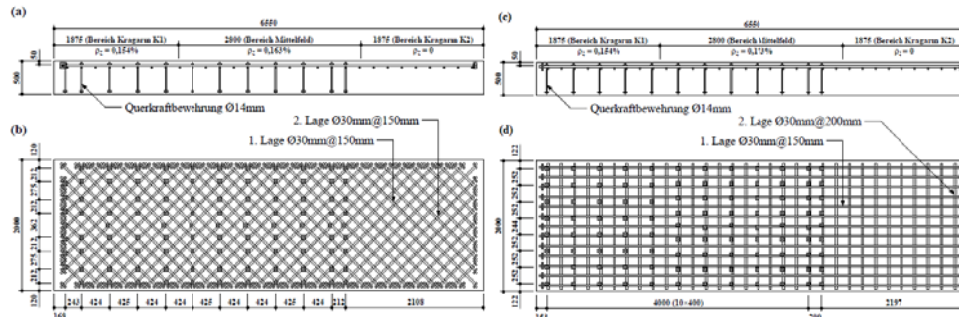


Fig. 4.19: a) Longitudinal section of reinforcement of B4; b) Plan of reinforcement of B4; c) Longitudinal reinforcement of B5; d) Plan of reinforcement of B5, Jaeger (2005).

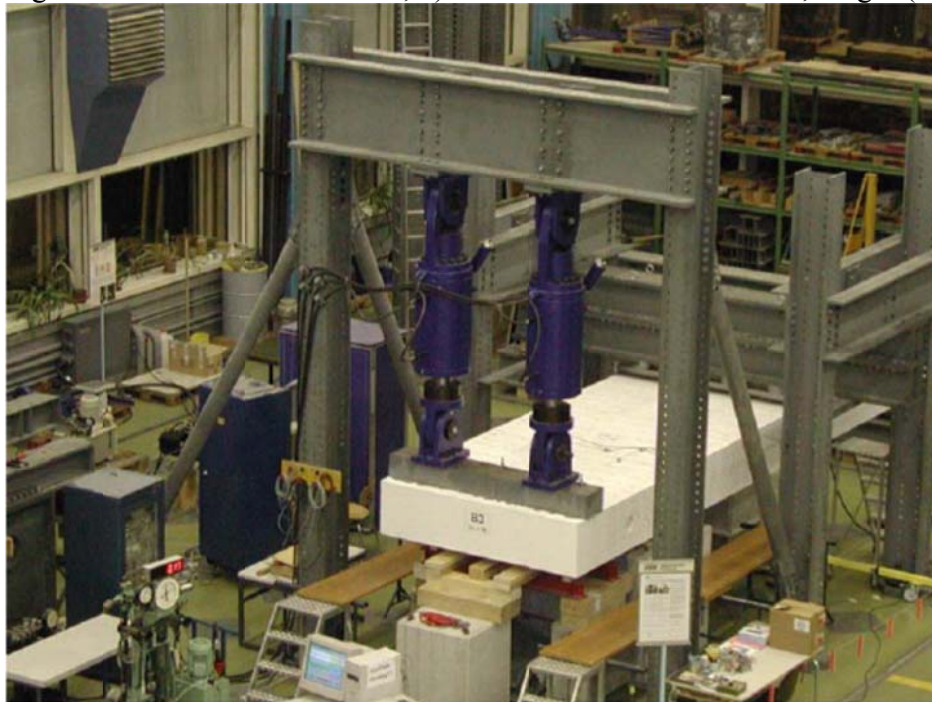


Fig. 4.20: Experimental setup, Jaeger (2005).

Table 4.9: Material properties of relevant tests, based on Jaeger and Marti (2009), Jäger (2005, 2007).

Slab	$f_{cw}$ (MPa)	$f_{cc}$ (MPa)	$E_c$ (GPa)	$f_{ct}$ (MPa)	$f_{sy,stat}$ (MPa)	$f_{su,stat}$ (MPa)
A1V1	58,1	52,4	29,2	4,56	480,8	558,7
A3V1	63,3	58,8	37,7	4,16	546,0	630,3
A4V1	58,5	46,8	36,7	3,62	546,0	630,3
A5V1	59,1	56,7	36,1	4,00	546,0	630,3
B1V1	58,7	52,4	31,8	4,29	539,0	619,0
B3V1	59,5	53,7	36,0	3,9	539,0	619,0
B4V1	61,3	54,2	35,4	3,75	533,6	613,7
B5V1	59,4	51,8	33,9	4,14	533,6	613,7

Table 4.10: Geometric properties of relevant tests, based on Jaeger and Marti (2009), Jäger (2005, 2007).

Slab	$h$ (mm)	$\varphi_0$ (°)	$d_m$ (mm)	$\rho_x$ (%)	$P_u$ (kN)
A1V1	200	45	156	1,538	169,2
A3V1	200	0	162	1,745	265,6
A4V1	200	45	168	0,952	140,5
A5V1	200	0	174	1,056	222,1
B1V1	500	45	390	1,538	852
B3V1	500	0	405	1,745	1282
B4V1	500	45	420	0,952	804
B5V1	500	0	435	1,056	1170

In which:

$h$	slab thickness;
$\varphi_0$	direction of bending reinforcement;
$d_m$	average effective depth;
$\rho_x$	effective reinforcement ratio in x-direction;
$f_{cw}$	concrete cube strength;
$f_{cc}$	concrete cylinder strength;
$E_c$	modulus of elasticity;
$f_{ct}$	tensile strength;
$f_{sy,stat}$	yield strength of 30mm bar;
$f_{su,stat}$	ultimate strength of 30mm bar;
$P_u$	ultimate load.

#### 4.6. Experiments on wide beams and slabs

Graf (1933) carried out tests on reinforced concrete slabs under concentrated loads near to supports. The effective width was assumed to be  $b_{eff} = 5d$  but experiments were needed to confirm this. Three slabs (1243, 1244, 1245) are cast, Fig. 4.21, and on every slab, four tests are reported ( $a_1$ ,  $a_2$ ,  $b_1$ ,  $b_2$ ). The size of slab 1243 is 2500mm x 2000mm; slab 1244 is 2050mm x 2004mm and slab 1245 is 2050mm x 2404mm. The size of the load was 100mm x 150mm. Bent bars are provided close to  $a_1$  and  $a_2$ , but the shear reinforcing action of these bars is questionable as the bars did not cross the shear span. The distance  $d_l$  is 115mm for 1243, 104mm for 1244 and 106mm for 1245 and  $d_t$  is 105mm for 1243, 92mm for 1244 and 94mm for 1245. The maximum aggregate size is 30mm. Conversion

of kg-m units to N-m units is made assuming  $g=9,807 \text{ m/s}^2$ . The results are given in Table 4.11, in which

$\rho$	the amount of longitudinal reinforcement;
$f_y$	the yield strength of the reinforcement steel;
$f_u$	the ultimate strength of the reinforcement steel;
$f_c'_{begin}$	the mean concrete compressive strength of cylinders tested at beginning of a series of tests on a specimen;
$f_c'_{end}$	the mean concrete compressive strength of cylinders tested at end of a series of tests on a specimen.

Photographs of the failed specimens are given in Graf (1933), and from the cracking pattern it is determined whether the failure mode is punching (P) or wide beam shear failure (WB). Some photographs show a partial punching cone; these failures have been denoted P/WB. The failure pattern of  $a_2$  (Fig. 4.22) for example shows a half developed punching cone at the left side and then shear cracks running towards the free edge at the right side.

Table 4.11: Results of tests by Graf (1933).

Specimen	Test	$a/d$	$\rho_l$ (%)	$\rho_t$ (%)	$f_y$ (MPa)	$f_u$ (MPa)	$f_c'_{begin}$ (MPa)	$f_c'_{end}$ (MPa)	$P_u$ (kN)	Failure mode
<b>1243</b>	$a_1$	1,13	0,65	0,27	289	400	16,6	21,6	314	WB
	$a_2$	2,17							235	P/WB
	$b_1$	0,65							355	P
	$b_2$	1,52							206	WB
<b>1244</b>	$a_1$	1,92	1,14	0,44	435	708	12,7	13,9	275	WB
	$a_2$	2,40							196	WB
	$b_1$	1,68							157	WB
	$b_2$	2,16							147	WB
<b>1245</b>	$a_1$	1,89	1,52	0,43	412	616	23,7	23,5	333	P/WB
	$a_2$	2,36							257	WB
	$b_1$	1,65							196	P/WB
	$b_2$	2,12							206	P/WB

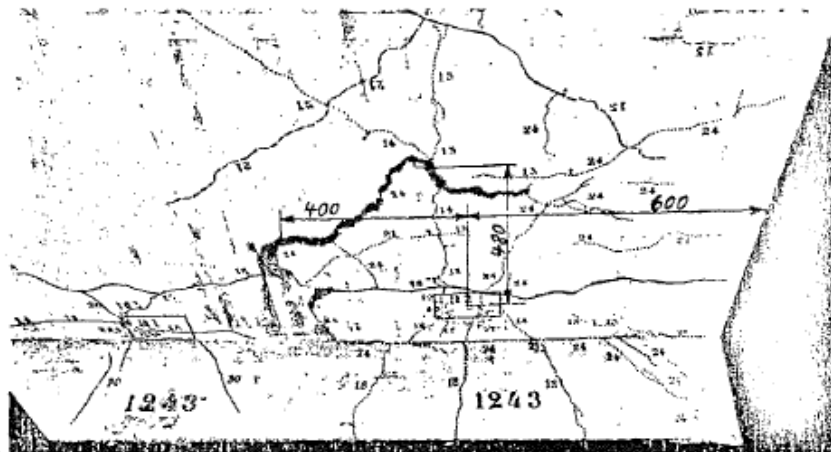
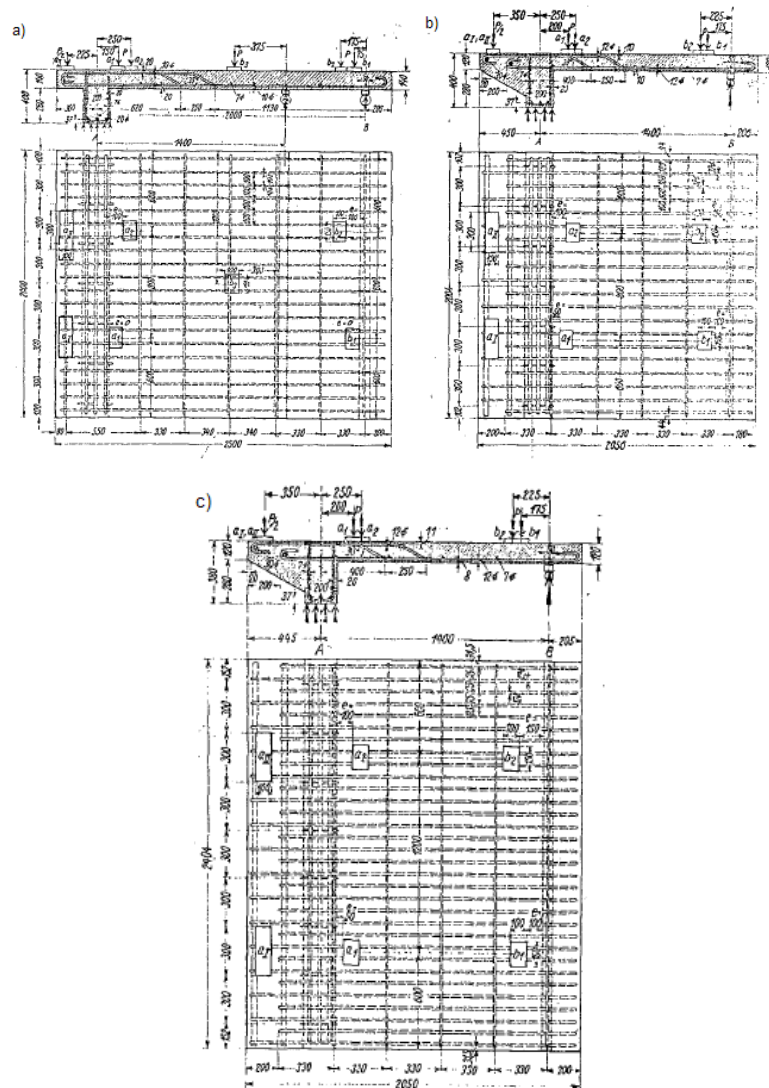


Fig. 4.22: Picture from the bottom face of 1243 showing the failure patterns of  $a_1$  and  $a_2$ . (Graf, 1933).

Richart and Kluge (1939) tested two one-way slabs on which they changed the position of the load, Fig. 4.23. The relevant tests are: Slab No. 1, test 2 and test 3; and Slab No. 2, test 2. The authors wrote: “In *most* cases the slab punched through...” and therefore it is concluded that the tests with loading close to the support might have shown a wide beam shear failure, but pictures of the slabs after failure are not included in the report for these particular tests. The effective depth was 139,7mm to the longitudinal reinforcement and 127mm to the transverse reinforcement. The support width was 101,6mm. The compressive strength of the concrete is measured on 6in by 12in cylinders (15,2cm x 30,5cm). The first slab is graded from 6,35mm to 38,1mm and the second slab from 6,35mm to 25,4mm. The relevant test data have been converted to SI units and are shown in Table 4.12, in which  $b_{edge}$  equals the distance from the load to the free edge.

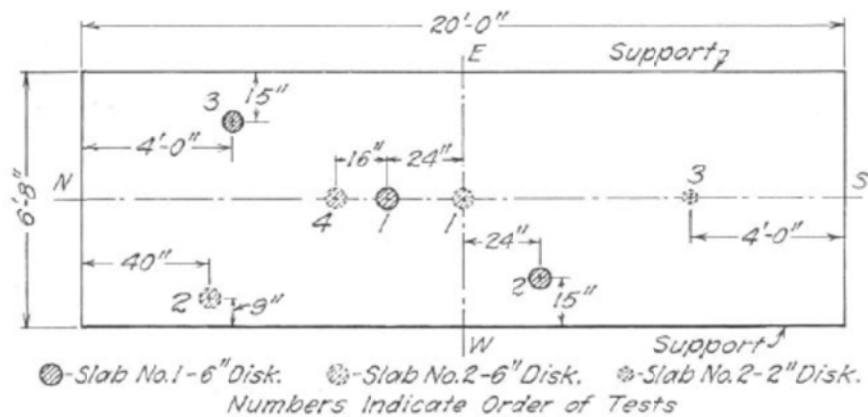


Fig. 4.23: Location and points of application of loads producing local failure (Richart and Kluge, 1939).

Table 4.12: Relevant test data from Richart and Kluge (1939).

Specimen	Test	$a/d$	$b_{edge}$ (mm)	$\rho_l$ (%)	$\rho_t$ (%)	$f_y$ (MPa)	$f_u$ (MPa)	$f_c'$ (MPa)	$P_u$ (kN)
Slab 1	2	2,72	2438	0,907	0,998	313,7	501,9	25,6	342,5
	3	2,72	1219	0,907	0,998	313,7	501,9	25,6	391,4
Slab 2	2	1,64	1016	0,907	0,998	313,7	501,9	29,1	369,2

Richart (1948) tested a series of rectangular slabs. Six footings of 1,83m x 2,74m (501 – 503) and six footings of 1,52m x 3,05m (504 – 506) are tested. The loading area is a 356mm square concrete stub. The test setup is shown in Fig. 4.24. The maximum

aggregate size is 25,4mm. Jones and Laughlin hard grade deformed billet steel bars are used. The bars of footings 503 and 506 are welded into mats. All bars are hooked at the ends, except in footings 503 and 506. The compressive strength of the concrete is measured on 6in by 12in cylinders (15,2cm x 30,5cm) and is found to be 24,8 MPa. The test data of series 5 have been converted to SI units and are given in Table 4.12. The failure mode is abbreviated as DT (diagonal tension) or T (tensile failure of the reinforcement). The main flexural reinforcement ratio is denoted  $\rho_{lx}$  and the transverse flexural reinforcement  $\rho_{ly}$ . The measured strains in the reinforcement bars are shown in Fig. 4.25 and Fig. 4.26.

Richart (1948) concluded that the average stress in the long bars in the rectangular footings agree very well with that calculated from the full static bending moment at loads approaching the ultimate capacity of the footing. Further, he concluded that the maximum shearing stresses in these footings are definitely greater than those developed in square footings. The main bars running lengthwise of the footing behaved normally, but the stress in the short bars was highly concentrated at mid-length of the footing. This suggests that in these footings a somewhat greater width of shearing section is effective than that prescribed in the ACI design procedure of that time. It seems logical that as the ratio of length to width of the footings increases, the failure section must change from a pyramidal punching surface to the usual inclined diagonal plane across the width of the member, as in a beam.

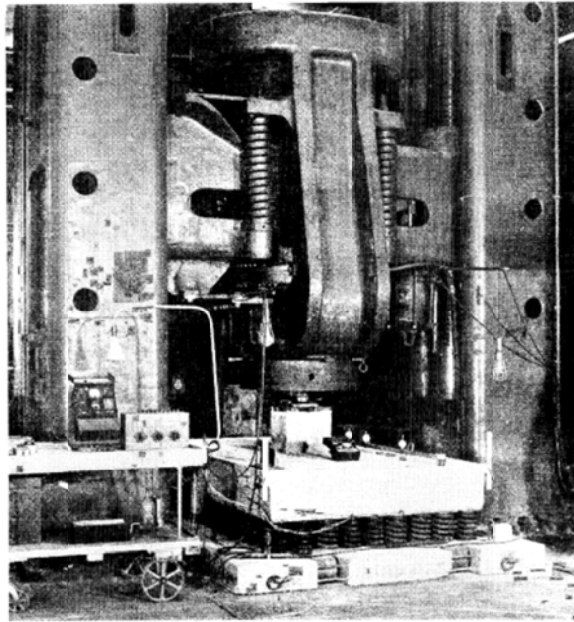


Fig. 4.24: Rectangular footing in test machine (Richart, 1948).

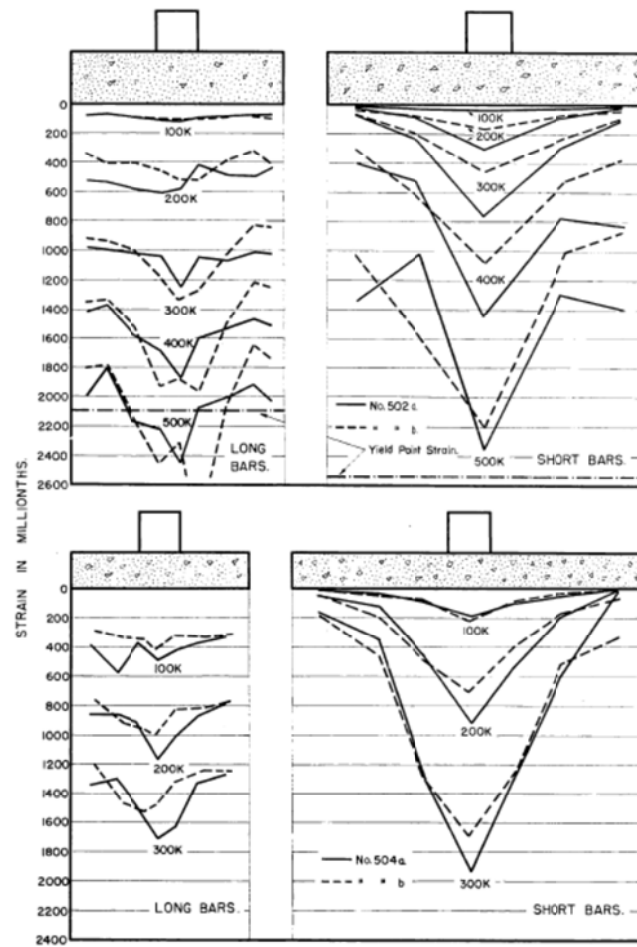


Fig. 4.25: Measured tensile strains across standard moment section (Richart, 1948).

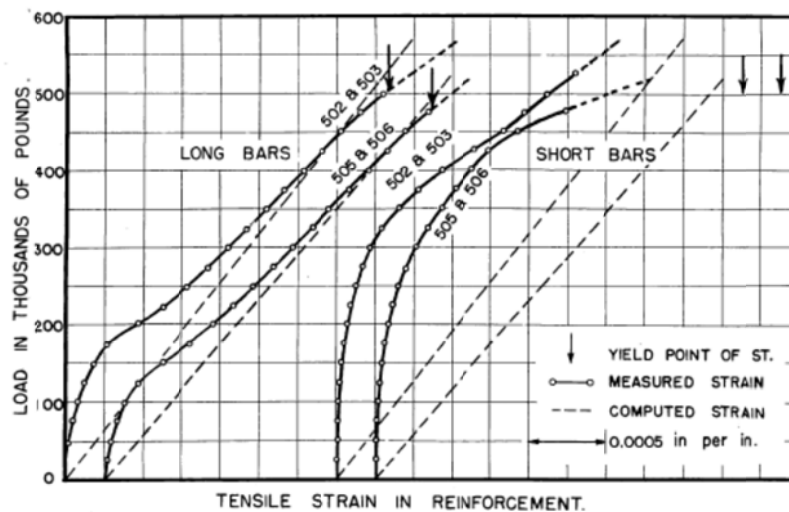


Fig. 4.26: Measured and computed average tensile strains across standard moment section (Richart, 1948).

Table 4.13: Test data from rectangular footings by Richart (1948).



No.	$h$ (mm)	$d$ (mm)	$a/d$	$\rho_{lx}$ (%)	$f_y$ (MPa)	$\rho_{ly}$ (%)	$f_y$ (MPa)	$f_c'$ (MPa)	$P_u$ (kN)	Failure mode
501a	305	254	3,60	1,38	424,7	0,53	530,2	25,4	1753	DT
501b	305	254	3,60	1,38	424,7	0,53	530,2	25,7	1690	DT
502a	457	406	2,25	0,54	419,9	0,20	530,2	24,3	2464	T/DT
502b	457	406	2,25	0,54	419,9	0,20	530,2	22,6	2571	T/DT
503a	457	406	2,25	0,54	419,9	0,20	530,2	24,4	2607	T/DT
503b	457	406	2,25	0,54	419,9	0,20	530,2	24,0	2447	T/DT
504a	305	254	3,00	1,77	510,2	0,34	530,2	24,9	1446	DT
504b	305	254	3,00	1,77	510,2	0,34	530,2	25,8	1557	DT
505a	457	406	1,88	0,68	424,7	0,13	530,2	25,4	2438	T/DT
505b	457	406	1,88	0,68	424,7	0,13	530,2	25,7	2335	T/DT
506a	457	406	1,88	0,68	424,7	0,13	530,2	23,1	2224	T/DT
506b	457	406	1,88	0,68	424,7	0,13	530,2	26,3	2224	T/DT

Serna-Ros et al. (2002) tested wide beams (750mm) with an effective depth of 206mm and a total height of 250mm. Given the dimensions in Fig. 4.27, the  $a/d$  ratio of all tests is 4. The longitudinal reinforcement is kept constant along the beam. The compression reinforcement is 7 16mm bars ( $\rho = 0,94\%$ ) and the tension reinforcement is 7 20mm bars ( $\rho = 2,2\%$ ). The size of the loading plate, the yield strength of the reinforcement bars and the maximum aggregate size are not given. The results of the relevant tests are given in Table 4.14.

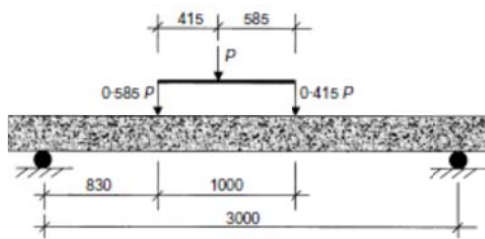


Fig. 4.27: Test arrangement, dimensions in millimeters (Serna-Ros et al., 2002).

Table 4.14: Relevant test data from Serna-Ros et al. (2002).

Specimen	$b_{sup}$ (mm)	$f_c'$ (MPa)	$V_{u exp}$ (kN)
R0	750	29,2	244
A0	750	24,5	187
C0	750	25,2	182
D0	300	32,6	218

Collins, Bentz and Sherwood (2008) have collected a database of 1601 shear tests. The tests on wide beams ( $b \geq 500\text{mm}$  and  $h/b \geq 1$ ) have been represented in Table 4.15, in which  $b_{sup}$  is the longitudinal length of the bearing plate. The value of the failure capacity  $V_u$  includes the self weight of the specimen. “R & F” refers to Rajagopalan and Ferguson. Specimens 11, 16, 2, 12 and 3 of Aster and Koch have bar cutoffs. The original data can be found in: Leonhardt and Walther (1962); de Cossio (1962); Kani (1979); Rajagopalan and Ferguson (1968) and discussion by Brock et al. (1969); Aster and Koch (1974); Reineck, Koch and Schlaich (1978) and Heger and McGrath (1980). The size of the loading plate is not given in the paper by Collins, Bentz and Sherwood (2008). Diaz de Cossio (1962) uses different lengths of loading plate: tests A50-25A, A50-25B, 64-8A and 64-8B use a line load, 64-8C and 64-8D use a load width equal to half the total width and 64-8E and 64-8F use a load width equal to a quarter of the total width. Rajagopalan and Ferguson (1968) use a line load for testing specimen S-15. Aster and Koch (1974) do not specify the size of the loading plate. Leonhardt and Walther (1962) use a concentrated load at one side and a line load at the other side, Fig. 4.29. All slab strips except P2 and P4 failed at the side of the concentrated load. Heger and McGrath (1980) use a loading plate of 25,4mm wide over the full length of the specimen.

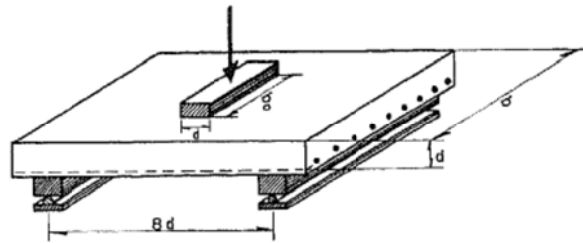


Fig. 4.28: Slab test setup, Diaz de Cossio (1962).

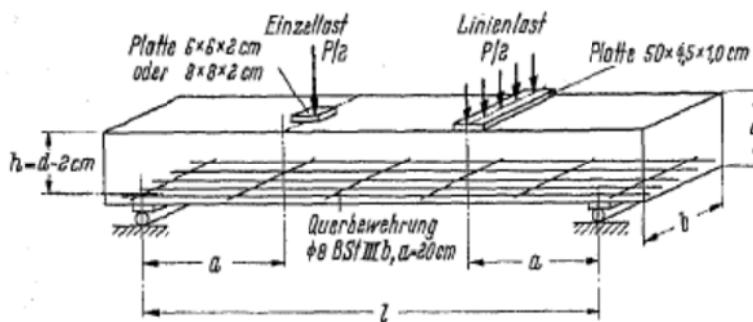


Fig. 4.29: Test setup, Leonhardt and Walther (1962).

Table 4.15: Wide beam test data from Collins, Bentz and Sherwood (2008).

Author	Beam Name	$b$ (mm)	$h$ (mm)	$d$ (mm)	$a/d$	$b_{sup}$ (mm)	$\rho_w$ (%)	$f'_c$ (MPa)	$a_g$ (mm)	$f_y$ (MPa)	$V_u$ (kN)
Leonhardt & Walther	P2	503	162	142	3,45	45	0,95	13,4	30	427	76,2
	P3	502	162	142	3,45	45	1,11	13,4	30	427	81,1
	P4	500	165	145	3,38	45	1,40	14,5	30	427	100,8
	P5	503	165	145	3,38	45	1,86	13,4	30	427	100,8
	P8	502	168	148	3,31	45	0,91	24,9	30	427	88,0
	P9	500	166	146	3,36	45	1,86	24,9	30	427	105,8
	P10	503	122	102	3,43	45	1,10	12,4	30	427	59,3
	P11	498	203	183	3,44	45	1,11	13,7	30	427	101,2
	P12	501	162	142	2,46	45	0,95	12,6	30	427	100,5
de Cossio	64-8F	639	102	83	4	17	1,88	30,4	12	373	71,3
	64-8E	639	102	87	4	17	1,92	31,2	12	373	67,7
	64-8C	640	102	82	4	16	1,90	28,5	12	383	85,2
	64-8D	640	102	81	4	16	1,95	28,5	12	383	81,6
	48-8B	505	102	82	4	16	1,98	27,8	12	399	65,3
	64-8A	640	105	82	4	16	1,90	28,5	12	397	87,0
	64-8B	636	102	81	4	16	1,94	29,2	12	440	85,5
	A50-25A	501	305	253	2,67	51	1,81	34,5	12	399	188,7
	A50-25B	502	305	252	2,67	50	1,85	34,1	12	394	171,2
Kani	271	611	305	269	6,07	152	2,75	27,0	19	377	217,2
	272	611	305	271	5,02	152	2,73	27,0	19	377	227,8
	273	612	305	271	4,01	152	2,72	27,2	19	377	206,2
	274	612	305	270	3,02	152	2,73	27,2	19	377	250,2
R & F	S-15	761	311	269	4,16	50	0,63	33,0	13	524	150,8
Aster & Koch	11	1000	539	500	3,65	100	0,46	24,6	30	535	267,4
	16	1000	794	750	3,67	150	0,42	30,4	30	536	406,7
	2	1000	281	250	3,68	50	0,64	26,9	30	554	218,0
	12	1000	540	500	3,65	100	0,65	27,3	30	535	330,2
	3	1000	289	250	3,68	50	0,91	27,3	30	535	222,5
	8	1000	544	500	5,50	100	0,63	31,1	30	535	287,1
	9	1000	544	500	5,50	100	0,63	19,9	30	535	260,6
	10	1000	544	500	5,50	100	0,63	20,0	30	535	261,6
Reineck Koch Schlaich	17	1000	794	750	3,67	150	0,42	28,7	30	535	363,5
	N8	500	250	226	3,50	10	0,79	25,8	16	501	101,5
	N6	500	250	226	2,50	10	0,79	25,8	16	501	117,5
Heger & McGrath	N7	500	250	225	2,50	10	1,39	24,6	16	441	139,5
	SW9-0A	914	224	184	3,24	50	0,62	48,5	19	603	167,6
	SW9-0B	914	227	190	3,14	50	0,60	48,5	19	603	155,5
	SW9-6A-15	914	225	188	2,03	50	0,61	48,5	19	603	267,7
	SW9-0B-15	914	225	186	2,05	50	0,62	48,5	19	603	270,7
	SW9M-0A	914	225	197	3,19	50	0,61	48,5	19	594	155,7
	SW9M-0B	914	226	185	3,23	50	0,62	48,5	19	594	174,3
	SW9M-0A-15	914	225	190	2,01	50	0,60	48,5	19	594	299,8
	SW9M-0B-15	914	226	174	2,19	50	0,66	48,5	19	594	308,1
	SW14-0A	914	227	191	3,13	50	0,93	49,0	19	673	197,2
	SW14-0B	914	226	186	3,21	50	0,96	49,0	19	673	195,9
	SW18-0A	914	225	184	3,25	50	1,24	48,3	19	633	202,6
	SW18-0B	914	225	180	3,31	50	1,27	48,3	19	633	222,8
	SW18-0A-15	914	227	179	2,13	50	1,28	48,3	19	633	378,9
	SW18-0B-15	914	227	176	2,17	50	1,30	48,3	19	633	390,2

Cullington, Daly and Hill (1996) tested a slab strip on site and two similar slab strips in the laboratory. The dimensions of the specimens are  $h = 305\text{mm}$ ,  $l = 4,37\text{m}$  and  $b = 1\text{m}$ . The concrete cover is assumed to be  $35\text{mm}$ , resulting in  $d = 257\text{mm}$ . The longitudinal reinforcement is  $\varphi = 25\text{mm}$  with spacing  $s = 115\text{mm}$ . This results in  $\rho_w = 1,54\%$ . The support width is  $b_w = 350\text{mm}$  on site. The support width of the laboratory tests is unknown. The load is a full width knife-edge load. The maximum aggregate size is unknown. The test setup in the laboratory is shown in Fig. 4.30. The test results are given in Table 4.16.

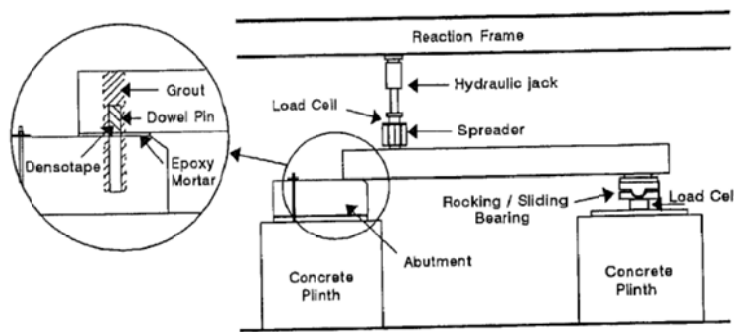


Fig. 4.30: Configuration for laboratory test (Cullington, Daly and Hill, 1996).

Table 4.16: Test results from Cullington, Daly and Hill (1996).

Specimen	$a/d$	$f'_c$ (MPa)	$f_y$ (MPa)	$V_u$ (kN)	Failure Mode
on site	3,7	56	254	440	Flexure
lab 1	2	60	300	700	Shear
lab 2	1	60	300	1060	Shear

Coin and Thonier (2007) tested 7 slabs in one-way shear. The concrete cover is  $1\text{cm}$ , concrete class B25/30 and steel with  $f_{yk} = 500\text{MPa}$  is used. The maximum aggregate size is  $20\text{mm}$ . The dimensions of the specimens are given in Fig. 4.31. The reinforcement layout of slabs 1, 2 and 3 is given in Fig. 4.32 and of slabs 5, 6 and 7 is given in Fig. 4.33. The results are given in Table 4.17. The value of  $a/d$  has been determined by taking  $a$  as the distance from the center of the support to the center of the load ( $37\text{cm}$ ) and  $d = 8,5\text{cm}$  and equals  $4,35$  for all tests.

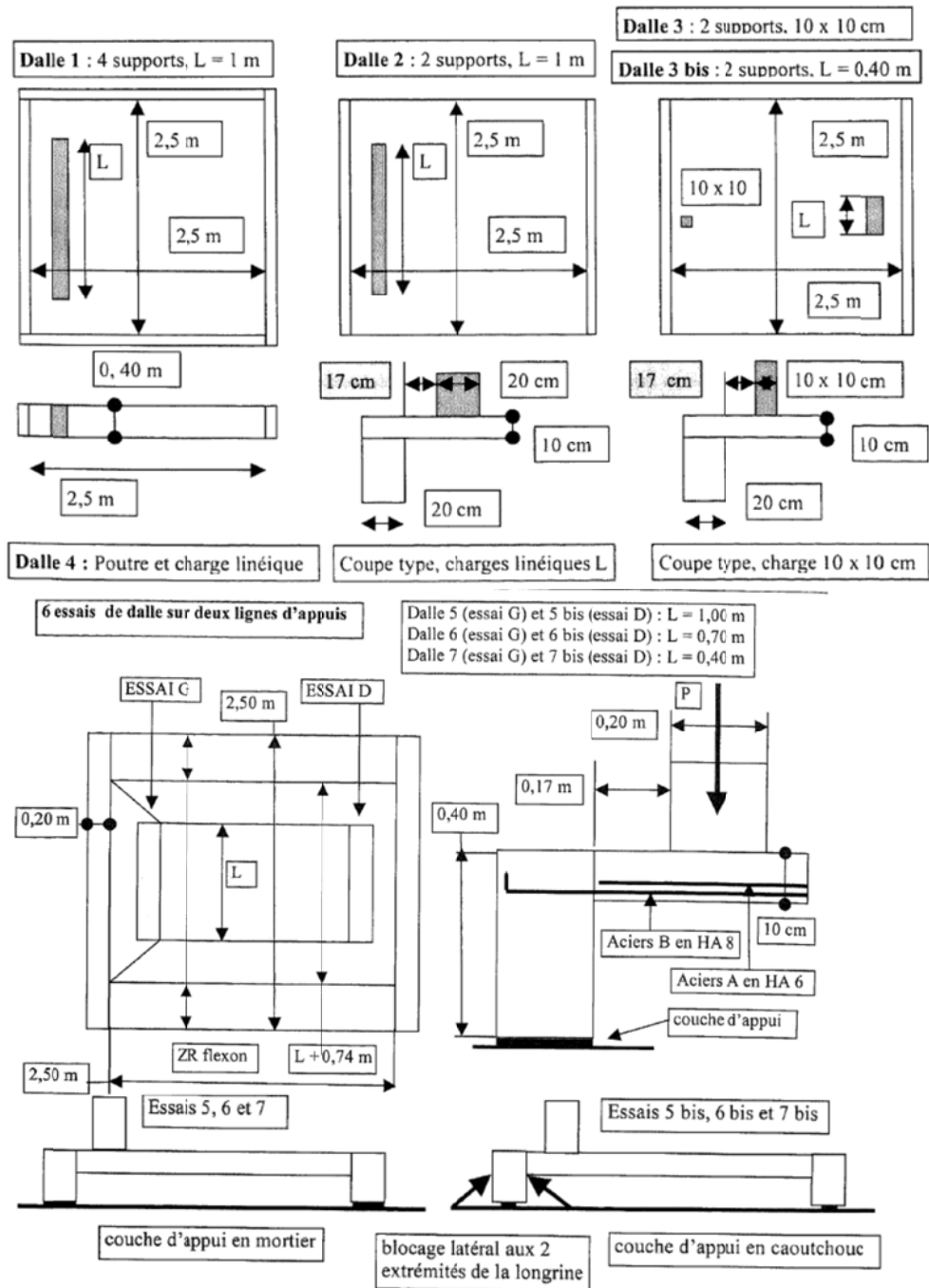
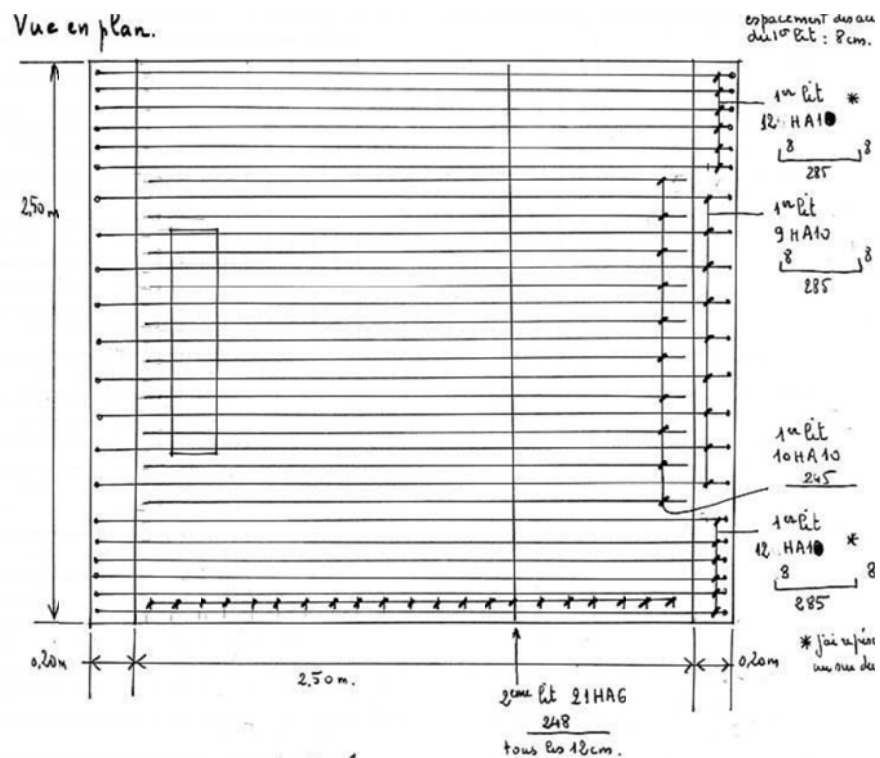
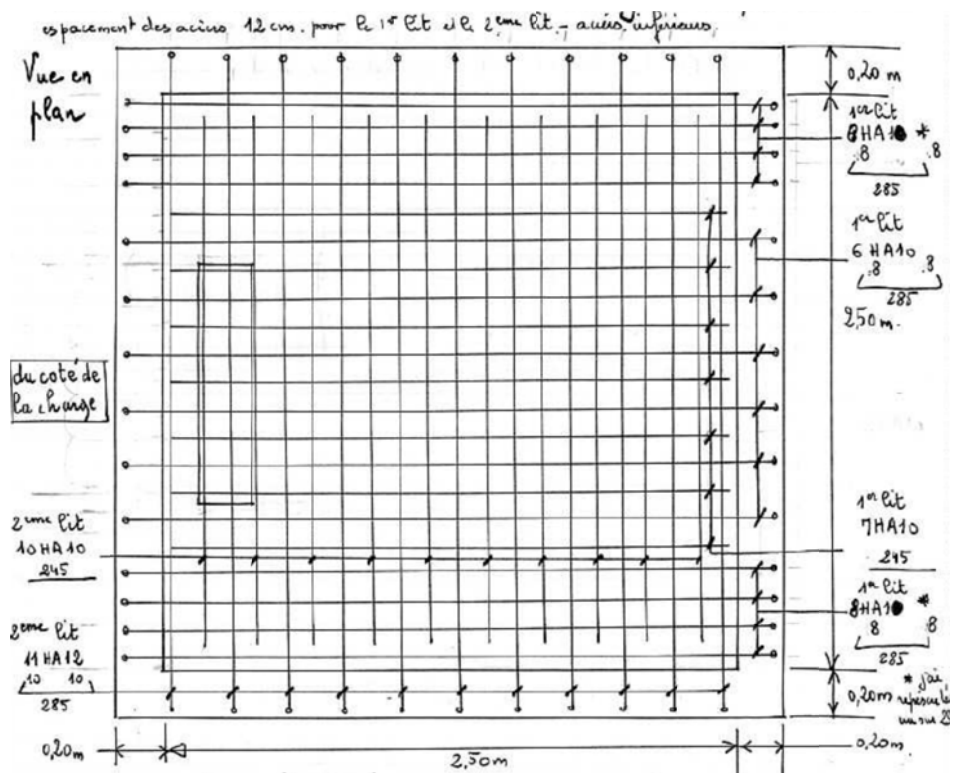


Fig. 4.31: Specimens 1 to 7 (Coin and Thonier, 2007).



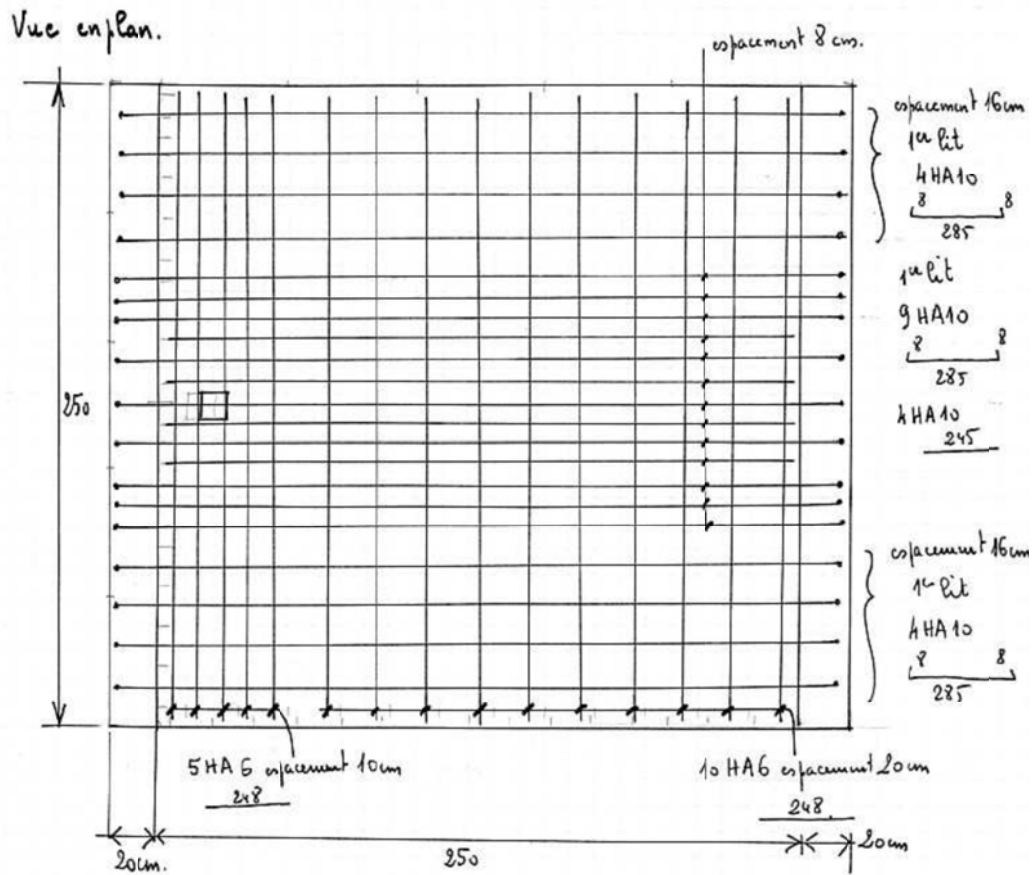
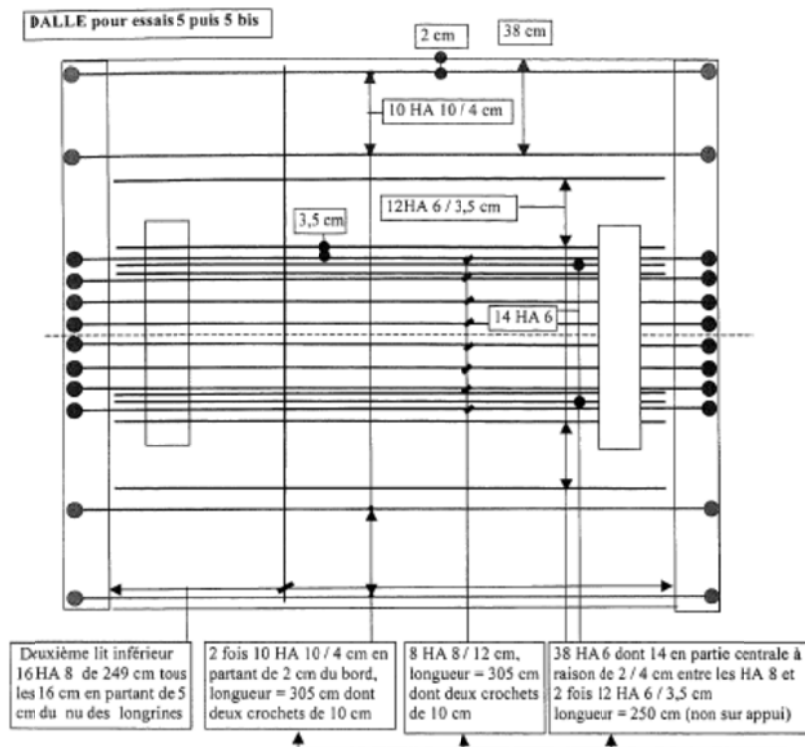


Fig. 4.32: Reinforcement of slabs 1,2 and 3. (Correspondence with Mr. Coin).



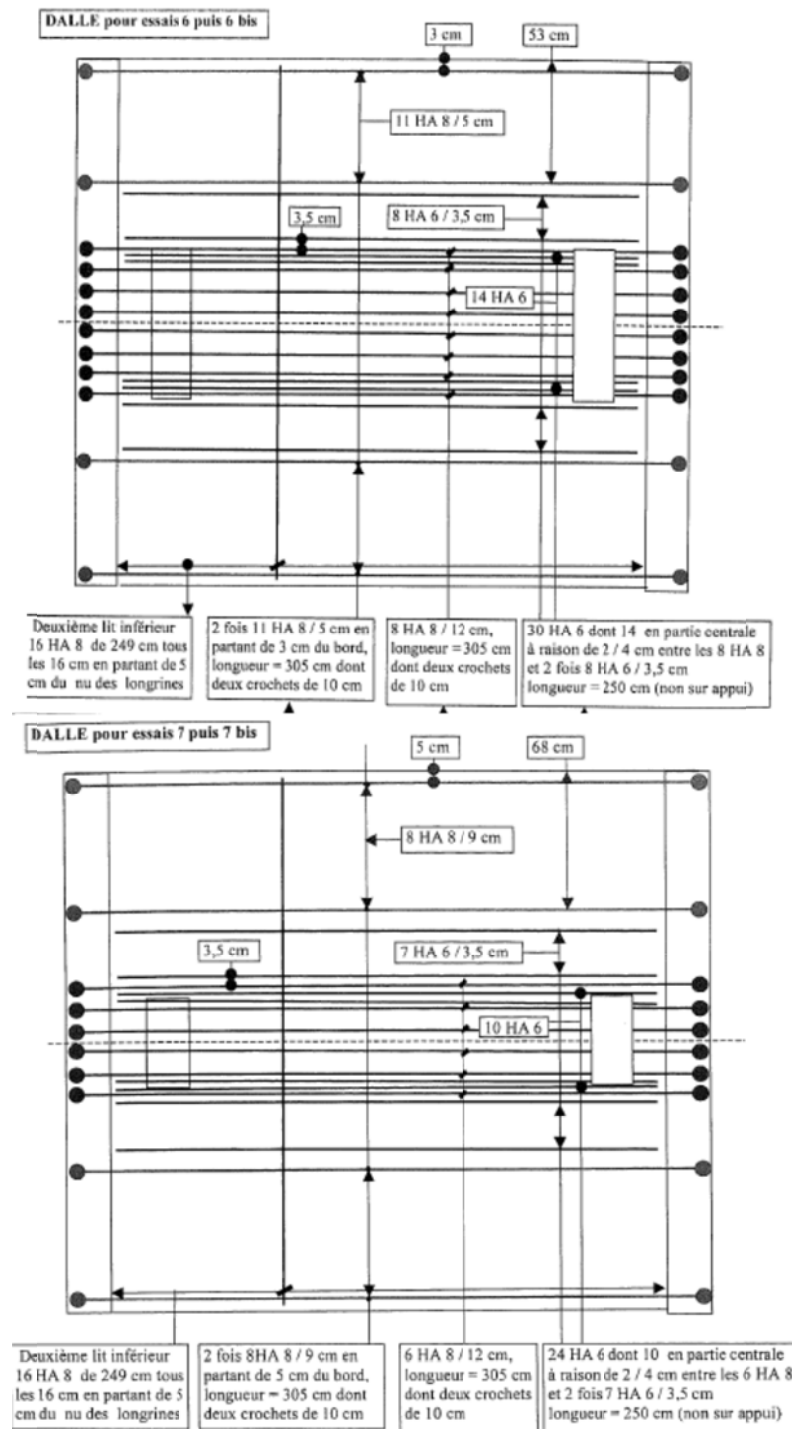


Fig. 4.33: Reinforcement of specimens 5, 6 and 7 (Coin and Thonier, 2007).

Table 4.17: Results from slabs tested by Coin and Thonier, 2007.

Name	$f_c'$ (MPa)	$f_t$ (MPa)	load (cm)	$P_u$ (kN)
------	-----------------	----------------	--------------	---------------



<b>1</b>	25,8	2,9	20 x 100	257
<b>2</b>	30,4	3,1	20 x 100	272
<b>3bis</b>	30,4	3,1	20 x 40	174
<b>5</b>	30,2	3,4	20 x 100	306
<b>5bis</b>	30,2	3,4	20 x 100	312
<b>6</b>	30,2	3,4	20 x 70	356
<b>6bis</b>	30,2	3,4	20 x 70	250
<b>7</b>	19,2	2,3	20 x 40	165
<b>7bis</b>	19,2	2,3	20 x 40	151

Olonisakin and Alexander (1999) tested 4 slabs in one-way shear. The dimensions and reinforcement layout are shown in Fig. 4.34. The slabs are 155mm thick, 750mm wide and 1,4mm long. The reinforcement consists of grade 400 no. 15M bars spaced at 150mm each way. The effective depth of the main reinforcement is 128mm. The reinforcement ratio is 1,04%. CB1 and CB2 use epoxy coated bars to study the influence of bond. The compressive cylinder strength of the concrete is 32,5MPa. The maximum aggregate size is not given. The test setup is shown in Fig. 4.35. Test results are given in Table 4.18. The size of the loading plate in CB1(a) is 380mm x 750mm (38 x 75 HSS) and for the other tests a 200mm channel with an estimated flange thickness of 9,9mm is used.

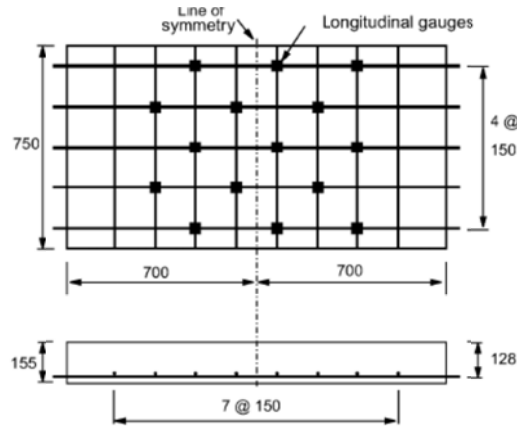


Fig. 4.34: Description of test specimens (Olonisakin and Alexander, 1999).

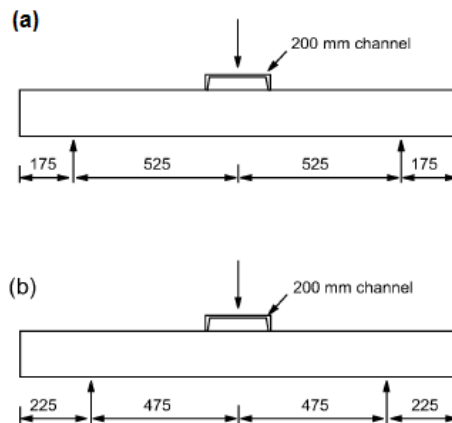


Fig. 4.35: Test setup, a) CB1(b) and RB1; b) CB2 and RB2 (Olonisakin and Alexander, 1999).

Table 4.18: Result of tests (Olonisakin and Alexander, 1999).

Mark	$a/d$	$f_y$ (MPa)	$V_{max}$ (kN)
CB1(b)	3,32	439	129
CB2	2,93	439	130
RB1	3,32	425	123
RB2	2,93	425	128

Ekeberg et al. (1982) carried out in-situ tests on a four story concrete warehouse building which was scheduled for demolition (Fig. 4.36). The distance from the loaded area to the nearest support is varied (Fig. 4.37). In two slabs in the building the two-way effect is neutralized by sawing through the slab along the two short sides. This is found not to have essential importance for the collapse load. In one of the two slabs mentioned above, the slab is also sawed along the long sides on the outer side of the supporting beams. This is done to test if the reduction in the restraining of the slab has any influence on the load-carrying capacity. The collapse load for this slab is not significantly different from the collapse load for slabs without sawed sides.

The building slabs have a height of 170mm plus a mortar layer of 40mm, a length of 2,5m and a width of 5m. The clear span in the length direction is 2,2m and in the width direction 4,6m. The maximum aggregate size is not known. The measured concrete cylinder (10cm diameter) compressive strength is 25MPa for the first floor and 17,8 MPa for the second floor. The yield strength of the reinforcement consisting of smooth bars is 310 MPa. The results with  $a/d < 7$  are given in Table 4.19, in which

$d_x$  the effective depth to the main reinforcement;

$d_y$  the effective depth to the transverse reinforcement;  
 $p_x$  the main reinforcement ratio;  
 $p_y$  the transverse reinforcement ratio;  
 $s$  the side length of the square loaded area.

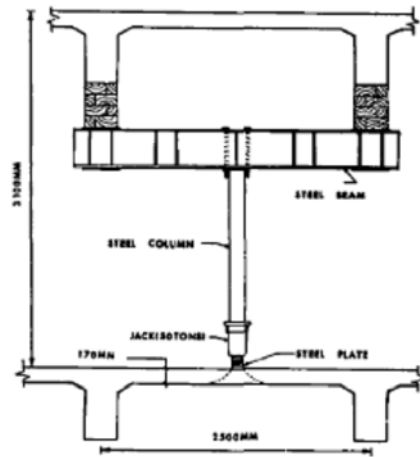


Fig. 4.36: Test rig used for the tests in the building. (Ekeberg et al., 1982).

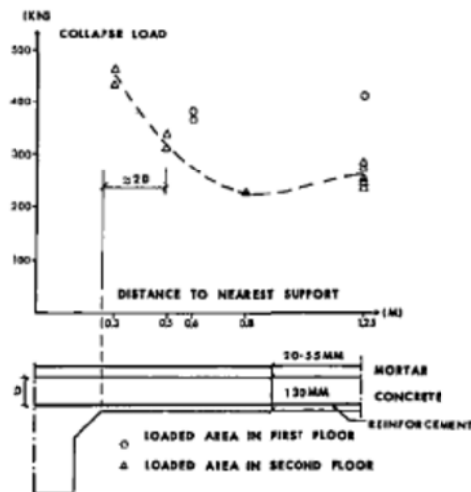


Fig. 4.37: Collapse loads as a function of the distance from the center of the loaded area to the center of the nearest support. (Ekeberg et al., 1982). Note that a minimum occurs at  $a/d = 7,3$ .

Table 4.19: Data from in-situ tests (Ekeberg et al., 1982).

Floor	n°	$d_x$ (mm)	$d_y$ (mm)	$p_x$ (%)	$p_y$ (%)	$s$ (mm)	$a$ (mm)	$a/d$	$P$ (kN)
1 <sup>st</sup> floor	3	110	100	0,649	0,157	100	610	5,55	371
	4	110	100	0,649	0,157	100	610	5,45	385
2 <sup>nd</sup> floor	3	108	98	0,519	0,102	100	300	2,78	465

	5	115	105	0,488	0,095	100	300	2,61	435
	6	115	105	0,488	0,095	100	800	6,96	230
	7	113	103	0,497	0,097	100	500	4,42	340
	8	113	103	0,497	0,097	100	500	4,42	315

Hegger and Reißer (2011) tested six slabs and two double T-beams to estimate the effective width and study the shear strength of slabs under concentrated loads. Each T-beam had one straight and one haunched cantilever slab. The new German Code requires stirrups in slabs where previous versions of the code did not require this. The effective width is studied by testing elements of different width. Parameter studies in non-linear finite elements are used to study the influence of:

- the concrete compressive strength,
- the yield strength of the steel,
- the reinforcement detailing, and
- the  $a/d$  or  $M/V$  ratio.

The loading configuration of the first four slabs (9 tests) is shown in Fig. 4.38. The size of the loading plate is 400mm x 400mm and  $d = 240$ mm (cover = 20 mm), leading to  $a/d = 4,16$ . The loading configuration of the next two slabs is shown in Fig. 4.39, with  $a/d$  ratios of 5,41 and 2,91. The cantilever slabs of Tb2 are preloaded by a preload of  $f_q = 85$ kN/m at the cantilever end in order to increase the bending moment and the vertical component of the compression force. The details of the loading and support conditions are shown in Fig. 4.41, showing that the size of the support is 100mm x 3500mm.

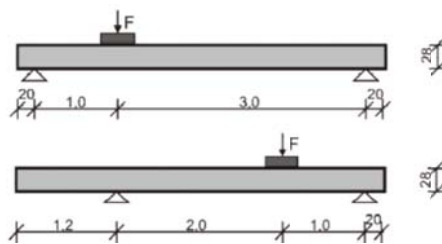


Fig. 4.38: Static system of first five specimens (Hegger and Reißer, 2011).

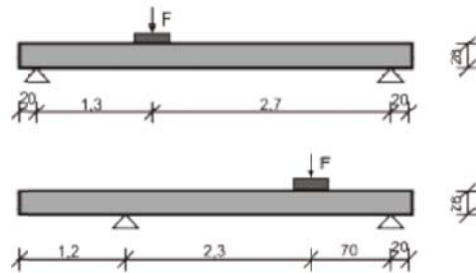


Fig. 4.39: Static system of last two specimens (Hegger and Reiben, 2011).

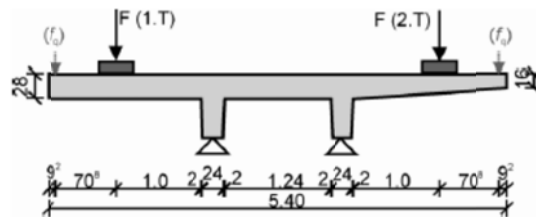


Fig. 4.40: Static system of the second test series: Tb1: without preload  $f_q$ , Tb2: with preload  $f_q$ .

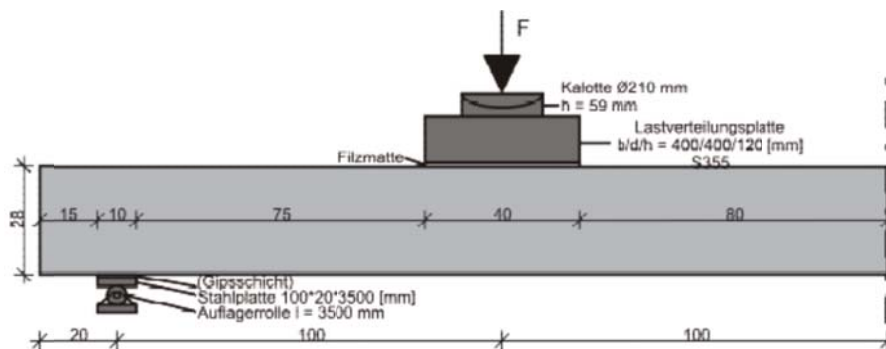


Fig. 4.41: Layout of loading plate and support conditions (Hegger and Reiben, 2011).

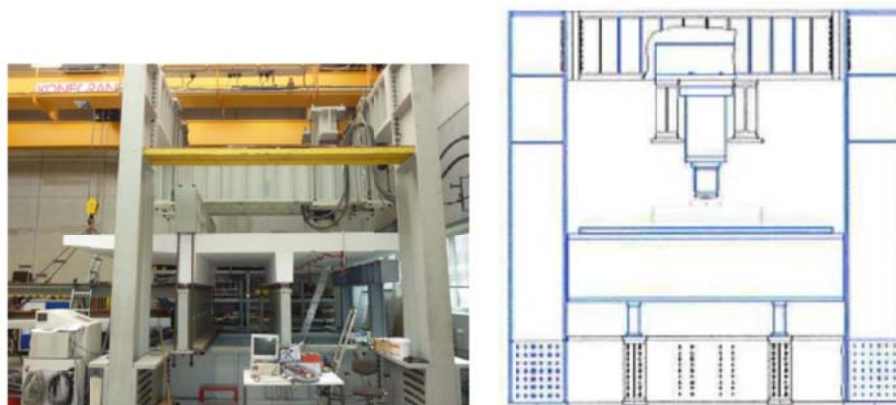


Fig. 4.42: Picture of double T beam in the test setup (Hegger and Reiben, 2011; Golus, 2011).

Table 4.20: Overview of test program (Hegger and Reiben, 2011).



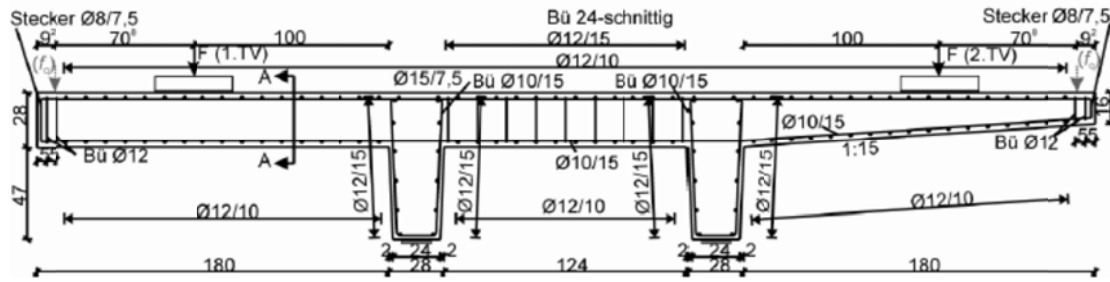


Fig. 4.43: Reinforcement of slabs with  $b = 50\text{cm}$ ,  $b = 150\text{cm}$ ,  $b = 250\text{cm}$ ,  $b = 350\text{cm}$  and double T beams (Hegger and Reiben, 2011).

Table 4.21: Reinforcement properties (Hegger and Reiben, 2011).

Versuchskörper	$\varnothing$	$f_{y,0.2}$	$f_t$	$E_s$
	mm	N/mm <sup>2</sup>	N/mm <sup>2</sup>	N/mm <sup>2</sup>
b=50, b=50_W, b=150, b=250, b=350, b=350_a1	12	573	672	200387
b=350_a2, Pb1, Pb2	12	556	639	200215
b=50, b=150, b=250, b=350	15	885	1082	199481
b=50_W, b=350_a1, Pb1, Pb2	15	920	1077	199710
b=350_a2	15	905	1095	198104

Regular concrete  $f_{cm} = 34\text{N/mm}^2$  is used for all slabs. The concrete properties are measured on cubes, cylinders, small beams for the E-modulus and cores drilled from the slabs for axial tension tests. The results of these tests are shown in Table 4.22, in which  $f_{c,cube,Güte}$  is the cube compressive strength at 28 days. The results of the first 9 tests (5 slabs) are shown in Table 4.23. The authors noted that the shear cracks further developed to the side face after exceeding the ultimate load within the descending branch, Fig. 4.44. Because of the unknown involved width, the dead weight was not considered in the evaluation.

Table 4.22: Concrete properties (Hegger and Reiben, 2011).



Versuch		Betonalter	$f_{c,cube}$	$f_{c,cube,Güte}$	$f_{c,cyl}$	$f_{ctm}$	$f_{ct,sp}$	$E_{cm}$
	Teilversuch	d	N/mm <sup>2</sup>	N/mm <sup>2</sup>	N/mm <sup>2</sup>	N/mm <sup>2</sup>	N/mm <sup>2</sup>	N/mm <sup>2</sup>
b=50	2.TV	21	40,1	42,0	33,7	2,8	3,0	26200
b=50_W	1.TV	18	43,7	51,3	39,2	3,0	3,5	26200
	2.TV	20	46,1		40,5	2,8	2,8	28100
b=150	1.TV	18	43,4	47,4	37,7	2,8	3,1	27300
	2.TV	23	45,0		38,2	3,0	3,6	27600
b=250	1.TV	25	32,7	34,6	27,9	2,5	2,3	22400
	2.TV	30	33,4		29,5	2,6	2,5	21000
b=350	1.TV	15	45,3	53,1	35,9	2,8	3,1	28200
	2.TV	21	47,8		38,2	3,0	3,1	24900 <sup>(1)</sup>
b=350_a1	1.TV	21	47,4	52,7	39,6	2,4	3,1	27200
	2.TV	26	47,5		41,3	2,7	3,2	29900
b=350_a2	1.TV	28	31,0	31,4	29,5	2,5 <sup>(2)</sup>	2,5	22700
	2.TV	30	31,0		29,0	2,7 <sup>(2)</sup>	2,4	23300
Pb1	1.TV	16	43,4	47,5	37,0	2,2	2,6	25900
	2.TV	21	44,9		38,4	2,2	2,7	26900
Pb2	1.TV	18	42,2	46,1	34,3	2,7	2,8	25500
	2.TV	21	42,0		34,8	2,6	3,0	26800

Table 4.23: Results of slab tests (Hegger and Reiben, 2011).

Last- stufe Soil	b=50		b=50_W				b=150				b=250				b=350			
	2.TV		1.TV		2.TV		1.TV		2.TV		1.TV		2.TV		1.TV		1.TV	
	F	Stufe ist	F	Stufe ist	F	Stufe ist	F	Stufe ist	F	Stufe ist	F	Stufe ist	F	Stufe ist	F	Stufe ist	F	Stufe ist
[%]	[kN]	[%]	[kN]	[%]	[kN]	[%]	[kN]	[%]	[kN]	[%]	[kN]	[%]	[kN]	[%]	[kN]	[%]	[kN]	[%]
12,50	28	13,7	23	12,8	26	12,1	70	12,9	76	11,9	85	12,8	94	12,1	104	10,6	138	13,5
25,00	56	27,5	46	25,1	52	24,2	140	25,8	152	23,8	170	25,6	188	24,1	208	21,1	276	27,0
37,50	84	41,2	69	37,7	78	36,3	210	38,7	228	35,7	255	38,4	282	36,2	312	31,7	414	40,4
50,00	112	54,9	92	50,3	104	48,4	280	51,6	304	47,6	340	51,2	376	48,2	416	42,2	552	53,9
56,25	126	61,8	103,5	56,6	117	54,4	315	58,0	342	53,6	382,5	57,6	423	54,2	468	47,5	621	60,6
62,50	140	68,6	115	62,8	130	60,5	350	64,5	380	59,6	425	64,0	470	60,3	520	52,8	690	67,4
68,75	154	75,5	126,5	69,1	143	66,5	385	70,9	418	65,5	467,5	70,4	517	66,3	572	58,1	759	74,1
75,00	168	82,4	138	75,4	156	72,6	420	77,3	456	71,5	510	76,8	564	72,3	624	63,4	828	80,9
81,25	182	89,2	149,5	81,7	169	78,6	455	83,8	494	77,4	552,5	83,2	611	78,3	676	68,6	897	87,6
87,50	196	96,1	161	88,0	182	84,7	490	90,2	532	83,4	595	89,6	658	84,4	728	73,9	966	94,3
93,75	210	102,9	172,5	94,3	195	90,7	525	96,7	570	89,3	637,5	96,0	705	90,4	780	79,2	1035	101,1
100,00	224	100,0	184	100,0	208	100,0	560	100,0	608	100,0	680	100,0	752	100,0	832	100,0	1104	100,0
$F_{max}$ [kN]		204		183		215		543		638		684		780		985		1024
$F_{max} / F_{max,act}$ [%]		91,1		99,5		103,4		97,0		104,9		97,6		103,7		118,4		92,8

Versuch		$F_u$	$V_{F,u}$	$V_{Rm,ct}$	$V_g$	$b_{aq,exp}$	$b_{eff,H240}$	$V_{Rm,ct,H240}$
		kN	kN	kN/m	kN/m	m	m	kN
b=50	2.TV	204	136	255	5,4	0,55	0,5	127
b=50_W	1.TV	183	137	269	10,5	0,54	0,5	135
	2.TV	215	143	273	5,4	0,54		136
b=150	1.TV	543	407	266	10,5	1,60	1,18	313
	2.TV	683	425	267	5,4	1,63		315
b=250	1.TV	664	498	237	10,5	2,21	1,18	279
	2.TV	780	520	242	5,4	2,20		286
b=350	1.TV	985	739	261	10,5	2,96	1,18	308
	2.TV	1024	683	267	5,4	2,62		315
b=350_a1	1.TV	1166	787	270	9,5	3,02	1,33	360
	2.TV	1143	876	275	6,4	3,27	1,03	283
b=350_a2	1.TV	924	624	242	9,5	2,69	1,33	322
	2.TV	892	684	240	6,4	2,93	1,03	248



Versuch		$F_{u+GL} = V_{F,u+GL}$	$f_{q+GL} = V_{q+GL}$	Schnitt	$V_{Rm,d}$	$b_{aq,exp\_GL(16)}$	$b_{aq,exp\_GL(17)}$	$b_{eff,H240}$	$V_{Rm,d,H240}$
		kN	kN/m	m von An-schnitt	kN/m	m	m	m	kN
Pb1	1.TV	571	0	0,46	264	2,24	2,24	0,98	258
	2.TV	477	0	0,59	248	1,97	1,67	0,91	226
Pb2	1.TV	539	86,4	0,59	256	3,34	3,34	0,98	251
	2.TV	453	86,4	0,59	239	3,09	2,10	0,91	218

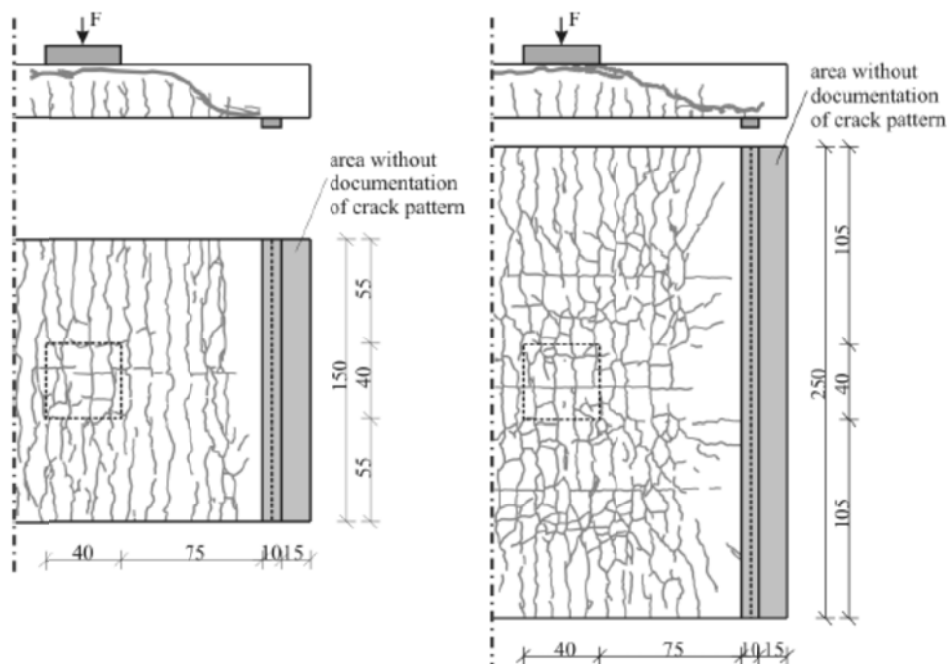


Fig. 4.44: Crack pattern of  $b=150$ , 2.T and of  $b=250$ , 2.T (Reißen and Hegger, 2011).

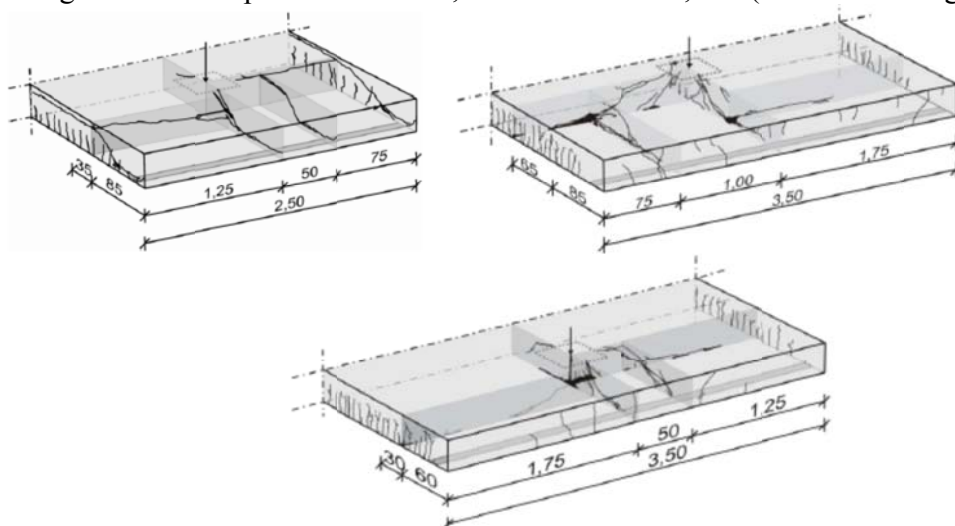


Fig. 4.45: Three-dimensional crack pattern of  $b=250$  1.TV,  $b=350\_a2$ , 1.TV and  $b=350\_a2$ , 2.TV (Reißen and Hegger, 2011).

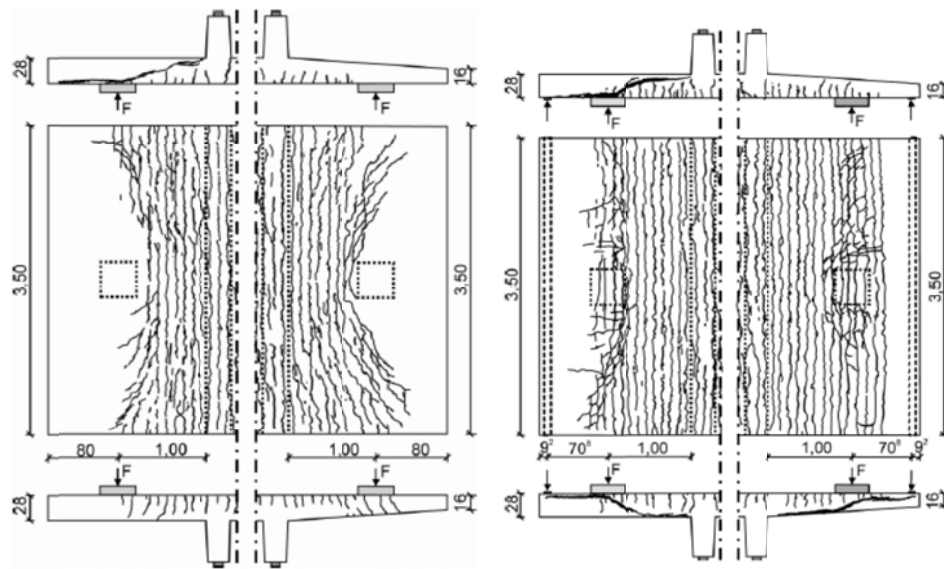


Fig. 4.46: Crack patterns of double T beams Pb1 and Pb2 (left 1.TV and right 2.TV) (Reißen and Hegger, 2011).

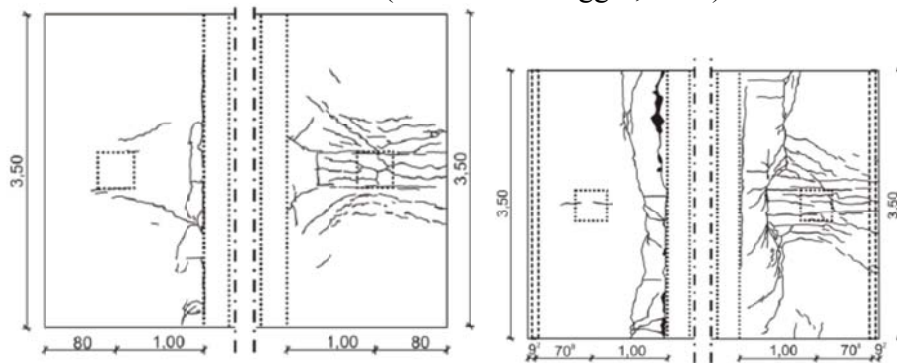


Fig. 4.47: Cracks at bottom face of double T beams Pb1 and Pb2 (left 1.TV and right 2.TV) (Reißen and Hegger, 2011).

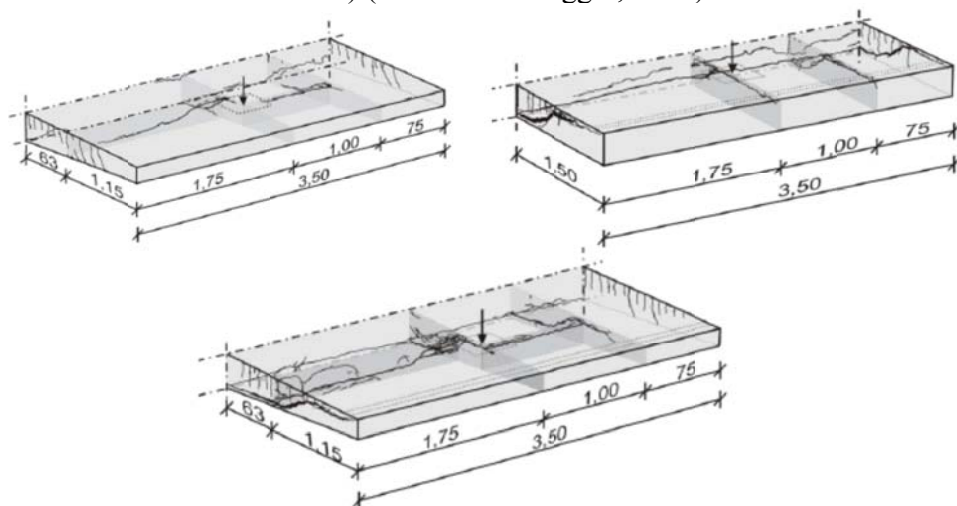


Fig. 4.48: Three-dimensional crack patterns of double T beams: Pb1 2.TV and Pb2 1.TV and 2.TV (Reißen and Hegger, 2011).

#### 4.7. Experiments on bridge decks

Rombach and Latte (2008, 2009) carried out tests on cantilever slabs (with and without haunches) to examine whether bridge deck slabs under concentrated wheel loads exhibit reserves of shear capacity which are not represented by EN 1992-1-1:2005. The test setup is shown in Fig. 4.49 and the specimens are shown in Fig. 4.50. The reinforcing steel has a yield strength of 550MPa. The maximum aggregate size is 16mm and the water-cement ratio is 0,49. The size of the load plate is 400mm x 400mm. The cover in VK1 is 45mm and in the other slabs 25mm. A line load the represent the edge loading is applied. The results are given in

Table 4.27, in which:

$f_{c,cyl}$	the concrete cylinder compressive strength;
$f_{ct,sp}$	the split tensile strength of the concrete;
$e$	the eccentricity of the line load.

Failure occurred over the full width of the specimen (2,40m wide) while a 45° load spreading gives an effective width of 2,10m and load spreading based on linear elasticity results in an effective width of 1,42m. The failure crack pattern is shown in Fig. 4.51.

Due to the restraint of the middle slab, normal forces result and the failure mode is punching. The following reasons are summed up to explain the much higher shear capacities than calculated with EN 1992-1-1:2005:

- redistribution of forces in the cracked specimen,
- influence of the moment-shear force ratio,
- direct load transfer between the load and the support,
- influence of the transverse flexural reinforcement.

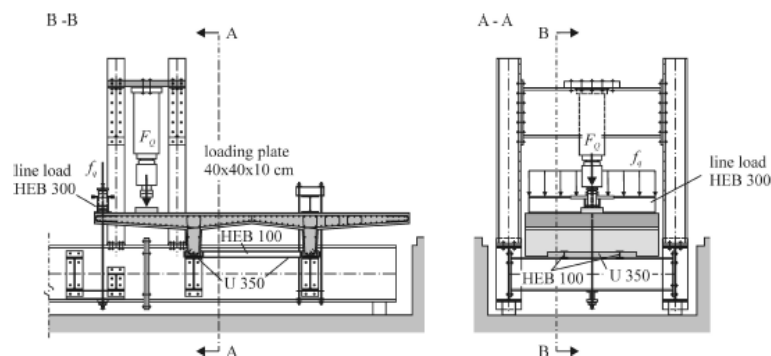


Fig. 4.49: Test setup and load arrangement of the cantilever test for the test specimen VK1 (Rombach and Latte, 2008).

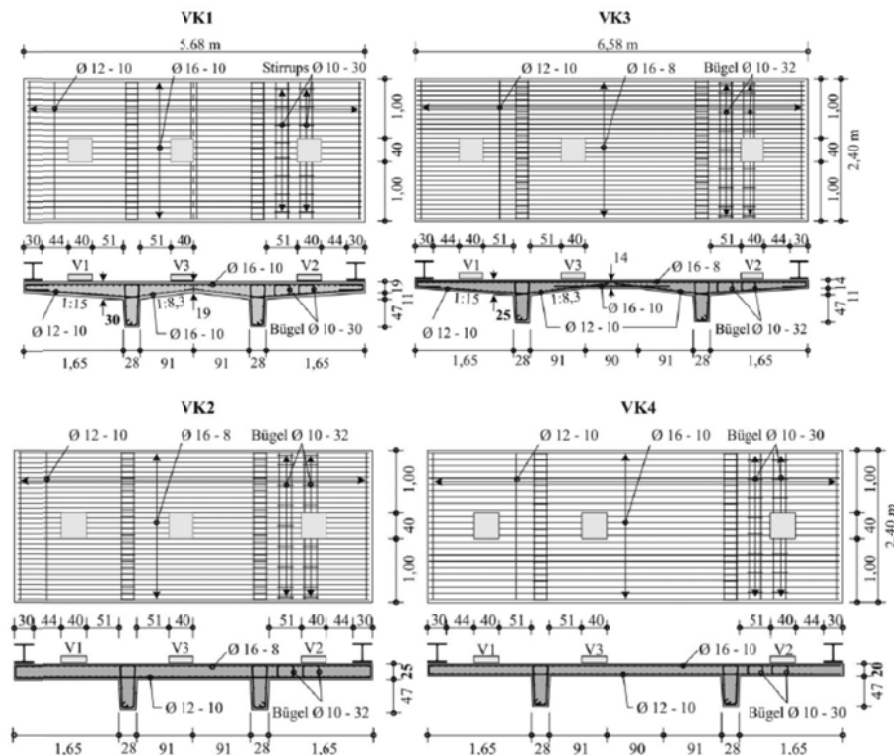


Fig. 4.50: Dimensions and reinforcement layout of the test specimens VK1 to VK4, (Rombach and Latte, 2009).

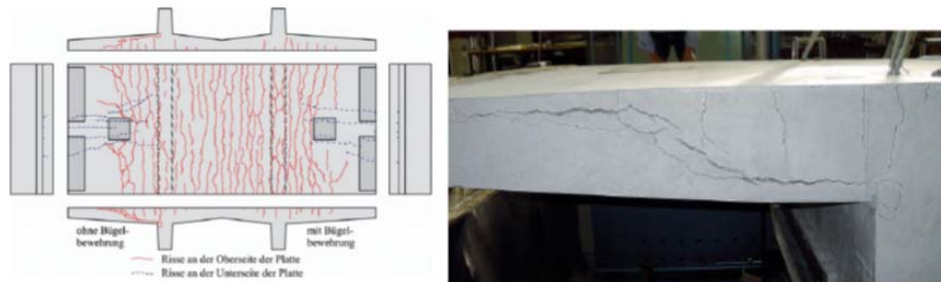


Fig. 4.51: Crack pattern of test specimen VK1 after loading (Rombach and Latte, 2009).

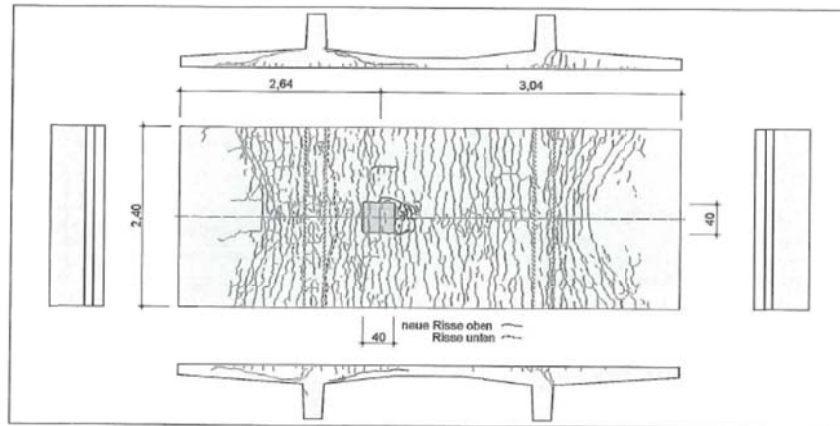


Fig. 4.52: VK3V3 cracking pattern (Rombach et al., 2009).

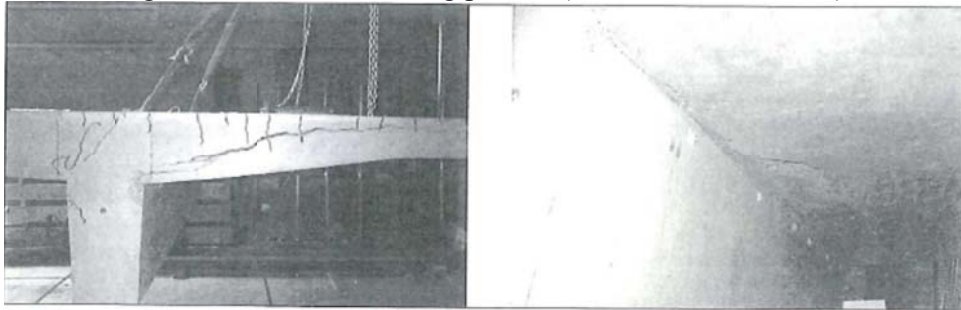


Fig. 4.53: Crack pattern at failure of VK3V3 (Rombach et al., 2009).

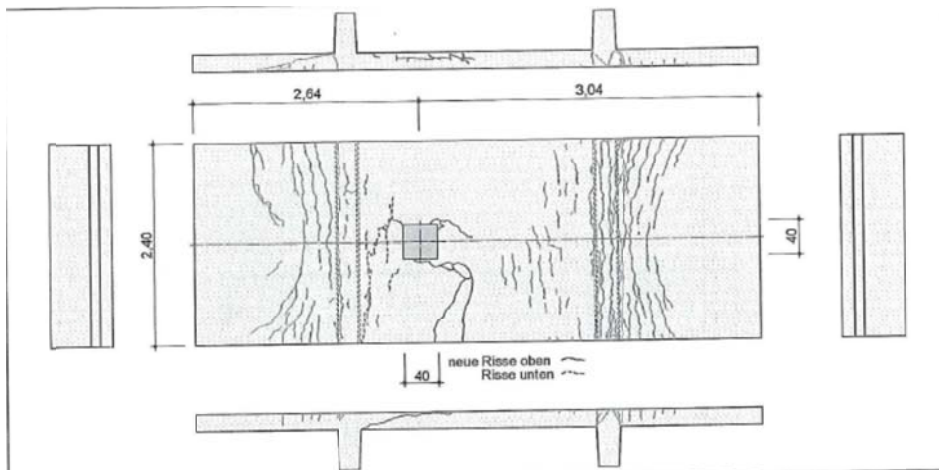


Fig. 4.54: VK4V3 cracking pattern (Rombach et al., 2009).

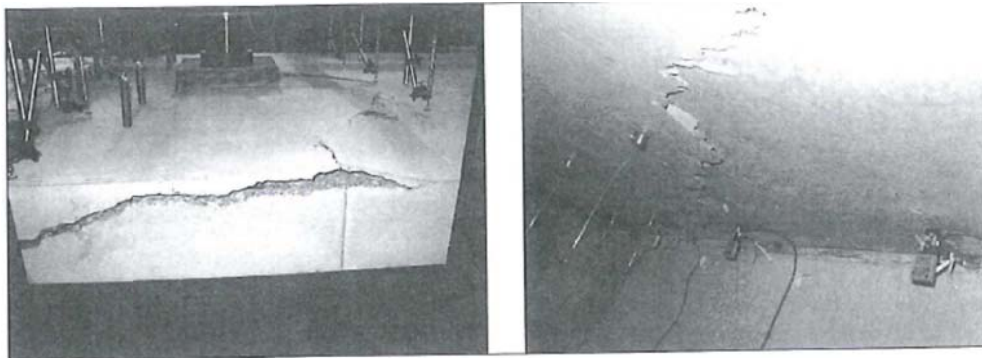


Fig. 4.55: Crack pattern at failure of VK4V3 (Rombach et al., 2009).

Table 4.24: Tested specimens (Rombach et al., 2009).

Ver- suchs- körper	Beton- deckung	Längsbewehrung oben				Längsbewehrung Kragarme unten				Längsbewehrung Innenplatte unten				Bügelbewehrung rechter Kragarm Ø 10	
	$c_v$ [mm]	Ø [mm]	$a_{sx}$ [cm <sup>2</sup> /m]	$\rho_x^{(1)}$ [%]	Ø [mm]	$a'_{sx}$ [cm <sup>2</sup> /m]	$\rho'_x^{(1)}$ [%]	Ø [mm]	$a'_{sx}$ [cm <sup>2</sup> /m]	$\rho'_x^{(1)}$ [%]	Ø [mm]	$a'_{sx}$ [cm <sup>2</sup> /m]	$\rho'_x^{(1)}$ [%]	$s_x - s_y$ [cm]	$a_{sw}$ [cm <sup>2</sup> /m <sup>2</sup> ]
VK1	45	16-10	20,1	0,81	12-10	11,3	0,46	16-10	20,1	0,81	20-30	13,1			
VK2	25	16-8	25,1	1,16	12-10	11,3	0,52	12-10	11,3	0,52	20-32	12,3			
VK3	25	16-8	25,1	1,16	12-10	11,3	0,52	12-10	11,3	0,52	20-32	12,3			
VK4	25	16-10	20,1	1,20	12-10	11,3	0,68	12-10	11,3	0,68	20-30	13,1			

(1) Berechnet mit der statischen Nutzhöhe  $d$  am Anschnitt zum Steg

Table 4.25: Concrete properties (Rombach et al., 2009).

Ver- suchs- körper	Versuch	Beton- alter	Mittelwerte		$E_c$
		[d]	$f_{c,cyl,dry}$ [MPa]	$f_{ct,sp}$ [MPa]	[GPa]
VK1	V1	46	35,0	2,85	29,17
	V3	71	37,9	3,05	-
VK2	V1	45	46,0	3,42	33,99
	V3	58	45,2	3,54	33,19
VK3	V1	44	46,5	3,34	33,34
	V3	80	51,5	3,61	33,67
VK4	V1	36	42,5	3,23	32,49
	V3	50	46,0	3,38	32,23

Table 4.26: Steel properties (Rombach et al., 2009).



Ø [mm]	Mittelwerte		$\epsilon_u$ [%]	$\frac{f_t}{f_y}$	$E_s$ [GPa]
	$f_y$ [MPa]	$f_t$ [MPa]			
10 BSt500 WR	540	598	4,70	1,11	194
12 BSt500 WR	550	607	5,09	1,11	195
16 BSt500 S	554	646	11,61	1,17	195

Table 4.27: Relevant test results from Rombach and Latte (2008).

		Concrete		Line load		Wheel load		Test results	
Test	$\rho$ (%)	$f_{c,cyl}$ (MPa)	$f_{ct,sp}$ (MPa)	$f_q$ (kN/m)	$e$ (m)	$a_v$ (m)	$a_v/d$	Shear cracking $F_{Q,ct}$ (kN)	Failure $F_{Qu}$ (kN)
VK1V1	0,81	35,0	2,85	32,1	1,5	0,51	2,91	350	690
VK2V1	1,16	46,0	3,42	22,5	1,5	0,51	2,35	360	678
VK3V1	1,16	46,5	3,34	22,5	1,5	0,51	2,35	400	672
VK3V3	0,52	51,5	3,61	-	-	0,51	2,35		677
VK4V1	1,20	42,5	3,23	-	-	0,51	3,05	260	487
VK4V3	0,68	46	3,38	-	-	0,51	3,05		935

Table 4.28: Test results and reported failure modes (Rombach et al., 2009).

1	2	3	4		5		6		7	8
Versuchs- körper	b/d <sup>(1)</sup>	Versuch	Vorlast $f_q$		Konz. Last $F_Q$		Fließen		Bruchlast	Versagen
			$f_q$ [kN/m]	$e$ [m]	$a$ [m]	$a/d^{(1)}$	$F_{Q,mitte}^{(2)}$ [kN]	$F_{Q,gesamt}^{(3)}$ [kN]		
VK1	9,7	V1	32,1	1,50	0,71	2,88	-	-	690	Querkraft
		V2	32,1	1,50			671	732	758	Biegung
		V3	-	-			-	-	-	Höchstlast 978 kN
VK2	11,1	V1	22,5	1,50	0,71	3,27	-	-	678	Querkraft
		V2	22,5	1,50			808	851	877	Biegung
		V3	-	-			-	-	-	Höchstlast 945 kN
VK3	11,1	V1	22,5	1,50	0,71	3,27	-	-	677	Querkraft
		V2	22,5	1,50			767	850	870	Biegung
		V3	-	-			-	-	898	Querkraft
VK4	14,4	V1	-	-	0,71	4,25	-	-	487	Querkraft
		V2	-	-			548	579	590	Biegung
		V3	-	-			-	-	935	Querkraft

<sup>(1)</sup> Mit der statischen Nutzhöhe  $d$  am Anschnitt zum Steg  
<sup>(2)</sup> Überschreiten der Fließdehnung von 3,3 ‰ in beiden mittleren Stäben (Messstellen D3 u. D4)  
<sup>(3)</sup> Maximallast beim Übergang in den horizontalen Verlauf des Last-Weg-Diagramms  
<sup>(4)</sup> Bei den Versuchen V2 wurde der Versuch vor dem Bruch der Längsbewehrung beendet

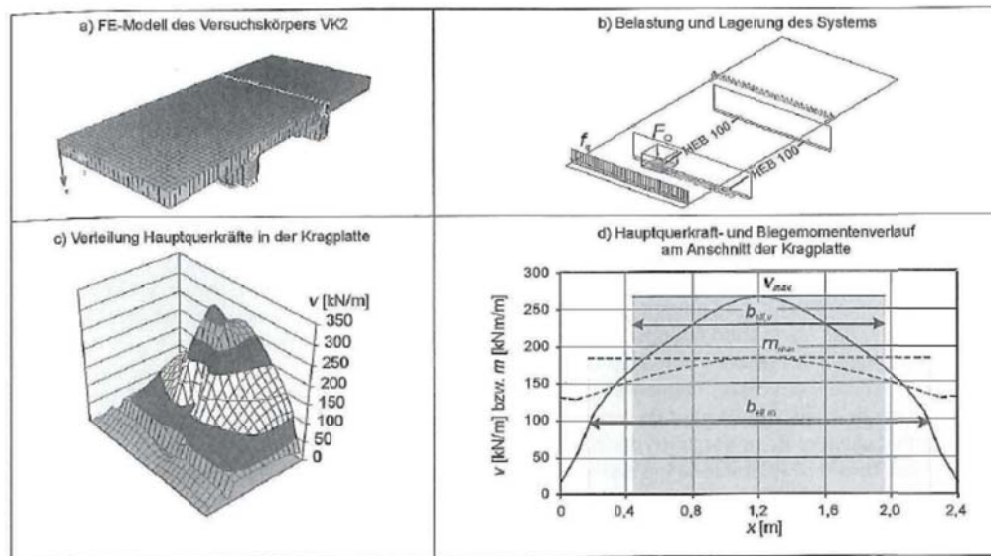


Fig. 4.56: Finite element model of bridge deck tests (Rombach et al., 2009).

Table 4.29: Comparison between experimental result and calculated values, also showing the effective width resulting from linear elastic load spreading (Rombach et al., 2009).

1	2	3	4	5	6	7	8	9	10	11	12	13	
Versuch		Versuchsergebnisse			Elastische Lastausbreitung				Volle Lastausbreitung $b_{eff,m} = b_{eff,v} = 2,4 \text{ m}$				
		Schubbriss $F_{Q,ct}^{1)}$ [kN]	Fließen $F_{Q,ymitte}^{2)}$ [m]	Bruch $F_{Qu}$ [kN]	$b_{eff,m}$ [m]	$F_{y,cal}$ [kN]	$b_{eff,v}$ [m]	$F_{ct,cal}$ [kN]	$\frac{F_{Qu}}{F_{ct,cal}}$	$F_{vu,cal}$ [kN]	$\frac{F_{Qu}}{F_{vu,cal}}$	$F_{mu,cal}$ [kN]	$\frac{F_{Qu}}{F_{mu,cal}}$
VK1	V1	350	-	690	1,93	537	1,40	290	2,38	518	1,33	684	1,00
	V2	-	671	758				-	-	-	-		1,11
VK2	V1	360	-	678	2,07	691	1,52	392	1,73	613	1,11	807	0,84
	V2	-	808	877				-	-	-	-		1,09
VK3	V1	400	-	672	1,93	645	1,40	359	1,87	621	1,08	817	0,82
	V2	-	767	870				-	-	-	-		1,06
VK4	V1	260	-	487	2,01	469	1,43	308	1,58	516	0,94	558	0,87
	V2	-	548	590				-	-	-	-		1,06

<sup>1)</sup> Aus den berechneten Vertikaldehnungen abgelesener Lastwert bei ersten Biegeschubbrissen an den Messstellen (siehe Kapitel 4.5.1)

<sup>2)</sup> Lastwert beim Überschreiten der Fließdehnung von 3,3 ‰ in den beiden mittleren Stäben (siehe Kapitel 4.5.1)

Miller et al. (1994) tested a decommissioned 38-year-old concrete slab bridge up to failure. The abutments and pier lines of the bridge are skewed 30° to the roadway. The concrete is heavily deteriorated with the reinforcement in the shoulder area completely exposed. The dimensions of the bridge are shown in Fig. 4.57 and the reinforcement layout is shown in Fig. 4.58. The deck is 438mm thick. Only one lane is loaded with a load simulating the stationary load of an HS20-44 truck, Fig. 4.59, showing that the load is placed at  $a/d = 3,51$ . The bridge failed in shear at 3200kN, which corresponds to 22 HS20-44 trucks. The theoretical flexural failure load is not reached. Yield is reached only



just before failure. The bridge failed in a brittle flexural shear mode. The final failure is shown in Fig. 4.60. The average shear stress at failure is  $0.95\sqrt{f'_c}$ , much lower than the estimated  $3.8\sqrt{f'_c}$ . The measured concrete compressive strength is 54 MPa. The final failure surface is not typical punching shear. The damage had a great effect on the final failure.

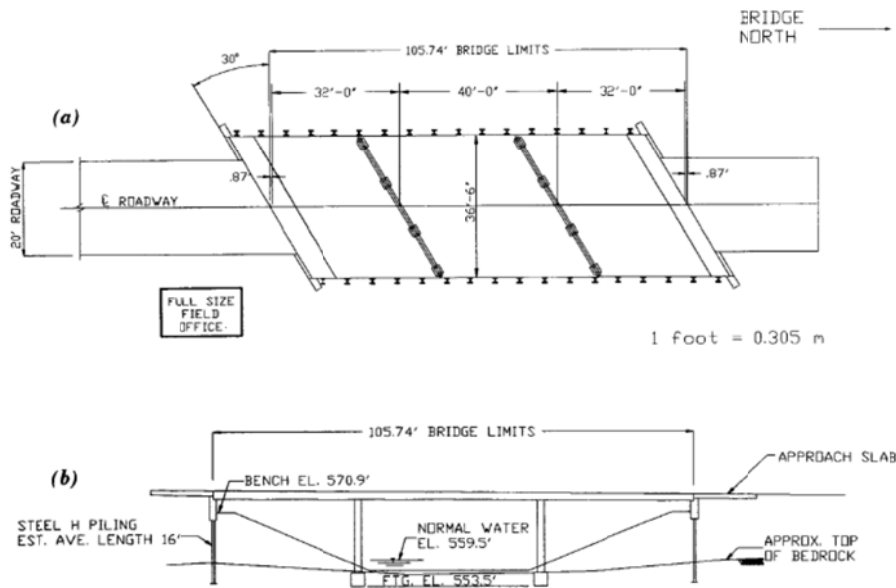


Fig. 4.57: Bridge dimensions: (a) Plan; and (b) Elevation (Miller et al., 1994).

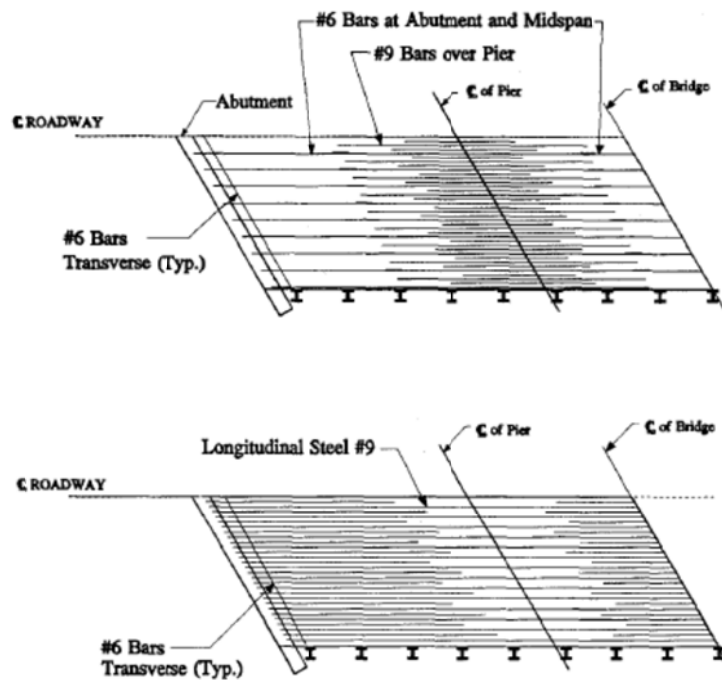


Fig. 4.58: Reinforcement: (a) top of slab; and (b) bottom of slab (Miller et al., 1994)

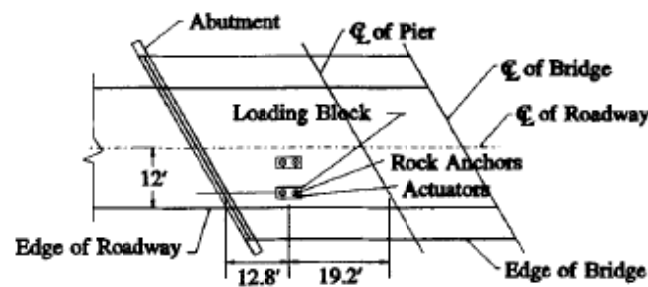


Fig. 4.59: Loading system, Miller et al. (1994).

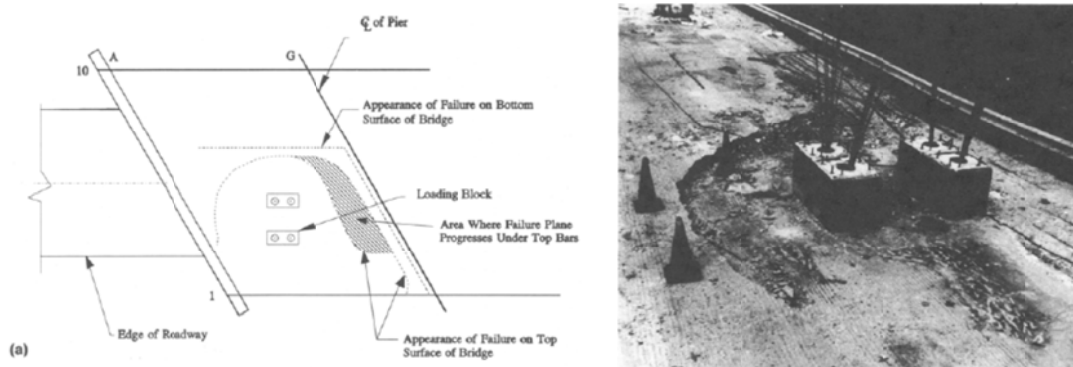


Fig. 4.60: Final failure plane: (a) diagram; and (b) photo (Miller et al., 1994).

Fang et al. (1990) tested a full scale bridge deck of 6,10m by 15,24m. The plan view and cross section are shown in Fig. 4.61 and Fig. 4.62. The specimen is a full size composite bridge with a 191mm thick concrete deck on three 914mm steel W-sections, spaced at 2,13m. Half the deck has two layers of isotropic reinforcement (#4 bars at 222mm). The compressive strength of the concrete is measured as 29MPa. The yield strength of the reinforcement is measured as 504 MPa. The maximum aggregate size is not given. The size of the load is 203,2 mm x 508mm. The cracking patterns are given in Fig. 4.63. The single load test has an ultimate load of 632kN, and the tandem wheel load 907kN. The failure mode is reported as punching, but the slab never actually punched through. The real failure angles could not be measured, but judging the distance between the top and bottom cracks the failure angle was estimated at about 39 degrees. Further analysis suggests that the slab showed a combination of beam shear and punching shear failure. The predictions with ACI and AASHTO codes are very conservative, as the failure load is about seven times the service wheel load for the single load test.

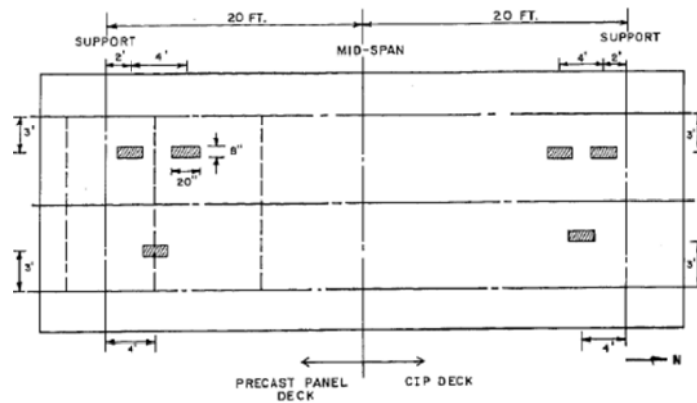


Fig. 4.61: Plan view of test specimen. (Fang et al., 1990)

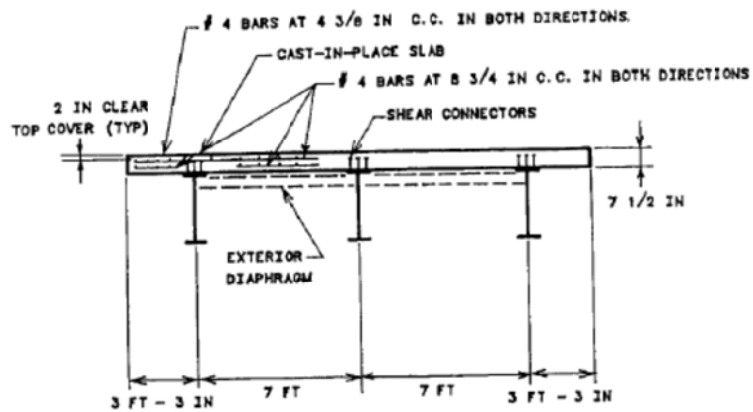


Fig. 4.62: Cross section of test specimen. (Fang et al., 1990)

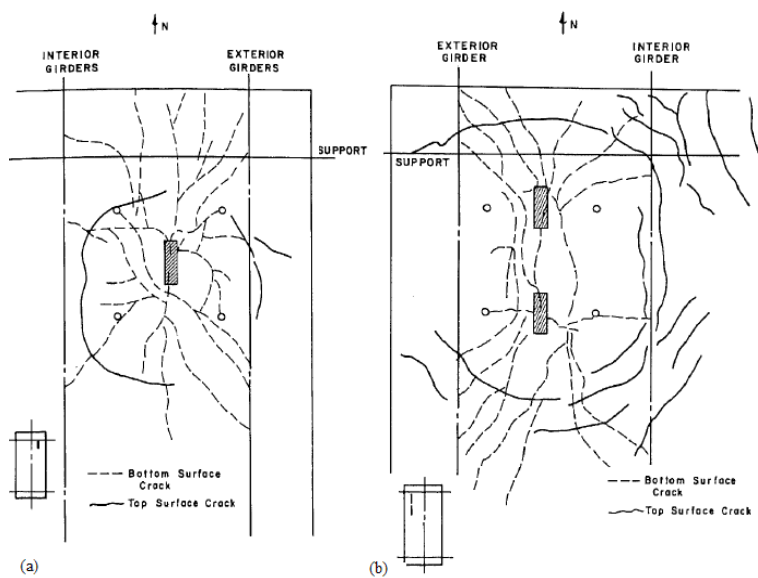


Fig. 4.63: Deck cracking from (a) single load test and (b) tandem load test. (Fang et al., 1990)

## 5. Code provisions

### 5.1. NEN 6720

The Dutch code NEN 6720 uses the following criterion for one-way shear:

$$\tau_d \leq \tau_u \quad (5.1)$$

in which

$$\tau_u = \tau_l + \tau_s \leq \tau_2;$$

$$\tau_2 = 0,2 f_b' k_n k_\theta;$$

with

$$k_n = \frac{5}{3} \left(1 - \frac{\sigma_{bmd}'}{f_b'}\right) \leq 1,0 \text{ in which } \sigma_{bmd}' = \frac{N_d'}{A_b} \text{ the average concrete}$$

compressive stress due to the design value of the normal force including the prestressing and  $f_b'$  the design value of the compressive strength of the concrete;

$$k_\theta = 2 \frac{\cot \theta + \cot \alpha}{1 + \cot^2 \theta} \text{ for } 45^\circ \leq \alpha < 90^\circ;$$

$k_\theta = 1$  for  $\alpha = 90^\circ$  and if no stirrups are used, with  $\alpha$  the angle between the stirrups and the axis of the member and  $\theta$  the angle between the compression diagonal and the axis of the member;  
 $f_b'$  = concrete compressive strength.

$\tau_1$  the ultimate shear capacity of the concrete without stirrups; its value for reinforced concrete members in bending is  $\tau_1 = 0,4 f_b k_\lambda k_h \sqrt[3]{w_o} \geq 0,4 f_b$

with

$f_b$  = concrete tensile strength;

$$k_\lambda = \frac{12}{g_\lambda} \sqrt[3]{\frac{A_o}{bd}} \geq 1 \text{ for corbels and members at end supports where a}$$

compression strut can be formed between the load and the support,

$$g_\lambda = 1 + \lambda_v^2 \text{ if } \lambda_v \geq 0,6;$$

$$g_\lambda = 2,5 - 3\lambda_v \text{ if } \lambda_v < 0,6.$$

$$k_\lambda = 1 \text{ for all other cases;}$$

$\lambda_v = \frac{M_{d\max}}{dV_{d\max}}$  the shear slenderness with  $M_{d\max}$  the maximum

absolute value of  $M_d$  in the member and  $V_{d\max}$  the maximum absolute value of  $V_d$  in the member;

$A_o$  is the smallest value of the area of the load or support, not exceeding  $bd$ ;

$k_h = 1,6 - h \geq 1,0$  with  $h$  in meters;

$$w_o = \frac{100(A_s + A_p)}{bd} \leq 2,0 \text{ and } \geq 0,7 - 0,5\lambda_v ;$$

$\tau_s$  the shear capacity of the stirrups;

$\tau_d$  the shear stress in the section,  $\tau_d = \frac{V_d}{bd}$ .

The concrete tensile strength  $f_b$  is taken as the long-term tensile strength (CUR rapport 94-13):

$$f_{bm} = 0,7(1,05 + 0,05f'_{cm}) \quad (5.2)$$

in which  $f'_{cm}$  is the measured mean cube concrete compressive strength.

The NEN 6720 uses the following criterion for punching shear for concentrated loads of which the length is not larger than three times the width:

$$\tau_d \leq \tau_u \quad (5.3)$$

in which

$$\tau_u = \tau_I + \tau_s \leq \tau_2 ;$$

$\tau_I$  the ultimate shear capacity of the concrete without stirrups

$$\tau_1 = 0,8f_b k_d \sqrt[3]{w_o} \geq 0,8f_b ;$$

$$\text{for } a_l > 2a_b, \tau_I \text{ has to be multiplied with } k_1 = (2 - \frac{a_l}{2a_b}) \geq 0,5 ;$$

$$\text{for } a > 2d, \tau_I \text{ has to be multiplied with } k_2 = \frac{4}{2 + \frac{a}{d}} \geq 0,5 ;$$

$d$  = the effective depth around the concentrated load;

$k_d$  = the size factor  $1,5 - 0,6d \geq 1,0$  with  $d$  in meters;

$w_o = \sqrt{w_{ox}w_{oy}} \leq 2,0$  with  $w_{ox}$  and  $w_{oy}$  the reinforcement ratio of the flexural reinforcement in the x- and y-direction;

$a$  = the diameter of a circular loaded area, taken as  $a = \frac{2}{\pi}(a_l + a_b)$  for a rectangular loaded area;

$\tau_s$  the shear capacity of the stirrups;

$\tau_2 = 0,15f'_b \leq 5,0\text{N/mm}^2$ ;

$\tau_d$  the design value of the largest shear stress,  $\tau_d = \frac{\alpha_e F_d}{pd}$

with

$F_d$  = the design value of the punching force;

$\alpha_e$  = the eccentricity factor  $\alpha_e = 1 + \alpha_x \frac{|e_x - e_z|}{d + a} + \alpha_y \frac{|e_y|}{d + a}$ ;

$e_x, e_y$  = the eccentricity of punching force with respect to the centroid of the loaded area in x- resp. y-direction;

$e_z$  = the eccentricity of the centroid of the periphery with respect to the centroid of the loaded area;

$d$  = the effective depth;

$a$  = the diameter of circular loaded area,  $a = \frac{2}{\pi}(a_l + a_b)$  for a rectangular loaded area;

$p$  = the perimeter:

middle column:  $p = \pi(d + a)$ ;

edge column:  $p = 0,5\pi(d + a) + 2a_r$ ;

corner column:  $p = 0,25\pi(d + a) + 2a_r$ ;

$a_r$  = the distance from the centroid of the loaded area to the edge of the slab:

edge column :  $a_r = 0,25\pi(d + a)$ ;

corner column:  $a_r = 0,375\pi(d + a)$ ;

$\alpha_x, \alpha_y$  = a factor from tables 30 to 34 of the NEN 6720, Table 5.1 to Table 5.5.

Table 5.1: Values of  $a$  for a rectangular column. Table 30 from NEN 6720.

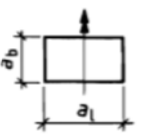
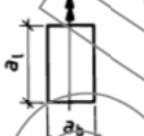
$\frac{a_l + d}{a_b + d}$		
	$\alpha_x$	$\alpha_y$
1,0	2,0	2,0
1,2	2,2	1,8
1,4	2,4	1,6
1,6	2,6	1,4
1,8	2,7	1,3
2,0	2,8	1,2

Table 5.2: Values of  $\alpha_x$  for an edge column with moment vector parallel to the edge. Table 31 from NEN 6720.

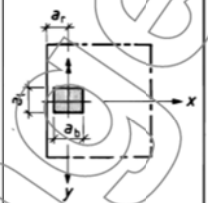
	$\frac{a_b + d + 2a_r}{2(a_l + d)}$	$\frac{2a_r}{d + a}$					
		0,2	0,4	0,8	1,2	1,6	2,0
$e_x \geq e_z$	0,4	0,6	0,5	0,4	0,4	0,3	0,3
	0,8	1,9	1,7	1,3	1,1	1,0	0,9
	1,2	3,0	2,6	2,1	1,8	1,5	1,4
	1,6	3,8	3,3	2,6	2,2	1,8	1,6
$e_x < e_z$	0,4	1,0	0,9	0,6	0,5	0,4	0,3
	0,8	3,2	2,7	2,0	1,6	1,3	1,2
	1,2	5,1	4,3	3,2	2,5	2,1	1,8
	1,6	6,1	5,3	4,0	3,2	2,6	2,3

Table 5.3: Values for  $\alpha_y$  for an edge column with moment vector perpendicular to the edge. Table 32 from NEN 6720.

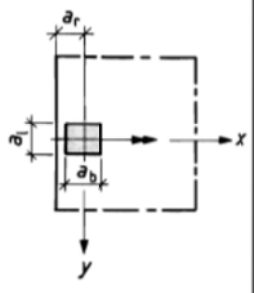
	$\frac{a_l + d}{a_b + d + 2a_r}$	$\frac{2a_r}{d + a}$					
		0,2	0,4	0,8	1,2	1,6	2,0
	0,2	0,5	0,4	0,4	0,4	0,4	0,4
	0,4	0,9	0,8	0,7	0,7	0,7	0,7
	0,6	1,2	1,2	1,0	1,0	0,9	0,9
	0,8	1,5	1,4	1,3	1,2	1,2	1,2
	1,0	1,8	1,7	1,5	1,4	1,4	1,4

Table 5.4: values for  $a_x$  for a corner column with moment vector perpendicular to bissectrice. Table 33 from NEN 6720.

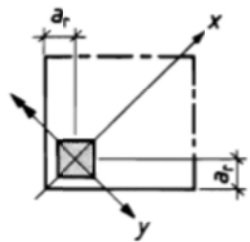
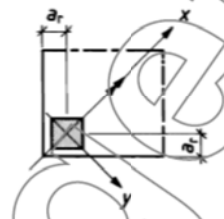
	$\frac{2a_r}{d+a}$					
	0,2	0,4	0,8	1,2	1,6	2,0
$e_x \geq e_z$	5,0	3,8	2,7	2,1	1,8	1,6
$e_x < e_z$	9,3	6,5	4,1	3,0	2,4	2,0

Table 5.5: Values for  $a_y$  for a corner column with moment vector parallel to bissectrice. Table 34 from NEN 6720.

	$\frac{2a_r}{d+a}$					
	0,2	0,4	0,8	1,2	1,6	2,0
	1,9	1,6	1,2	1,0	0,9	0,8

## 5.2. EN 1992-1-1:2005

In EN 1992-1-1:2005 §6.2.2., the maximum shear force for a section without stirrups is calculated as follows:

$$V_{Rd,c} = \left[ C_{Rd,c} k (100 \rho_l f_{ck})^{1/3} + k_1 \sigma_{cp} \right] b_w d \geq (v_{\min} + k_1 \sigma_{cp}) b_w d \quad (5.4)$$

with

$\rho_l$  the reinforcement ratio,  $\rho_l = \frac{A_{sl}}{b_w d} \leq 0,02$  ;

$A_{sl}$  the area of the reinforcement which extends  $\geq (l_{bd} + d)$  beyond the section considered, Fig. 5.1;

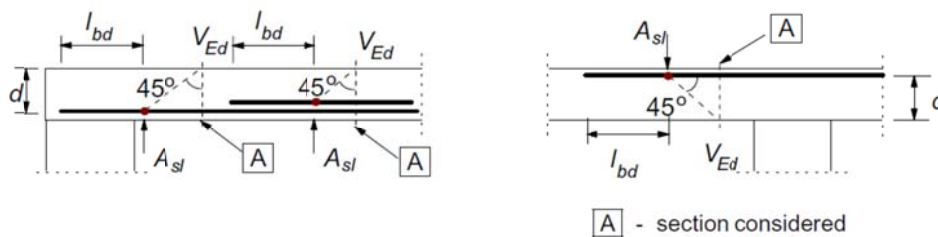


Fig. 5.1: Definition of  $A_{sl}$ , Figure 6.3 from EN 1992-1-1:2005



$b_w$  the smallest width of the cross-section in the tensile area;

$f_{ck}$  the characteristic concrete strength in MPa;

$$k = 1 + \sqrt{\frac{200}{d}} \leq 2,0 ;$$

$d$  the effective depth in mm;

$$\sigma_{cp} = (\sigma_{cy} + \sigma_{cz}) / 2 ;$$

$\sigma_{cy}, \sigma_{cz}$  the normal concrete stresses in the critical section in y- and z-directions

$$(\text{MPa, positive if compression}) \quad \sigma_{cy} = \frac{N_{Ed,y}}{A_{cy}} \quad \text{and} \quad \sigma_{cz} = \frac{N_{Ed,z}}{A_{cz}} ;$$

$N_{Ed,y}, N_{Ed,z}$  is the axial force in the cross-section due to loading or prestressing ( $N_{Ed} > 0$  for compression). The influence of imposed deformations on  $N_E$  may be ignored.

$A_c$  the area of concrete according to the definition of  $N_{Ed}$ .

The values of  $C_{Rd,c}$ ,  $v_{min}$  and  $k_I$  depend on the National Annex. The recommended values, also used in the Dutch annex, are:

$$C_{Rd,c} = 0,18/\gamma_c ;$$

$$v_{min} = 0,035 k^{3/2} f_{ck}^{1/2} ;$$

$$k_I = 0,15.$$

In the French National Annex (Chauvel et al., 2007) a different approach is used for  $v_{min}$ :

$$v_{min} = 0,34 f_{ck}^{1/2} \quad \text{for slabs benefiting from a transverse redistribution effect under the load case considered;}$$

$$v_{min} = 0,053 k^{3/2} f_{ck}^{1/2} \quad \text{for beams and for slabs other than those above.}$$

The effective width from the French professional recommendations (Cortade, 2007) is obtained by spreading the load from the far corners of the load under 45° towards the face of the support.

The value for  $C_{Rd,c}$  is based on a reliability analysis of 176 tests by König and Fischer (1995). A coefficient of  $C = 0,12$  was found as a good lower bound for characteristic values and  $C = 0,15$  can be used for average values. To distinguish between different

loading combinations for which different safety levels apply,  $C_{Rd,c}$  is taken as  $0,18/\gamma_c$  (Walraven, 2002).

The expression for  $v_{min}$  is based on the idea that for low reinforcement ratios the capacity can never be lower than the flexural capacity (Walraven, 2010):

$$V_{uk} = 0,15k(100\rho_l f_{cm})^{1/3} bd \quad (5.5)$$

At  $a/d = 2,5$  the flexural moment is:

$$M_{uv} = V_{uk} \cdot 2,5d = 0,375k(100\rho_l f_{cm})^{1/3} bd^2 \quad (5.6)$$

The maximal moment resistance is approximated as:

$$M_{u,fl} = 0,9d(\rho_l bd)f_{yk} \quad (5.7)$$

Equating (5.6) and (5.7) and taking  $f_{yk} = 500\text{MPa}$  results in the percentage of reinforcement  $\rho_l$  at which shear capacity and moment capacity are equal:

$$\rho_l = 0,00024k^{3/2} f_{cm}^{1/2} \quad (5.8)$$

Substituting this into equation (5.5) leads to:

$$\frac{V_{ud}}{bd} = 0,035k^{3/2} f_{cm}^{1/2} \quad (5.9)$$

Finally, replacing  $f_{cm}$  by  $f_{ck}$  leads to the recommended value of  $v_{min}$ :

$$v_{min} = 0,035k^{3/2} f_{ck}^{1/2} \quad (5.10)$$

According to Walraven (2007), it would be scientifically more correct to directly involve the fracture energy  $G_F$  and the concrete tensile strength  $f_{ct}$  instead of the factor  $k$  for the size effect. These parameters can be introduced by using the characteristic length  $l_{ch}$ , defined as:

$$l_{ch} = \frac{EG_F}{f_{ct}^2} \quad (5.11)$$

The mean ultimate nominal shear strength can then be formulated as:

$$v_u = Cf_{ct} \sqrt[3]{\frac{l_{ch}\rho_l}{d}} \quad (5.12)$$

For members with loads applied within a distance  $0,5d \leq a_v \leq 2d$  from the edge of a support, the contribution of this load to the shear force may be multiplied by  $\beta = \frac{a_v}{2d}$ , Fig. 5.2. This is only valid provided that the longitudinal reinforcement is fully anchored at

the support. The multiplication factor  $\frac{a_v}{2d}$  is the lowest of multiplication factors for different cases as discussed in Walraven (2002). More background is available in Regan (1998). In DIN 1045-1, this factor is taken as  $\beta = \frac{x}{2,5d} \leq 1$  (Rombach et al., 2009).

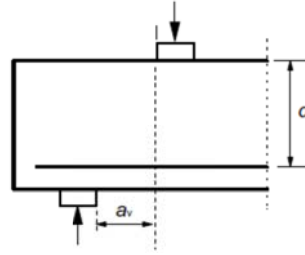


Fig. 5.2: Loads near supports, for example beam with direct support. Figure 6.4 from EN 1992-1-1:2005.

The shear force  $V_{Ed}$ , calculated without the reduction, should always satisfy the condition

$$V_{Ed} \leq 0,5b_w d v f_{cd} \quad (5.13)$$

where  $v$  is a strength reduction factor for concrete cracked in shear:  $v = 0,6 \left[ 1 - \frac{f_{ck}}{250} \right]$

with  $f_{ck}$  in MPa. Background for these formulas can also be found in Regan (1987).

A comparison of test data to the Eurocode shear provision is given in Fig. 5.3. König and Fischer (1995) found that a lognormal distribution enables the best description of the

distribution of  $\frac{v_{calc}}{v_{test}}$ .

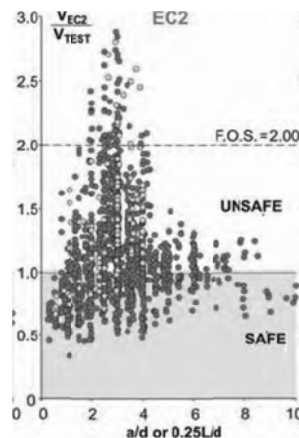


Fig. 5.3: Accuracy of EC2 in predicting shear strength of members without links. Total factor of safety listed for case where live load is 50% of dead load (Collins, Mitchell and Bentz, 2008).

In EN 1992-1-1:2005, the design punching shear capacity is calculated as follows (equation 6.47 in the EN 1992-1-1:2005):

$$v_{Rd,c} = C_{Rd,c} k (100 \rho_l f_{ck})^{1/3} + k_1 \sigma_{cp} \geq (v_{\min} + k_1 \sigma_{cp}) \quad (5.14)$$

with

$$\rho_l = \sqrt{\rho_{ly} \cdot \rho_{lz}} \leq 0,02$$

$\rho_{ly}, \rho_{lz}$  relate to the bonded tension steel y- and z-directions respectively. The values  $\rho_{ly}$  and  $\rho_{lz}$  should be calculated as mean values taking into account a slab width equal to the column width plus  $3d$  each side.

The shear stress  $v_{Ed}$  should not exceed  $v_{Rd,c}$ .

$$v_{Ed} = \beta \frac{V_{Ed}}{u_i d} \quad (5.15)$$

with

- $V_{Ed}$  the shear force;
- $u_i$  the perimeter of the critical section;
- $d$  the effective depth;
- $\beta$  a factor, approximate values are:
  - internal column:  $\beta = 1,15$ ;
  - edge column:  $\beta = 1,4$ ;
  - corner column:  $\beta = 1,5$ .

The critical section is taken at  $2d$  from the loaded area (Fig. 5.4). Around rectangular loaded areas, rounded corners are used (Fig. 5.5).

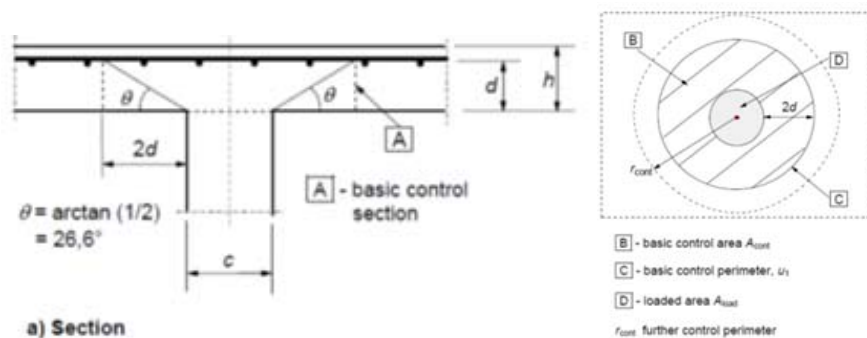


Fig. 5.4: Verification model for punching shear at the ultimate limit state, Figure 6.12 from EN 1992-1-1:2005.

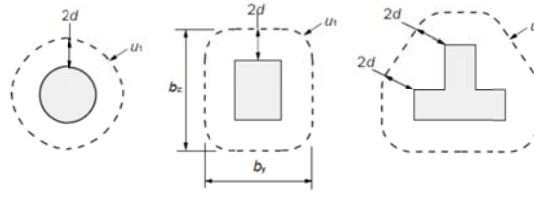


Fig. 5.5: Typical basic control perimeters around loaded areas, Figure 6.13 from EN 1992-1-1: 2004.

### 5.3. ACI 318-08

In ACI 318-08, two formulas are given to calculate the shear strength provided by concrete for members subject to shear and flexure only (US customary units):

$$V_c = 2\lambda\sqrt{f'_c}b_wd \quad (5.16)$$

$$V_c = \left( 1,9\lambda\sqrt{f'_c} + 2500\rho_w \frac{V_u d}{M_u} \right) b_w d \leq 3,5\lambda\sqrt{f'_c}b_w d \quad (5.17)$$

in which

$f'_c$  the specified concrete cylinder strength, in psi;

$\lambda$  the factor to account for concrete density (1,0 for normal density concrete);

$b_w$  the web width;

$d$  the distance from the extreme compression fiber to the centroid of tensile reinforcement;

$\rho_w$  the reinforcement ratio,  $\frac{A_s}{b_w d}$ ;

$V_u$  the factored shear force at a section;

$M_u$  the factored moment at a section.

Equation (5.17) is based on the work of ACI-ASCE committee 326 (1962), originally developed by I.M. Viest (Bresler and MacGregor, 1967) and has not changed since (except for the addition of the factor  $\lambda$ ). In the discussion by Sozen and Hawkins (1962) it reads: “However, if part of the short-time shear strength of the beam is due to doweling of the reinforcement, this action is likely to decay with time and cause tensile stresses in the web comparable to those corresponding to a nominal shear stress of about  $2\sqrt{f'_c}$  in a

short-time test.” Earlier work by Moody and Viest (1955) related the factors  $\frac{M}{Vd}$  and  $f_c'$  to the shear capacity. Morrow and Viest (1957) showed  $2\sqrt{f_c'}$  to be the lower bound for diagonal tension failure of their test data which are related to the modulus of rupture  $f_r$ . The expression for  $V_c$  determines the diagonal cracking load, which is lower than or equal to the ultimate shear force. The formula is based on the test results of 194 beams, Fig. 5.6, and shows significant scatter.

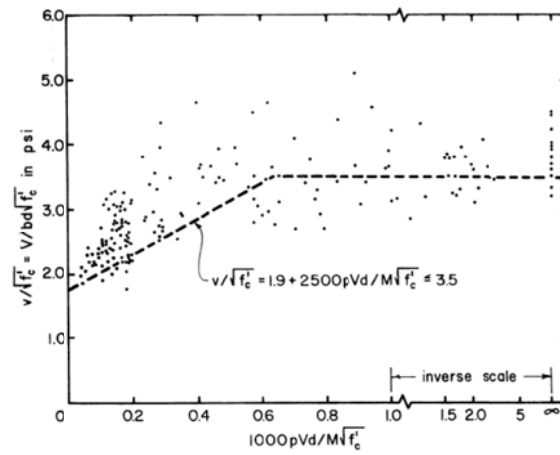


Fig. 5.6: Derivation of Equation (11-5) from ACI 318-08, here Equation (5.17), from ACI-ASCE committee 326 (1962).

Determining the exact conditions of cracking is subject to the interpretation of each researcher and to the variability of testing procedures in each laboratory (Lubell, 2006). The database contained test results of members usually narrower than about 350mm. The width-to-height aspect ratio of the specimens is usually well below 1,0 (Lubell, 2006). These specimens have an average depth of 340mm and an average width of 194mm (Lubell, 2006). The data set includes members with a wide range of  $a/d$  ratios, including ratios below 2,5 where slender beam analysis equations are not strictly valid. According to MacGregor and Wight, 2005, the use of (5.17) is not recommended in practice. Since the shear design formula for beams without stirrups is set at about 55% below the mean of the test data, a covert understrength factor is present in ACI 318-08 (Yu and Bažant, 2011).

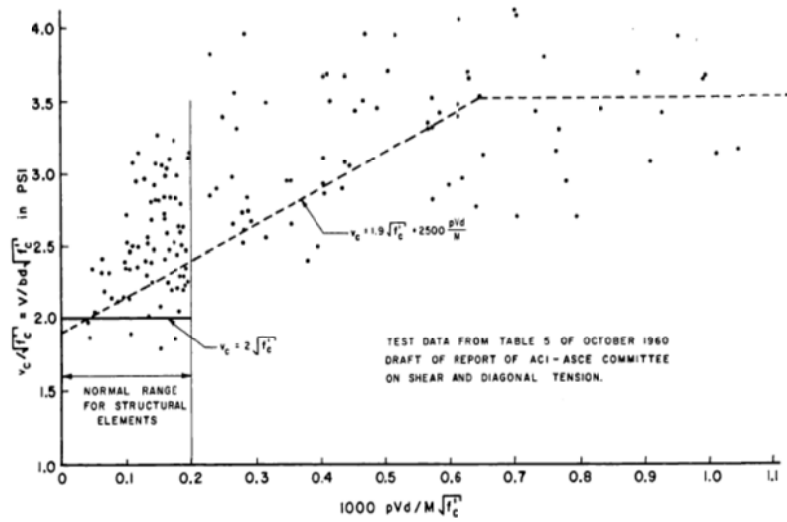


Fig. 5.7: Derivation of ACI 318-08 formula (11-3), here (5.16). (Bresler and Scordelis, 1963).

The two basic assumptions for the shear force  $V_c$  are that  $V_c$  is the shear force at cracking and  $V_c$  is the same for members with and without stirrups. Reineck (2009) showed by reviewing tests that these assumptions are not valid.

While equation (5.16) depends fully on the concrete compressive strength, Angelakos, Bentz and Collins (2001) concluded from experiments that the concrete cylinder strength has almost no effect on the load at which shear failure occurred. For small concrete strengths relatively ductile post-peak behavior is observed, while for high-strength concrete a large, sudden drop in the capacity is registered.

According to Rangan (1973) the ACI procedure is unsafe for  $\rho < 1\%$ . Reineck et al. (2003) showed by analyzing a database with 690 test results that the ACI 318-08 equations become increasingly unsafe as the members become larger and more lightly reinforced. The influence of size on the safety of the code formula is also shown in Fig. 5.8. A comparison of the ACI 318-08 code procedure with 1601 tests is shown in Fig. 5.9.

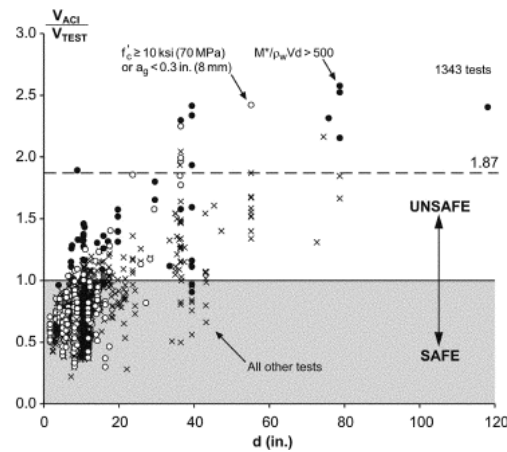


Fig. 5.8: Ability to accurately predict breakdown of beam action (Collins, Bentz and Sherwood, 2008).

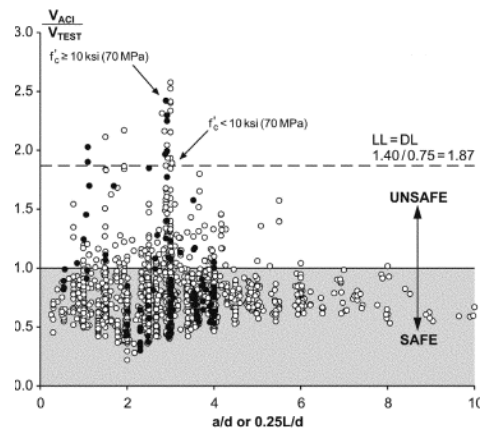


Fig. 5.9: Ability to accurately predict 1601 observed shear failure loads (Collins, Bentz and Sherwood, 2008).

Nowak and Paczkowski (2009) calculated the reliability index based on more than 300 experiments for equations (5.16) and (5.17), Fig. 5.10.

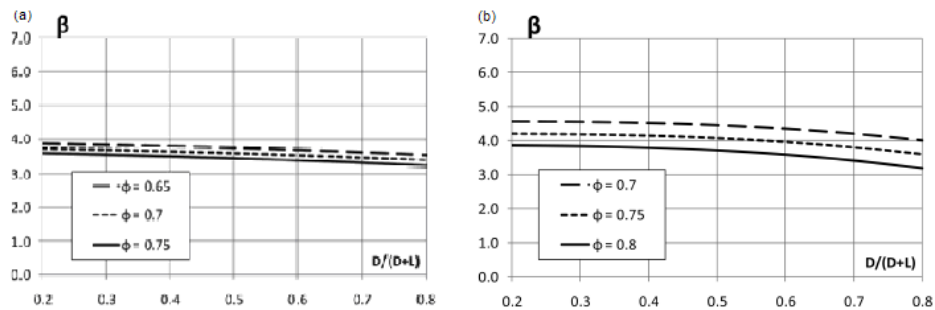


Fig. 5.10: Reliability index for different values of the resistance factor: (a) ACI 318-08 Eq. (11-3), here (5.16); (b) ACI 318-08 Eq. (11-5), here (5.17), Nowak and Paczkowski, 2009.



The nominal punching shear strength  $V_c$  shall be taken as the smallest of (ACI 318-08 §11.11.2.1, in US customary units):

$$V_c = \left(2 + \frac{4}{\beta}\right) \lambda \sqrt{f'_c} b_o d \quad (5.18)$$

$$V_c = \left(\frac{\alpha_s d}{b_o} + 2\right) \lambda \sqrt{f'_c} b_o d \quad (5.19)$$

$$V_c = 4 \lambda \sqrt{f'_c} b_o d \quad (5.20)$$

in which:

$\beta$  the ratio of the long side to the short side of the column, concentrated load or reaction area;

$b_o$  the perimeter of the critical section for shear;

$\alpha_s$  40 for interior columns, 30 for edge columns, 20 for corner columns.

The other parameters are calculated in the same way as for formulas (5.16) and (5.17).

The critical section is taken at a distance of  $d/2$  away from the periphery of the loaded area. Formulas (5.18), (5.19) and (5.20) are based on the work done by ACI-ASCE committee 326 (1962), ASCE-ACI committee 426 (1974) and Moe (1961). Widiyanto et al., (2009) showed that this leads to unsafe predictions for lightly reinforced slabs.

#### **5.4. Model Code 2010**

The draft of the Model Code 2010 (fib, 2010) proposes a shear resistance attributed to the concrete as:

$$V_{Rd,c} = k_v \frac{\sqrt{f_{ck}}}{\gamma_c} z b_w \quad (5.21)$$

in which:

$f_{ck}$  the characteristic cylinder compressive strength of the concrete;

$z$  the effective shear depth, Fig. 5.12;

$b_w$  the width of the web, Fig. 5.12 or for slabs under concentrated loads Fig. 5.11.

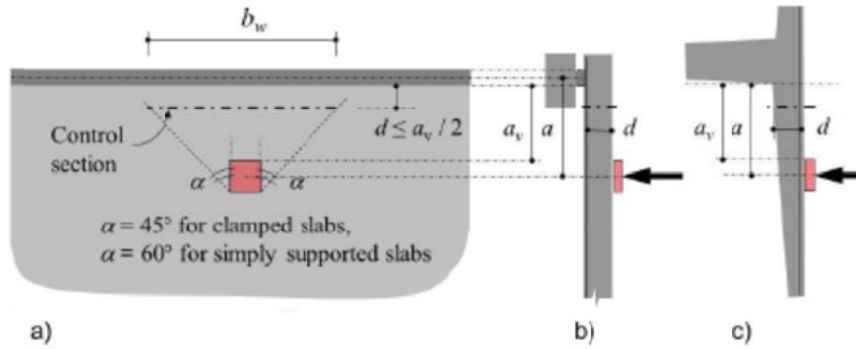


Fig. 5.11: Location and length of the control section,  $b_w$ , for the determination of the shear resistance of slabs with point loads located near a support-line; (b) simple edge support; (c) clamped edge support (fib, 2010).

The value of  $\sqrt{f_{ck}}$  shall not be taken greater than 8MPa.

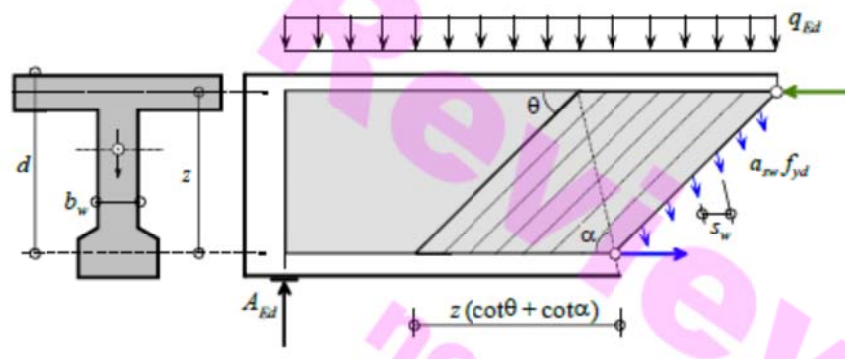


Fig. 5.12: Geometry and definitions. (fib, 2010).

The factor  $\beta$  as used in EN 1992-1-1:2005 is included in the same way. The value of  $k_v$  depends on the level of approximation. For level I approximation,  $k_v$  is taken as:

$$k_v = \frac{180}{1000 + 1,25z} \quad (5.22)$$

For level II approximation,  $k_v$  is taken as:

$$k_v = \frac{0,4}{1 + 1500\varepsilon_x} \frac{1300}{1000 + k_{dg}z} \quad (5.23)$$

which is based on the Modified Compression Field Theory and consists of:

$$k_{dg} = \frac{32}{16 + d_g} \geq 0,75 \quad (5.24)$$

in which  $d_g$  is the aggregate diameter; and

$$\varepsilon_x = \frac{\frac{M_{Ed}}{z} + V_{Ed} + N_{Ed} \left( \frac{1}{2} \mp \frac{\Delta e}{z} \right)}{2(E_s A_s)} \quad (5.25)$$

with  $M_{Ed}$ ,  $V_{Ed}$  and  $N_{Ed}$  as shown in Fig. 5.13 and Fig. 5.14.

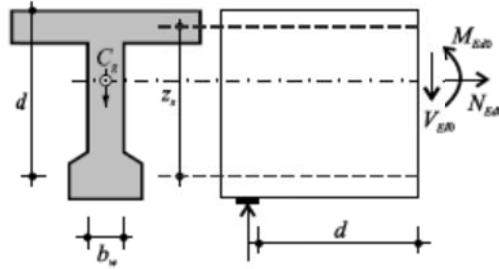


Fig. 5.13: Definition of control section for sectional design. (fib, 2010).

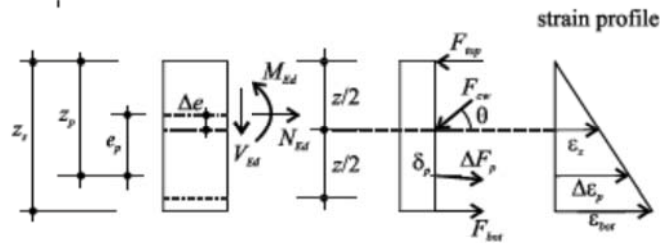


Fig. 5.14: Definitions. (fib, 2010).

Comparison of the results of 1725 experiments leads to a mean observed to predicted shear strength ratio of 2,10 with a COV of 22,4% and 5<sup>th</sup> percentile of 1,33 for a level I approximation. For level III, the comparison is based on 1921 experiments leading to a mean value of 1,27, a COV of 15,1% and a 5<sup>th</sup> percentile of 0,96 (Bentz, 2010). These results are based on a previous draft of ModelCode 2010, in which slightly different values for  $k_v$  were used and level III is now called level II.

For punching, the design shear force is compared to the punching shear strength. The design shear force is calculated as the sum of design forces acting on a basic control perimeter  $b_l$ . The basic control perimeter  $b_l$  may normally be taken at a distance  $d_v$  from the loaded area and should be determined to minimize its length. The length of the control perimeter is limited by slab edges, Fig. 5.15. The shear-resisting effective depth  $d_v$  is the distance from the centroid of the reinforcement layers to the loaded area. The shear-resisting control perimeter can also be obtained on the basis of a detailed shear field analysis as:

$$b_0 = \frac{V_{Ed}}{v_{perp,d,max}} \quad (5.26)$$

where  $v_{perp,d,max}$  is the maximum shear force per unit length perpendicular to the basic control perimeter.

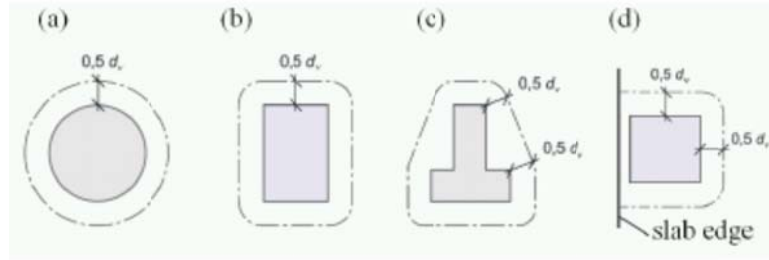


Fig. 5.15: Basic control perimeters around loaded areas (fib, 2010).

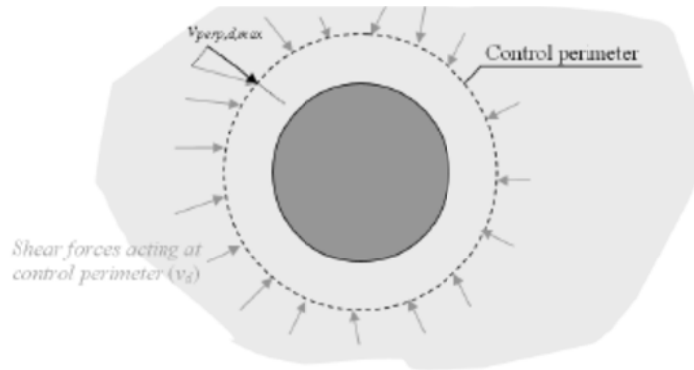


Fig. 5.16: Shear force per unit length,  $v_d$ , and maximum value perpendicular to the basic control perimeter.

The contribution of the shear forces due to moment transfer between the slab and the loaded area can be taken into account by using an eccentricity factor  $k_e$ . In cases where the lateral stability does not depend on frame action of slabs and columns and where the adjacent spans do not differ in length by more than 25%, the following approximated values can be used for the coefficient  $k_e$ :

- 0,90 for inner columns
- 0,70 for edge columns
- 0,65 for corner columns
- 0,75 for corners of walls.

The design punching shear resistance is based on the critical shear crack theory and can be taken as:

$$V_{Rd,c} = k_{\psi} \frac{\sqrt{f_{ck}}}{\gamma_c} b_0 d_v \quad (5.27)$$

with  $f_{ck}$  in [MPa].

The parameter  $k_{\psi}$  depends on the deformations (rotations) of the slab and follows from

$$k_{\psi} = \frac{1}{1,5 + 0,9 k_{dg} \psi d} \leq 0,6 \quad (5.28)$$

where  $d$  is the mean value in [mm] of the flexural effective depth for the  $x$ - and the  $y$ -directions. Provided that the size of the aggregates is not less than 16mm  $k_{dg}$  can be taken as 1,0. If the aggregate size is smaller than 16mm, then Eq. (5.24) can be used.

The rotations around the loaded area can be calculated according to different levels of approximation. Level I is for a regular flat slab designed according to an elastic analysis without significant redistribution of internal forces:

$$\psi = 1,5 \frac{r_s}{d} \frac{f_{yd}}{E_s} \quad (5.29)$$

where  $r_s$  denotes the position where the radial bending moment is zero with respect to the support axis. In the cases where significant bending moment redistribution is considered in the design, the slab rotation can be calculated as:

$$\psi = 1,5 \frac{r_s}{d} \frac{f_{yd}}{E_s} \left( \frac{m_{sd}}{m_{Rd}} \right)^{1,5} \quad (5.30)$$

where:

- $m_{sd}$  the average moment per unit length for calculation of the flexural reinforcement in the support strip (for the considered direction);
- $m_{Rd}$  the design average flexural strength per unit length in the support strip (for the considered direction).

The rotation has to be calculated along the two main directions of the reinforcement. The width of the support strip for calculating  $m_{sd}$  is:

$$b_s = 1,5 \sqrt{r_{sx} r_{sy}} \leq L_{\min} \quad (5.31)$$

The same value for  $r_s$  as in a level I approximation can be used. The commentary also provides formulas for determining  $m_{sd}$  for inner, edge and corner columns.

For a level III approximation, the factor of 1,5 in Eqs. (5.29) and (5.30) can be replaced by 1,2 if:

- $r_s$  is calculated according to a linear elastic model;
- $m_{sd}$  is calculated from a linear elastic model as the average value of the moment for design of the flexural reinforcement over the width of the support strip  $b_s$

The width of the support strip can be calculated as in Level II taking  $r_{sx}$  and  $r_{sy}$  as the maximum value in the direction investigated.

In a level IV approximation, the rotation  $\psi$  can be calculated on the basis of a nonlinear analysis of the structure and accounting for cracking, tension-stiffening effects, yielding of the reinforcement and any other non-linear effects relevant for providing an accurate assessment of the structure.

An design example for punching of flat slabs can be found in Lips et al. (2010).

## 6. Discussion

Most of our knowledge on shear is the result of experiments on small, heavily reinforced slender beams under two concentrated loads, and most of our knowledge on punching shear is the result of experiments on slab-column specimens. It might be questionable to extrapolate this knowledge to the case of a slab bridge under traffic loads. In chapter 2, it is shown that slab bridges are robust structures, typically designed to fail in flexure instead of shear. However, due to compressive membrane action the actual flexural capacity is a multiple of the design capacity and shear failure modes become governing. Another aspect in slabs is that, due to the extra dimension as compared to beams, transverse moments and shears should be taken into account.

In chapter 3, the different types of shear failure are explained as a function of their shear-span-to-depth ratio. It is assumed that, as in Kani's valley, a minimum capacity can be observed for  $a/d = 2,5$ . However, in chapter 4, the results of Ekeberg et al. (1982) show a minimum for  $a/d = 7,3$ . Another point of discussion is the breakdown of shear into the shear carrying mechanisms. It is difficult to experimentally investigate these mechanisms separately, and to prove that the total shear capacity is the result of the sum of the capacities of these mechanisms. The distinction between one-way and two-way shear in slabs is not clear and there seems to be a transition zone between these two failure mechanisms. Also, there seems to be no consensus in the literature on how to determine the failure mode based on pictures and the cracking pattern as observed in experiments. A limited amount of guidelines exist to give an estimate of the effective width in shear and the origins of these guidelines and national practices seems to be based on tradition rather than on experiments or theoretical work. Up to date, the only code which gives guidelines for the determination of the effective width in shear is ModelCode 2010. Even though the recommendations for the effective width do not lead to satisfactory results when compared to test results, it is a positive evolution that a code is providing guidelines for the determination of the effective width in shear. One of the observations made in the sideline of this literature review is that there exist different schools which adhere to their theory on shear in a sometimes rather rigid way. As a result, several theoretical approaches to the problem of shear in concrete members exist, none of which seems to be able to fully explain the mechanics at the basis of this problem. For the problem of a one-

way slab under a concentrated load, the additional dimension of the slab needs to be taken into account, thus further complicating the mechanics behind the failure mechanism. For design, therefore, simplified methods need to be used. The only method which is tailored for the problem of shear in slabs under concentrated loads close to the support, is the method developed by Regan (1982). The modified compression field theory seems to be less suitable for loads close to the support, and cannot be applied to the problem of punching. Therefore, it is questionable if this method can adequately model the transitional problem of shear in one-way slabs under a concentrated load. The critical shear crack theory uses the same approach for one-way shear as well as for punching shear. However, in the case of a concentrated load close to the support, the non-axis-symmetrical layout needs to be taken into account, and finite element packages need to be used to determine the stress distribution along the punching perimeter. Strut and tie models can be applied for the problem of a concentrated load on a slab. There is however an art to choosing the right strut and tie model which might make the approach not suitable for the design practice. Both plasticity-based and fracture mechanics models need to be considered with regard to the assumptions that were made when developing the model. These assumptions are a simplification of reality and may not always be applicable to the problem under study. For example, the ductility requirement for using plasticity-based models is not always fulfilled for shear failures. Ideally, the empirical code formulas should be replaced by calculation methods with a theoretical basis.

A database with relevant test results is gathered in the Annex. In this database, a distinction is made between punching shear failures and one-way shear failures. This distinction, however, is not based on guidelines on how to interpret cracking patterns as different authors seem to use different approaches. Different categories are also subdivided in the database, as not all design approaches are suitable for all cases. Databases with test results typically show crowding in the small size and relatively large reinforcement percentage region. A way to analyze these data is by using a knowledge-based system, which uses a database of knowledge in combination with a method that mimics the problem-solving strategy of a human. This method is discussed in Jung and Kim, 2008.



When comparing results from a database to a suggested method, the variability of the material should be taken into account. Reineck (1997a) points out that different control specimens could yield differences in tensile strength of more than 20% and up to 30%. Therefore it is futile to demand more from a prediction of the ultimate load capacity in shear than this scatter. Reineck (1997b) emphasizes the importance of a discrete model for shear in concrete.

## 7. Conclusions

A study of slab bridges shows that for existing bridges the failure mode for which these bridges are designed (flexure) does not always occur in practice. As a result of compressive membrane action, shear can become the governing failure mode. Previous research, however, shows that solid slab bridges can typically carry loads that are a multiple of their design load.

An overview of the research on beam shear and punching shear from the past decades is given. Also, the difference between and the transition from beam shear to punching shear is studied. An overview of past research on the effective width in shear is also given. These results show that the currently existing models for shear cannot fully cover the problem, and especially the problem of concentrated loads near to the support on slabs requires an alteration of existing methods. The forces in the transverse direction have to be taken into account.

A database of existing test results is compiled. This database shows that a very limited amount of experimental results on slabs under concentrated loads close to the support is available. Most of the available results are based on small-scale specimens in which the size effect might have resulted in higher shear capacities as compared to slabs in practice. The lack of consensus in the literature on how to deal with shear in concrete members is also reflected by the code provisions. The studied codes (NEN 6720, EN 1992-1-1, ACI 318 and ModelCode 2010) all recommend very different approaches which also result in different design shear capacities.

Therefore, experiments on slabs under concentrated loads close to the support are necessary to gain a better understanding of the problem.

## 8. References

- AASHTO, 2007, *AASHTO LRFD Bridge Design Specifications*, American Association of State Highway and Transportation Officials, Washington D.C., 4086 pp.
- ACI Committee 318, 2008, *Building Code Requirements for Structural Concrete (ACI 318-08) and Commentary*, American Concrete Institute, Farmington Hills, MI, USA, 465 pp.
- ACI-ASCE Committee 326, 1962, "Shear and Diagonal Tension: Part 1 – General Principles." *Journal of the American Concrete Institute*, Vol 59, No. 1, pp. 1-30.
- ACI-ASCE Committee 326, 1962, "Shear and Diagonal Tension: Part 2 - Beams and Frames." *Journal of the American Concrete Institute*, Vol 59, No. 2, pp. 277-333.
- ACI-ASCE Committee 326, 1962, "Shear and Diagonal Tension: Part 3 - Slabs and Footings." *Journal of the American Concrete Institute*, Vol 59, No. 3, pp. 353-396.
- Adebar, P., Collins, M. P., 1996, "Shear strength of members without transverse reinforcement." *Canadian journal of civil engineering*, Vol. 23, No. 1, pp. 30-41.
- Adebar, P., 2000, "One-way shear strength of large footings." *Canadian journal of civil engineering*, Vol. 27, pp. 553-562.
- Aktan, A. E., Zwick, M., Miller, R., Shahrooz, B., 1992, "Nondestructive and Destructive Testing of Decommissioned Reinforced Concrete Slab Highway Bridge and Associated Analytical Studies." *Transportation Research Record: Journal of the Transportation Research Board*, 1371, pp. 142-153.
- Alexander, S., Simmonds, S., 1986, *Shear-Moment Transfer in Slab-Column connections*, Structural Engineering Report No. 141, University of Alberta, Edmonton, Alberta, 95 pp.
- Alexander, S. D. B., Simmonds, S. H., 1987, "Ultimate Strength of Slab-Column connections." *Aci Structural Journal*, Vol. 84, No. 3, pp. 255-261.
- Alexander, S., Simmonds, S., 1992, "Bond Model for Concentric Punching Shear," *ACI Structural Journal*, V. 89, No. 3, pp. 325-334.
- Amer, A., Arockiasamy, M., Shahawy, M., 1999, "Load distribution of existing solid slab bridges based on field tests." *Journal of Bridge Engineering*, Vol. 4, No. 3, pp. 189-193.
- Anderson, B. G., 1957, "Rigid Frame Failures." *ACI Journal Proceedings*, Vol. 53, No. 2, pp. 625-636.
- Angelakos, D., Bentz, E. C., and Collins, M. P., 2001, "Effect of concrete strength and minimum stirrups on shear strength of large members." *ACI Structural Journal*, Vol. 98,

No. 3, pp. 290-300.

ASCE-ACI Committee 445 on Shear and Torsion, 1998, "Recent approaches to shear design of structural concrete." *Journal of Structural Engineering*, Vol. 124, No. 12, pp. 1375-1417.

ASCE-ACI Committee 426 on Shear and Diagonal Tension, 1973, "The shear strength of reinforced concrete members." *Journal of the Structural Division*, Vol. 99, No. 6, pp. 1091-1187.

ASCE-ACI Task Committee 426, 1974, "The shear strength of reinforced concrete members - slabs." *Journal of the Structural Division*, Vol. 100, No. 8, pp. 1543-1591.

Aster, H., Koch, R., 1974, "Schubtragfähigkeit dicker Stahlbetonplatten." *Beton- und Stahlbetonbau*, Vol. 69, No. 11, pp. 266-270.

Azad, A. K., Baluch, M. H., Abbasi, M. S. A., Kareem, K. (1994). "Punching Capacity of Deck Slabs in Girder-Slab Bridges." *ACI Structural Journal*, Vol. 91, No. 6, pp. 656-662.

Azizinamini, A., Boothby, T. E., Shekar, Y., Barnhill, G., 1994, "Old Concrete Slab Bridges. I: Experimental Investigation." *Journal of Structural Engineering-ASCE*, Vol. 120, No. 11, pp. 3284-3304.

Azizinamini, A., Shekar, Y., Boothby, T. E., Barnhill, G., 1994, "Old Concrete Slab Bridges. II: Analysis." *Journal of Structural Engineering-ASCE*, Vol. 120, No. 11, pp. 3305-3319.

Bahen, N., Sanders, D. H., 2009, "Investigation of strut strength using a deep-beam database." *SP-265 Thomas T.C. Hsu Symposium on Shear and Torsion in Concrete Structures*, American Concrete Institute., ed., New Orleans, LA, USA, pp. 385-404.

Baker, A. L. L., Abeles, P. W., Ashdown, A. J., Bennett, A. W., Brock, G. C., Bunn, E. W., Guest, J. E., Jones, L. L., Matthews, D. D., Regan, P. E., Smith, R. B. L., Yu, C. W., Taylor, R. (The Shear Study Group), 1969, *The shear strength of reinforced concrete beams: a report*, Institution of Structural Engineers, London, U.K, 170pp.

Bazant, Z. P., Kim, J. K., 1984, "Size Effect in Shear Failure of Longitudinally Reinforced Beams." *Journal of the American Concrete Institute*, Vol. 81, No. 5, pp. 456-468.

Bazant, Z. P., Kazemi, M. T., 1991, "Size effect on Diagonal Shear Failure of Beams without Stirrups." *ACI Structural Journal*, Vol. 88, No. 3, pp. 268-276.

Bazant, Z. P., 2004, "Shear database for reinforced concrete members without shear reinforcement. Paper by Karl-Heinz Reineck, Daniel A. Kuchma, Kang Su Kim, and Sina Marx - Discussion." *ACI Structural Journal*, Vol. 101, No. 1, pp. 139-140.

Bazant, Z. P., Kazemi, M. T., 2006, "Repeating a classic set of experiments on size effect in shear of members without stirrups. Discussion." *ACI Structural Journal*, Vol. 103, No. 5, pp. 754-755.

Bazant, Z. P., Pang, S. D., 2006, "Mechanics-based statistics of failure risk of quasibrittle structures and size effect on safety factors." *Proceedings of the National Academy of Sciences of the United States of America*, Vol. 103, pp. 9434-9439.

Bazant, Z. P., Yu, Q., Gerstle, W., Hanson, J., and Ju, W., 2007, "Justification of ACI 446 proposal for updating ACI code provisions for shear design of reinforced concrete beams." *ACI Structural Journal*, Vol. 104, No. 5, pp. 601-610.

Bazant, Z. P., Yu, Q., Gerstle, W., Hanson, J., and Ju, W., Bentz, E.C., 2008, "Justification of ACI 446 proposal for updating ACI code provisions for shear design of reinforced concrete beams: discussion and authors' closure." *ACI Structural Journal*, Vol. 105, No. 4, pp. 511-515.

Bazant, Z. P., Yu, Q., 2008, "Minimizing Statistical Bias to Identify Size Effect from Beam Shear Database." *ACI Structural Journal*, Vol. 105, No. 6, pp. 685-691.

Bazant, Z. P., Yu, Q., Chen, S. M., Jiao, Y. Q., 2009, "Minimizing Statistical Bias to Identify Size Effect from Beam Shear Database Discussion." *ACI Structural Journal*, Vol. 106, No. 5, pp. 737-739.

BBK 79, *Bestämmelser för betongkonstruktioner, band 1, Konstruktion (Regulations for concrete structures – Part 1, Design)*, Statens Betong Kommitté, Stockholm, pp.114-116.

Beal, D. B., 1982, "Load capacity of concrete bridge decks." *Journal of the Structural Division-Asce*, Vol. 108, No. 4, pp. 814-832.

Bentz, E. C., 2005, "Empirical modeling of reinforced concrete shear strength size effect for members without stirrups." *ACI Structural Journal*, Vol. 102, No. 2, pp. 232-241.

Bentz, E. C., Buckley, S., 2005. "Repeating a classic set of experiments on size effect in shear of members without stirrups." *Aci Structural Journal*, Vol. 102, No. 6, pp. 832-838.

Bentz, E. C., Buckley, S., 2006, "Repeating a classic set of experiments on size effect in shear of members without stirrups. Closure." *ACI Structural Journal*, Vol. 103, No. 5, pp. 761-763.

Bentz, E. C., Collins, M. P., 2006, "Development of the 2004 Canadian Standards Association (CSA) A23.3 shear provisions for reinforced concrete." *Canadian Journal of Civil Engineering*, Vol. 33, No. 5, pp 521-534.

Bentz, E. C., Vecchio, F. J., Collins, M. P., 2006, "Simplified modified compression field theory for calculating shear strength of reinforced concrete elements." *ACI Structural Journal*, Vol. 103, No. 4, pp. 614-624.

Bentz, E. C., 2010, "MC2010: Shear strength of beams and implications of the new approaches." *Shear and punching shear in RC and FRC elements – Proceedings of a workshop held on 15-16 October 2010 in Salò, Lake Garda, Italy*, fib bulletin 57, pp. 15-30.

Bhide, S. B., Collins, M. P., 1989, "Influence of Axial Tension on the Shear Capacity of Reinforced-Concrete Members." *ACI Structural Journal*, Vol. 86, No. 5, pp. 570-581.

Birkle, G., Dilger, W. H., 2008, "Influence of slab thickness on punching shear strength." *ACI Structural Journal*, Vol. 105, No. 2, pp. 180-188.

Blaauwendraad, J., and Wang, Q. B., 1991, "Systematic fracture mechanics study of shear failure in beams under distributed load." *IABSE colloquium on structural concrete*, pp. 637-642.

Blaauwendraad, J., Walraven, J., 1992, "Ultimate Shear Force of Structural Concrete Members without Transverse Reinforcement Derived from a Mechanical Model - Discussion." *ACI Structural Journal*, Vol. 89, No. 4, pp. 475-476.

Braestrup, M. W., Rangan, B. V., Springfield, J., Windisch, A., Alexander, S. D. B., Simmonds, S. H., 1988, "Ultimate Strength of Slab-Column connections - Discussion and Closure." *ACI Structural Journal*, Vol. 85, No. 2, pp. 226-232.

Braestrup, M. W., 2009, "Structural concrete beam shear – still a riddle?" SP-265 Thomas T.C. Hsu Symposium on Shear and Torsion in Concrete Structures, ACI, New Orleans, LA, USA, pp. 327-344.

Bresler, B., Scordelis, A. C., 1963, "Shear Strength of Reinforced Concrete Beams." *ACI Journal Proceedings*, Vol. 60, No. 1, pp. 51-74.

Bresler, B., MacGregor, J. G., 1967, "Review of concrete Beams failing in Shear." *Journal of the Structural Division-ASCE*, Vol. 93, ST1, pp. 343-372.

Brock, G. C., Fenwick, R. C., Paulay, T., Goswami, M. M., Katow, T., Loov, R. E., Neville, A. M., MacGregor, J., Mehta, K. C., Ojha, S. K., Rensaa, E. M., Sollid, E., Zielinski, Z. A., Kani, G. N. J., 1964, "The riddle of shear failure and its solution: Discussion and closure." *ACI Journal Proceedings*, Vol. 61, No. 12, pp. 1587-1636.

Brock, G. C., MacGregor, J., Patel, M. N., Rensaa, E. M., and Kani, G. N. J. (1967). "How Safe Are Our Large Reinforced Concrete Beams - Discussion and Closure." *ACI Journal Proceedings*, 64(9), 602-612.

Brock, G., Dutta, S. C., Kani, G. N. J., Wittkopp, R. B. R., Rajagopalan, K. S., Ferguson, P. M., 1969, "Exploratory shear tests emphasizing percentage of longitudinal steel: discussion and authors' closure." *ACI Journal Proceedings*, Vol. 66, No. 2, pp. 150-154.

Broms, B., 1964, "Stress Distribution, Crack Patterns, and Failure Mechanisms of Reinforced Concrete Members." *ACI Journal Proceedings*, Vol. 61, No. 12, pp. 1535-1557.

Brown, M. D., Bayrak, O., Jirsa, J. O., 2006, "Design for shear based on loading conditions." *ACI Structural Journal*, Vol. 103, No. 4, pp. 541-550.

CEN, 2002, *Eurocode 1 – Actions on Structures - Part 2: Traffic loads on bridges, EN 1991-2*, Comité Européen de Normalisation, Brussels, Belgium, 164 pp.

CEN, 2005, *Eurocode 2 – Design of Concrete Structures: Part 1-1 General Rules and Rules for Buildings, EN 1992-1-1*, Comité Européen de Normalisation, Brussels, Belgium, 225 pp.

Chamululu, G., 2009, *The ultimate load carrying capacity of laterally restrained concrete decks*, MSc thesis, Delft University of Technology, Delft, The Netherlands, 164pp.

Chana, P. S., 1988, "Analytical and experimental studies of shear failures in reinforced concrete beams." *Proceedings of the Institution of Civil Engineers, Structural Engineering group*, Vol. 85, No. 2, pp. 609-628.

Chauvel, D., Thonier, H., Coin, A., and Ile, N. (2007). "Shear Resistance of slabs not provided with shear reinforcement CEN/TC 250/SC 02 N 726." France, 32 pp.

Cho, S. H., 2003, "Shear strength-prediction by modified plasticity theory for short beams." *ACI Structural Journal*, Vol. 100, No. 1, pp. 105-112.

Clark, A. P., 1951, "Diagonal Tension in Reinforced Concrete Beams." *ACI Journal Proceedings*, Vol. 48, No. 10, pp. 145-156.

Coin, A., and Thonier, H., 2007, "Essais sur le cisaillement des dalles en beton arme." *Annales du batiment et des travaux publics*, pp. 7-16.

Collins, M. P., 1978, "Towards a Rational Theory for Rc Members in Shear." *Journal of the Structural Division-ASCE*, Vol. 104, No. 4, pp. 649-666.

Collins, M. P., Mitchell, D., 1980, "Shear and Torsion Design of Prestressed and Non-Prestressed Concrete Beams." *Journal Prestressed Concrete Institute*, Vol. 25, No. 5, pp. 32-100.

Collins, M. P., Mitchell, D., Adebar, P., Vecchio, F. J., 1996, "A general shear design method." *ACI Structural Journal*, Vol. 93, No. 1, pp. 36-45.

Collins, M.P., Kuchma, D., 1999, "How safe are our large, lightly reinforced concrete beams, slabs, and footings?," *ACI Structural Journal*, Vol. 96, No. 4, pp.482-490.

Collins, M. R., Bentz, E. C., Sherwood, E. G., 2008, "Where is shear reinforcement required? Review of research results and design procedures." *ACI Structural Journal*, Vol. 105, No. 5, pp. 590-600.

Collins, M. P., Bentz, E. C., Sherwood, E. G., Xie, L., 2008, "An adequate theory for the shear strength of reinforced concrete structures." *Magazine of Concrete Research*, Vol. 60, No. 9, pp. 635-650.

Collins, M. P., Mitchell, D., Bentz, E., 2008, "Shear design of concrete structures," *The Structural Engineer*, Vol. 86, No. 10, pp.32-39.

Cope, R.J., Rao, P.V., Edwards, K.R., 1983, *Shear in skew reinforced concrete slab bridges – analytical and experimental studies – A report to the Department of Transport*, D.Tp. ref. BE 22/2/0137, University of Liverpool, Liverpool, UK, 219 pp.

Cope, R. J., Clark, L. A., 1984, *Concrete slabs : analysis and design*, Elsevier Applied Science, London, 502pp.

Cope, R. J., 1985, "Flexural Shear Failure of Reinforced Concrete Slab Bridges." *Proceedings of the Institution of Civil Engineers Part 2-Research and Theory*, Vol. 79, 9, pp. 559-583.

Coronelli, D., Radaelli, E. O., 2010, "Analysis of shear critical corroded RC members." *Structural Faults and Repair*, 13th International Conference and Exhibition, Edinburgh, UK, pp. 1-15.

Cortade, J., 2007, "Recommandations professionnelles." *FF Batiment*, 36 pp.

Criswell, M. E., Hawkins, N. M., 1973, "Shear Strength of Slabs: Basic Principle and Their Relation to Current Methods of Analysis." *ACI symposium March and October 1973*, pp. 641-676.

Cullington, D. W., Daly, A. F., Hill, M. E., 1996, "Assessment of reinforced concrete bridges: Collapse tests on Thurloxtan underpass." *Bridge Management*, Vol. 3, pp. 667-674.

CUR., 1994, "CUR rapport 94-13, 1994, Achtergronden bij de VBC 1990." *Civiltechnisch Centrum Uitvoering Research en Regelgeving*, Gouda, The Netherlands, pp. 68-113



- den Uijl, J. A., 2005, *Dwarskrachtdraagvermogen van bestaand plaatviaduct*. Delft University of Technology, Delft, 98pp.
- Desalegne, A. S., Lubell, A. S., 2010, "Shear Behavior of Concrete Slabs Longitudinally Reinforced with High-Performance Steel." *ACI Structural Journal*, Vol. 107, No. 2, pp. 228-236.
- Diaz de Cossio, R., Moe, J., Gould, P. L., Meason, J. G., 1962, "Shear and diagonal tension - Discussion." *ACI Journal Proceedings*, Vol. 59, No. 11, pp. 1323-1339.
- Dulacska, H., 1972, "Dowel Action of Reinforcement Crossing Cracks in Concrete." *ACI Journal Proceedings*, Vol. 69, No. 12, pp. 754-757.
- Ebeido, T., Kennedy, J. B., 1996, "Punching Strength of Deck Slabs in Skew Composite Bridges." *Journal of Bridge Engineering*, Vol. 1, No. 2, pp. 59-66.
- Ehmann, J., 2006, "Shear resistance of concrete bridge decks in tension." *Composite construction in steel and concrete, Proceedings of the 5th international conference*, Vol. 5, pp. 67-76.
- Ekeberg, P. K., Sjursen, A., and Thorenfeldt, E., 1982, "Load-carrying capacity of continuous concrete slabs with concentrated loads." *Nordisk betong*, 2-4, pp. 153-156.
- Elzanaty, A. H., Nilson, A. H., Slate, F. O., 1986, "Shear Capacity of Reinforced Concrete Beams Using High-Strength Concrete." *Journal of the American Concrete Institute*, Vol. 83, No. 2, pp. 290-296.
- Enright, M. P., and Frangopol, D. M., 2000, "Survey and Evaluation of Damaged Concrete Bridges." *Journal of Bridge Engineering*, Vol. 5, No. 1, pp. 31-38.
- Estes, A. C., and Frangopol, D. M., 2001, "Bridge lifetime system reliability under multiple limit states." *Journal of Bridge Engineering*, Vol. 6, No. 6, pp. 523-528.
- Eyre, J. R., 1997, "Direct assessment of safe strengths of RC slabs under membrane action." *Journal of Structural Engineering*, Vol. 123, No. 10, pp. 1331-1338.
- Fang, I. K., Tsui, C. K. T., Burns, N. H., Klingner, R. E., 1990, "Load Capacity of Isotropically Reinforced, Cast-in-Place and Precast Panel Bridge Decks." *PCI Journal*, Vol. 35, No. 4, pp. 104-113.
- Feldman, L. R., Bartlett, F. M., 2005, "Bond strength variability in pullout specimens with plain reinforcement." *ACI Structural Journal*, Vol. 102, No. 6, pp. 860-867.
- Feldman, L. R., Bartlett, F. M., 2008, "Bond in flexural members with plain steel reinforcement." *ACI Structural Journal*, Vol. 105, No. 5, pp. 552-560.

- Fenwick, R. C., Paulay, T., 1968,. "Mechanisms of Shear Resistance of Concrete Beams." *Journal of the Structural Division - ASCE*, Vol. 94, ST10, pp. 2325-2350.
- Ferguson, P.M., Breen, J.E., Jirsa, J.O, 1988, *Reinforced Concrete Fundamentals*, Wiley, 746pp.
- Fernandez Ruiz, M., Muttoni, A., 2007, "On development of suitable stress fields for structural concrete." *Aci Structural Journal*, Vol. 104, No. 4, pp. 495-502.
- Fernandez Ruiz, M., Vaz Rodrigues, R., Muttoni, A., 2009, "Dimensionnement et verification des dalles de roulement des ponts routiers." Ecole Polytechnique Federale de Lausanne, Laboratoire de Construction en Beton, 53 pp.
- fib. (2010). *Model Code 2010 - First complete draft Vol. I*, fib Bulletin 55, 317 pp.
- fib. (2010). *Model Code 2010 - First complete draft Vol. II*, fib Bulletin 56, 311 pp.
- Fischer, J., König, G., 1997, "Mechanical Model for Diagonal Tension Failure." *CEB Bulletin 237*, pp. 231-246.
- Fischer, J., and König, G. (1997). "Parabel-Schrägriß-Modell für das Versagen van schubschlanken Balken 2)." *Beton- und Stahlbetonbau*, Vol. 92, No. 8, pp. 220-224.
- Forrest, R. W. B., Higgins, C., Senturk, A. E., 2010, "Experimental and Analytical Evaluation of Reinforced Concrete Girders under Low-Cycle Shear Fatigue." *ACI Structural Journal*, Vol. 107, No. 2, pp. 199-207.
- Frenaij, J. W. I. J., 1989, *Time-dependent shear transfer in cracked reinforced concrete*, PhD thesis, Delft University of Technology, Delft, The Netherlands, 190 pp.
- Furuuchi, H., Takahashi, Y., Ueda, T., Kakuta, Y., 1998, "Effective width for shear failure of RC deep slabs," *Transactions of the Japan concrete institute*, Vol. 20, pp.209-216.
- Gambarova, P. G., 1981, "On Aggregate Interlock Mechanism in Reinforced Concrete Plates with Extensive Cracking." *IABSE Colloquium*, pp. 105-134.
- Gastebled, O. J., May, I. M., 2001, "Fracture mechanics model applied to shear failure of reinforced concrete beams without stirrups." *ACI Structural Journal*, Vol. 98, No. 2, pp. 184-190.
- Gettu, R., 2006, "Repeating a classic set of experiments on size effect in shear of members without stirrups. Discussion." *ACI Structural Journal*, Vol. 103, No. 5, pp. 760-761.

Ghazavy-Khorasgany, M., Gopalaratnam, V., 1993, "Shear Strength of Concrete - Size and other influences." *Proceedings of the JCI International workshop on size effect in concrete structures*, oct. 31 - nov. 2, 1993, Sendai, Japan, pp. 51-62.

Goldbeck, A. T., 1917, "The influence of total width on the effective width of reinforced concrete slabs subjected to central concentrated loading." *ACI Journal Proceedings*, Vol. 13, No. 2, pp. 78-88.

Goldbeck, A. T., Smith, E. B., 1916, "Tests of large reinforced concrete slabs." *ACI Journal Proceedings*, Vol. 12, No. 2, pp. 324-333.

Golus, P., 2011, "Numerische Untersuchungen zur mitwirkenden Plattenbreite für Querkraft von Fahrbahnplatten ohne Querkraftbewehrung." Diplomarbeit, Rheinsch-Westfälischen Technische Hochschule Aachen, 116 pp.

Graf, O., 1933, "Versuche über die Widerstandsfähigkeit von Eisenbetonplatten unter konzentrierter Last nahe einem Auflager (Tests of the strengths of reinforced concrete slabs under concentrated loads near supports)," *Deutscher Ausschuss für Eisenbeton*, Heft 73, Berlin, Germany, pp.1-16.

Guandalini, S., Burdet, O. L., Muttoni, A., 2009, "Punching Tests of Slabs with Low Reinforcement Ratios." *ACI Structural Journal*, Vol. 106, No. 1, pp. 87-95.

Guadalini, S., Burdet, O., Muttoni, A., Theodorakopoulos, D., Swamy, N., 2009, "Punching Tests of Slabs with Low Reinforcement Ratios: discussion and authors' closure." *ACI Structural Journal*, Vol. 106, No. 6, pp. 911-912.

Guice, L. K., Slawson, T. R., Rhomberg, E. J., 1989, "Membrane analysis of flat plate slabs." *ACI Structural Journal*, Vol. 86, No. 1, pp. 83-92.

Hallgren, M., Bjerke, M., 2002, "Non-linear finite element analyses of punching shear failure of column footings," *Cement & Concrete Composites*, V. 24, No. 6, pp. 491-496.

Gurley, C., 2011, "Exact" theoretical plane-stress yield-line analysis of shear in 'ordinary' beams." *Magazine of Concrete Research*, in press, 21pp.

Gustafsson, P. J., and Hillerborg, A., 1988, "Sensitivity in Shear Strength of Longitudinally Reinforced Concrete Beams to Fracture Energy of Concrete." *ACI Structural Journal*, Vol. 85, No. 3, pp. 286-294.

Hamadi, Y. D., Regan, P. E., 1980, "Behaviour in shear of beams with flexural cracks." *Magazine of Concrete Research*, Vol. 32, No. 111, pp. 67-78.

Hassan, A. A. A., Hossain, K. M. A., Lachemi, M., 2010, "Strength, cracking and deflection performance of large-scale self-consolidating concrete beams subjected to shear failure." *Engineering Structures*, Vol. 32, No. 5, pp. 1262-1271.

- Hawkins, N. M., Mitchell, D., 1979, "Progressive Collapse of Flat Plate Structures," *Journal of the American Concrete Institute*, Vol. 76, No. 7, pp. 775-808.
- Heger, F. J., McGrath, T. J., 1980, "Design method for reinforced concrete pipe and box sections." Simpson Gumpertz & Heger Inc., Cambridge, Massachusetts; San Francisco, California, 251 pp.
- Hegger, J., and Reißer, K., 2011, "Zwischenbericht: Anpassung des DIN-Fachberichtes "Betonbrücken" an endgültige Eurocodes und nationale Anhänge einschließlich Vergleichsrechnungen - Speziell: Querkrafttragfähigkeit von Fahrbanplatten." 116pp.
- Hegger, J., and Reißer, K., 2011. "Entwurf Schlussbericht: Anpassung des DIN-Fachberichtes "Betonbrücken" an endgültige Eurocodes und nationale Anhänge einschließlich Vergleichsrechnungen - Speziell: Querkrafttragfähigkeit von Fahrbanplatten." 86pp.
- Hewitt, B. E., de Batchelor, B. V., 1975, "Punching shear strength of restrained slabs." *Journal of the Structural Division*, Vol. 101, No. 9, pp. 1837-1853.
- Hofbeck, J. A., Ibrahim, I. O., Mattock, A. H., 1969, "Shear Transfer in Reinforced Concrete." *ACI Journal Proceedings*, Vol. 66, No. 2, pp. 119-128.
- Hon, A., Taplin, G., Al-Mahaidi, R. S., 2005, "Strength of reinforced concrete bridge decks under compressive membrane action." *ACI Structural Journal*, Vol. 102, No. 3, pp. 393-401.
- Hsu, T. T. C., 1996, "Towards a unified nomenclature for reinforced-concrete theory." *Journal of Structural Engineering*, Vol. 122, No. 3, pp. 275-283.
- Hsu, T. T. C., Mau, S. T., Chen, B., 1987, "Theory of Shear Transfer Strength of Reinforced Concrete." *ACI Structural Journal*, Vol. 84, No. 2, pp. 149-160.
- Iguero, M., Shioya, T., Nojiri, Y., Akiyama, H., 1984, "Experimental studies on shear strength of large reinforced concrete beams under uniformly distributed load." *Proceedings of JSCE*, Vol. 5, No. 345, pp. 137-154.
- Jackson, P., Zheng, Y., Taylor, S., Robinson, D., Cleland, D., 2010, "Investigation of Ultimate Strength of Deck Slabs in Steel-Concrete Bridges - Discussion and Author's closure." *ACI Structural Journal*, Vol. 107, No. 6, pp. 747-748.
- Jaeger, T., 2002, "Shear Strength and Deformation Capacity of Reinforced Concrete Slabs," *Proceedings of the 4<sup>th</sup> International PhD Symposium in Civil Engineering*, Fédération Internationale du Béton, Munich, Germany, pp.280-286.
- Jäger, T., 2005, *Versuche zum Querkraftwiderstand und zum Verformungsvermögen von Stahlbetonplatten*, ETH Zurich, Zurich, Switzerland, 362pp.

Jäger, T., 2007, *Querkraftwiderstand und Verformungsvermögen von Stahlbetonplatten*, PhD Thesis, ETH Zurich, Zurich, Switzerland, 123pp.

Jaeger, T. and P. Marti, 2009, "Reinforced Concrete Slab Shear Prediction Competition: Experiments." *ACI Structural Journal*, Vol. 106, No. 3, pp. 300-308.

Jaeger, T., Marti, P., 2009, "Reinforced Concrete Slab Shear Prediction Competition: Entries and Discussion." *ACI Structural Journal*, Vol. 106, No. 3, pp.309-318.

Joint committee on concrete and reinforced concrete, 1916, "Final report on concrete and reinforced concrete." *Proceedings of the American Society of Civil Engineers*, Vol. 42, No. 10, pp. 167-1708.

Jung, S., Kim, K. S., 2008, "Knowledge-based prediction of shear strength of concrete beams without shear reinforcement." *Engineering Structures*, Vol. 30, No. 6, pp. 1515-1525.

Kani, G. N. J., 1964, "The Riddle of Shear Failure and Its Solution." *ACI Journal Proceedings*, Vol. 61, No. 4, pp. 441-467.

Kani, G. N. J., 1966, "Basic Facts Concerning Shear Failure." *ACI Journal Proceedings*, Vol. 63, No. 6, pp. 675-692.

Kani, G. N. J., 1967, "How Safe Are Our Large Reinforced Concrete Beams." *ACI Journal Proceedings*, Vol. 64, No. 3, pp. 128-141.

Kani, G. N. J., 1969, "A Rational Theory for the function of Web Reinforcement." *ACI Journal Proceedings*, Vol. 66, No. 3, pp. 185-197.

Kani, M. W., Huggins, M. W., Wittkopp, R. R., 1979, *Kani on Shear in Reinforced Concrete*, University of Toronto, Dept of Civil Engineering, Toronto, 225 pp.

Kaufmann, W., Marti, P., 1998, "Structural concrete: Cracked membrane model." *Journal of Structural Engineering-ASCE*, Vol. 124, No. 12, pp. 1467-1475.

Kazemi, M. T., Broujerdian, V., 2006, "Repeating a classic set of experiments on size effect in shear of members without stirrups. Discussion." *ACI Structural Journal*, Vol. 103, No. 5, pp. 757-758.

Khuntia, M., Stojadinovic, B., 2001, "Shear strength of reinforced concrete beams without transverse reinforcement." *ACI Structural Journal*, Vol. 98, No. 5, pp. 648-656.

Kim, D., Kim, W., White, R. N., 1999, "Arch action in reinforced concrete beams - A rational prediction of shear strength." *ACI Structural Journal*, Vol. 96, No. 4, pp. 586-593.

- Kim, W., Jeong, J., 2011, "Decoupling of Arch Action in Shear-Critical Reinforced Concrete Beams." *ACI Structural Journal*, Vol. 108, No. 4, pp. 395-404.
- Kinnunen, S., Nylander, H., 1960, *Punching of Concrete Slabs without Shear Reinforcement*, Stockholm, 112pp.
- Kirkpatrick, J., Rankin, G. I. B., Long, A. E., 1984, "Strength evaluation of M-beam bridge deck slabs." *The structural engineer*, Vol. 62B, No. 3, pp. 60-68.
- König, G., Fischer, J., 1995, "Model Uncertainties concerning Design Equations for the Shear Capacity of Concrete Members without Shear Reinforcement." *CEB Bulletin 224, "Model Uncertainties and Concrete Barrier for Environmental Protection"*, pp. 49-100.
- Kotsovos, M. D., 1984, "Behavior of Reinforced Concrete Beams with a Shear Span to Depth Ratio Between 1.0 and 2.5." *Journal of the American Concrete Institute*, Vol. 81, No. (3), pp. 279-286.
- Kotsovos, M. D., 1992, "Ultimate Shear Force of Structural Concrete Members without Transverse Reinforcement Derived from a Mechanical Model - Discussion" *Aci Structural Journal*, Vol. 89, No. 4, pp. 477-477.
- Kuang, J. S., Morley, C. T., 1992, "Punching Shear Behavior of Restrained Reinforced-concrete slabs." *Aci Structural Journal*, Vol. 89, No. 1, pp. 13-19.
- Kuang, J. S., Morley, C. T., 1993, "A Plasticity Model for Punching shear of Laterally Restrained Slabs with Compressive Membrane Action." *International Journal of Mechanical Sciences*, Vol. 35, No. 5, pp. 371-385.
- Labib, M., Moslehy, Y., Ayoub, A. S., 2009, "Behavior of Reinforced Concrete Elements Subjected to Tri-Directional Shear Using a State-of-the-Art Panel Tester." *SP-265 Thomas T.C. Hsu Symposium on Shear and Torsion in Concrete Structures*, American Concrete Institute., ed., New Orleans, LA, USA, pp. 455-476.
- Lantsoght, E., 2009, *Literature review of punching shear in reinforced concrete slabs*, Research Report No. 09-10, School of Civil and Environmental Engineering – Structural Engineering, Mechanics and Materials, Georgia Institute of Technology, Atlanta, GA, USA, 93 pp.
- Laupa, A., Siess, C. P., Newmark, N. M., 1953, "The shear strength of simple-span reinforced concrete beams without web reinforcement." University of Illinois, Urbana, 81 pp.
- Lee, S. C., Cho, J. Y., Oh, B. H., 2010, "Shear Behavior of Large-Scale Post-Tensioned Girders with Small Shear Span-Depth Ratio." *ACI Structural Journal*, Vol. 107, No. 2, pp. 137-145.

Leonhardt, F., Walther, R., 1962, *The Stuttgart shear tests, 1961; contributions to the treatment of the problems of shear in reinforced concrete construction*, Translation No. 111, Cement and Concrete Association, London, 134 pp.

Leonhardt, F., Walther, R., 1962, "Beitrage zur Behandlung der Schubprobleme in Stahlbetonbau - 2. Fortsetzung des Kapitels II. Versuchsberichte." *Beton- und Stahlbetonbau*, Vol. 57, No. 3, pp. 54-64.

Leonhardt, F., 1965, "Reducing the Shear Reinforcement in Reinforced Concrete Beams and Slabs." *Magazine of Concrete Research*, Vol. 17, No. 53, pp.187-198.

Leonhardt, F., 1978, "Shear in concrete structures." CEB Bulletin 126, pp. 67-124.

Li, Y., Vrouwenvelder, T., Wijnants, G. H., Walraven, J., 2004, "Spatial variability of concrete deterioration and repair strategies." *Structural Concrete*, Vol. 5, No. 3, pp. 121-129.

Lips, S., Muttoni, A., and Ruiz, M. F. (2010). "Punching of flat slabs: Design example.", 13pp.

Long, A. E., 1975,. "A two-phase Approach to the Prediction of the Punching Strength of Slabs." *ACI Journal Proceedings*, Vol. 72, No. 2, pp. 37-45.

Lubell, A.S., 2006, *Shear in wide reinforced concrete members*, PhD Thesis, University of Toronto, 2006, 455pp.

Lubell, A.S., Bentz, E.C., Collins, M.P., 2009, "Influence of Longitudinal Reinforcement on One-way Shear in Slabs and Wide Beams," *Journal of Structural Engineering*, Vol. 135, No. 1, pp.78-87.

Lubell, A. S., Bentz, E. C., Collins, M. P., 2009, "Shear Reinforcement Spacing in Wide Members." *ACI Structural Journal*, Vol. 106, No. 2, pp. 205-214.

Lubell, A. S., Sherwood, E. G., Bentz, E., Collins, M. P., 2004, "Safe shear design of large, wide beams." *Concrete international*, Vol. 26, No. 1, pp. 67-78.

Mabsout, M., Tarhini, K., Jabakhanji, R., Awwad, E., 2004, "Wheel Load Distribution in Simply Supported Concrete Slab bridges." *Journal of Bridge Engineering*, Vol. 9, No. 2, pp. 147-155.

MacGregor, J. G., Walters, J. R. V., 1967, "Analysis of Inclined Cracking Shear in Slender Reinforced Concrete Beams." *ACI Journal Proceedings*, Vol. 64, No. 10, pp. 644-653.

MacGregor, J. G., Hanson, J., 1969, "Proposed changes in shear provisions for reinforced and prestressed concrete beams." *ACI Journal Proceedings*, Vol. 66, No. 4, pp. 276-288.

- MacGregor, J. G., 1973, "The Design of Reinforced Concrete Beams for Shear." *ACI symposium March and October 1973*, pp. 503-537.
- MacGregor, J. G., Gergely, P., 1977, "Suggested Revisions to ACI Building Code Clauses Dealing with Shear in Beams." *Journal of the American Concrete Institute*, Vol. 74, No. 10, pp. 493-500.
- MacGregor, J. G., Wight, J. K., 2005, *Reinforced concrete: mechanics and design*, 4<sup>th</sup> edition, Prentice Hall, Upper Saddle River, N.J., 1132pp.
- Manuel, R. F., 1973, "Failure of Deep Beams." *ACI symposium March and October 1973*, pp. 425-440.
- Marti, P. 1990, "Design of concrete slabs for transverse shear," *ACI Structural Journal*, Vol. 87, No. 2, pp.180-190.
- Marti, P., 1999, "How to treat shear in structural concrete." *ACI Structural Journal*, Vol. 96, No. 3, pp. 408-415.
- Marti, P., 2003, "Kraftfluß in Stahlbetonplatten." *Beton- und Stahlbetonbau*, Vol. 98, No. 2, pp. 85-93.
- Massicotte, B., 2007, "Etude des causes de l'effondrement du pont du boulevard de la Concorde." Ecole polytechnique de Montreal Groupe de recherche en genie des structures, 263 pp.,  
[http://www.cevc.gouv.qc.ca/UserFiles/File/Autres\\_pieces\\_deposees/PieceMTQ\\_6.pdf](http://www.cevc.gouv.qc.ca/UserFiles/File/Autres_pieces_deposees/PieceMTQ_6.pdf)
- Mathey, R. G., Watstein, D., 1963, "Shear strength of beams without web reinforcement containing deformed bars of different yield strengths." *ACI Journal Proceedings*, Vol. 60, No. 2, pp. 183-207.
- McCabe, S. L., Niwa, J., 1993, "Size effect in reinforced concrete members subjected to shear loading." *Proceedings of the JCI International workshop on size effect in concrete structures*, oct. 31 - nov. 2, 1993, Sendai, Japan, pp. 335-358.
- McCabe, S. L., 1997, "Fracture Mechanics Evaluation of Structural Concrete Members." *CEB Bulletin 237*, pp. 171-184.
- Menétrey, P., 2002, "Synthesis of punching failure in reinforced concrete." *Cement & Concrete Composites*, Vol. 24, No. 6, pp. 497-507.
- Mihashi, H., Nomura, N., 1993, "How to predict size effect in concrete structures." *Proceedings of the JCI International workshop on size effect in concrete structures*, oct. 31 - nov. 2, 1993, Sendai, Japan, pp. 235-246.



Millard, S. G., Johnson, R. P., 1984, "Shear transfer across cracks in reinforced concrete due to aggregate interlock and dowel action." *Magazine of Concrete Research*, Vol. 36, No. 126, pp. 9-21.

Miller, R. A., Aktan, A. E., Shahrooz, B. M., 1994, "Destructive Testing of Decommissioned Concrete Slab Bridge." *Journal of Structural Engineering*, Vol. 120, No. 7, pp.2176-2198.

Mitchell, D., Collins, M. P., 1974, "Diagonal Compression Field Theory - A Rational Model for Structural Concrete in Pure Torsion." *ACI Journal Proceedings*, Vol. 71 , No. 8, pp. 396-408.

Moe, J., 1961, *Shearing strength of reinforced concrete slabs and footings under concentrated loads*, Portland Cement Association Research and Development laboratories, Skokie, IL, 135 pp.

Moody, K. G., Viest, I. M., Elstner, R. C., Hognestad, E., 1954, "Shear strength of reinforced concrete beams. Part 1 - Tests of simple beams." *ACI Journal Proceedings*, Vol. 51, No. 4, pp. 317-332.

Moody, K. G., Viest, I. M., 1955, "Shear strength of reinforced concrete beams: Part 4 - Analytical Studies." *ACI Journal Proceedings*, Vol. 51, No. 7, pp. 697-730.

Morita, S., Fujii, S., Kondo, G., 1993, "Experimental Study on Size Effect in Concrete Structures." *Proceedings of the JCI International workshop on size effect in concrete structures*, oct. 31 - nov. 2, 1993, Sendai, Japan, pp. 21-40.

Morrow, J., Viest, I. M., 1957, "Shear Strength of Reinforced Concrete Frame Members Without Web Reinforcement." *ACI Journal Proceedings*, Vol. 53, No. 3, pp. 833-869.

Mörsch, E., 1922, *Der Eisenbetonbau : Seine Theorie Und Anwendung*, Verlag Von Konrad Wittwer, Stuttgart, 368 pp.

Muttoni, A., Schwartz, J., 1991, "Behaviour of Beams and Punching in Slabs without Shear Reinforcement." *IABSE colloquium on structural concrete*, pp. 703-708.

Muttoni, A., 2003, "Schubfestigkeit und Durchstanzen von Platten ohne Querkraftbewehrung (Shear and punching strength of slabs without shear reinforcement)," *Beton- und Stahlbetonbau*, Vol. 98, No. 2, pp.74-84.

Muttoni, A., 2008, "Punching shear strength of reinforced concrete slabs without transverse reinforcement." *ACI Structural Journal*, Vol. 105, No. 4, pp. 440-450.

Muttoni, A., Fernández Ruiz, M., 2008a, "Shear strength in one- and two-way slabs according to the Critical Shear Crack Theory," *Proceedings of the International FIB*

*Symposium 2008*, Fédération Internationale du Béton , Amsterdam, The Netherlands, pp. 559-563.

Muttoni, A., Fernández Ruiz, M., March- April 2008b, "Shear Strength of Members without Transverse Reinforcement as Function of Critical Shear Crack Width," *ACI Structural Journal*, Vol. 105, No. 2, pp.163-172.

Muttoni, A., Windisch, A., Subramanian, N., 2009, "Punching Shear Strength of Reinforced Concrete Slabs without Transverse Reinforcement: Discussion an author's closure." *ACI Structural Journal*, Vol. 106, No. 3, pp. 381-382

Muttoni, A., Fernández Ruiz, M., 2010, "MC2010: The Critical Shear Crack Theory as a mechanical model for punching shear design and its application to code provisions." *Shear and punching shear in RC and FRC elements – Proceedings of a workshop held on 15-16 October 2010 in Salò, Lake Garda, Italy*, fib bulletin 57, pp. 31-59.

Naumann, J. (2010). "Bruecken und Schwerverkehr - eine Bestandsaufnahme." *der Bauingenieur*, 85(01), 1-9.

Nielsen, M. P., 1984, *Limit analysis and concrete plasticity*, Prentice-Hall, Englewood Cliffs, N.J. ; London, 420 pp.

Niwa, J., Yamada, K., Yokozawa, K., and Okamura, H., 1987, "Revaluation of the equation for shear strength of reinforced concrete beams without web reinforcement." *Proceedings of JSCE*, Vol. 5, No. 372, pp. 65-84.

Niwa, J., 1997, "Size effect in Shear of Concrete Beams Predicted by Fracture Mechanics." *CEB Bulletin* 237, pp. 147-158.

Normcommissie 351 001, 1995, *Technische Grondslagen voor Bouwvoorschriften, Voorschriften Beton TGB 1990 – Constructieve Eisen en Rekenmethoden (VBC 1995), NEN 6720*, Civieltechnisch centrum uitvoering research en regelgeving, Nederlands Normalisatie-instituut, Delft, The Netherlands, 245 pp.

Nowak, A. S., 1995, "Calibration of LRFD bridge code." *Journal of Structural Engineering-Asce*, Vol. 121, No. 8, pp. 1245-1251.

Nowak, A. S., Paczkowski, P., 2009, "Reliability models for shear in reinforced concrete beams." SP-265 Thomas T.C. Hsu Symposium on Shear and Torsion in Concrete Structures, pp. 627-646.

Olonisakin, A. A., Alexander, S. D. B., 1999, "Mechanism of shear transfer in a reinforced concrete beam." *Canadian journal of civil engineering*, Vol. 26, No. 6, pp. 810-817.

Ozbolt, J., Eligehausen, R., 1997, "Size effects in concrete and RC structures - diagonal

shear and bending." *CEB Bulletin 237*, pp. 103-145.

Paulay, T., Loeber, P. J. (1973) "Shear Transfer by Aggregate Interlock." *ACI symposium March and October 1973*, pp. 1-15.

Pearson-Kirk, D., 2010, "Improving the management of bridges - the benefits of condition monitoring." *Structural Faults and Repair*, 13th International Conference and Exhibition, Edinburgh, UK, 12 pp.

Pujol, S., Muttoni, A., Fernandez Ruiz, M., Jaeger, T., Marti, P., 2009, "Reinforced Concrete Slab Shear Prediction Competition: Entries and Discussion: Discussion and Authors' closure ." *ACI Structural Journal*, Vol. 107, No. 2, pp. 249-250.

Pruijssers, A. F., 1986, *Shear resistance of beams based on the effective shear depth*. Stevinreport No. 5-86-1, Delft University of Technology, Delft, The Netherlands, 69 pp.

Rajagopalan, K. S., Ferguson, P. M., 1968, "Exploratory shear tests emphasizing percentage of longitudinal steel." *ACI Journal Proceedings*, Vol. 65, No. 8, pp. 634-638.

Rafla, K., 1971, "Empirische Formeln zur Berechnung der Schubtragfähigkeit von Stahlbetonbalken." *Strasse Brücke Tunnel*, Vol. 23, No. 12, pp. 311-320.

Rahal, K. N., Collins, M. P., 1995, "Analysis of Sections Subjected to Combined Shear and Torsion - a Theoretical-Model." *ACI Structural Journal*, Vol. 92, No. 4, pp. 459-469.

Rahal, K. N., Collins, M. P., 1999, "Background to the general method of shear design in the 1994 CSA-A23.3 standard." *Canadian Journal of Civil Engineering*, Vol. 26, No. 6, pp. 827-839.

Rangan, B. V., 1973, "A comparison of code requirements for shear strength of reinforced concrete beams." *ACI symposium March and October 1973*, pp. 285-303.

Reineck, K. H., 1991, "Ultimate Shear Force of Structural Concrete Members without Transverse Reinforcement Derived from a Mechanical Model." *ACI Structural Journal*, Vol. 88, No. 5, pp. 592-602.

Reineck, K. H., 1992, "Ultimate Shear Force of Structural Concrete Members without Transverse Reinforcement Derived from a Mechanical Model - Closure" *ACI Structural Journal*, Vol. 89, No. 4, pp. 479-481.

Reineck, K.-H., 1997a, "Modelling the shear behaviour and size effect of structural concrete members without transverse reinforcement." *CEB Bulletin 237*, pp. 185-197.

Reineck, K.-H., 1997b, "Concrete Tension and Size Effect - Summary and Discussion." *CEB Bulletin 237*, pp. 247-253.

- Reineck, K.-H., 2002, "Shear design in a consistent design concept for structural concrete based on strut-and-tie models." *Design Examples for the 1996 FIP recommendations "Practical design of structural concrete"*, fib bulletin 16, pp. 165-186.
- Reineck, K.H., 2009, "Review of Basic Assumptions for the Shear Design." Thomas T.C. Hsu Symposium on Shear and Torsion in Concrete Structures, American Concrete Institute, New Orleans, LA, USA, pp. 367-384.
- Reineck, K. H., 2010, "Strut-and-tie models utilizing concrete tension fields." 3rd fib International Congress, Washington DC, USA, 12 pp.
- Reineck, K. H., Kuchma, D. A., Kim, K. S., Marx, S., 2003, "Shear database for reinforced concrete members without shear reinforcement." *ACI Structural Journal*, Vol. 100, No. 2, pp. 240-249.
- Reineck, K.-H., Ozbolt, J., Tepfers, R., 1997, "Introduction to the CEB Bulletin Concrete Tension and Size Effect - Utilization of concrete tension in structural concrete design and relevance of size effect." *CEB Bulletin 237*, pp. 7-15.
- Reinhardt, H. W., 1986, "The role of Fracture Mechanics in Rational Rules for Concrete Design." *IABSE Periodica*, Vol. 34, No. 1, pp. 1-15.
- Reißen, K., and Hegger, J., 2011, "Experimental Study on the Shear Capacity of Concrete Slabs." IABSE 2011, 8 pp.
- Regan, P. E., 1969, "Shear in Reinforced Concrete Beams." *Magazine of Concrete Research*, Vol. 21, No. 66, pp. 31-42.
- Regan, P.E., 1982, *Shear Resistance of Concrete Slabs at Concentrated Loads close to Supports*, Engineering Structures Research Group, Polytechnic of Central London, London, United Kingdom, 24 pp.
- Regan, P. E., 1987, "Shear resistance of members without shear reinforcement; proposal for CEB Model Code MC90." Polytechnic of Central London, London, UK, 28 pp.
- Regan, P.E., Rezai-Jorabi, H., 1988, "Shear resistance of one-way slabs under concentrated loads," *ACI Structural Journal*, Vol. 85, No.2, pp.150-157.
- Regan, P. E., 1993, "Research on shear: a benefit to humanity or a waste of time," *The structural engineer*, Vol. 71, No. 19, pp. 337-347.
- Regan, P. E., 1998, "Enhancement of shear resistance in short shear spans of reinforced concrete - an evaluation of UK recommendations and particularly of BD44/95." University of Westminster, London, UK, 16 pp.
- Regan, P. E., Kennedy-Reid, I. L., Pullen, A. D., Smith, D. A., 2005, "The influence of

aggregate type on the shear resistance of reinforced concrete." *The structural engineer*, Vol. 83, No. 23, pp. 27-32.

Richart, F. E., Kluge, R.W., 1939. "Tests of reinforced concrete slabs subjected to concentrated loads; a report of an investigation", *Bulletin*, Vol. 36, No. 85, The engineering experiment station, University of Illinois, Urbana, 86 pp.

Richart, F. E., 1948, "Reinforced Concrete Wall and Column Footings: part 1." *ACI Journal Proceedings*, Vol. 45, No. 2, pp. 97-127.

Richart, F. E., 1948, "Reinforced Concrete Wall and Column Footings: part 2." *ACI Journal Proceedings*, Vol. 45, No. 2, pp. 97-127.

Ritter, W., 1899, "Die Bauweise Hennebique." *Schweizerische Bauzeitung*, Vol. 33, No. 7, pp. 59-61.

Rombach, G. A., Velasco, R. R., 2005, "Schnittgrößen auskragender fahrbahnplatten infolge von radlasten nach DIN-fachbericht." *Beton- und Stahlbetonbau*, Vol. 100, No. 5, pp. 376-389.

Rombach, G.A., Latte, S., 2008, "Shear resistance of bridge decks without shear reinforcement," *Proceedings of the International FIB Symposium 2008*, Fédération Internationale du Béton , Amsterdam, The Netherlands, pp.519-525.

Rombach, G., Latte, S., 2009, "Querkrafttragfähigkeit von Fahrbahnplatten ohne Querkraftbewehrung." *Beton- und Stahlbetonbau*, Vol. 104, No. 10, pp. 642-656.

Rombach, G. A., Latte, S., and Steffens, R., 2009, *Querkrafttragfähigkeit von Fahrbahnplatten ohne Querkraftbewehrung*. Forschung Straßenbau under Straßenverkehrstechnik, Institut für Massivbau, Technische Universität Hamburg-Harburg, Bonn, 91pp.

Russo, G., Zingone, G., Puleri, G., 1991, "Flexure-Shear Interaction-Model for Longitudinally Reinforced Beams." *ACI Structural Journal*, Vol. 88, No. 1, pp. 60-68.

Sabnis, G. M., 1993, "Size Effects in concrete - its impact on experimental work and related design standards." *Proceedings of the JCI International workshop on size effect in concrete structures*, oct. 31 - nov. 2, 1993, Sendai, Japan, pp. 359-368.

Sagaseta, J., Muttoni, A., Ruiz, M. F., Tassinari, L., 2011, "Non-axis-symmetrical punching shear around internal columns of RC slabs without transverse reinforcement." *Magazine of Concrete Research*, in press, 17 pp.

Salim, W., Sebastian, W. M., 2002, "Plasticity model for predicting punching shear strengths of reinforced concrete slabs." *ACI Structural Journal*, Vol. 99, No. 6, pp. 827-835.

- Schlaich, J., Schafer, K., Jennewein, M., 1987, "Toward a Consistent Design of Structural Concrete." *Journal Prestressed Concrete Institute*, Vol. 32, No. 3, pp. 74-150.
- Serna-Ros, P., Fernandez-Prada, M. A., Miguel-Sosa, P., Debb, O. A. R., 2002, "Influence of stirrup distribution and support width on the shear strength of reinforced concrete wide beams." *Magazine of Concrete Research*, Vol. 54, No. 3, pp. 181-191.
- Shank, J. R., 1931, "Bond, Shear and Diagonal Tension in Reinforced Concrete." *ACI Journal Proceedings*, 28(11), 187-192.
- Sherwood, E. G., Bentz, E. C., Collins, M. P., 2007, "Effect of aggregate size on beam-shear strength of thick slabs." *ACI Structural Journal*, Vol. 104, No. 2, pp. 180-190.
- Sherwood, E.G., Lubell, A.S., Bentz, E.C, Collins, M.P., 2006, "One-way Shear Strength of Thick Slabs and Wide Beams," *ACI Structural Journal*, Vol. 103, No. 6, pp.794-802.
- Sherwood, E. G., Lubell, A. S., Bentz, E.C., Collins, M.P., 2007, "One-way shear strength of thick slabs and wide beams – Discussion and Authors' closure." *ACI Structural Journal*, Vol 104, No. 5, pp. 640-641.
- Sherwood, E. G., 2008, *One-way shear behaviour of large, lightly-reinforced concrete beams and slabs*, PhD dissertation, University of Toronto, 547 pp.
- Shioya, T., Iguro, M., Nojiri, Y., Akiyama, H., Okada, T., 1989, "Shear strength of large reinforced concrete beams." *Fracture Mechanics: Application to Concrete*, ACI SP-118, pp. 259-279.
- Shioya, T., Akiyama, H., 1993, "Application to Design of Size Effect in Reinforced Concrete Structures." *Proceedings of the JCI International workshop on size effect in concrete structures*, oct. 31 - nov. 2, 1993, Sendai, Japan, pp. 327-334.
- Sneed, L. H., Ramirez, J. A., 2010, "Influence of Effective Depth on Shear Strength of Concrete Beams - Experimental Study." *ACI Structural Journal*, Vol. 107, No. 5, pp. 554-562.
- Stewart, M. G., Val, D. V., 2003, "Multiple limit states and expected failure costs for deteriorating reinforced concrete bridges." *Journal of Bridge Engineering*, Vol. 8, No. 6, pp. 405-415.
- Sun, S., Kuchma, D. A., 2007, *Shear Behavior and Capacity of Large-Scale Prestressed High-Strength Concrete Bulb-Tee Girders*. University of Illinois at Urbana-Champaign, 147 pp.

Sundquist, H., 2005, "Punching Research at the Royal Institute of Technology (KTH) in Stockholm," *SP-232*, Ed. Polak, M.A., American Concrete Institute, Farmington Hills, MI, pp. 229-256.

Swamy, R. N., Andriopoulos, A. D., 1973, "Contribution of Aggregate Interlock and Dowel Forces to the Shear Resistance of Reinforced Beams with Web Reinforcement." *ACI symposium March and October 1973*, pp. 129-166.

Talbot, A. N., 1904, *Tests of reinforced concrete beams*. University of Illinois, Urbana, 70 pp.

Talbot, A. N., 1905, *Tests of reinforced concrete beams*. University of Illinois, Urbana, 92 pp.

Talbot, A. N., 1906, *Tests of reinforced concrete T-beams*. University of Illinois, Urbana, 42 pp.

Talbot, A. N., 1908, *A test of three large reinforced concrete beams*. University of Illinois, Urbana, 42 pp.

Talbot, A. N., 1909, *Tests of reinforced concrete beams: resistance to web stresses*. University of Illinois, Urbana, 90 pp.

Taylor, H. P. J., 1972, "Shear Strength of Large Beams." *Journal of the Structural Division*, Vol. 98, ST11, pp. 2473-2490.

Taylor, H. P. J., 1973, "The fundamental behavior of reinforced concrete beams in bending and shear." *ACI symposium March and October 1973*, pp. 285-303.

Taylor, R., Hayes, B., 1965, "Some tests on the effect of edge restraint on punching shear in reinforced concrete slabs." *Magazine of Concrete Research*, Vol. 17, No. 50, pp. 39-44.

Taylor, S. E., Rankin, G. I. B., Cleland, D. J., 2003, "Real strength of high-performance concrete bridge deck slabs." *Proceedings of the Institution of Civil Engineers, Bridge Engineering*, 156, Issue BE2, pp. 81-90.

Taylor, S. E., Rankin, B., Cleland, D. J., and Kirkpatrick, J., 2007, "Serviceability of bridge deck slabs with arching action." *Aci Structural Journal*, Vol. 104, No. 1, pp. 39-48.

Theodorakopoulos, D. D., Swamy, R. N., 2002. "Ultimate punching shear strength analysis of slab-column connections." *Cement & Concrete Composites*, Vol. 24, No. 6, pp. 509-521.

TNO Bouw en Ondergrond, Van der Veen, C., 2010, "Viaduct in de A1 over de Tolnegenweg bij Stroe, Controle dwarskrachtcapaciteit." TNO Bouw en Ondergrond, Delft, The Netherlands, 67 pp.

Tompos, E. J., Frosch, R. J., 2002, "Influence of beam size, longitudinal reinforcement, and stirrup effectiveness on concrete shear strength." *ACI Structural Journal*, Vol. 99, No. 5, pp. 559-567.

Tureyen, A. K., Frosch, R. J., 2004, "Concrete shear strength: Another perspective." *ACI Structural Journal*, Vol. 101, No. 4, pp. 584-585.

Uzel, A., Podgorniak, B., Bentz, E. C., Collins, M. P., 2011, "Design of Large Footings for One-Way Shear." *Aci Structural Journal*, Vol. 108, No. 2, pp. 131-138.

van den Berg, F. J., 1962, "Shear strength of reinforced concrete beams without web reinforcement: Part 1 - Distribution of stresses over beam cross section." *ACI Journal Proceedings*, Vol. 59, No. 10, pp. 1467-1478.

van den Beukel, A., Monnier, T., 1985, "Rapport No. B-84-522A/62.5.0804: Dwarskracht." Instituut TNO voor bouwmaterialen en bouwconstructies, Delft, The Netherlands, 69 pp.

Vaz Rodrigues, R., Muttoni, A., Olivier, O., 2006, "Large Scale Tests on Bridge Slabs Cantilevers Subjected to Traffic Loads," *Proceedings of the 2<sup>nd</sup> international Congress*, Fédération Internationale du Béton, Naples, Italy, 10 pp.

Vaz Rodrigues, R., 2007, *Shear strength of reinforced concrete bridge deck slabs*, PhD thesis, Ecole Polytechnique Fédérale de Lausanne, Lausanne, Switzerland, 293 pp.

Vaz Rodrigues, R., Ruiz, M. F., Muttoni, A., 2008, "Shear strength of R/C bridge cantilever slabs." *Engineering Structures*, Vol. 30, No. 11, pp. 3024-3033.

Vaz Rodrigues, R., Muttoni, A., Fernández Ruiz, M., 2010, "Influence of shear on rotation capacity of reinforced concrete members without shear reinforcement." *ACI Structural Journal*, Vol. 107, No. 5, pp. 516-525.

Vecchio, F. J., Collins, M. P., 1986, "The Modified Compression-Field Theory for Reinforced-Concrete Elements Subjected to Shear." *Journal of the American Concrete Institute*, Vol. 83, No. 2, pp. 219-231.

Vecchio, F.J., Collins, M.P., 1990, "Investigating the collapse of a warehouse," *Concrete International*, Vol. 12, No. 3, pp. 72-78.

Vecchio, F. J., 2000, "Disturbed stress field model for reinforced concrete: Formulation." *Journal of Structural Engineering-ASCE*, Vol. 126, No. 9, pp. 1070-1077.

Vintzileou, E., 1997, "Shear transfer by dowel action and friction as related to size effects." *CEB Bulletin 237*, pp. 53-77.



- Voormeeren, L. (2011). "Extension and Verification of Sequentially Linear Analysis to Solid Elements." M.Sc. thesis, Delft University of Technology, Delft, 95 pp.
- Wang, N., O'Malley, C., Ellingwood, B. R., Zureick, A.-H., 2010, "Bridge rating using system reliability assessment Part I: Assessment and verification by load testing." *Journal of Bridge Engineering*, in press, 31pp.
- Wang, N., Ellingwood, B. R., Zureick, A.-H., 2010, "Bridge rating using system reliability assessment Part II: Improvement to bridge rating practices." *Journal of Bridge Engineering*, in press, 33pp.
- Walraven, J.C., 1980, "Aggregate interlock: a theoretical and experimental analysis," PhD Thesis, Delft University of Technology, Delft, The Netherlands, 197 pp.
- Walraven, J.C., 1981, "Fundamental Analysis of Aggregate Interlock." *Journal of the Structural Division-ASCE*, Vol. 107, No. 11, pp. 2245-2270,
- Walraven, J.C., 1981, "Scheurverstanding." *Cement*, Vol. 33, No. 6, pp. 406-412.
- Walraven, J., Frenay, J., Pruijssers, A., 1987, "Influence of Concrete Strength and Load History on the Shear Friction Capacity of Concrete Members." *Journal Prestressed Concrete Institute*, Vol. 32, No. 1, pp. 66-84.
- Walraven, J. C., 1993, "Size Effects: their nature and their recognition in building codes." *Proceedings of the JCI International workshop on size effect in concrete structures*, oct. 31 - nov. 2, 1993, Sendai, Japan, pp. 295-314.
- Walraven, J., Lehwalter, N., 1994, "Size Effects in Short Beams Loaded in Shear." *ACI Structural Journal*, Vol. 91, No. 5, pp. 585-593.
- Walraven, J. C., 2002, *Background document for EC-2, Chapter 6.2 Shear*, Delft University of Technology, Delft, The Netherlands, 30 pp.
- Walraven, J. C., 2007, "Fracture mechanics of concrete and its role in explaining structural behaviour." *Fracture Mechanics of Concrete and Concrete Structures*, Vols. 1-3, pp. 1265-1275.
- Wei, W.-w., Che, Y., Gong, J.-x., 2011, "Shear strength prediction for reinforced concrete beams without stirrups." *Magazine of Concrete Research*, in press, 8 pp.
- Westergaard, H. M., 1930, "Computation of stresses in bridge slabs due to wheel loads." *Public roads*, Vol. 11, No. 1, pp. 1-23.
- Widianto, Bayrak, O., Jirsa, J. O., 2009, "Two-Way Shear Strength of Slab-Column Connections: Reexamination of ACI 318 Provisions." *Aci Structural Journal*, Vol. 106, No. 2, pp. 160-170.

Windisch, A., Rodrigues, R. V., Muttoni, A., Ruiz, M. F., 2011, "Influence of Shear on Rotation Capacity of Reinforced Concrete Members Without Shear Reinforcement: Discussion and Authors' Closure." *ACI Structural Journal*, Vol. 108, No. 4, pp. 505-506.

Wood, J. G. M., 2008, "Implications of the collapse of the de la Concorde overpass." *The structural engineer*, Vol. 86, No. 1, pp. 16-18.

Xu, S., Reinhardt, H. W., 2005, "Shear Fracture on the basis of Fracture Mechanics." *Otto Graf Journal*, Vol. 16, No. 1, pp. 21-78.

Yang, K.-H., 2010, "Tests on Lightweight Concrete Deep Beams." *ACI Structural Journal*, Vol. 107, No. 6, pp. 663-670.

Yang, K.-H., Sim, J.-I., Choi, B.-J., and Lee, E.-T., 2011, "Effect of Aggregate Size on Shear Behavior of Lightweight Concrete Continuous Slender Beams." *ACI Materials Journal*, Vol. 108, No. 5, pp. 501-509.

Yu, Q., 2004, "Shear database for reinforced concrete members without shear reinforcement. Paper by Karl-Heinz Reineck, Daniel A. Kuchma, Kang Su Kim, and Sina Marx - Discussion." *ACI Structural Journal*, Vol. 101, No. 1, pp. 141-143.

Yu, Q., Bazant, Z. P., 2006, "Repeating a classic set of experiments on size effect in shear of members without stirrups. Discussion." *ACI Structural Journal*, Vol. 103, No. 5, pp. 755-757.

Yu, Q., Bazant, Z. P., 2011, "Can Stirrups Suppress Size Effect on Shear Strength of RC Beams?" *Journal of Structural Engineering-ASCE*, Vol. 137, No. 5, pp. 607-617.

Zararis, P. D., Papadakis, G. C., 2001, "Diagonal shear failure and size effect in RC beams without web reinforcement." *Journal of Structural Engineering-ASCE*, Vol. 127, No. 7, pp. 733-742.

Zheng, Y., Taylor, S., Robinson, D., Cleland, D., 2010, "Investigation of Ultimate Strength of Deck Slabs in Steel-Concrete Bridges." *ACI Structural Journal*, Vol. 107, No. 1, pp. 82-91.

Zokaie, T., 1992, "Distribution of wheel loads on highway bridges - Final report of NCHRP Project 12-26." *Research results digest*, Number 187, pp. 1-31.

Zsutty, T., 1971, "Shear Strength Prediction for Separate Categories of Simple Beam Tests." *ACI Journal Proceedings*, vol. 68, No. 2, pp. 138-143.

## **9. Annex: Database of test results**